Photochemical Internalisation to Improve the Therapeutic Indices of Chemotherapy Drugs and Nanoformulations

Christopher Marc Barnett

EPSRC Centre for Doctoral Training in
Advanced Therapeutics and Nanomedicines
UCL School of Pharmacy
UCL

A thesis submitted in fulfilment of the degree of
Doctor of Philosophy (PhD)

2018

I, Christopher Marc Barnett, confirm that the work presented in this thesis is my own. Where information has been derived from other sources, I confirm that this has been indicated in the thesis.

Abstract

Photochemical internalisation (PCI) is a novel, minimally-invasive, drug delivery technology that facilitates the delivery of therapeutic molecules into the cytosol of cells. Owing to PCI being initiated by light, treatment is confined to the specific area of illumination and adverse effects in distant tissues are therefore minimised. PCI can enhance the targeted intracellular delivery of therapeutics unable to penetrate cellular membranes and of those sequestered within endosomes and lysosomes whereby they are unable to exert their therapeutic potential. To date, PCI studies have predominantly used immunotoxins as the chemotherapeutic component with relatively few investigating the benefit of PCI in the delivery of clinically-approved small molecule chemotherapy drugs.

Three-dimensional (3D) *in vitro* cell culture models of breast cancer (MDA-MB-231 and MCF-7 cells) and pancreatic cancer (MiaPaCa-2 cells) were used in this work. First, the performance of a range of chemotherapy drugs was tested in 3D breast cancer models with key parameters identified for subsequent use in light treatment experiments. PDT and PCI experiments were then performed and novel PCI-drug combinations compared to PCI of bleomycin (a model PCI chemotherapeutic drug). Excitingly, several promising new PCI-drug combinations were seen to outperform PCI-bleomycin. In particular, PCI-vincristine and PCI delivery of the vinca alkaloids, in general, was seen to perform impressively across all of the treatment outcomes of potency, efficacy, and synergy - as determined by means of a cell viability assay.

Key PCI-drug combinations were then taken forward to investigations with alterations made in both PCI regimen and cell culture conditions. Both variations were seen to significantly impact upon PCI treatment outcomes. Finally, PCI-drug combinations were then tested in a 3D model of pancreatic cancer. In addition to this, novel gemcitabine nanoformulations (gemcitabine-squalene and gemcitabine-polymer) were combined in PCI regimens and the former bioconjugate was seen to vastly improve treatment outcomes in both pancreatic and breast cancer models.

Impact Statement

Photochemical internalisation (PCI) is a powerful means to improve the delivery of anticancer drugs to tumours. The focus of this project was to study the therapeutic modality of PCI in monolayer and 3D *in vitro* environments and to improve the therapeutic index of eight clinically-used anticancer drugs and two experimental nanoformulations. The results of this Thesis could make an impact in multifarious ways and in different contexts.

First, the *in vitro* models that are reported and contrasted in this Thesis provide a valuable insight which will be beneficial to a range of scientists that use cell culture as a standard means of drug screening and development; namely, biologists, medical scientists, and medicinal chemists.

Secondly, PCI utilises light and hence the protocols developed herein will be highly interesting to biophotonics experts, as well as, clinical scientists that utilise light sources in therapeutics in a wider context. For example, in oncology and precision medicine, as well as, in diagnostics and imaging.

More importantly, there are several interesting and quite serendipitous findings throughout the Thesis. For instance, it was found that under our proposed PCI protocols and experimental conditions, several of the tested drugs enhanced their cytotoxic properties by two or even three (and sometimes even more) orders of magnitude. In addition, we showed that PCI can be combined with novel nanoformulations which could lead to the development of even more potent therapeutic modalities. It is therefore apparent that these findings will be of interest to a wide range of medical scientists spanning from oncologists, molecular biologists, to pharmacologists, and nanomedicinal scientists.

These findings will pose a direct impact upon the development of future therapeutic modalities for breast and pancreatic cancer which harbour clinical phenotypes with limited treatment options and poor prognoses. From this viewpoint, it is expected that this Thesis could potentially direct the field of precision medicine towards the clinical development of PCI therapeutics which could ultimately find use in the clinical setting.

Finally, the key results of the Thesis have been communicated in national and international conferences and have been published in top-tier academic journals. It is therefore anticipated that these findings will be inspirational to colleagues, scholars, clinicians, and students across the respective research fields of nanomedicine, biophotonics, interventional science, and the pharmaceutical technologies.

Table of Contents

List of Figures and Tables

List of Abbreviations

$^1O_2$	Singlet oxygen
3D	Three-dimensional
5-FU	5-fluorouracil
$AlPcS_{2a}$	Aluminium phthalocyanine disulphonate [adjacently-substituted]
APC	Antigen-presenting cell
CDT	Centre for Doctoral Training in Advanced Therapeutics & Nanomedicines
CYP3A4	Cytochrome P450 enzyme 3A4
Da	Dalton
DLS	Dynamic light scattering
DMEM	Dulbecco's Modified Eagle's Medium
DMSO	Dimethyl sulfoxide
ECM	Extracellular matrix
EGF	Epidermal growth factor
EGFP	Enhanced green fluorescent protein
EMA	European Medicines Agency
E_{max}	Maximum efficacy
EMT	Epithelial to mesenchymal transition
EPR	Enhanced permeability and retention
ER+	Oestrogen-receptor positive
EtOH	Ethanol
FDA	Food and Drug Administration
FOLFIRINOX	FOL – folinic acid; F – fluorouracil; IRIN – irinotecan; OX – oxaliplatin
HPD	Haematoporphyrin
HSP	Heat shock protein
$IC_{50/70}$	Inhibitory concentration 50%/70%
IL	Interleukin
LB	Light-before
LDL	Low-density lipoprotein
LDLR	Low-density lipoprotein receptor
LED	Light emitting diode
MCF-7	MCF-7 human mammary gland/breast adenocarcinoma

MDA-MB-231	MDA-MB-231 human mammary gland/breast adenocarcinoma
MDR	Multi-drug resistance
MiaPaCa-2	MiaPaCa-2 human pancreatic carcinoma
NICE	National Institute for Health and Clinical Excellence
nM	Nanomolar
NSCLC	Non-small cell lung cancer
PAMAM	Polyamidoamine
PCI	Photochemical internalisation
PDI	Polydispersity index
PDT	Photodynamic therapy
PR	Progesterone receptor
PS	Photosensitiser
RLU	Relative light units
ROS	Reactive oxygen species
RTC	Rat rail collagen
SCC	Squamous cell carcinoma
SqGem	Squalene-gemcitabine
TLR	Toll-like receptor
TNBC	Triple-negative breast cancer
TNF	Tumour necrosis factor
$TPCS_{2a}$	Fimaporfin/Amphinex®
TPZ	Tirapazamine
UCL	University College London
VLDL	Very low density lipoproteins

Acknowledgements

"Gorau adnabod, d'adnabod dy hun." – The best knowledge is to know yourself

This Thesis was conducted at the Engineering and Physical Sciences Research Council (EPSRC) Centre for Doctoral Training in Advanced Therapeutics and Nanomedicines (CDT) at UCL School of Pharmacy, University College London. I would like to thank all of my fellow CDT members with whom I have shared this journey. It has not been the easiest path but I have learned a great deal both of myself and of life, more generally. I also learned a bit of science along the way!

I would like to say thank you to my supervisors Dr. George Pasparakis and Prof. Ijeoma Uchegbu. George, particularly, your honest and spirited advice was always very welcoming and it was an immense help to me at some difficult times. Thank you. All things considered, I am immensely proud of what we have managed to achieve with this Thesis.

I would also like to say a massive thank you to my partner and best friend, Saja. Suffice to say that this Thesis simply would not have been completed without your ever-present intellect, support, and atonal melodies! To my twin brother and oldest friend, Dai, thank you for always being there and providing the hammer of truth when I needed it. We have certainly come a long way and it has always been together. That was yesterday…

I would also like to thank my parents, sister, and nephews and to say a special thank you to the Muwaffak's – many fun times have already been had, and here's to many more..! I would also like to say thank you to Prof. Steve Brocchini – a truly kind and generous (and busy!) man.

This Thesis is dedicated to my uncle, Tudor.

Christopher M. Barnett

September 20, 2018

Section A: Background and Introduction

Chapter 1: Photodynamic Therapy and Photochemical Internalisation

1. Photodynamic Therapy and Photochemical Internalisation

Although the majority of this body of work pertains to the light-initiated treatment photochemical internalisation (PCI), it is important to recognise that it shares many parallels with the already clinically-established light-initiated treatment called photodynamic therapy (PDT). Despite each being separate treatment modalities in their own right, both rely upon the fundamental use of a photosensitiser in conjunction with the focal application of light. Thus, it is necessary to first introduce the underlying principles and applications of PDT as many of them are also directly applicable to PCI.

1.1 Photodynamic Therapy

1.1.1 General background

Photodynamic therapy (PDT) is a minimally-invasive, targeted anticancer treatment modality which induces photo-oxidative damage in cells and tissues of specific therapeutic interest. It achieves this by means of a light-activated photosensitive drug (photosensitiser) which, upon light-irradiation, combines with molecular oxygen to produce the required cytotoxic moiety. Each of the three components of photosensitiser, light, and oxygen are crucial to the overall PDT effect and site-specificity is achieved by virtue of the spatially-confined area of illumination.

The history of PDT and light-treatments in general has previously been described in detail by Dolmans and colleagues (1). As outlined in this review, the relatively recent advent of PDT use in oncology has been preceded by attempts to use light as therapy for more than four thousand years. For instance, it has been documented that the ancient Egyptians used the combination of orally-ingested Amni Majus plant (which contains psoralen – today used to treat psoriasis) and sunlight, to successfully manage vitiligo (2). More recently, in his 19th century Nobel Prize-winning work (Physiology or Medicine, 1903), Niels Finsen used the "Finsen lamp" to successfully demonstrate 'phototherapy' in the treatment of cutaneous tuberculosis (*lupus vulgaris*) (3). The first modern use of chemicals and light in combination occurred in the early 20th century with acridine and eosin (both are dyes – as are many newer sensitisers) being found to be cytotoxic to infusoria and skin carcinoma, respectively (4,5). It

was also at this time that a French neurologist named Jean Prime noted the development of sunlight-induced dermatitis in epilepsy patients treated with oral eosin – an adverse effect that is still a major limitation of photosensitisers today (6). In the 1903 eosin work by von Tappeiner and Jesionek, they were also the first to describe the phenomena they saw as "photodynamic action". In 1911, further advancements were seen when W. Hausmann first utilised the photosensitising porphyrin haematoporphyrin (7). Incidentally, the combination of iron and porphin (the central structure of porphyrins) forms the vital biomolecule haem (1). In 1913, the first human use of haematoporphyrin followed shortly after Hausmann's work in mice. Here, German scientist Friedrich Meyer-Betz, self-administered haematoporphyrin and reported pain and swelling in light-exposed areas (8).

In the 1960's, Richard Lipson and his colleagues at the Mayo Clinic then ushered in the modern era of PDT by showing that haematoporphyrin derivative (HpD) – a compound with twice the phototoxicity of haematoporphyrin; developed by Samuel Schwartz (9) – localised to tumours where it emitted fluorescence (10). A decade later, Diamond et al. reported that HpD could treat cancer *in vivo* following their observation that glioma growth was retarded by several weeks using HpD treatment (11). In the 1970s, the *in vivo* tumour-eradicating effect of HpD and red light was then revealed by Dougherty (12); prompting clinical administration in humans using HpD for the PDT treatment of skin and bladder cancers (13,14). Following the preliminary successes seen in these clinical studies, numerous other PDT studies then followed for various malignancies including those of the lung, oesophagus, and stomach (1). A partially-purified HpD derivative later gave rise to the clinical compound Photofrin® (Porfimer sodium); which first gained regulatory approval for bladder cancer treatment (Canada, 1993) but is now licensed in over 40 countries for the treatment of several other cancers, too, including those of the lung, stomach, and oesophagus (1,15).

Despite its numerous clinical indications, Photofrin® is not without its limitations. For example, this 1st generation sensitiser has suboptimal tumour selectivity, a relatively short wavelength of absorption (630 nm), and a low molar absorption coefficient (1,170 $M^{-1}cm^{-1}$); which means that high concentrations of both sensitiser and light must be administered (1,2). Moreover, as it exists, Photofrin® actually consists of about 60 compounds (all of which contain the porphyrin moiety) which gives rise to issues in composition reproducibility. Photofrin® also

accumulates in the skin which results in prolonged cutaneous photosensitivity for patients requiring 4-6 weeks of sunlight avoidance following illumination (1). As a result of these limitations, significant efforts have been made to develop *2nd generation* compounds with improved chemical purity, light absorbance wavelengths (the red light region is preferable), tumour specificity, and less skin photosensitivity (1,2). These revised agents have been developed since the late 1980s and are based upon a host of porphyrin/chlorophyll analogue chemical structures (Figure 1). Indeed, a disulphonated aluminium phthalocyanine derivative (maximum absorbance: 670 nm) has been used in the present work. Third generation photosensitisers have subsequently been developed which refer to those 2nd generation sensitisers which have been coupled to carrier-moieties such as cholesterol, antibodies, and liposomes (2).

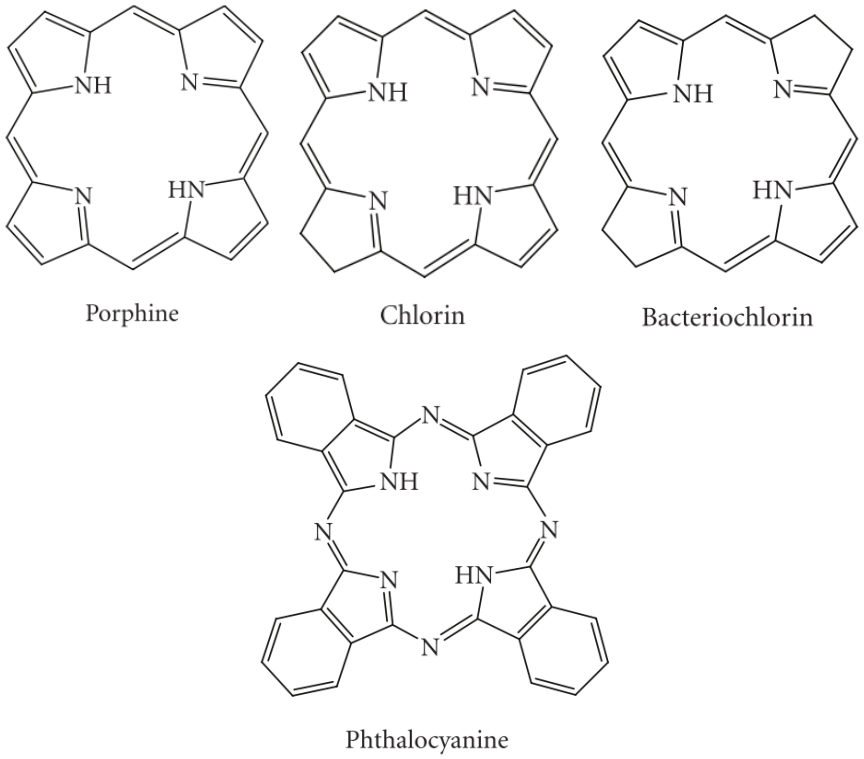

Figure 1. Chemical structures of porphine, chlorin, bacteriochlorin, and phthalocyanine photosensitisers. *Modified from* (2).

The first light sources used in clinical PDT were non-coherent light sources (e.g. conventional arc lamps) and although these were safe, easy to use, and inexpensive, they retained a significant thermal effect, together with a low, variable light intensity (16). Today, laser light sources are most commonly used in clinical PDT as they produce high energy, coherent, monochromatic light of a specific wavelength. Furthermore, laser light can be

delivered directly to the target site using optical fibres – a feature that is also useful for treating larger tumours that require intraluminal or interstitial placement of multiple light sources (aided by radiological guidance). More recently, Light Emitting Diodes (LED) have also been investigated which are powerful, inexpensive, and easy to manufacture (17). Clinical light penetration is complex owing to heterogeneous tissues and the attenuation of shorter light wavelengths by endogenous chromophores (e.g. haemoglobin) and at longer wavelengths by water. Optimal tissues penetration is thus achieved between 600-1300 nm although wavelengths >850 nm do not provide sufficient energy to induce sensitiser triplet state (more details below in *Photochemistry*). As such, the 'therapeutic window' lies in the visible red spectrum region between 620-850 nm (18).

Table 1. Overview of clinically-approved photosensitisers. *Modified from* (18).

Photosensitiser	Excitation Wavelength (nm)	Approved	Indication
Porfimer sodium/Photofrin®	630	Worldwide, withdrawn in EU for commercial reasons	High grade dysplasia in Barret's oesophagous; obstructive oesophageal or lung cancer
5-ALA/Ameluz®/Levulan®	635	Worldwide	Mild to moderate actinic keratosis
Metvix®/Metvixia®	570–670	Worldwide	Non-hyperkeratotic actinic keratosis; basal cell carcinoma
Temoporfin/mTHPC/Foscan®	652	Europe	Advanced head and neck cancer
Talaporfin/NPe6/Laserphyrin®	664	Japan	Early centrally located lung cancer
Verteporfin/Visudyne®	690	Worldwide	Age-related macular degeneration
Synthetic hypericin/SGX301	570–650	Orphan status in EU	Cutaneous T-cell lymphoma
Redaporfin®/LUZ1	749	Orphan status in EU	Biliary tract cancer

Photodynamic therapy has been studied extensively in the preclinical and clinical setting and at the time of writing, *eight* photosensitive drugs are clinically-approved for treating various indications – predominantly malignancies (Table 1). Exceptions include: sensitisers for diagnosis (e.g. hexyl aminolevulinate: Hexvix®) and for age-related macular degeneration (e.g. Verteporfin/Visudyne®). As shown in Table 1, PDT is capable of treating a range of solid tumour malignancies but its widespread clinical use has been stalled by the need to administer

photosensitisers at high doses; thus, predisposing patients to the risk of prolonged skin photosensitisation (2). Moreover, from a more mechanistic standpoint, PDT efficacy is reliant upon many independent factors, including: light dose and fluence rate, molecular oxygen availability, photosensitiser uptake and localisation, photosensitiser charge, hydrophobicity, and three-dimensional shape, as well as, the time between photosensitiser administration and light exposure (1,18). Consequently, a standardised clinical approach has been difficult to develop and has kept PDT at the fringes of medicine despite its clear promise (15,18).

1.1.2 PDT Mechanism of Action

1.1.2.1 Photochemistry

Although the precise mechanism of action of PDT is an ongoing topic of investigation, its molecular effects are well-characterised (18). These fundamental photochemical processes are based upon the reaction of a light-activated photosensitiser with other cellular components and substrates to create radicals – a mechanism central to the therapeutic action of PDT (and PCI). In order to optimise photosensitiser activation, the spectral output of the light source is typically matched to its absorption spectrum. Figure 2 illustrates a simplified summary of the process of photosensitisation.

Briefly, following the absorption of light (photons) at a given wavelength (preferably matched to the photosensitiser), the sensitiser is transformed from its ground state (singlet state) into a relatively long-lived electronically-excited state (triplet state; “excited state”) by means of a short-lived excited singlet state (2,18). The excited triplet state (Figure 3, “activated photosensitiser”) can then partake in type I or type II reactions. Type I reactions occur when the triplet reacts directly with adjacent cellular substrates such as the cell membrane (or a molecule) and transfers an electron (hydrogen atom) to form radicals which then, in turn, interact with oxygen to generate oxygenated products (e.g. superoxide anions) (2,18). Alternatively, type II reactions occur when the triplet (activated photosensitiser) transfers its energy directly to oxygen, to form the extremely labile and reactive singlet oxygen moiety ($^1O_2$). Photomolecules can also decay back to the ground state by other means including by converting their energy into heat or fluorescence – a feature useful for diagnostics and optical monitoring (18).

.

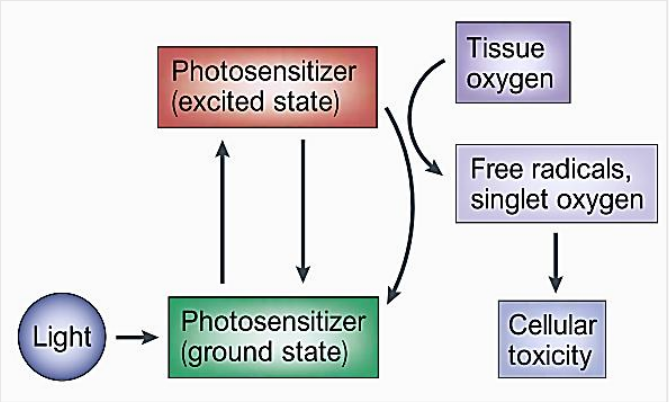

Figure 2. Mechanism of action of photodynamic therapy (PDT). *Modified from (1).*

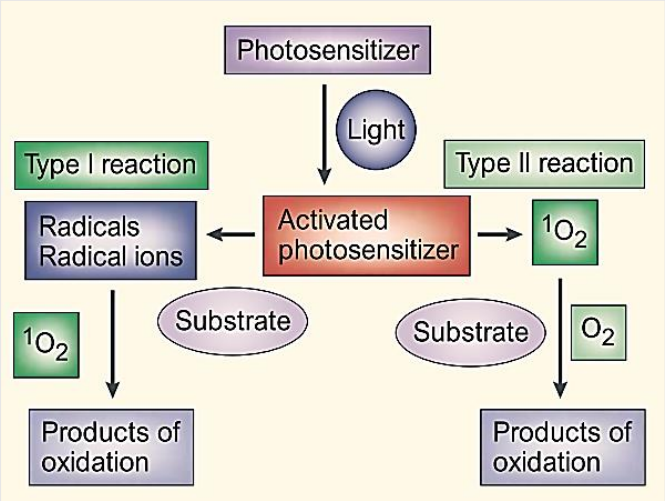

Figure 3. Type I and type II reaction in photodynamic therapy (PDT). *Modified from (1).*

Most photosensitisers are thought to act through type II reactions (particularly, $^1O_2$) (18). However, both type I and type II reactions can occur concurrently, and their relative ratio depends upon the type of sensitiser used, substrate and molecular oxygen concentration, and sensitiser-substrate binding affinity (1). Moreover, both type II and type I (e.g. superoxide anions) reactions are cytotoxic as they directly react with, and cause damage to, vital cellular biomolecules such as lipids, proteins, and nucleic acids (2,19). In biological tissues, the half-life of singlet oxygen is 40 ns and its maximum radius of action is about 20 nm (20). These short-lived reactive oxygen species (ROS) are particularly beneficial in PCI as their limited diffusion confines ROS action to the area of ROS generation (i.e. at the lysosome membrane and away from lumen-situated therapeutics). In addition, the formation of ROS during light treatment depletes oxygen at a rate directly linked to light fluence rate (19). Consequently,

low light fluence rates are desirable as the availability of sufficient molecular oxygen is critical to PDT efficacy (anoxic or hypoxic regions are considered PDT-resistant) (18).

1.1.2.2 Photosensitiser uptake and localisation

Due to the limited radius of action of ROS (in particular, $^1O_2$), the exact intracellular localisation of the sensitiser can be crucial to its therapeutic effect. Key structural characteristics that influence the cellular uptake and subcellular localisation of photosensitisers include their charge, lipophilicity, and three-dimensional shape (1,2,18). In addition to these physicochemical parameters, photosensitiser concentration and incubation times, environmental factors (e.g. temperature, pH), and serum concentration also impact upon photosensitiser accumulation. To the latter point, upon intravenous administration, photosensitisers will encounter and quickly bind plasma proteins and because they associate with these proteins to varying degrees, their pharmacokinetics and biodistribution will also vary (18).

The net photosensitiser charge determines the interaction between the sensitiser and cellular membranes (18). In general, positively-charged (cationic) sensitisers readily cross cellular membranes (which are negatively-charged) and primarily localise to mitochondrial membranes. By contrast, negatively-charged (anionic) sensitisers are taken up *via* endocytosis which favours localisation to the lysosome (21). In addition, the spatial distribution of charges can also impact upon photosensitiser-membrane electrostatic interactions and therefore photosensitiser uptake, subcellular distribution, and their resulting photocytotoxic effect (18).

Photosensitiser lipophilicity affects its plasma distribution and, subsequently, its uptake and localisation. Specifically, more hydrophilic sensitisers generally bind albumin, amphiphilic bind high-density lipoproteins, and more hydrophobic sensitisers bind the inner lipid core of low-density lipoproteins (22). Interestingly, increased lipophilicity permits higher photosensitiser uptake and increased amphiphilicity increased partitioning from lysosomes to mitochondria (23).

Additional structural alterations such as the central incorporation of metal ions (e.g. aluminium) and the substitution of the peripheral pyrrole rings (e.g. sulphonate groups to

aluminium phthalocyanine) can also strongly influence the photophysical properties and biodistribution of photosensitisers (2). For instance, the disulphonated derivative of aluminium phthalocyanine ($AlPcS_{2a}$) is water-soluble, amphiphilic and preferentially localises to lysosomal membranes – favourable properties for PCI applications (24). Sensitiser subcellular locale will also therefore have a material impact upon the type of photooxidative damage elicited (e.g. mitochondrial or lysosomal) and the type of cell death that is initiated.

1.1.3. PDT at a Cellular Level

Photosensitiser localisation is key in determining cellular responses to photooxidative damage and, ultimately, cell fate (25). For example, the photosensitisers crystal violet and methylene blue were equally efficient in inducing cell death despite the former producing 10-fold fewer radicals. Here, its mitochondrial cytolocation was key – the latter sensitiser localised to the cytosol (and lysosome) (26). Although PDT affects numerous targets (including the cytoskeleton and cell adhesion molecules), three primary mechanisms of photodamage-induced cell death have been recognised: (i) apoptosis, (ii) necrosis, and (iii) autophagy. This activation of various cell death pathways could also bypass the issue of apoptosis-resistant tumour cells which is a major mechanism of treatment resistance (27).

1.1.3.1 Apoptosis

Apoptosis is a controlled and tightly-regulated mechanism of cell death which can be initiated naturally *via* various pathways and also in response to key physiological cues, such as, those emanating from photooxidative damage to intracellular organelles. Apoptotic cells are morphologically-distinct (e.g. membrane blebbing) and tissues characteristically remain inflammation-free (2). Mitochondrial-localised photosensitisers are most likely to induce apoptosis as photodamage here results in membrane permeabilisation and leakage of cytochrome c into the cytosol – a key activator of the caspase-mediated apoptotic pathway (28).

1.1.3.2 Necrosis

In contrast to apoptosis, necrosis is an uncontrolled and less-ordered form of cell death which is characterised by tissue inflammation (which can also trigger immune responses – see later).

Other features include cytoplasmic swelling and organelle destruction (18). Plasma membrane-localised sensitisers and higher PDT doses are more likely to cause necrosis – the latter due to damage to the constituent components of the apoptotic apparatus. Correspondingly, apoptosis predominates at lower PDT doses. Importantly, however, both necrotic and apoptotic cell death mechanisms ensue following PDT and the initiation of either process involves complex intracellular mechanisms along with specific sensitiser considerations (29).

1.1.3.3 Autophagy

Autophagy (literally, 'self-eating') allows the cell to recycle damaged organelles and cytoplasmic components and is thought to be initiated by calcium ion release from damaged mitochondria and/or endoplasmic reticulum. Damaged components are engulfed by double-membrane *autophagosomes* which then fuse with lysosomes for degradation (30). Autophagy also appears to be PDT-dose dependent. At lower doses autophagy exhibits cytoprotective functions whereas, at higher doses, autophagic cell death can be activated (31). Interestingly, lysosome-targeted photosensitisers have been shown to compromise the autophagy mechanism (32).

Overall, determining the outcome of PDT at the cellular level is complex. However, the general themes are as follows: *necrosis* predominates at high PDT doses and plasma membrane-localised sensitisers; *apoptosis* is common after mild PDT and photodamage to mitochondria; and, cytoprotective *autophagy* results from low PDT damage to organelles which can later switch to a cytotoxic capacity, if necessary (18).

1.1.4 PDT at a Tumour Level

In general, there appears to be good concordance between *in vitro* and *in vivo* outcomes with regard to PDT-initiated cell death mechanisms (18). However, as aforementioned, PDT effects are multifaceted and complex and so are the factors that contribute to them. In relation to *in vivo* work, even the earliest photosensitisers have demonstrated some preferential localisation and accumulation within tumour tissue (1,10,18). However, photosensitisers are

still internalised by both healthy and diseased cells which means the overall treatment effect is not entirely confined to the area of PDT treatment.

It has been posited that the selective uptake of photosensitisers by tumour tissue stems from the ability of normal tissues to more-efficiently eliminate sensitisers (and other xenobiotics) *via* lymphatic drainage. Moreover, the rapid growth of cancer cells leads to malformed and 'leaky' tumour vasculature which permits the extravasation and retention of macromolecules within tumours *via* the enhanced permeability and retention (EPR) effect (33). The overexpression of certain receptors has also been posited to contribute to the favourable tumoural retention of photosensitisers (18,33). For instance, hydrophobic sensitisers bind low-density plasma lipoproteins (LDLs) and tumour cells are known to overexpress LDL-receptors (as do some normal tissues, e.g. the liver and kidney) in order to gain the cholesterol needed for the rapid turnover of cellular membranes. Other theories pertain to the effect of the low intratumoural pH on the relative ionisation/unionisation of sensitisers which could influence their membrane penetration and cellular retention. Another involves tumour-associated macrophages "delivering" photosensitiser during tumour infiltration (18,33).

The route of administration can also substantially affect photosensitiser pharmacokinetics and biodistribution (18,33). Administration may occur *via* the intravenous, intraperitoneal, or topical route; although the former route is typically used for non-cutaneous carcinomas. The major limitation here is the necessarily high photosensitiser doses resulting in prolonged periods of skin photosensitivity (during which patients have to avoid exposure to both natural and artificial light). Attempts to increase tumour selectivity and to decrease systemic photosensitiser doses have subsequently spawned various advanced formulations utilising sensitiser-polymer conjugates (e.g. dendrimer or miceller nano-carriers) and targeting ligands (e.g. antibodies) (18,33).

1.1.4.1 PDT mechanisms of anti-tumour effects

Photodynamic therapy is considered to elicit three distinct mechanisms of tumour destruction: (i) direct cytotoxicity; (ii) anti-vascular effects; and (iii) immune reaction (1,18,33). Firstly, ROS generated by tumour-localised photosensitisers can directly kill tumour cells by apoptosis and/or necrosis. Secondly, photooxidative damage to tumour vasculature can impair

perfusion and thus compromise the supply of oxygen and essential nutrients to the tumour. Thirdly, PDT can induce an inflammatory and immune response against malignant cells. These three mechanisms combine to produce the therapeutic effect of PDT and can also influence each other.

1.1.4.1.1 Direct ROS effects

The PDT site of action is also fundamentally important at the tumour level. Like healthy tissues, solid tumours also comprise of distinct tissues with various cell types: namely, the parenchyma (malignant cells) and the stroma (supportive, vascularised tissue). The most direct form of cytotoxicity is photooxidative damage to the parenchyma cells, however, studies have shown that this is not sufficient enough for tumour cure (1,33). Instead, damage to stromal cells such as structural proteins (e.g. integrins) and fibroblasts may also play a vital role in PDT efficacy through disruption of stromal-tumour signalling pathways.

The direct killing of parenchymal and stromal cells is ultimately predicated on the sufficient distribution and accumulation of photosensitiser, as well as, the availability of oxygen for ROS generation. Crucially, levels of both can be impaired as a result of the chaotic growth and organisation of tumour vasculature. Indeed, both intra- and inter-tumour variations in photosensitiser concentration have also been observed (33). Furthermore, oxygen can be rapidly depleted by high light fluence rates hence why low light fluence rates are preferred. Alternatively, fractionated illumination may be employed in order to conserve oxygen whereby tissue reoxygenation is thought to occur during the *dark* interval (34).

1.1.4.1.2 Vasculature effects

Angiogenesis is a key process in cancer development and the importance of adequate perfusion is demonstrated by necrotic regions found within the tumour. Vascular destruction is therefore directly detrimental to tumour growth as destroying the tumour blood supply evidently prevents the delivery of oxygen and nutrients upon which it relies for sustenance.

Post-PDT, both endothelial and subendothelial cells are damaged. Indeed, post-PDT treatment, microvascular collapse is readily observable alongside a severe and persistent tumour hypoxia (33). Although photooxidative damage to the tumour endothelium ultimately

induces ischemic cell death, the underlying mechanisms to achieving this are photosensitiser-dependent. Typically, damaged endothelial cells release clotting factors which activate platelets, leading to thrombus formation and vessel occlusion. Activated platelets then also induce vasoconstriction, thus decreasing perfusion yet further, and leading to tissue hypoxia and tumour destruction (18). Indeed, antivascular-PDT is a deliberate strategy in its own right (1,18,33).

1.1.4.1.3 Immune reaction

The third mechanism of PDT-induced tumour destruction is the initiation of inflammation followed by host anti-tumour immunity (1,18,33). The oxidative stress induced by PDT can upregulate heat shock protein expression (HSP) and prompt the release of inflammatory cytokines such as tumour necrosis factor (TNF)-α, interleukin (IL)-6 and IL-1β that stimulate neutrophilia (1,35). Moreover, HSPs can bind tumour antigens as well as interact with Toll-like receptors (TLRs) – a key route for activating antigen-presenting cells (APC) (36). Indeed, this post-PDT inflammatory signalling initiates a massive, regulated invasion of neutrophils, mast cells, and macrophages; cells which have been shown to potentiate the anti-tumour effects of PDT (33).

Following the acute inflammatory response (innate immunity), host anti-tumour immunity can develop (adaptive immunity). Demonstrating the importance of the induced immune reaction, mice with normal immunity have been shown to outperform their immunosuppressed counterparts in PDT treatment outcomes including in resistance to tumour cell rechallenge. Moreover, the transfer of T-lymphocytes from normal mice to immunocompromised mice achieved improved cure rates (33,35). Although the adaptive immune reaction is not essential to initial tumour damage, it primes the host for subsequent recurrences of similar tumours through the formation of tumour-specific memory cells (37).

This anti-tumour immunity effect also forms the basis of PDT-generated cancer vaccines (38). Interestingly, tumour-cell lysates recovered post-PDT treatment were more effective anti-cancer vaccines than those from tumour cells exposed to ultraviolet or ionising irradiation (1).

1.1.5 Clinical PDT

Due to its mode of action, PDT can be used in conjunction with many current mainstay clinical oncology treatments such as surgery, radiotherapy, and chemotherapy. Furthermore, PDT is minimally-invasive and activated locally which means it is relatively tissue-sparing. This permits favourable healing and good cosmetic results, particularly in skin and head and neck cancers (18,39). This is, at least in part, because PDT is a cold photochemical process (i.e. there is no tissue heating) so connective tissues such as collagen remain largely unaffected by treatment (39). Moreover, unlike radiotherapy, PDT can be repeated several times (39). Its main limitation remains the prolonged periods of skin photosensitivity for patients following intravenous sensitiser administration.

As aforementioned, the 1st-generation photosensitiser Photofrin® (porfimer sodium) was first to obtain regulatory approval for several malignancies but has well-recognised limitations. This was followed by approval of the 2nd-generation sensitiser Foscan® (temporfin), in Europe, for treating advanced head and neck cancers. However, due to the relative ease of accessibility of skin legions, most clinical PDT experience has been gained in the dermatological field (39). Notwithstanding, the utility of PDT in treating deeply-seated and locally-advanced interstitial tumours is still being realised (e.g. in prostate cancer) (40). Despite this, only *four* sensitisers currently have regulatory approval for cancer treatment from both the Food and Drug Administration (FDA) and the European Medicines Agency (EMA) (Table 1).

Encouragingly, there are extensive clinical trials still ongoing. As of the time of writing (September, 2018), a cursory look at www.clinicaltrials.gov using the search terms “photodynamic therapy” and “cancer” shows that there are currently 43 open, actively-recruiting trials utilising a host of both new and existing photosensitisers. Inevitably, the more clinical trials that are performed, the sooner a standardised PDT approach is likely to be developed. This, coupled with the development of sensitisers and sensitiser formulations with improved therapeutic indices, increased computing power for *in silico* simulations, along with advancements in light sources (e.g. the cylindrical diffuser fibre), will all contribute to the increased clinical appeal of PDT and, indeed, other light-based treatments.

1.1.6 Chemophototherapy

Photodynamic therapy can cure early tumours and small lesions for advanced cancers but, alone, PDT rarely achieves a cure and recurrence is common (33,41). Numerous strategies have therefore been adopted in order to try to improve the therapeutic indices of PDT: including advanced formulation by conjugation to carrier molecules (e.g. peptides), but also by combining with chemotherapy (termed, 'chemophototherapy'). In theory, each treatment modality would employ a distinct mechanism in order to exert its therapeutic effect and thus produce a more effective overall treatment. Indeed, both *in vitro* and *in vivo* studies have shown that the combination of both modalities can produce a more potent treatment than using either treatment alone – that is, treatment *synergy* was produced (42). Synergy is achieved when the combined effect of two (or more) treatments is greater than the effect obtained by applying each modality separately. Importantly, treatment synergy (or, indeed, additivity) could lead to reduced systemic drug doses and therefore improved overall therapeutic indices.

PDT in combination with chemotherapy is of particular relevance to this Thesis, although PCI may be more accurately viewed as a distinct branch of this general approach. Doxorubicin, mitomycin, and cisplatin have been the most frequently studied chemotherapeutics in combination with PDT in preclinical studies. Other chemotherapy drugs include gemcitabine and methotrexate. With regards to photosensitisers, Photofrin® appears to be the choice in the majority of studies (19). Now over thirty years ago, Cowled et al., first paired HpD-PDT with doxorubicin chemotherapy *in vitro* and *in vivo* and observed a slight enhancement of anti-tumour effect in a lung carcinoma mouse model (43). Utilising $AlPcS_2$-PDT against inoculated L1210 leukemia and P388 lymphoma cells *in vivo*, Canti and co-workers reported an additive cytotoxicity in combination with doxorubicin and cisplatin chemotherapy (44). This study demonstrated that, indeed, favourable therapeutic outcomes could be achieved even with low chemotherapy doses when used in a combined PDT-chemotherapy regimen. In addition, Sun et al., also found that combining HPPH (2-[1-hexyloxyethyl]-2-devinyl pyropheophorbide)-PDT with gemcitabine led to a synergistic cytotoxic effect in pancreatic cancer cell lines (45). The sequence and timing of drug and

sensitiser administration also emerged as an important consideration in such combined drug-PDT regimens.

The combination of PDT and chemotherapy in chemophototherapy regimens is still a relatively rare occurrence, with many traditional drugs still yet to be tested (19). As aforementioned, PCI may be regarded as a discrete form of chemophototherapy as it also combines chemotherapeutics with photosensitisers and light (PDT). Importantly, however, the main purpose of the photochemical component in PCI is to specifically increase the cytosolic concentration of the chemotherapeutic. Consequently, the primary cytotoxic effect of PCI is exerted by the chemotherapeutic rather than the photochemical treatment.

1.2 Photochemical Internalisation

1.2.1 General background

Photochemical internalisation (PCI) is a novel, minimally-invasive, drug delivery technology originally conceived by Berg and colleagues in 1999 (46). The technique facilitates the delivery of therapeutic molecules into the cytosol of cells (47) and, much like PDT, is regarded to be a site-specific therapy owing to treatment being initiated and confined to the specific area of illumination.

The PCI approach (Figure 4) was developed in order to enhance the targeted intracellular delivery of therapeutics unable to penetrate cellular membranes due to, for example, their molecular size, charge, or subcellular localisation (48). Following endocytosis, these molecules accumulate within endosomes and lysosomes where they are trapped or enzymatically-degraded and are therefore unable to exert their therapeutic potential (47). Subsequently, PCI acts to increase the cytosolic concentrations of these endocytosed therapeutics through a form of targeted intracellular PDT utilising amphiphilic photosensitisers (49).

In fact, early pioneering work by de Duve and colleagues discovered that all endocytosed substances are trafficked to the lysosome (50). These membrane-enclosed organelles contain about 50 different degradative enzymes and function to degrade and digest xenobiotics (including chemotherapy drugs) and obsolete cellular components (51). The

precise targeting of a drug-laden lysosome (or endosome) is therefore an ideal target for attempts to increase cytosolic drug concentrations for therapeutic means. As previously outlined, the macrocyclic and aromatic chemical structure of photosensitisers allows for an almost infinite number of structural variations and derivatives which can have a material impact upon sensitiser distribution, uptake, localisation, and therapeutic action. Nonetheless, only relatively few photosensitisers have achieved regulatory approval to date (18). Among the variants, though, is a group of amphiphilic photosensitisers with a unique subcellular localisation following endocytosis. Namely, instead of being diffusely localised in the cytosol, these sensitisers specifically localise to the same endocytic vesicle membranes that enclose the therapeutics – making them particularly useful for PCI applications (52).

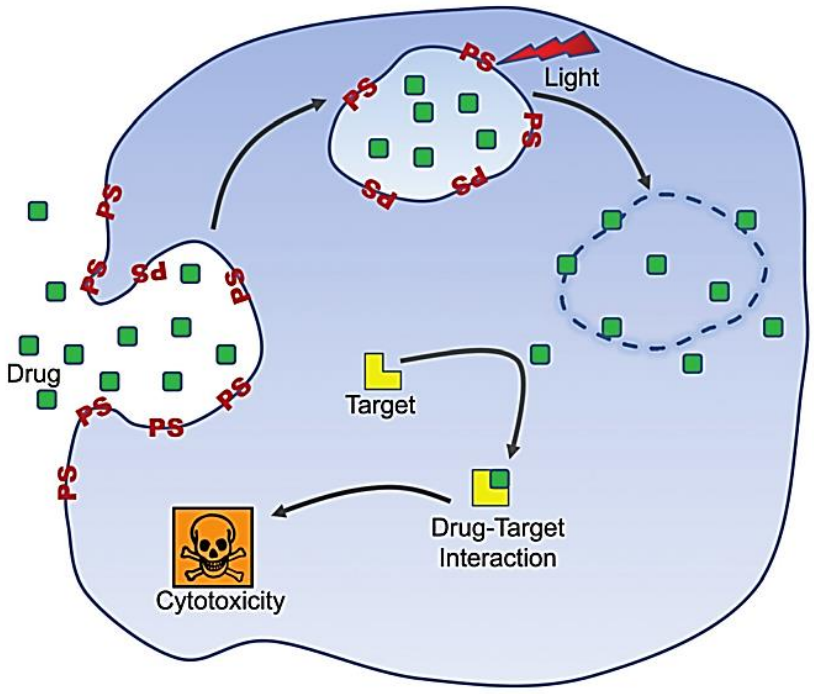

Figure 4. Mechanism of action of photochemical internalisation. *Modified from (48).*

Upon light illumination and ROS generation, endosomal and lysosomal membranes are ruptured releasing both lysing enzymes and entrapped contents into the cytosol and thus allowing the administered drugs to reach their intracellular targets. The fact that PCI is initiated by the application of external energy, *light*, can be beneficial for both targeting specific tissues (e.g. tumours) and for initiating the drug delivery process at the optimum time following systemic drug administration (53). Moreover, by site-directed illumination, PCI can be

employed to target drugs preferentially to tumour sites and therefore reducing adverse effects in distant normal tissues (47).

As aforementioned, the primary aim of PCI is to aid the release of cytotoxic chemotherapeutics using what is essentially a type of targeted and low-dose (essentially, sub-lethal) intracellular PDT. Accordingly, the chemotherapeutic component is the primary agent causing tumour cell death and not the photochemical component, as is the case with PDT. The PCI-release of sequestered and previously "inactive" cytotoxic drugs could therefore reduce light and sensitiser dose requirements and lead to treatment synergy.

Berg and colleagues initially recognised the clinical potential of PCI to improve the delivery of various therapeutics including anti-cancer therapy, gene therapy, and vaccinations (46). Indeed, both *in vitro* and *in vivo* models have now shown that PCI can potentiate the effect of many types of macromolecules and also some small molecule chemotherapy agents, too (47). With regard to *in vitro* investigations with chemotherapeutics, bleomycin has emerged as exceptional candidate for PCI delivery. *In vivo* PCI studies have also analysed various therapeutic agents, regimen parameters (e.g. drug-light interval), and treatment outcomes including tumour response, tumour selectivity, and immunological response (47). Importantly, $AlPcS_{2a}$-induced PCI delivery of bleomycin has been demonstrated to be superior to PDT in *in vivo* animal models (54). Bleomycin-PCI (also utilising $AlPcS_{2a}$) has also shown a synergistic effect when combined with radiotherapy, or after surgery, in mouse xenograft models of human cancer (55,56). In addition, this drug-photosensitiser combination has been shown to induce a systemic anti-tumour immunity *in vivo* (57).

Photochemical internalisation has shown considerable promise in the preclinical setting which warrants further investigation in humans. The limitations associated with current PDT photosensitisers and their intravenous administration may be addressed by the advent of new and improved sensitisers such as Amphinex® (47). In addition, the use of PCI in cancer therapy could improve the therapeutic indices of traditional cytotoxic chemotherapy drugs by ameliorating some of the common limitations associated with their use. Namely, (i) to reduce systemic toxicity resulting from the off-target effects of high systemic drug doses, (ii) the advent of multi-drug resistant tumour cells, and (iii) to better target chemotherapeutics to

tumour tissue (58). The specific use of PCI to deliver chemotherapy drugs is the modality of particular relevance to the present work and will thenceforth be the foremost concern (with some exceptions).

1.2.2 Mechanism of PCI

Photochemical internalisation relies upon the cellular internalisation of both a photosensitiser and chemotherapeutic agent by endocytosis (53,54). Endocytosed molecules are rapidly processed and sometimes directed to other organelles or they may be retained within the endocytic vesicles to later fuse with lysosomes and there be subjected to enzymatic degradation. Thus, cytotoxic agents that target intracellular sites such as the nucleus or microtubules either have to penetrate the plasma membrane or escape from endocytic vesicles in order to exert their therapeutic effect. PCI facilitates drug release from these endocytic vesicles into the cytosol (Figure 5).

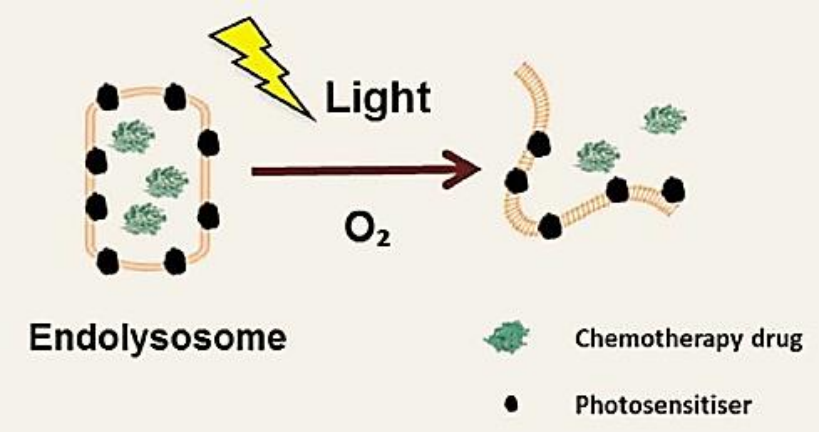

Figure 5. PCI-induced cold photochemical release of an entrapped chemotherapy drug into the cytosol*. Modified from* (52).

The *conventional* PCI approach involves the concurrent incubation of photosensitiser and chemotherapy (although the exact timing and duration depends upon the agents used), meaning that both agents are present at the time of illumination. As such, light irradiation should proceed only when sensitisers are sufficiently localised to intracellular membranes and drugs internalised and entrapped within endocytotic vesicles. Furthermore, timing has to be such that the sequestered drugs have not yet undergone enzymatic degradation. Then, upon exposure to visible light of an appropriate wavelength, the photosensitiser generates ROS which act to rupture and/or permeabilise the endocytic membrane, thus releasing the confined

drug to act on its intracellular target. Favourably for PCI, oxygen solubility in organelle membranes is relatively high therefore only strongly hypoxic cells should remain unaffected (53). The short-range action of singlet oxygen ($^1O_2$) is particularly important and is more efficient in cellular membranes than aqueous environments (54). It stands that therapeutic agents may also be liable to oxidation, however, studies suggest that photochemical inactivation by ROS is minimal (54). Further, the sensitisers' membrane localisation should limit photochemical damage to the therapeutic cargo. In addition, both fluorescence imaging and immunohistochemistry have shown PCI capable of inducing intracellular redistribution of photosensitisers, cytotoxic drugs, and nanoparticles from endocytic vesicles both *in vitro* (46,52) and *in vivo* (59).

As previously outlined, PCI is a technology that shares fundamental characteristics with the clinically-established technique PDT (53,54). For example, both are minimally-invasive techniques which utilise photosensitisers in order to generate ROS and induce photo-oxidative damage to cells. Moreover, the same three key tumour-eradicating effects of PDT are also present with PCI: that is, (i) direct cytotoxicity (60), (ii) vascular starvation (61) and, (iii) the potential activation of an immune response (62,63). However, PCI also presents a fourth novel effect (46): the cold photochemical release of endocytic vesicle contents into the cytosol (e.g. a chemotherapeutic drug). In addition, and as previously discerned, due to their respective uses of ROS in therapy, PCI also requires lower photosensitiser doses than PDT which could limit its post-treatment skin phototoxicity.

An alternative PCI regimen also exists whereby the 'PDT' element of treatment is carried out *before* the addition and subsequent uptake of the chemotherapeutic. Interestingly, in some cases, this "light-before" approach has been found to improve treatment effects versus the conventional PCI regimen *in vitro* (52). It has been posited that this PCI approach operates *via* the fusion of both undamaged and photochemically-damaged endocytic membranes. Together, the resultant vesicle membranes exhibit increased permeability, leading to entrapped drug leakage and release to the cytosol (Figure 6). One advantage of the light-before method is the diminished risk of photochemical effects on the therapeutic agent. An ideal PCI chemotherapeutic would therefore produce synergy with both conventional (light-after) *and* light-before regimens.

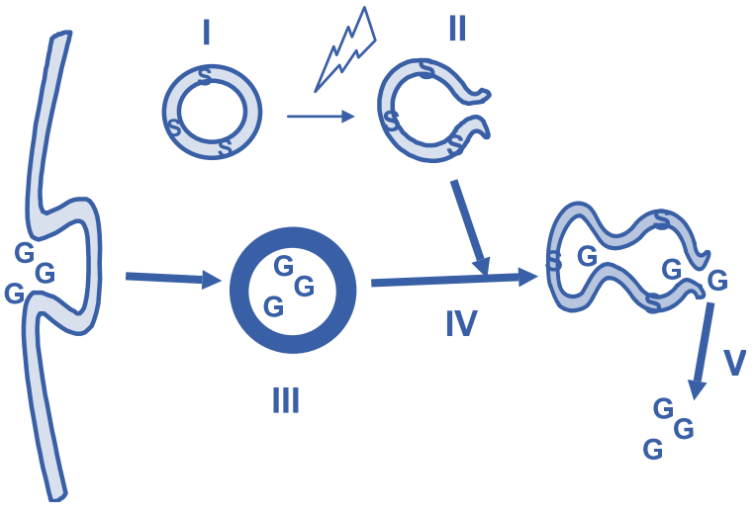

Figure 6. A proposed mechanism of action for the "light-before" PCI regimen. *From stages I-V: (I) sensitiser (S) uptake; (II) illumination; (III) drug (G) incubation; (IV) vesicle membrane fusion; (V) drug release from 'leaky' vesicle. Modified from* (52).

Photochemical internalisation therefore aims to achieve maximum clinical efficacy from the synergistic action of combined lower photosensitiser and chemotherapy drug doses whilst, concomitantly, decreasing the risk of serious adverse effects associated with their use at conventional treatment doses.

1.2.3 Photosensitisers

1.2.3.1 Photosensitiser uptake – endocytosis

The process of photosensitiser uptake and the key physiochemical factors of influence has been outlined previously - a general overview of endocytosis is therefore provided here. Endocytosis intimately regulates many processes, including: drug delivery, nutrient uptake, cell adhesion and migration, signalling, pathogen entry, synaptic transmission, receptor downregulation, antigen presentation, and cell polarity, mitosis, growth and differentiation (64).

An *active* budding structure from the plasma membrane is a prerequisite for the uptake of extracellular substances (including chemotherapeutics and macromolecules) by any endocytic pathway (64). Endocytosed molecules are then contained within membrane-bound vesicles derived from the cellular plasma membrane itself. Endocytosis pathways can be broadly subdivided into three main categories: (i) phagocytosis, (ii) pinocytosis, and, (iii) receptor-mediated endocytosis. In humans, phagocytosis is restricted to specialised cells

called phagocytes (e.g. neutrophils) and therefore pinocytosis (fluid endocytosis) and, possibly, receptor-mediated endocytosis (with the presence of targeting ligands, for example) are the endocytic processes of particular importance to PCI. In simplified terms, pinocytosis is the process by which small particles suspended in extracellular fluid are brought into the cell. Receptor-mediated endocytosis is substrate-driven and refers to the process of solute-binding to specific high-affinity extracellular receptors (although *non-specific* binding also occurs) which precedes specialised intracellular molecular transport with the formation of protein-coated vesicles. Many other diverse endocytic pathways also exist, including: macropinocytosis, flotillin-dependent, caveolae-dependent, clathrin- and caveolae-independent endocytosis, and entosis (64).

Photosensitisers are known to enter the cell through the pinocytosis pathway and then to target endocytic vesicles (65). The most efficient PCI sensitisers are chlorin, porphyrin, or phthalocyanine aromatic dye molecules of an amphiphilic structure; particularly, the adjacently-substituted sulphonated derivatives (53). Furthermore, the specific partition of amphiphilic sensitisers to the vesicle membrane is particularly favourable in PCI; with optimal localisation typically occurring 18-24 hours after administration *in vitro* (47). Amphiphilic sensitisers are useful for two primary reasons: first, the entrapped therapeutic cargo will be released upon photochemical rupture of the endocytic membrane; and second, photooxidative damage to the lumen-localised macromolecules will be limited, as the ROS generated at the vesicular membrane (particularly, $^1O_2$) can only diffuse very short distances (20 nm) (20).

1.2.3.2 Subcellular localisation

Figure 7 shows the two amphiphilic photosensitisers most commonly used in PCI studies *in vitro* and *in vivo* ($AlPcS_{2a}$ and $TTPS_{2a}$); although a relatively new chlorin derivative ($TPCS_{2a}$) is also being increasingly used (47). The latter purports to improve upon some limitations associated with the aforementioned including improved synthetic reproducibility whilst retaining an equivalent efficiency to the long-standing chlorin sensitiser temoporfin (Foscan®) (53).

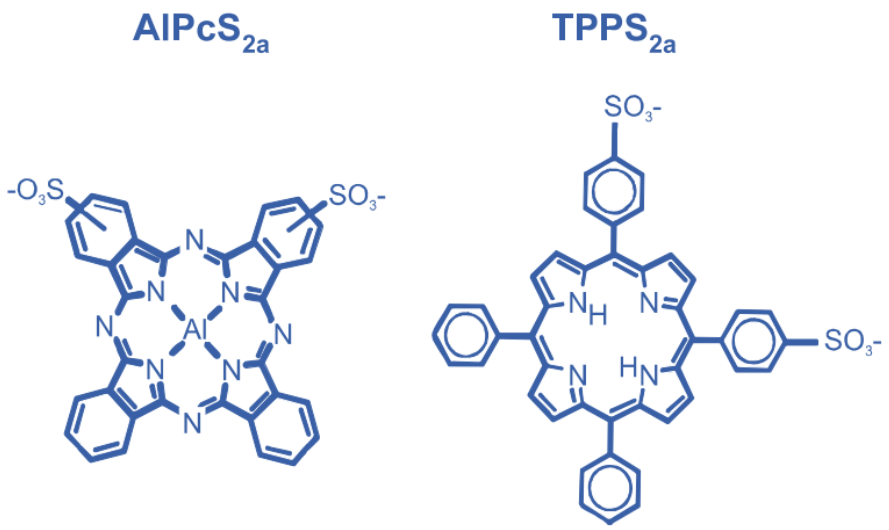

Figure 7. Chemical structures of amphiphilic disulphonated photosensitisers. *$AlPcS_{2a}$ (left) and $TPPS_{2a}$ (right); modified from* (52).

Notably, the two sulphonate group substitutions on adjacent phthalate/phenyl rings is common to all three photosensitiser molecules. The effect of this chemical structure modification therefore appears to be crucial in producing the desired amphiphilic sensitisers required for use in PCI. As aforementioned, these sensitisers localise to and are retained within the endo/lysosome membrane following endocytosis. Specifically, the hydrophobic portion is found inserted into the lipid membrane and the hydrophilic portion protrudes inward toward the vesicular lumen (Figure 8).

The importance of endocytic membrane localisation in PCI delivery has been extensively reported (46,66,67). In particular, this was demonstrated to great effect in a key early PCI study by Prasmickaite et al (66). Using a polylysine-mediated gene transfection model in human melanoma THX cells, this work determined that PCI could only be mediated by photosensitisers localised to endocytic vesicles and that the amphiphilic sensitisers (e.g. $AlPcS_{2a}$ and $TPPS_{2a}$) were most efficient at transfection of a plasmid-encoding enhanced green fluorescent protein (nor did either sensitiser affect transfecting DNA uptake). By contrast, sensitisers that did not localise to endocytic vesicles (e.g. 5-ALA, 3THPP) failed to stimulate [PCI-induced] gene transfection.

As aforementioned, for clinical applications, the photosensitiser should exhibit strong absorbance at red/near-infrared wavelengths in order for therapy to benefit from the deeper

tissue penetration of red light (2,18,53). Due to phthalocyanines having strong absorption in the far-red region (>670nm) of the visible light spectrum, $AlPcS_{2a}$ would be preferred over $TPPS_{2a}$ for preclinical or clinical studies.

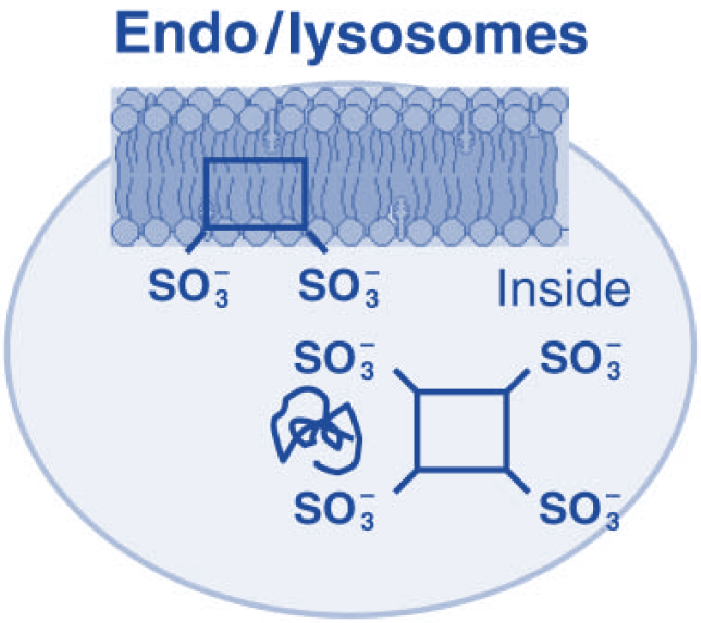

Figure 8. Endo/lysosomal membrane localisation of amphiphilic photosensitisers.
Disulphonated photosensitisers localise to the endo-lysosomal membranes compared with the cytosol localisation of tetrasulphonated sensitisers and chemotherapy drugs (squiggly line). Modified from (77).

1.2.3.3 Aluminium phthalocyanine disulphonate [adjacent] ($AlPcS_{2a}$)

Phthalocyanine was first observed in 1907; its name derives from the Greek terms for naphtha (rock oil) and cyanine (dark blue). In addition to its biomedical use as a photosensitiser in PDT and PCI therapy, this blue pigment is also used commercially as a colourant for paint, inks, and textiles. The sulphonated phthalocycanine derivatives are water-soluble and therefore do not require an additional vehicle for *in vivo* administration. In addition, the disulphonated AlPcS analogue is the most photoactive among the sulphonated derivatives (68).

In order to maximise the effectiveness of PCI therapy, photosensitisers should ideally possess several properties, including: efficient induction of ROS generation, low aggregation propensity (since monomeric molecules are more photoactive), exhibit strong absorption at red or near-infrared wavelengths (e.g. 670 nm), and the ability to partition to intracellular

endo/lysosomal membranes (53). Aluminium phthalocyanine disulphonate [adjacently-substituted] ($AlPcS_{2a}$) retains all of these features, and extensive *in vitro* and preclinical studies (several of which are aforementioned) have shown it to be an effective model photosensitiser for PCI applications. Moreover, the formulation Photosense® – which contains a mixture of aluminium sulphonated phthalocyanine analogues (including $AlPcS_{2a}$) – has been safely used clinically in the Russian Federation for the PDT treatment of various malignancies (2,69,70). Moreover, this clinical formulation has recently been shown capable of eliciting a classical PCI effect (70). Notwithstanding, $AlPcS_{2a}$ itself contains a number of regioisomers and batch-to-batch ratio variations which has so far prevented its routine clinical use (47). Recently, a disulphonated tetraphenyl chlorin photosensitiser ($TPCS_{2a}$ - Amphinex®, PCI Biotech AS, Oslo, Norway) was developed which produces just three regioisomers with low batch-to-batch variations and also exhibits strong absorption at 650 nm (71). Importantly, the photosensitisers used in PCI have no serious *in vivo* toxic effects in the absence of light (47).

1.2.4 Cytotoxic agents used in PCI

Of the PCI studies published to date, the majority have utilised macromolecular toxins (e.g. gelonin) as the cytotoxic agent, with only relatively few having investigated small molecule anticancer chemotherapy drugs (i.e. those of low molecular weight <900 daltons (72)) (53). The chemotherapeutic agents that have currently been investigated fall within three broad categories and have varying clinical use and applicability: (i) macromolecules (e.g. ribosome-inactivating proteins; immunotoxins); (ii) glycopeptide antibiotics (e.g. bleomycin); (iii) small molecule chemotherapy drugs (e.g. doxorubicin, mitoxantrone).

In addition, strategies to further enhance drug delivery specificity to tumour tissue has included both *passive* and *active* targeting. Passive approaches have comprised the use of macromolecular drug carriers (e.g. dendrimers) in order to exploit the EPR effect. Active targeting includes the method of conjugating chemotherapeutic agents to targeting moieties such as monoclonal antibodies or growth factors (e.g. epidermal growth factor, EGF) (8). Combined with PCI, these targeting approaches may improve therapeutic indices yet further.

1.2.4.1 Bleomycin

The bleomycins were first isolated in 1966 by Japanese scientist Hamao Umezawa from culture filtrates of the bacterium *Streptomyces verticillus*. This family of water-soluble glycopeptidic antibiotics retain four functional domains which bind DNA and metal ions (e.g. iron). Indeed, even in its clinical form, bleomycin exists as a mixture of compounds with bleomycin A_2 and B_2 predominating (Figure 9). Although its exact mechanism of action is yet to be elucidated, bleomycin is known to cause both single and double-stranded DNA scission, as well as, inhibition of RNA and protein synthesis (73). Bleomycin is indicated for the treatment of several cancers, particularly squamous cell carcinoma of the skin and head and neck, and malignant lymphomas such as Hodgkin's lymphoma (47,73). Bleomycin has also been used in the treatment of brain tumours such as glioblastomas and astrocytomas *via* intratumoral injection (74).

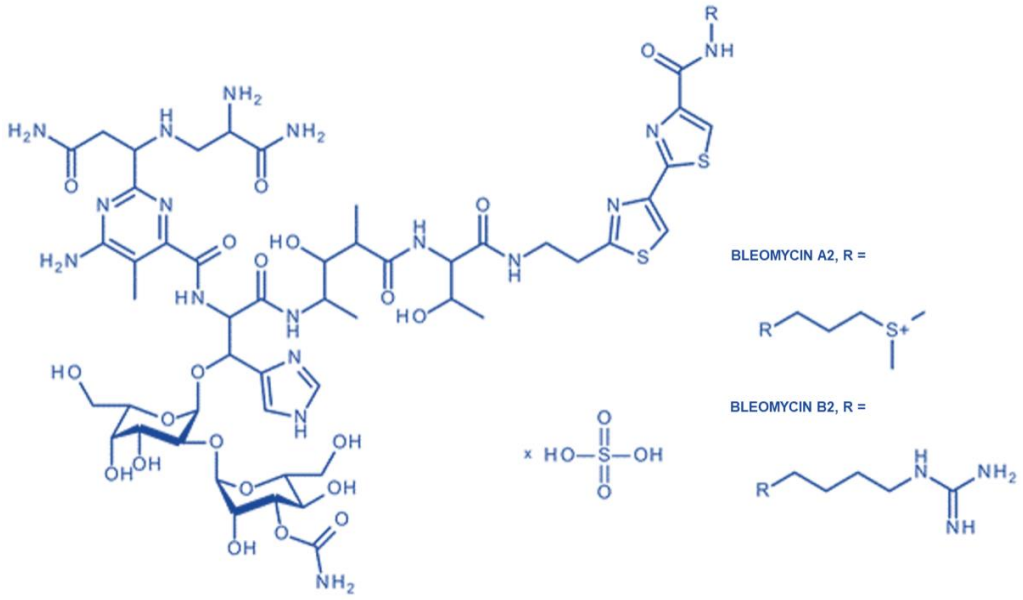

Figure 9. The chemical structure of bleomycin A_2 and B_2.

By contrast to most other anticancer cytotoxic drugs, bleomycin is unusual in that it is hydrophilic and also large in size (1.4 kDa). These properties mean that the drug penetrates membrane structures poorly and necessitates its uptake *via* endocytosis. Consequently, bleomycin is sequestered within endocytic vesicles which severely restricts its therapeutic activity (47). Indeed, both *in vitro* and preclinical studies have shown that the subsequent intracellular release of bleomycin using PCI strongly enhances antitumour activity (71). At

conventional clinical doses, bleomycin can cause serious dose-related toxicities including interstitial pneumonia and pulmonary fibrosis (73). Thus, lower bleomycin doses and fewer treatment cycles (owing to its clinically-effective delivery *via* PCI) could decrease the risk of these serious adverse effects. Preclinical PCI-bleomycin studies have also shown important clinical advantages over PDT alone: including an increased depth of tumour necrosis and better targeting of proliferating cells at the tumour periphery (54).

1.2.4.2 Small molecule drugs

In vitro studies have shown that PCI can increase the cytosolic concentrations of chemotherapeutic agents that do not easily cross cellular membranes. As outlined previously, drug absorption across biological membranes is a complicated interplay between cell biology and the physiochemical properties of the therapeutic. Barriers to drug uptake by *passive* diffusion include the molecular size and molecular charge of the drug – however, other *active* routes to absorption (e.g. clathrin-mediated endocytosis) are also present. In general, larger, hydrophilic drugs and macromolecules are endocytosed before being trafficked to lysosomes. In the acidic lysosome, basic drugs are also protonated/ionized and therefore they do not easily penetrate the membrane in order to reach the cytosol.

As previously alluded to, there is a relative dearth of literature pertaining to the specific use of small molecule chemotherapy drugs in PCI regimens (49,53). Doxorubicin (543.52 Da) and mitoxantrone (444.48 Da) are examples of small-molecule anthracycline chemotherapy drugs that have been successfully delivered *via* PCI. Doxorubicin and mitoxantrone inhibit DNA and RNA synthesis, respectively, and are weakly basic and relatively hydrophobic drugs which will influence their tissue distribution and cellular localisation.

Key early PCI studies demonstrated that PCI delivery of doxorubicin and mitoxantrone (using the photosensitiser hypericin) reversed the multi-drug resistant phenotype of both breast and bladder cancer cell lines previously resistant to each of these respective agents (75). It was posited that, in addition to PCI releasing entrapped drugs from the endocytic vesicles, photooxidative damage to P-glycoprotein efflux pumps (a common resistance mechanism for anthracyclines) also occurred which caused these pumps to shutdown and thus increased intracellular drug concentrations. Interestingly, a study by Lou et al., found a

synergistic effect on MDR MCF-7 cells exposed to doxorubicin-PCI but only an additive effect in non-MDR MCF-7 breast cancer cells ("ADR" denotes that the cells were originally grown in increasing adriamycin [ADR]/doxorubicin concentrations) (76). More recently, Ali et al., reported the use of deliberately-low-dose Photosense® PDT in conjunction with doxorubicin and mitoxantrone chemotherapy on human cervical and breast cancer (HeLa and MCF-7, respectively) and rat brain tumour (RG2) cell lines (70). Here, several treatment regimen variations were investigated – including what could be described as both conventional and light-before PCI – and, encouragingly, treatment synergy was observed for each chemotherapy drug in all three cell lines (70). These studies therefore highlight the potential of PCI to produce favourable treatment outcomes with small molecule chemotherapy drugs.

1.2.4.3 Macromolecular toxins

1.2.4.3.1 Type I ribosome inactivating proteins

Protein toxins have been widely studied for use as cancer therapies (77). In relation to PCI, the small type I ribosome-inactivating proteins gelonin and saporin (approximately, 30 kDa) have been extensively evaluated and their use – either alone or combined with targeting moieties – makes up the bulk of the PCI literature (53). The RIPs are plant-derived protein toxins that inhibit cellular protein synthesis by damaging ribosomes of which there are two main types: type I and type II. Type II RIPs (e.g. ricin) consist of an enzymatically active A chain linked to a B chain which contains a binding domain (Figure 10). By contrast, type I RIPs lack this B chain and only consist of the A chain.

Consequently, type I RIPs enter the cell *via* pinocytosis whereas type II toxins enter *via* the more efficient receptor-mediated endocytosis owing to B-chain binding to the cell surface (77). Type I RIPs are typically directed to the lysosome where they remain sequestered until they are eventually degraded. Type I RIPs therefore exert a low cytotoxic effect and make good candidates for PCI due to their vesicular entrapment. Interestingly, both RIP types are extremely potent as free drugs with just 1-10 molecules required in the cytosol in order to kill the cell (78).

Both gelonin and saporin have been extensively evaluated for PCI studies (53). Crucially, though, neither protein is used clinically but rather serve as model PCI drugs due to their undergoing endo/lysosomal sequestration and degradation with low endocytic vesicle escape rates. Consequently, their low cytosolic concentrations mean their *de novo* therapeutic effect is minimal. By contrast, when delivered *via* PCI these proteins have achieved curative rates of 60-80% in animal models (61). Berg et al., used PCI-gelonin (utilising $AlPcS_{2a}$ and $TPPS_{2a}$) on the NHIK 3025 cervical carcinoma cell line and saw treatment synergy with up to a 200-fold increase in cell death when contrasted with either treatment alone (46). Another study utilising PCI-gelonin ($AlPcS_{2a}$ as sensitiser) on THX melanoma cells saw significant enhancements in PCI efficacy using the light-before PCI regimen (79).

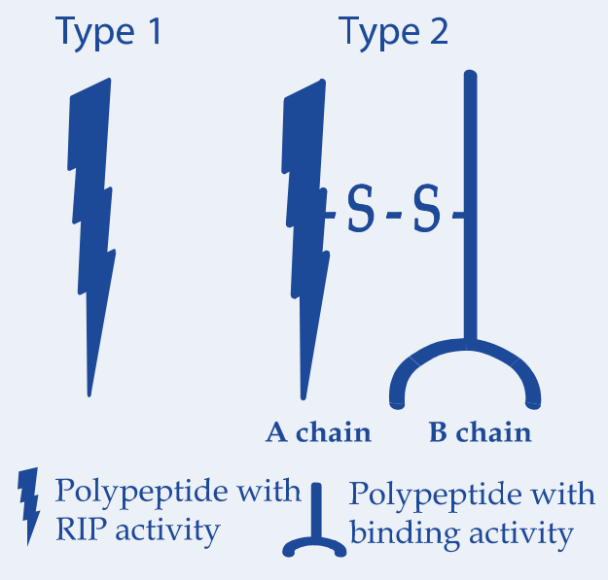

Figure 10. Main structural features of type 1 (I) and 2 (II) ribosome inactivation protein toxins. *Modified from (77).*

1.2.4.4 Macromolecular drug carriers

1.2.4.4.1 Nanocarriers

Photochemical internalisation is well-suited to delivering macromolecular drug carriers as their size dictates uptake by endocytosis and PCI can subsequently release them from intracellular sequestration. For instance, type I RIP proteins have been extensively conjugated to a wide range of macromolecular drug carriers including liposomes and dendrimers (80,81). For

example, PCI-delivery (using $TPPS_{2a}$) of saporin-containing liposomes increased treatment cytotoxicity over both saporin and saporin-liposomes as standalone therapies (80). However, more commonly, gelonin or saporin has been conjugated to antibody moieties (e.g. cetuximab) (53).

With regard to small molecule chemotherapy drugs, Lu et al., utilised a dendrimer-phthalocyanine photosensitiser in order to effect the lysosomal release of doxorubicin which killed doxorubicin-resistant MCF-7 cells (82). In another study by Tian et al., a pH-sensitive porphyrin-based amphiphilic block copolymer micelle formulation was loaded with doxorubicin and tested against A549 lung carcinoma cells. At low PDT doses, a significantly enhanced cytotoxic effect was seen versus dark controls which was ascribed to PCI-facilitated release of doxorubicin from endocytic vesicles (83).

An interesting study by Pasparakis et al., saw polymeric nanocarriers co-loaded with camptothecin (0.35 kDa) and the sensitiser haematoporphyrin. The nanocarrier structure was acid-labile and therefore endocytic entry saw the release and partition of the hydrophobic sensitiser to the lipid membrane. Subsequently, a synergistic increase in treatment cytotoxicity was observed utilising PCI (84). Zhu and colleagues also utilised camptothecin to prepare hybrid chemotherapy-photosensitiser nanoparticles. Here, it was demonstrated that following uptake by endocytosis, nanoparticles could be released from vesicular entrapment using Eosin Y-mediated and near-infrared light (980 nm) PCI and potentiate treatment cytotoxicity against HepG2 hepatocellular carcinoma cells versus controls (85).

1.2.4.5 Other targeted macromolecules and gene delivery

Although outside of the scope of the present work, numerous other PCI studies have also investigated the use of a diverse range of specific ligands in order to improve targeting to cellular receptors and markers such as EGFR, HER2, GP240, and CD133 (53). In addition, PCI has also been employed to successfully deliver other macromolecules including oligonucleotides and peptides, as well as, gene transfection vectors (86).

1.2.4.6 New PCI drug candidates

To date, only a few clinically-approved small molecule chemotherapy drugs have been tested for compatibility with PCI delivery. Owing, in part, to a combination of relatively uncommon physicochemical properties and wide-ranging clinical applicability, bleomycin has become the most widely-researched cytotoxic drug for use with PCI. Its relative success has been well-earned having demonstrated promising preclinical synergy and efficacy before progressing to the clinical trial stage in humans.

Notwithstanding, cancer is an inherently heterogeneous and dynamic malady with inter- and even intra-patient (!) variations in response to drug treatment widely-recognised. The development of new, safe, and potent anticancer treatment modalities such as PCI can therefore only benefit future clinical outcomes. More specifically to the present work, the identification of existing clinically-approved cytotoxic agents that could see their therapeutic indices improved *via* PCI delivery, is one important step toward the realisation of this goal.

In summary, non-clinical, macromolecular agents have primarily been used as the chemotherapeutic component of PCI. To date, only a few small molecule anticancer drugs (e.g. doxorubicin, mitoxantrone; camptothecin – in formulation) have been investigated with the clinical drug bleomycin also having been successfully delivered *via* PCI. Encouragingly, however, the enhanced cancer cell-killing potential of PCI drug delivery has been seen across many different types of cancer in the preclinical setting.

1.2.5 Potential advantages of PCI

1.2.5.1 Repurposing of existing drugs

Drug delivery *via* PCI could lead to the repurposing of existing commercial drugs, as well as, those previously earmarked for cessation of development in the industrial product development process. For instance, in early pharmaceutical compound screening experiments, inadequate plasma membrane penetration and/or low cytosolic concentrations of the new drug can lead to its exclusion from further clinical development (61). Hence, the ability of PCI to liberate entrapped drugs from endocytic vesicles – in order to increase their cytosolic concentration and to spare their degradation - could lead to the re-purposing of such compounds.

1.2.5.2 Overcoming drug resistance

The ability of cancer to exert resistance toward therapy is one of the primary reasons why several types of tumour remain difficult to cure (48). Resistance can be intrinsic or acquired as a result of selective pressure from chemotherapeutic agents. Resistance to anticancer therapy is well-recognised and is one of the main reasons why chemotherapy regimens typically comprise of several different drugs given concurrently (often from different drug classes). Moreover, resistance to treatment has also emerged as a major issue for newer targeted therapeutics such as monoclonal antibodies (mAbs) and tyrosine kinase inhibitors (TKIs) (48).

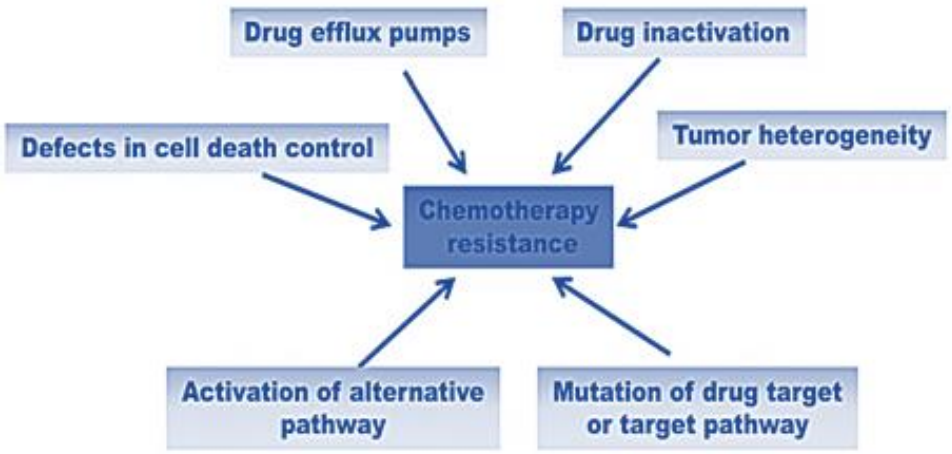

***Figure 11. Mechanisms of resistance to anticancer therapeutics**. Modified from (48).*

Two common mechanisms of multiple drug resistance (MDR) in cancer cells is the overexpression of p-glycoprotein efflux pumps and drug inactivation (Figure 11). With regard to the latter, for example, the increased acidification of endocytic compartments can lead to the 'ion-trapping' and inactivation of basic chemotherapy drugs (e.g. doxorubicin and mitoxantrone). Importantly, drug delivery *via* PCI has been shown capable of reversing the drug-resistant phenotype of cancer cell lines *in vitro* (and *in vivo*) – as mentioned previously in this chapter (75,76,82).

1.2.5.3 Adjuvant to surgical resection

The presence of microscopic residual disease after surgical resections has been posited as a major cause for local cancer recurrence which, ultimately, has a deleterious impact upon

treatment outcomes. One potential solution is therefore to use intraoperative PCI whereby the surgical bed is illuminated prior to wound closure in order to treat undetected viable cancer cells. Indeed, Norum et al., demonstrated that PCI (conventional regimen) in combination with marginal surgery can be highly effective in maximising tumour tissue removal (55). Specifically, following surgical resection, $AlPcS_{2a}$-mediated PCI-bleomycin was used to treat the wound bed (located on the rat hind leg) in an invasive human fibrosarcoma xenograft (HT1080) model which resulted in a significant delay in tumour growth when compared to surgery alone and PDT in combination with surgery. This intraoperative approach has also been trialled in clinical PDT treatments to highly positive effect (e.g. in lung cancers) (87).

1.2.5.4 Antivascular effects

As with PDT, PCI has also shown notable effects on tumour vasculature. However, PCI-induced vascular effects are greater than those achieved by PDT when the same photosensitiser is used (54). Moreover, damage to tumour microvasculature is also an important clinical mechanism for eradicating drug-resistant tumour cells and could cause therapeutic effects at deep tumour levels (47). Indeed, PCI has been shown to achieve deeper tumour necrosis than PDT *in vivo* (54).

1.2.5.5 Immunogenic response

As outlined previously, immunological responses have been reported in preclinical studies of photochemical treatments (35,88). For instance, PCI has been shown to enhance MHC class I antigen presentation – an important factor in immunogenic responses to tumours (63). Immunogenic stimulation by photooxidative damage results from the induction of cytokines, inflammation, and necrosis which could cause penetration into deep tissue layers exposed to suboptimal treatment (47). Moreover, recent PCI studies have demonstrated how the known post-photochemical tissue infiltration of phagocytes can also be exploited for drug delivery. Shin et al., loaded macrophages with doxorubicin and observed a PCI-induced (using $AlPcS_{2a}$) synergistic reduction of cellular growth in a 3D rat glioma (F98) *in vitro* model (89).

1.2.6 *In vivo studies*

Most *in vivo* cancer xenograft studies are performed using nude mice transplantation models which are not strictly ideal for PCI. This is because, as aforementioned, one of the main contributors to the overall therapeutic effect of PCI is the activation of the immune system itself which is ordinarily severely compromised in nude mice. To date, $AlPcS_{2a}$ is the most commonly-used photosensitiser for *in vivo* PCI studies (53).

Nevertheless, the first *in vivo* PCI study demonstrated the impressive potential of PCI technology (60). In a transplanted human colon adenocarcinoma (WiDr) model, gelonin-$AlPcS_{2a}$ PCI was shown to outperform PDT with respect to tumour growth attenuation and remission rates. Pertaining to the former outcome (a '5-fold increase in tumour volume') control groups took 9-14 days, PDT took 29 days, whereas, with PCI, tumours were almost completely eradicated after 20 days and tumour volume had only increased 2.5 times at 60 days post-treatment. With regard to remission rates, complete remission of the WiDr-tumours was seen in 67% of animals versus only 17% of animals in the PDT group.

Berg and colleagues have also demonstrated that $TPCS_{2a}$-mediated PCI of bleomycin can achieve positive results *in vivo* (71). Here, bleomycin alone was seen to delay tumour growth by 1.4 days compared with control. Next, PDT-induced a tumour growth delay of ~3 days whereby PCI-bleomycin induced a tumour growth delay of 10.4-12.4 days which was determined to be a synergistic effect. Interestingly, here, light treatment alone was found to induce a "small but significant" tumour growth enhancement. In addition, PCI-bleomycin was seen to approximately double the mean time to reach an 8-fold increase in tumour volume versus $TPCS_{2a}$-PDT.

Finally, a recent study by Norum and co-workers (57) investigated the impact of PCI-bleomycin (using $AlPcS_{2a}$) on systemic anti-tumour immunity in thymic and athymic mice. Although treatment synergy *was* seen, a curative effect was not observed in the latter group despite exposure to twice the light dose of the former group (30 J/cm^2 versus 15 J/cm^2, respectively). By contrast, thymic mice achieved cure rates over 90%. Impressively, cured thymic mice also rejected 57-100% of inoculated tumour cells when re-challenged up to 2 months post-treatment.

1.2.7 Clinical PCI

Preclinical studies have demonstrated that PCI treatment outcomes can vary between different chemotherapeutics and photosensitisers, not least, between different types of cancer. Notwithstanding, treatment synergy has been observed with both the conventional and light-before PCI regimens which presents additional options for clinicians. Again, this all demonstrates the need for careful parameter optimisation and planning prior to PCI initiation.

Sultan et al. (47) carried out the first phase I clinical trial to examine the safety and tolerability of $TPCS_{2a}$-mediated PCI of bleomycin, and documented the antitumour activity in patients with advanced (or recurrent) cutaneous and subcutaneous malignancies. This was a single-centre (University College Hospital, London, UK) dose-escalation phase I clinical trial of PCI using bleomycin and Amphinex® in 22 patients with superficial skin and head and neck neoplasms resulting from different primary histologies. The study met all of its primary outcomes with substantial antitumour effects seen in patients.

A multi-centre phase II study was subsequently initiated. In this study, both superficial (as per the phase I study) and more deep-seated head and neck tumours which required interstitial illumination (using multiple optical fibres inserted into the tumour) were investigated. Despite promising patient responses to surface illumination in particular (similar to the phase I study), the study was terminated prior to completion in June, 2015; both commercial and clinical considerations were cited. Importantly, to the latter point, the clinical placement of optical fibres and optimisation of light dose for interstitial illumination was found to be more complicated than anticipated (90).

At the time of writing (September, 2018) there is currently only one actively recruiting trial pertaining to “photochemical internalization” for cancer patients according to www.clinicaltrials.gov. This is a phase I/II dose escalation study of fimaporfin ($TPCS_{2a}$)-induced PCI of gemcitabine followed by gemcitabine/cisplatin chemotherapy in patients with advanced inoperable cholangiocarcinomas (91).

1.3 Summary

Drug delivery *via* PCI could have many positive effects in the drug delivery space. Existing drugs could be repurposed due to the ability of PCI to increase cytosolic drug concentrations in focal regions of specific therapeutic interest. This focal nature of PCI treatment makes the technique particularly suited to tumour eradication in the context of anticancer therapy. Moreover, these higher cytosolic drug concentrations might even be able to be achieved from lower systemic drug doses which would reduce the risk of off-target adverse effects associated with mainstay chemotherapy treatments.

Photochemical internalisation has been shown to be effective for the delivery of chemotherapeutic agents exhibiting diverse physicochemical properties; however, the bulk of the current PCI literature pertains to its use with protein toxins rather than more clinically-translatable small molecule cytotoxic drugs. Studies have, to date, highlighted that various factors require optimisation in order to achieve maximum therapeutic benefit from PCI, including: light dosimetry, chemotherapeutic and photosensitiser doses, and, crucially, the timing and sequence of their administration.

In theory, PCI could be used to treat all solid tumours. It could be suitable for early-stage cancers, as a neoadjuvant to standard treatment procedures and for the treatment of innate or acquired treatment-resistant tumours (47). Its focal nature could also be utilised in advanced disease in the treatment of cancer metastases. Recent studies also suggest that PCI could induce a systemic immune response which could further improve long-term tumour control.

Chapter 2: Modelling Cancer, 3D Cell Culture, Squalene

2. Modelling Cancer, 3D Cell Culture, Squalene

Traditionally, preclinical cancer studies could be broadly divided into two categories, that is*, in vitro* models and *in vivo* models. Typically, studies would begin with *in vitro* experiments using cancer cells grown in monolayer before promising candidates and therapies would advance to the more complex environment afforded by *in vivo* animal models. However, there are limitations associated with each of these modes of testing and the complexity of experimental conditions between the two differ to a large extent.

Increasingly, technological and computational advances are now beginning to 'bridge-the-gap' and provide further insight into anticancer treatment outcomes. Important examples of this would be the advent of computational 'in silico' modelling and the emergence of hybrid *in vitro-in vivo* technologies such as three-dimensional (3D) cell culture models.

With regard to anticancer therapy, chemotherapy drugs still remain at the forefront of preferred treatment options for the majority of solid and haematological malignancies. Many of these cytotoxic agents have well-recognised modes of action and, in corollary, modes of toxicity which commonly manifest in a dose-dependent manner.

Thus, improving the therapeutic indices of these vital anticancer compounds still remains a significant challenge confronting clinicians and patients alike. At the head of this challenge, though, are novel technologies such as photochemical internalisation and other, recently emerged, nano-formulation strategies aimed precisely at improving treatment specificity and patient outcomes.

2.1 Breast Cancer

2.1.1 General background

Breast cancer is the most frequently diagnosed cancer in women both of Europe and the United States of America with an estimated 1.7 million new cases diagnosed in 2012 (92). This represents around 25% of all cancers in women and 12% of all new cancer cases. Importantly, breast cancer is not a single disease but rather a collection of breast diseases that each have diverse histopathologies, genetic and genomic variations, and, crucially,

clinical outcomes. Subsequently, there are significant challenges in producing experimental preclinical model systems that recapitulate this complex and heterogeneous malady with no single model likely to mimic all characteristics of the disease. For example, inherently diverse and dynamic metastatic disease remains the principal cause of mortality in breast and, indeed, most other types of solid cancers (93).

2.1.2 Cell lines

The process of cell culturing was originally developed by Harrison, in 1907, while investigating the origin of nerve fibres (94). However, another half century would elapse before the first human cancer cell line was established by George Gey in 1951 (95). Famously, it bore the name “HeLa” - after the cervical carcinoma patient Henrietta Lacks from whom it was derived. Subsequently, *in vitro* cell culture research expanded rapidly into a mainstay experimental tool thanks to Gey’s pioneering vision. In fact, the use of established breast cancer cell lines in *in vitro* model systems has been the most common method of investigating drug screening and the molecular biological aspects of breast cancer (93). Their extensive use owes, in part, to their straight-forward propagation in standard cell culture medium in order to produce an infinite supply of a relatively homogeneous cancer cells which generally yield reproducible and quantifiable results (96).

Just seven years later, in 1958, the BT-20 human breast carcinoma cell line became the first breast cancer cell line to be established (97). However, 20 years would elapse before additional breast cancer cell lines were established including the famous MD Anderson (“MDA”) series (98) and MCF-7 cell lines which are still immensely popular today (99). The SUM series of cell lines are more recent additions and include the inflammatory breast cancer cell lines SUM149 and SUM190 (100). Finally, the incidence of male breast cancer is increasing and there is now also a cell line derived from male breast cancer (101). Interestingly, genomic sequencing of this male cell line revealed that there was no evidence of somatic mutation in any of the established female breast cancer driver genes which suggests that it could be a valuable tool in modelling this disease (102).

2.1.3 Heterogeneity

The long-standing morphological observations of histopathologists that breast cancer is a heterogeneous disease has now been unequivocally confirmed by modern molecular profiling techniques. Clinical classification of disease denotes the histological type, tumour grade, lymph node status, and the presence of prognostic cellular markers such as the oestrogen receptor (ER) and human epidermal growth factor receptor (HER2). Latterly, gene expression profiling has revealed that breast cancer could be classified into at least five subtypes: (i) luminal A, (ii) luminal B, (iii) HER2, (iv) basal and (v) normal (103).

Crucially, clinical experience has shown that each subtype has a different prognoses and corresponding treatment options (104). For instance, most recognised breast cancer subtypes are hormone-related and are thus amenable to hormone therapy. The luminal A and luminal B subtypes are oestrogen receptor positive (ER+) which is a druggable target (e.g. with tamoxifen) as is the HER2 receptor (e.g. with trasuszumab) of the HER2 subtype. By contrast, basal tumours lack expression of a recognised therapeutic target (93,104). The basal phenotype is characterised by the absence of expression of the three predictive biomarkers of ER, progesterone receptor (PR), and HER2 and is thus commonly referred to as “triple-negative” (NB. the ‘basal’ and ‘triple-negative’ phenotypes are not identical) (93,104). Due to the lack of druggable targets, these tumours are more difficult to treat and are also characteristically aggressive in their progression and exhibit a poor prognosis. TNBC and basal-like tumours account for around 15% of all invasive breast cancers and correlate highly with the BRCA1 mutation (>75% of women with this mutation will present with these tumours) (93).

2.1.3.1 Representativeness

The molecular classifications of breast cancer are now firmly established, and so, the persistent questions pertain to whether the heterogeneous molecular profiles observed in breast carcinoma are accurately represented in immortalised cell lines. Despite this uncertainty, the use of cell lines has undoubtedly produced findings that have translated into clinical benefit. A key example being the recognition that anti-oestrogens regulated the growth of tamoxifen-stimulated MCF-7 cells (105). This, for example, directly led to the clinical

development and subsequent regulatory approval of the selective anti-oestrogen fulvestrant (Faslodex®) (106).

A comprehensive study by Neve et al., (107) compared the molecular profiles and genomic alterations of 51 breast cancer cell lines and human breast tumours and found many of the recurrent genomic abnormalities detected in primary tumours faithfully represented in the immortalised cells. The process of establishing these tumours as cultured cell lines did not therefore markedly alter the common genomic aberrations which suggests that these model systems provide a powerful means for investigating breast cancer. Although, notably, not all of the five recognised breast cancer subtypes were represented.

In the event that marked genomic differences are observed between cell lines and primary tumours, it is worth noting that many cell lines are obtained from advanced-stage and metastatic tumours and pleural effusions. Accordingly, these cells could represent the most malignant and genetically-unstable variants capable of being adapted to culture. Although, that said, gene-expression profile studies comparing primary tumours and their metastatic counterparts found them to be very similar (108).

In the *in vitro* space, improved methods for both identifying new cancer subtypes and immortalising and culturing human cells should help facilitate the establishment of new cell lineages from primary tumours. In turn, this will make studies more representative of clinical disease and thus expand the utility of *in vitro* cell culture models yet further (93).

2.1.4 Monolayer and 3D *in vitro* culture

Traditional cell culture methods typically involve the use of immortalised cancer cell lines grown on plastic substrates in two dimensions (monolayer culture). Despite the recognition that the complex *in vivo* inter-relationships between cells and stroma are subsequently lost by this method, monolayer culture remains the most favoured mechanism for *in vitro* cancer research (100). Importantly, cell culture conditions can dramatically influence cell morphology, inter–cell and cell–matrix interactions (109) and gene expression (110).

As aforementioned, cancer cell lines have been found to retain many of the important genetic and genomic alterations found in the primary tumours that they attempt to imitate.

However, the majority of these studies were performed using cell lines cultured by traditional means on a plastic substrata (100). That is, monolayer cultures involving whole cell-based screening assays comprised of a flat layer of cells attached to a stiff plastic surface. Principally, these cells propagate in a two-dimensional environment that differs markedly from the actual three-dimensional (3D) tumour microenvironment (Figure 12): devoid of supportive stromal cells and with planar mechanical cues and nutrition/oxygenation exchange. Moreover, the importance of tissue-specific architecture and microenvironment to tumour formation and development is being increasingly realised. There therefore exists a clear need to look beyond simple two-dimensional cancer models in order to 'bridge-the-gap' between *in vitro* and *in vivo* model systems. Fortunately, these are elements able to be at least partially recapitulated with advanced *in vitro* 3D cell culture models and so-called "heterotypic" models comprised of multiple cell types. These models therefore add the further layers of complexity and physiological relevance necessary for modelling this varied disease *in vitro* (109).

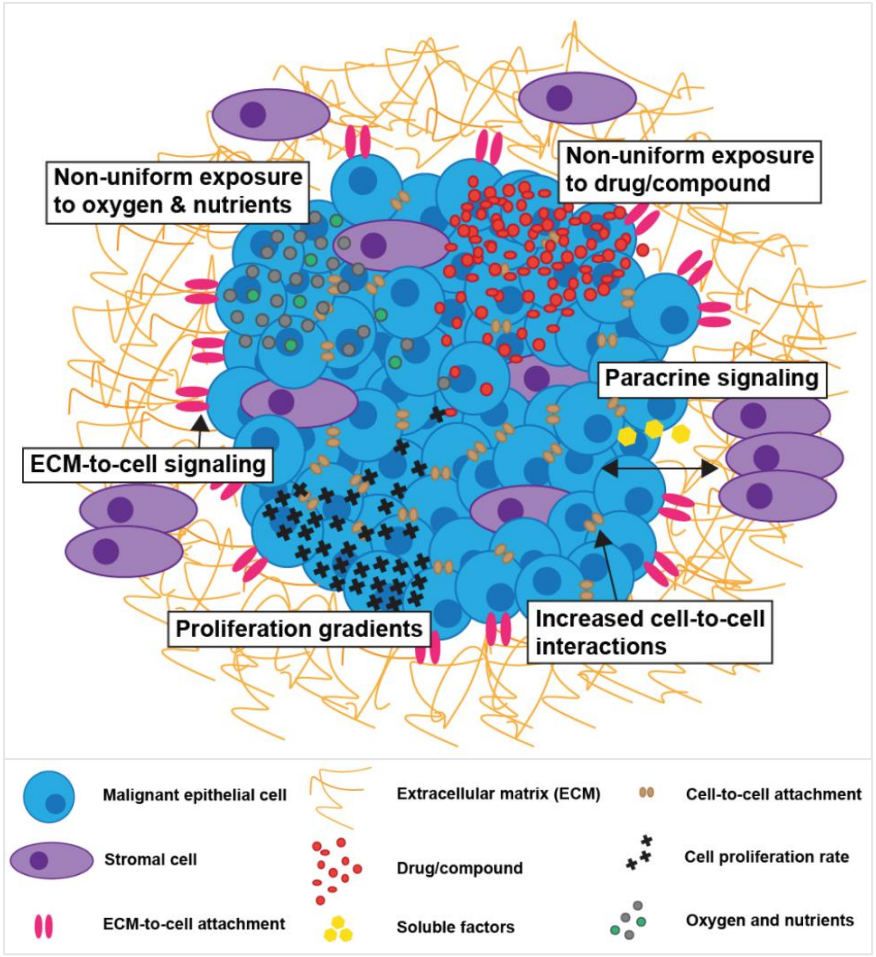

Figure 12. The tumour microenvironment can be recaptured, in part, by 3D cell culture. *Modified from* (144).

2.1.4.1 Types of 3D culture

In addition to differences in cellular spatial arrangement between cells grown in monolayer or 3D, there are also important biological differences that contribute to how cells are exposed (e.g. cell morphology) and therefore how they subsequently respond to therapeutic agents (111). For example, Weaver et al. studied non-malignant and malignant HMT-3522 breast cells (S-1 and T4-2 sublines, respectively) grown in 3D using Matrigel as an anchorage-dependent substrate (112). Here, normal/benign S-1 cells formed organised, polarised acini, similar to those found in healthy breast tissue whereas, by contrast, tumorigenic T4-2 cells formed disorganised, loose aggregates. Three-dimensional cell cultures may be achieved by various methods and there even exists some debate as to what actually constitutes a "3D" cell culture. Broadly speaking, though, there are the anchorage-independent and anchorage-dependent types, respectively.

The anchorage-independent approach involves the aggregation of cells in non-adherent culture conditions without a substrate for cellular attachment – substrates include, for example, extracellular matrix (ECM) proteins such as collagen. Examples of this approach include those utilising low-attachment plates (113), polymer-coating of plate surfaces (114), and the hanging drop method (115). By contrast, anchorage-dependent 3D cultures (Figure 13) result from cells adhering to specific substrates such as laminin-rich ECM (112) and type I collagen (116,117). Incidentally, these biomimetic matrices promote cellular 3D-structure formation in a time-dependent manner (118). Commonly in anchorage-dependent models, cells are either seeded on top of matrices/scaffolds (referred to as the 3D "on top" assay) or mixed into the substrate itself (the 3D "embedded" assay) (119). Inevitably, there are merits and demerits associated with the respective 3D model system approaches which have been reviewed in detail elsewhere (111). One major limitation of anchorage-independent spheroid cultures, for example, is that prior to experimentation cells require prolonged periods of time (e.g. 3-6 days or more) in order to sufficiently aggregate and grow.

2.1.4.2 Chemotherapy and 3D culture

In addition to observed biological differences between monolayer and 3D cell culture, differences in cellular response to classical chemotherapy drugs (as well as, other therapeutic

agents) has also been revealed (111). For example, Tung et al., generated 3D spheroid cultures of A431/H9 human skin cancer cells and showed that cellular response to 5-fluorouracil (5-FU) and tirapazamine (TPZ) differed substantially between monolayer and 3D (115). For example, 5-FU chemotherapy (10 mM, 96 h) reduced cell viability to 5% and 75% in monolayer and 3D cultures, respectively. This signifies that cells grown in 3D were much more resistant to the anti-proliferative effects of 5-FU. Conversely, TPZ chemotherapy (10 mM, 96 h) reduced cell viability to 72% and 40% in monolayer and 3D cultures, respectively. Thus in the latter case, cells in monolayer were found to be more resistant to the effects of TPZ.

In another study, David et al., showed that SA87 (derived from a brain metastases of gastric adenocarcinoma), NCI-H460 and H460M (both lung carcinoma) cultured in 3D (spheroids) exhibit a higher resistance to both 5-FU and doxorubicin chemotherapy compared to monolayer (120). In addition, Chen et al., demonstrated that 3D-cultured (Matrigel, embedded) MCF-10A breast cancer cells treated with paclitaxel were two-fold less susceptible to its cytotoxic effects than were cells in monolayer (121).

These data show that the *in vitro* cell culture method (i.e. monolayer or 3D) can substantially influence the cytotoxic effect of conventional chemotherapy drugs. In addition, they demonstrate that 3D-cultured cells do not necessarily exhibit a higher drug resistance. Moreover, that cellular responses to chemotherapy are mediated by a combination of the specific drug and its mode of action, as well as, the cellular microenvironment (115). Thus, although more technically challenging to establish (particularly in the case of heterotypic cultures), these more biomimetic 3D models have important implications for drug screening in vitro.

2.1.4.3 ECM stiffness in 3D culture

As aforementioned, *in vitro* modelling in a more biomimetic 3D microenvironment has shone light upon the important factors influencing both normal and malignant tumour biology and their responses to chemotherapeutic intervention. Moreover, studies have also revealed how stromal rigidity can have profound effects on cell morphogenesis when modelled in 3D cultures.

Tissue stiffening is frequently observed at the stage of clinical diagnosis of cancer (particularly in cases of breast and head and neck cancer) and when ECM stiffness has been increased in 3D experiments *in vitro*, this has been sufficient enough to induce a malignant phenotype from otherwise normal human mammary epithelial cells (122). Tumour-related changes in ECM stiffness and interstitial pressure also present challenges for the treatment of solid tumours with chemotherapy drugs (122). Indeed, an increase in interstitial fluid pressure can, itself, cause an increase in tissue stiffness (123).

In addition, some studies have demonstrated how different geometries of cell-matrix interactions and ECM microstructures can yield conflicting results pertaining to the epithelial to mesenchymal transition (EMT) process - a developmental program critical for tumour cell dissemination and metastasis (93,100,111). For example, breast cancer cells cultured 'on-top' of Matrigel- or type I collagen-coated polyacrylamide gels showed that increased stiffness (through increased polyacrylamide concentration) heightened EMT (124). By contrast, breast cancer spheroids embedded within 3D fibrillar type I collagen matrices showed decreased EMT upon increased ECM stiffness (collagen concentration) (125).

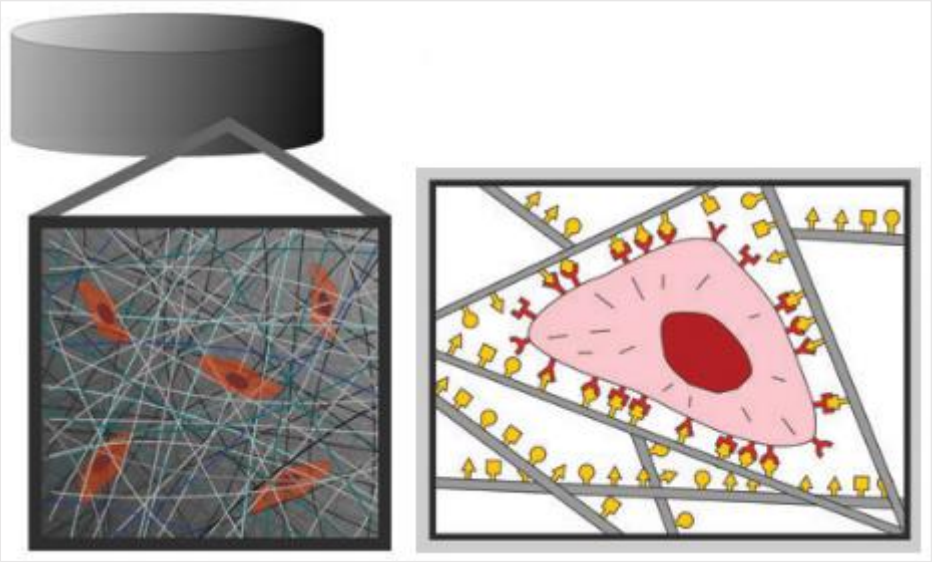

Figure 13. A representation of an anchorage-dependent, embedded-cell 3D in vitro model. *This type of 3D in vitro model was used in the present work with collagen type I hydrogels. Modified from* (117).

2.1.4.4 Heterotypic culture

Studies in 3D have generated an increased understanding of normal breast cell development, as well as, breast cells in the diseased state (111). In order to model the influence of tumour–

stromal cell interactions on cancer progression and therapeutic impact, cancer cells must be co-cultured with these stromal cells. Moreover, druggable targets within the tumour stromal environment itself may even present themselves (126). Provocatively, it has been posited that tumour stromal cells are genomically stable (whereas cancer cells are inherently genomically unstable) and would therefore be unlikely to acquire rapid resistance to therapeutic intervention (126).

Indeed, heterotypic 3D models incorporating various stromal cellular components including fibroblasts (127), macrophages (128), and endothelial cells (129) have already demonstrated therapeutic value. For example, Camp et al., reported that basal (e.g. MDA-MB-231) and luminal (e.g. MCF-7) breast cancers behaved very differently when co-cultured with stromal fibroblasts – with basal-like cells showing increased migration *in vitro* (130). In addition, cellular phenotypes were also found to be dependent upon the macrophage-mediated tumour–stromal cell interactions.

Intriguingly, heterotypic cell culture systems also make the choice of cell culture medium extremely important - for growth media can influence cell phenotype to a very great extent (100). This could present a not insignificant technical challenge and emphasises the need for correct controls and a robust standardisation of methodology.

2.1.5 Xenograft models

In order to evaluate the biological activity of novel drug candidates, drug discovery programmes employ both preclinical and clinical phases of which cell-based *in vitro* assays are commonly the starting point. Pertaining specifically to new anti-cancer drug candidates, attrition rates are extremely high at around 95% (131). Thus, it has been posited that developing more biologically-relevant tumour models *in vitro* (such as 3D culture techniques) could ultimately improve bench-to-bedside translation, as well as, reduce the number of animals used in preclinical testing in keeping with the three R's principal (119).

Human breast cancer cell lines have been used extensively as preclinical breast cancer models both *in vitro* and *in vivo* as xenografts. Chemotherapeutic intervention is normally evaluated as a measure of cytotoxic drug activity against these cells and, crucially,

both approaches have demonstrated clinical predictive value. However, xenograft models also have limitations and have, in general, fallen short of predicting therapeutic efficacy in humans (132).

Chief amongst these reasons is the fact that xenograft host animals are necessarily immunocompromised which can impact upon tumour formation and progression. Furthermore, and as previously outlined, the immune response is also central to the therapeutic response from many anticancer treatment modalities, not least, PDT and PCI. Furthermore, human breast tumour cells are transplanted into a foreign microenvironment (human and mouse mammary tissue has distinct differences) and there is lack of co-evolvement of the transplanted xenograft epithelial cells and the stromal compartments (100).

Of the cell lines commonly utilised in xenograft models, some cell lines representing basal subtypes (e.g. MDA- MB-231) have demonstrated inherent tumourigenicity whereas some ER^+ luminal A subtypes (e.g. MCF-7) are only tumourigenic in the presence of oestrogen. Surprisingly, xenograft models have also shown the limited capability of cell line-derived tumours to invade and metastasise which belies their often metastatic origin in humans (132). If metastasis does occur in xenograft models, it is usually to the lung – this is in contrast to the clinical situation whereby breast cancers most commonly metastasise to the bone (133).

2.1.6 Summary

Given the inherent complexity and heterogeneity of breast cancer, no individual model system is likely to faithfully replicate all aspects of the disease. Recent developments in 3D culture techniques have helped to identify key signalling interactions in both breast epithelial and cancer cells that are otherwise difficult to study *in vivo* (93,100,111). Thus, looking forward to the future, an integrated and multi-systems approach inclusive of 3D *in vitro* culture will likely become routine in modelling cancer and the impact of therapy.

2.2 Pancreatic Cancer

2.2.1 General background

Pancreatic cancer is currently the fourth highest cause of death from cancer in developed countries (134). The term 'pancreatic cancer' typically denotes ductal adenocarcinoma which is the most common pancreatic malignancy; it is also one of the deadliest known cancers with an extremely low estimated 5-year survival rate of around 5% (135). Rare pancreatic malignancies include hormone-secreting (e.g. insulin) neuroendocrine tumours and digestive-enzyme-releasing acinar carcinomas. In 2015, around 367,000 new cases of pancreatic cancer were diagnosed worldwide and an associated 359,000 deaths occurred in the same year (136). Moreover, more than half of diagnoses occurred in high-income countries (although, importantly, the possibility of under-diagnosis in developing countries must also be borne in mind). Interestingly, data from the United States found rates amongst black individuals to be ~30-50% higher than their white counterparts (137).

As aforementioned, pancreatic cancer carries an extremely poor prognosis and this occurs for several reasons (138). For instance, more than 80% of pancreatic cancers are locally advanced or metastatic at the time of diagnosis owing, in part, to characteristically non-specific symptoms such as unexplained weight loss, epigastric pain that radiates to the back, and jaundice (and sometimes there are no symptoms at all). Moreover, issues stem from a lack of sensitive and specific tumour markers, as well as, technical difficulties in imaging early-stage tumours, for example. Additional reasons include that pancreatic cancer is inherently aggressive with curative surgical resection often impeded by perineural invasion, localised vascular growth, and early distant metastases.

2.2.2 Chemotherapy

Surgery remains the only potentially curative option for pancreatic cancer, however, only about 20% of pancreatic cancers are resectable (139). Importantly, these patients make up the vast majority of survivors at the 5-year time point whereby survival rates are improved at ~15–25% (140). As with other malignancies (such as that of the breast), patients generally die from metastatic disease, therefore a better understanding of the drivers and contributory factors to

the metastatic phenotype (e.g. stromal ECM-cell influences) are vital to improving clinical outcomes (141). Pancreatic cancers exhibit a complex and dense tumour microenvironment and harbour multiple genetic and epigenetic alterations which impact upon available (and theoretical) treatment options. To date, pancreatic cancer has shown a remarkable resistance (or tolerance) to conventional chemotherapy and radiotherapy. Subsequently, adjuvant chemotherapy with radiation has been used widely in an attempt to improve treatment outcomes (138).

This resistance has also been show to extend to newer treatment modalities including molecular-targeted and immune therapies. Notwithstanding, cytotoxic chemotherapy remains the mainstay treatment for unresectable pancreatic cancer. Until recently, gemcitabine monotherapy was the standard chemotherapy regimen since its FDA approval in 1997 (139). Now, well-functioning patients presenting with metastatic disease in the UK are treated with the combinatorial regimen FOLFIRINOX (see below for further details). Frustratingly, though, despite numerous worldwide phase II and III clinical trials utilising numerous other cytotoxic agents (in both monotherapy and combination regimens), no significant improvement in prolongation of overall survival (OS) or progression-free survival (PFS) has been observed (142). Specifically, a recent systematic review found 27 agents or combinations were tested in 13,675 chemotherapy-naive patients with advanced pancreatic cancer between 1992-2015. From these, just *three* resulted in agents or combinations that are considered clinically meaningful (143).

2.2.3 3D Culture

The ECM associated with both normal and malignant tissues is comprised of two distinct types: basement membrane and interstitial matrix. Importantly, their composition differs markedly with the basement membrane being composed primarily of laminin, non-fibrillar type IV collagen, and heparan sulphate proteoglycan. By contrast, the interstitial matrix is composed primarily of fibrillar type I collagen (144).

Pancreatic cancers typically have an abundant and dense collagenous stroma (referred to as the desmoplasia) which results in a considerable hypoxic environment within which cancer cells propagate (138). Overactive pancreatic stellate cells (or, cancer-

associated fibroblasts) are responsible for the excessive depositing of ECM (predominantly, fibrillar type I collagen) which causes the stromal remodelling and dysregulated cell-ECM homeostasis implicated in promoting cancer progression, together with metastasis and chemotherapeutic resistance (145). Thus, more advanced preclinical models are required in order to achieve a more complete mechanistic understanding of these complex interactions (138,146).

By culturing cells in 3D *in vitro*, cells are prevented from attaching to the plastic substrata (i.e. the bottom of the plate) and are instead maintained in suspension or embedded within biomimetic matrices such as type I collagen. Subsequently, cells are able to maintain cell-cell and cell-matrix interactions and polarized structures which are ultimately more representative of the *in vivo* microenvironment (144). Ideal tumour models therefore replicate the 3D fibrillar microstructure given how interstitial matrix composition and physical properties (e.g. stiffness) are involved in facilitating EMT. Conventional epithelial to mesenchymal transition (EMT) schematics have tended to concentrate on intracellular events, however, the importance of alterations in the stroma are increasingly being recognised (141,144).

2.2.4 Summary

Collectively, pancreatic cancer therefore presents a substantial health problem and a significant challenge to scientists and clinicians alike. The foreboding features of pancreatic cancer such as aggressive disease and precarious survival rates could also support the case for intervention by novel experimental modalities such as PCI and formulation techniques. The stakes remain high, as pancreatic cancer is predicted to become the second leading cause of cancer-related mortality within the next decade should treatment outcomes not improve (134).

2.3 Chemotherapeutic Management

2.3.1 Breast cancer

As outlined in the National Institute for Health and Clinical Excellence (NICE, UK) guidelines (147), the chemotherapeutic management of advanced (stage 4) breast cancer is very much dependent upon the presence (or absence) of well-established clinical biomarkers. That is,

the presence of hormone-receptors (i.e. oestrogen or progesterone) and the HER-2 receptor; or, conversely, the absence of these biomarkers in triple-negative disease. In the advanced setting, only the triple-negative phenotype involves the exclusive administration of chemotherapy drugs; in the other clinical classifications, alternative therapeutic agents are recommended in the first instance (e.g. monoclonal antibodies and endocrine therapy). Chemotherapy (typically, anthracycline-based) may also be indicated in the neoadjuvant and adjuvant setting but surgery holds primacy in the early- and locally-advanced setting.

Chemotherapy in advanced triple-negative disease, is recommend as follows: (1st-line) single-agent docetaxel; (2nd-line) single-agent vinorelbine or capecitabine; (3rd-line) single-agent capecitabine or vinorelbine (whichever was not used as 2nd-line therapy). Dual-agent gemcitabine plus paclitaxel is also recommended as a treatment option for metastatic breast cancer (subject to certain clinical criterion). An important caveat here is with patients presenting with imminently life-threatening disease and whom have *not* previously been treated with anthracyclines (due to their risk of cumulative cardiotoxicity). These patients will typically be offered an anthracycline-containing regimen in line with what is used in the early and locally-advanced adjuvant setting (i.e. post-surgery) (147).

In essence, there are many treatment permutations in breast cancer but where chemotherapy is indicated in the advanced setting, it typically revolves around the following cytotoxic drugs (and drug classes): doxorubicin (anthracyclines), vinorelbine (vinca alkaloids), docetaxel and paclitaxel (taxanes), and gemcitabine and capecitabine (anti-metabolites). In the present work, therefore, the bulk of chemotherapy drugs tested for PCI compatibility principally derive from these chemotherapeutic drug classes which have already demonstrated clinical utility in the advanced breast cancer setting. In addition, PCI is currently most likely to be trialled in patients that are in the advanced stages of disease and who have exhausted other treatment options (47).

2.3.2 Pancreatic cancer

National Institute for Health and Clinical Excellence guidelines recommend 1st-line treatment for well-functioning patients presenting with metastatic disease should begin with a four-drug chemotherapy regimen called FOLFIRINOX (FOL – folinic acid; F – fluorouracil; IRIN –

irinotecan; OX – oxaliplatin). In many other clinical scenarios, such as in the adjuvant setting following surgery, or if patients are not well enough to tolerate the FOLFIRINOX regimen, chemotherapy regimens typically comprise of single- or combined-agent gemcitabine chemotherapy (e.g. with capecitabine) (148). Importantly, however, the FOLFIRINOX regimen is associated with significant toxicities including diarrhoea, nausea, fatigue, myelosuppression and neuropathy and hence why the regimen is only typically indicated for patients ≤76 years of age with an excellent performance status (149).

Interestingly, in 2012, the precedence was set for biomolecule-bound drug efficacy in pancreatic cancer when the combined regimen of gemcitabine and albumin-bound paclitaxel (now, FDA-approved) was found to be superior to single-agent gemcitabine (150). Although toxicities are also significant with this regimen, it can be safely given to older patients or those with a somewhat poorer performance status (138).

As previously alluded to, optimising therapy for patients with pancreatic cancer is a forbidding task due to the majority of patients presenting with unresectable, locally advanced, or widespread metastatic disease (e.g. in the liver). Moreover, the extensive stromal changes characteristic of the disease have previously been shown to impede drug delivery in preclinical models (151). Thus, to date, very few effective drugs have been identified and therefore finding new effective therapies is of the utmost importance.

2.4 New PCI drug candidates

The choice of potential cytotoxic agents to investigate for PCI compatibility is numerous so, in the present work, there has been a specific focus on those agents that feature prominently in the clinical guideline recommendations for breast and pancreatic cancer treatment. Crucially, however, the cytotoxic agents that have chosen for investigation are also clinically-indicated for use in other cancers across the spectrum of both solid and haematological malignancies. This certainly increases the potential benefit to patients should a positive outcome be observed from their delivery via PCI. Moreover, this approach also increases the likelihood of PCI transitioning from bench to bedside.

2.5 Formulation techniques – Squalene

2.5.1 General background

Formulation techniques are employed in order to improve upon the inherent characteristics of a drug which may be deficient or lacking in some way. In the context of anticancer treatment, formulation typically functions as a means of increasing drug specificity, bioavailability, and tumour accumulation (152,153). In order to overcome any potential limitations of biocompatibility, one particularly attractive strategy is the conjugation of chemotherapy drugs to biomolecules such as albumin and squalene (138,153).

Squalene (Figure 14) is a member of a group of molecules called terpenes (or terpenoids) which have an extraordinarily diverse chemistry, structure, and function (154). More specifically, squalene is a natural triterpene that has considerable potential as a biocompatible material for drug and gene delivery applications (152). In fact, numerous classes of terpenoids (which constitute the largest group of natural products) have already also been shown to possess exceptional pharmacological properties with major therapeutic value. Terpenoid examples include many of the important traditional chemotherapy drugs including taxanes such as paclitaxel and docetaxel (from *Taxus brevifolia*); vinca alkaloids such as vincristine and vinblastine (from *Catharanthus roseus*); camptothecin (from *Camptotheca acuminate*); and artemisinin (from *Artemisia annua*) (152).

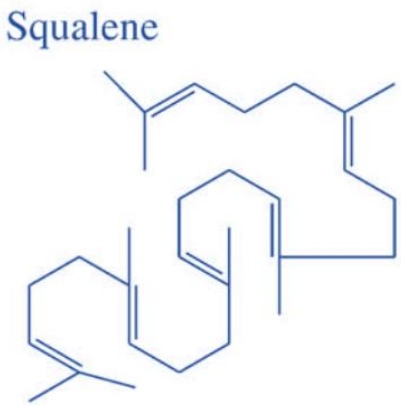

Figure 14. Chemical structure of squalene. *Squalene is a precursor biomolecule to cholesterol and potential drug carrier. Modified from* (152).

2.5.2 Correlations

Squalene is a polyunsaturated triterpene containing six isoprene units and is a biochemical precursor of cholesterol and other steroids (155). It is found throughout nature and is regularly consumed as a part of the human diet (e.g. it is present in: olives, wheat germ, and rice bran), in addition to being synthesised endogenously in the liver and skin. Interestingly, elevated squalene levels are seen in sharks (shark liver oil contains >40% squalene) which correlates with the absence of cancer in this animal species (156). Furthermore, high dietary consumption of squalene (olives) is thought to contribute to the low incidence of human cancer in the Mediterranean region (157).

Evidently, exogenously-derived squalene is therefore well-tolerated whether consumed orally or injected intravenously and is transported in the blood by low density lipoproteins (LDL) and very low density lipoproteins (VLDL) (158). Collectively, these features mean that squalene is favourably positioned from a toxicological perspective in its potential use as a carrier/adjuvant in therapeutics.

2.5.3 PCI applicability

Squalene is also secreted in sebum (~12% squalene content) and accumulates in high concentrations in the skin where, intriguingly, it has been shown to quench free ROS (particularly, singlet oxygen) (159). This is particularly important when considered in the context of PCI therapy, whose principal adverse effect stems directly from harmful cutaneous lipid peroxidation. On the other hand, though, the favourable accumulation of squalene in tumour cells could also potentially attenuate the beneficial effects of intracellular ROS in PCI-delivery. Although its anti-oxidant effect is thought to predominate, squalene has also been shown capable of exerting an oxygenation effect on cells which could potentiate the effect of PCI (particularly in hypoxic cells) and improve host immunity (152).

2.5.4 Drug carrier

The conjugation of chemotherapy drugs to drug carriers can confer many advantages to the passenger therapeutics (150,153). Namely, an increased aqueous solubility for hydrophobic drugs, decreased plasmatic metabolism, prolonged half-life, altered biodistribution, and

improved drug specificity (160). Lipids make good biocompatible drug carriers for numerous reasons including their ability to fuse to, and deliver therapeutics through, the cell membrane. Lipid-drug conjugates are typically covalently-bound and can improve chemotherapeutic therapeutic indices through modified pharmacokinetics and decreased toxicity (152).

Gemcitabine is a nucleoside analogue (antimetabolite) that features prominently in the chemotherapy regimens for both breast and pancreatic cancer treatment. Despite this, it retains some not insignificant limitations including a short biological half-life (due to rapid blood metabolisation), restricted intracellular diffusion, and varying mechanisms of resistance (e.g. the inhibition of gemcitabine metabolism to its active form) (161). Consequently, gemcitabine has been conjoined with squalene to give SqGem bioconjugates (153) that are also capable of spontaneous aqueous self-assembly in the form of nanoparticles (~100–200 nm) (162). Owing to their small size, nanoparticles themselves can passively target tumour tissue (via the EPR effect), but the added utility here is that squalene is transported by LDLs whose receptor is often over-expressed on cancer cells. SqGem conjugates have also been shown to interact with cellular membranes (163).

2.6 Summary

Breast and pancreatic cancers are highly prevalent and have well-defined clinical characteristics. Current chemotherapy treatment options are relatively limited and could potentially benefit from new technologies, such as PCI. Moreover, the current systems of modelling cancer *in vitro* are inadequate as they cannot recreate the complex tumour microenvironment that has been shown to influence both cellular morphology, disease progression, and therapeutic efficacy. Instead, biomimetic 3D *in vitro* models that utilise materials such as type I collagen have the potential to recapture important aspects of the disease and its response to treatment. Finally, formulation techniques such as novel drug-lipid bioconjugates have the potential to greatly enhance the therapeutic indices of chemotherapy drugs, yet further.

Chapter 3: Aims of Thesis & Methodology

3.1 Aims of Thesis

The first aim of this thesis is to determine the performance of a broad range of chemotherapy drugs (vinorelbine, vincristine, vinblastine; docetaxel, paclitaxel; gemcitabine, capecitabine; and, bleomycin) in a 3D hydrogel model of cancer *in vitro*. The novel combination of 3D model, cancer cell lines, and chemotherapy drugs, (and PCI treatment), used in this thesis means that it is imperative to first establish and optimise treatment parameters before they are taken forward to light treatments and nanoformulation studies. Primarily, chemotherapeutic cytotoxicity will be assessed by means of treatment potency and efficacy.

The next aim of this thesis is to test the amphiphilic photosensitiser $AlPcS_{2a}$ in PDT experiments in the 3D *in vitro* model before attempting to identify new drug candidates that are suitable for PCI delivery. Moreover, whether their therapeutic indices can be enhanced by PCI. Very few conventional chemotherapy drugs have been tested in PCI regimens and so, new compatible candidates could be of great clinical utility and help to accelerate the transition of PCI from bench to bedside.

Utilising a number of *in vitro* cancer models, new PCI-drug combinations will be compared and contrasted against PCI-bleomycin which is the most successful PCI therapy to date. Moreover, treatment performance by pharmacotherapeutic drug *class* will also be contrasted with PCI-bleomycin in order to try to highlight promising drug classes where other suitable PCI drug candidates could be found. Additional investigations will include the impact on treatment outcomes of an alternative light-before PCI regimen, as well as, variations in cell culture conditions. An advantage of 3D models is that specific ECM properties can be precisely manipulated and, indeed, the effect on treatment outcomes of varying hydrogel stiffness and hydrogel volume will also be investigated. These outcomes will also be compared and contrasted against results from monolayer cell culture.

Treatment outcomes will be assessed in terms of treatment potency, efficacy, and synergy. Fluorescence microscopy will also be used in order to probe the precise mechanisms of PCI action through drug-lysosome co-localisation studies. In addition, this method will be used to identify cellular distribution within the 3D model.

Finally, this thesis will aim to investigate the effect on therapeutic efficacy of novel nanoformulations in order to explore the potential of bioconjugation strategies for PCI applications.

3.2 Materials and Methods

3.2.1 Cell Culture

3.2.1.1 Chemicals

Aluminium(III) phthalocyanine chloride disulphonic acid, adjacent isomer ($AlPcS_{2a}$) was purchased from Frontier Scientific (distributed by Inochem, Lancashire, U.K.). $AlPcS_{2a}$ was first dissolved in 0.1 M NaOH, then diluted in sterile phosphate-buffered saline (PBS) to a final stock concentration of $AlPcS_{2a}$ 1.25 mg/mL ≡ 1.7 mM (NaOH 0.02 M). The photosensitiser ($AlPcS_{2a}$) was protected from light and stored at 4 °C (short-term) until use (long-term storage: -20 °C). Chemotherapeutic agents: bleomycin [sulphate], vinorelbine [tartrate], vincristine [sulphate], vinblastine [sulphate], paclitaxel, docetaxel, gemcitabine [hydrochloride], and capecitabine were purchased from Cambridge Bioscience (Cambridge, U.K.) and dissolved in sterilised dimethyl sulfoxide (DMSO) to a stock concentration of 50 mM. Stock solutions were then aliquoted and stored at -20 °C until use. All experimental procedures involving the use of photosensitisers were carried out under subdued laboratory light.

The first gemcitabine formulation, *gemcitabine-squalene* (SqGem), was kindly provided by Professor Patrick Couvreur and Dr. Didier Desmaelle (University Paris-Sud, France). The second gemcitabine formulation, *gemcitabine-polymer*, was synthesized in our lab based upon previously published methods (164). Briefly, a methacrylate-based gemcitabine-monomer conjugate was RAFT-polymerised to form a gemcitabine-polymer conjugate of well-characterised properties (for example, polymer molecular weight).

3.2.1.2. Cell lines

The MDA-MB-231 and MCF-7 human breast adenocarcinoma cell lines were a kind gift from Dr. Hazel Welch (UCL Department of Nanotechnology, Division of Surgery and Interventional Science, U.K.). Pancreatic cancer MiaPaCa-2 cells were from liquid nitrogen vapour-phase storage and originally from ATCC (Middlesex, U.K.). All cell lines were grown in “DMEM

Complete" medium which comprised of Dulbecco's Modified Eagle's Medium (DMEM) high glucose medium (Sigma-Aldrich, Gillingham, U.K.) supplemented with 10% (v/v) foetal calf serum (GIBCO BRL, Paisley, U.K.), 100 U/mL penicillin, 100 µg/mL streptomycin (Sigma-Aldrich, Gillingham, U.K.), and 2.5 mg/mL Plasmocin™ (InvivoGen, Toulouse, France). Cell lines were routinely subcultured by trypsinisation twice a week and experiments performed during three-month time periods (with passages approximately: 30-60). Cells were grown and incubated in 75 cm^2 flasks (Greiner Bio-One, Stonehouse, U.K.) at 37 °C in a humidified tissue culture incubator with 5% CO_2.

3.2.2 *In vitro* cell culture models

Three-dimensional (3D) *in vitro* cell culture models were predominantly used in this work; with the main cytotoxic treatment effects being quantified using a reagent and assay specifically designed for use with 3D cell-embedded cultures.

3.2.2.1 Three-dimensional (3D) cell culture

3D collagen hydrogels were prepared as follows: Collagen type I (rat-tail collagen type I, protein concentration 2.035 mg/mL or 5.000 mg/mL in 0.6% acetic acid; First Link UK Ltd, Birmingham, U.K.) was mixed with minimum essential medium (MEM, 10X with Earle's Salts, without L-glutamine, sodium bicarbonate, GIBCO 21430, Sigma-Aldrich, Gillingham, U.K.), and the pH adjusted to 7.0-7.7 (NaOH: 1 M) as determined by indicator colour change. MDA-MB-231, MCF-7, or MiaPaCa-2 cells (10,000 cells) were added immediately and the mixture shaken and micro-pipetted to ensure even cell dispersion. Collagen:medium:cell volume ratios were 8:1:1. The hydrogel mixture (25 µL; or, 75 µL) was then micro-pipetted into designated wells of a 96-well plate before being allowed to set for 15 min at 37 °C in a humidified tissue culture incubator with 5% CO_2. Hydrogels were then immersed in DMEM Complete medium and maintained at 37 °C in a humidified incubator with 5% CO_2 for 24 hours before experimentation (in order to allow cancer cells to rest after trypsinisation and also to minimise cell proliferation).

3.2.2.2 Monolayer culture

MDA-MB-231, and MCF-7 human breast cancer cells were trypsinised, counted, and re-suspended in DMEM Complete medium. A cell suspension in DMEM Complete medium was then added (10,000 cells) to designated wells of a 96-well plate before being allowed to settle and adhere to the well-base for 24 h at 37 °C in a humidified incubator with 5% CO_2.

3.2.3 Cytotoxic Treatments

3.2.3.1 Chemotherapy

Cell-containing 3D hydrogels (or, cells grown in monolayer) were incubated with various chemotherapeutic agents diluted in DMEM Complete cell culture medium for 18 h in dark conditions at a humidified 37 °C with 5% CO_2. Following incubation, cells were washed thrice with drug- and serum-free DMEM medium (200 µL) and incubated for 4 h in drug- and serum-free DMEM medium. Following this, fresh DMEM Complete medium was added to each well and cells were incubated at a humidified 37 °C with 5% CO_2. Cell viability was then determined at 48 h and 72 h (depending upon the regimen used) in order to assess treatment effects. More specifically, *viability* was a measurement of metabolic activity by means of luminescent ATP quantification. The treatment schedules for both 48 h and 72 h regimens are shown below in Figure 15. In order to correlate with the observed post-treatment reduction in cell viability, cell *death* was also determined by means of a qualitative live/dead assay (i.e., to prove that decreased cell viability was, in fact, due to cells being *dead*).

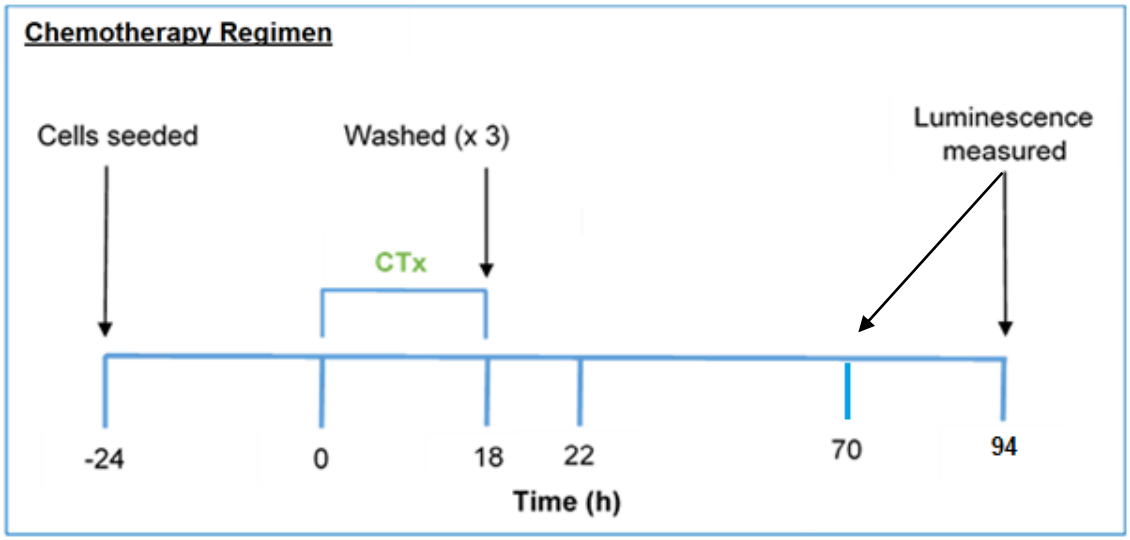

Figure 15. Timeline for the chemotherapy treatment schedule. *CTx: bleomycin; vinorelbine; vincristine; vinblastine; paclitaxel; docetaxel; gemcitabine; or, capecitabine.*

3.2.3.2 Photochemical treatments

3.2.3.2.1 Light source

For photochemical treatments, a mounted LED light source (Thorlabs M660L3, 1200 mA, 640 mW; Ely, U.K.) was used with peak wavelength of 660 nm (visible, deep-red range) and fluence rate of 2.0 mW/cm^2 for 1-5 min, to give a total energy density/light dose of 0.12-0.60 J/cm^2. The fluence rate in those 96-well plate regions to be illuminated was checked and measured using an optical power meter (Newport, Irvine, California, U.S.A.)

3.2.3.2.2 Photochemical internalisation

Cell-containing 3D hydrogels were incubated with either photosensitiser (AlPcS$_{2a}$) alone ("PDT"), or AlPcS$_{2a}$ together with various chemotherapeutic agents ("PCI") diluted in DMEM Complete medium for 18 h in dark conditions at a humidified 37 °C with 5% CO_2. Following incubation, cells were washed thrice with drug- and serum-free DMEM medium (200 µL) and incubated for 4 h in drug- and serum-free DMEM medium. Following this, fresh DMEM Complete medium was added to each well immediately prior to light exposure. In addition, PDT, drug-free, and light-free controls (wherever appropriate) were included in each experiment. DMSO controls were also carried out prior to experimentation which produced negligible cytotoxic effects. Following illumination, cells were incubated at a humidified 37 °C with 5% CO_2. In order to evaluate treatment effects, cell viability was determined at 48 h or 72 h post-irradiation (depending upon the PCI regimen used) using the same ATP-quantification assay as chemotherapy experiments. Treatment schedules follow for both conventional PCI (Figure 16) and "light-before" PCI (Figure 17) regimens.

3.2.4 Determination of treatment effects

3.2.4.1 CellTiter-Glo® luminescent cell viability assay

The CellTiter-Glo® Luminescent Cell Viability Assay (Promega UK Ltd, Southampton, U.K.) is a homogeneous method to determine the number of viable cells in 3D cell culture based upon quantification of the ATP present. ATP is a marker for the presence of metabolically active cells and its quantity is directly proportional to the number of viable cells present in culture (165).

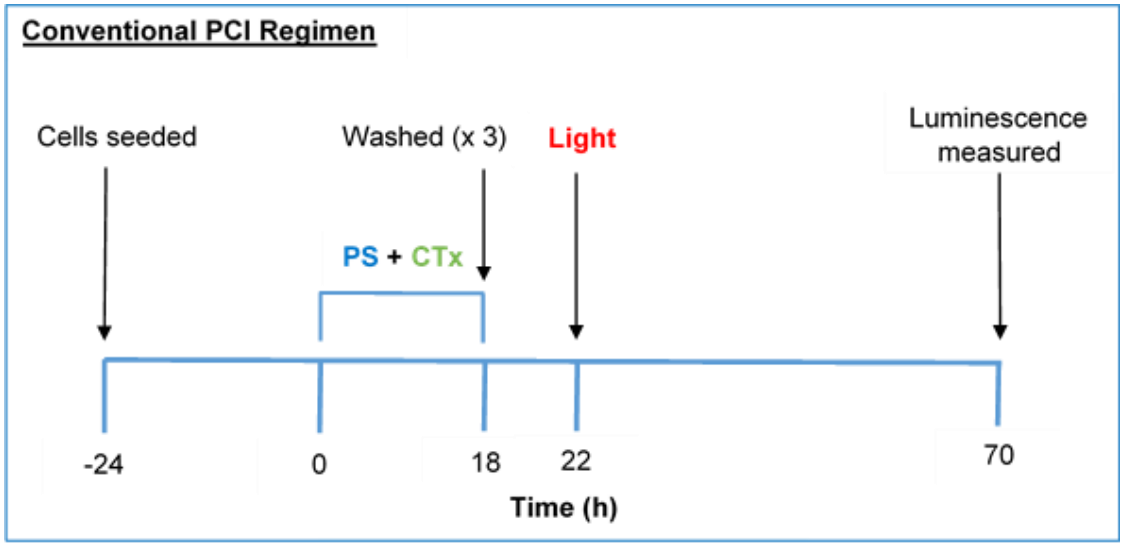

Figure 16. Timeline for the conventional PCI treatment schedule. *PS: photosensitiser ($AlPcS_{2a}$); CTx: bleomycin; vinorelbine; vincristine; vinblastine; paclitaxel; docetaxel; gemcitabine; or, capecitabine.*

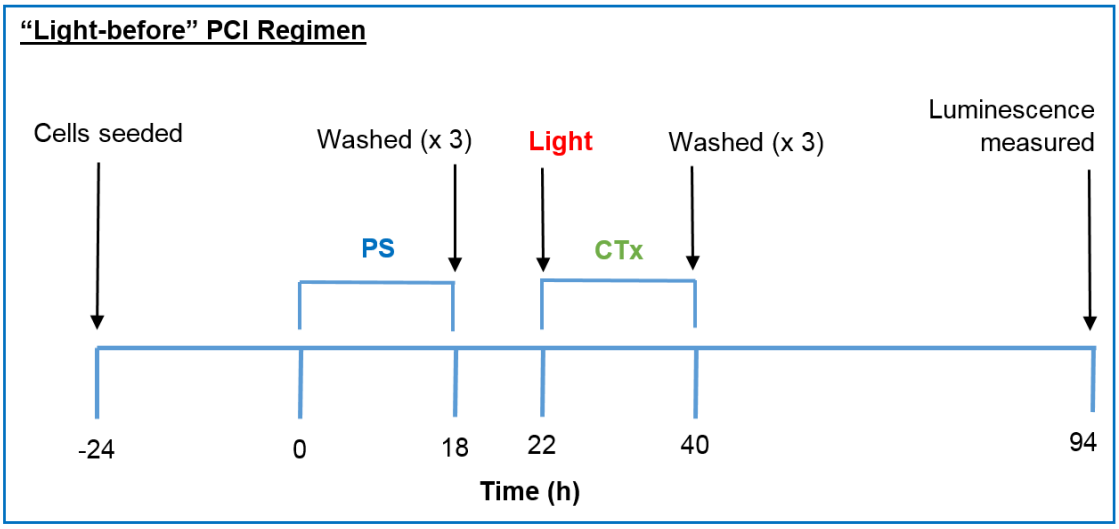

Figure 17. Timeline for the light-before PCI treatment schedule. *PS: photosensitiser ($AlPcS_{2a}$); CTx: bleomycin; vinorelbine; vincristine; vinblastine; paclitaxel; docetaxel; gemcitabine; or, capecitabine.*

The CellTiter-Glo® viability assay relies upon a thermostable luciferase to generate a stable "glow-type" luminescent signal. In accordance with an optimised protocol based upon the manufacturers' recommendations: at a specified time-point following PCI light irradiation (e.g. 48 h), CellTiter-Glo® 3D Reagent and experimental plates were equilibrated to room temperature for 30 min. Reagent was then added to each experimental well and mixed vigorously for 5 min to induce cell lysis. Experimental plates were then incubated for an additional 25 min at room temperature before luminescence was recorded using a SpectraMax M2e multi-mode microplate reader (Molecular Devices, California, USA).

Positive control (1% Triton X-100) and background luminescence readings were subtracted from experimental readings prior to statistical analysis. In addition, initial experiments were performed using acellular hydrogels incubated with the highest tested drug concentrations ($AlPcS_{2a}$, in particular) in order to confirm that no interaction existed between experimental drug compounds and the luminescent signal. Here, 3D reagent was added as per the cellularised-hydrogel protocols and luminescence readings were found to be comparable to background/empty well readings – thus confirming that there was no interaction. The term 'cell viability' thus refers to the cellular metabolic activity (as directly derived from cellular ATP quantity) measured for each experimental condition and are plotted as a percentage (%) of the negative control.

3.2.4.2 LIVE/DEAD Viability/cytotoxicity assay

In order to corroborate the findings from the cell viability assay, cell *death* was also determined using a combination live/dead preparation (LIVE/DEAD; Sigma-Aldrich, Gillingham, U.K.) consisting of the fluorescent dyes calcein AM (excitation 494 nm/emission 517nm) and ethidium homodimer-1 (excitation 517 nm/emission 617 nm).

In brief, MDA-MB-231 human breast cancer cells and MiaPaCa-2 human pancreatic cancer cells were cultured in monolayer as previously described. Next, cells were incubated with vinblastine diluted in DMEM Complete medium (10,000 nM) for 18 h at a humidified 37 °C with 5% CO_2. Cells were then washed thrice with drug- and serum-free DMEM media and fresh media added before staining with the LIVE/DEAD assay kit. The two components of the kit were mixed at equal volumes to prepare a 2X solution, and then a volume equal to that of the media in the wells added to the cells. After 15 min incubation at 25 °C, cells were then imaged using an EVOS FL fluorescent microscope (ThermoFisher Scientific, U.K.).

Next, in order to investigate cellular distribution within the 3D hydrogel model, the same staining protocol was used and cells visualised in 3D by confocal microscopy (Zeiss LSM 710, Germany) in conjunction with ZenTM software. Confocal images were obtained with the kind assistance of Ms. Maha Muwaffak. Negative controls were also similarly prepared and imaged (wherever appropriate).

3.2.4.3 Co-localisation of chemotherapy and lysosome

In order to evaluate whether the administered chemotherapy was localised to the lysosome, a fluorescently-tagged vinblastine preparation (BODIPY™ FL vinblastine conjugate; Sigma Aldrich, U.K.) was used in conjunction with Lysotracker™ (LysoTracker™ Red DND-99; Sigma Aldrich, U.K.).

Succinctly, MDA-MB-231 and MiaPaCa-2 human cancer cells were cultured in monolayer as previously described. Next, cells were incubated with BODIPY™-vinblastine diluted in DMEM Complete medium (10,000 nM) for 18 h at a humidified 37 °C with 5% CO_2. Cells were then washed thrice with drug- and serum-free DMEM media before staining with LysoTracker™. Lysotracker solution was prepared to a concentration of 75 nM (in serum free DMEM media) and incubated with cells for 2 h at a humidified 37 °C with 5% CO_2.

As with the LIVE/DEAD imaging, cancer cells containing both tagged-vinblastine and lysotracker were then imaged using the EVOS FL fluorescent microscope. Negative controls were also similarly prepared and imaged.

3.2.5 Statistical analysis

Cytotoxic treatment outcomes measures were primarily presented in terms of potency ($IC_{50/70}$), efficacy (E_{max}), and synergy (α). The IC_{50} is indicative of drug *potency*, and is defined as the concentration of drug at which the response is half (50%) of its theoretical maximum (here, the maximum effect is 0% of control cell viability). The E_{max} is indicative of drug *efficacy* and is the value of cell viability at the maximum tested drug concentration (here, 250,000 nM). $IC_{50/70}$ values were determined from the dose-response profiles for each respective treatment. In addition, for the purpose of graphical presentation and clarity, the x-axis concentration labelled “1” nM, in fact, represents ‘0.5’ nM (and therefore each increment to 5 nM is 0.5 nM). Furthermore, where applicable, PDT controls are shown as crosses on the y-axis (at 0 nM).

All cell culture experiments (e.g. chemotherapy, PDT, PCI) were carried out in 96-well plates and performed in triplicate on, at least, three separate occasions (n=3). The mean was then calculated from these sample data and tested for statistical significance *via* a mixed factorial ANOVA using IBM SPSS version 25. Error bars represent the standard error of the

mean (SE) – a statistic the denotes how far the sample mean deviates from the actual population mean (166). A minimum significance level of $p < 0.050$ was used for all statistical tests.

In order to test for synergistic interactions between treatment modalities - for example, vinorelbine and PDT as separate, standalone treatments then contrasted with vinorelbine-PCI - the following equation was used (167):

$$\alpha = \frac{[SF(\mathrm{PDT}) \times SF(\mathrm{chemotherapeutic})]}{SF(combination)}$$

Where the numerator *SF* is the survival fraction (survival fraction = %C metabolic activity ÷ 100) for each individual therapy (i.e. PDT; and, the chemotherapeutic alone), and the *SF* in the denominator is the survival fraction observed following the PCI combination treatment. When α > 1 then a synergistic effect has been observed whereas α < 1 denotes an antagonistic effect. When α = 1, this signifies an additive effect of the treatment combination. This analysis has been used previously by others in the field (and beyond) in order to identify synergistic effects resulting from PCI therapy (168,169).

3.2.6 Rheological studies

3.2.6.1 Mechanical analysis of hydrogel stiffness

Rheology measurements were carried out with the kind assistance of Ms. Saja Muwaffak.
In order to measure and compare the respective stiffnesses of 2 mg/mL and 5 mg/mL collagen type I hydrogels, acellular hydrogels were prepared as previously described only in 500 µL volumes (and in 24-well plates). Oscillometry rheology was then carried out using a Bohlin Gemini HR Nano (Malvern Instruments, U.K.). Parallel plates (PP20) were chosen and the measurement *gap* set to 400 µm for both types of collagen hydrogel. After carrying out an amplitude sweep the strain was set at 5% and the frequency range set between 0.1-10 H_z. The measurement platform temperature was set at 37 °C (to match cell culture conditions) and each run was repeated twice (in order to give a triplicate measurement in total). This was then repeated on two separate occasions in order to obtain n=3. Data (mean ± SE) was then plotted with the complex modulus (mechanical stiffness) on the y-axis and the frequency on the x-axis (logarithmic scale).

3.2.7 Nanoparticle Preparation: Gemcitabine-squalene and Gemcitabine-Polymer

3.2.7.1 Solvent evaporation technique

The preparation of these nanoparticles was kindly completed in collaboration with Ms. Alexandra Iliopoulou (gemcitabine-squalene conjugate; “SqGem”) and Mr. Raul Sanchez-Alvarez (gemcitabine-polymer conjugate).

Briefly, a stock solution of 1 mg/mL was prepared as follows: 5 mg of the formulation (either SqGem or gemcitabine-polymer) was dissolved in a 10 mL mixture of ethanol (EtOH) and distilled H_2O (1/1 v/v) and the solution sonicated (Fisher brand FB15051, Fisher Scientific, U.K) and vortexed (IKA Vortex Genius 3, Sigma Aldrich, U.K) in order to ensure correct mixing. The 10 mL solution was then transferred equally into five glass tubes and the 2 mL aliquot concentrated for 10 min using a Rotavapor® (R-300, Butchi, U.K) at 40 °C, 100 rpm, and 100 mBar. The resulting solution of ~1 mL was then characterised using dynamic light scattering (DLS) before proceeding to cell culture experiments.

3.2.7.2 Characterisation

Nanoparticle size was measured using a Zetasizer NanoS (Malvern Instruments, U.K). DLS measurements of particle size and polydispersity index (PDI) were conducted in distilled H_2O with a standard volume quartz cuvette (QS High Precision Cell, Helma Analytics, U.K) and the following parameters: a 30 s equilibration time, 10 x 10 s readings, and 3 sets of readings. Nanoparticle characterisation was performed in triplicate and all preparations were used within 2 h after preparation.

Section B: 3D *In Vitro* Studies – Chemotherapy & PCI

Chapter 4: Chemotherapy in Breast Cancer

4. Evaluation of Chemotherapy in a 3D Breast Cancer Model *In Vitro*

4.1 Introduction

As previously introduced, the chemotherapeutic agents selected for use in the 3D *in vitro* models of TNBC and ER+ breast cancer (and, later, pancreatic cancer) feature prominently in the current clinical recommendations for each malignancy.

In addition to biological differences between monolayer and 3D cell culture, differences in cellular response to classical chemotherapy drugs (as well as, other therapeutic agents) has also been revealed (111). In some cases, 3D-cultured cells have been more resistant to chemotherapy and at other times more sensitive (115). Thus, although more technically challenging to establish, 3D models are more biomimetic and have important implications for drug screening *in vitro*.

4.1.1 Vinca alkaloids

4.1.1.1 Vinorelbine, vincristine, and vinblastine

The vinca alkaloids are a class of cytotoxic chemotherapy drugs originally derived from the leaves of the *Catharanthus roseus* plant; formerly known as "*Vinca rosea"* or the "Madagascar periwinkle" (Figure 18). In fact, extracts from the *Catharanthus roseus* plant have been described in medicinal folklore as being effective for the treatment of haemorrhage, scurvy, toothache, wound healing, diabetic ulcers and hyperglycaemia (170). Initially, low yields of the active compound limited the range of compounds available for medicinal studies (171). Then, vincristine and vinblastine (Figure 19) were the compounds first derived from the plant; followed later by vinblastine derivatives including vindesine and vinorelbine. More recently, the fluorinated analogue vinflunine has been synthesized (172).

Vinca alkaloid-based drugs are established in the treatment of ovarian, breast, and lung cancers (173). Categorised as 'spindle poisons', these drugs target tubulin to cause microtubule destabilisation. Anti-tubulin vinca alkaloids inhibit tubulin polymerisation (from soluble dimers into microtubules) and spindle formation; resulting in the apoptosis of

susceptible cancer cells. Mitotic microtubule inhibition correlates with antitumor activity, whereas axonal microtubule inhibition seems to correlate with neurotoxicity – a common adverse effect of this therapeutic drug class (171).

The affinity for tubulin differs among the four most-common vinca alkaloid compounds in clinical use which could explain the distinct neurotoxic profiles of each drug (172); neurotoxicity decreases in order from: vincristine, vindesine, vinblastine, and, vinorelbine. Vincristine neurotoxicity is of particular importance as it can often be treatment-limiting. Vinorelbine, vincristine, and vinblastine were each tested in the 3D breast cancer model, as well as, in later PCI experiments.

Figure 18. Catharanthus roseus ("Madagascar periwinkle"). *The vinca alkaloid group of chemotherapy drugs are derived from the leaves of this plant.*

4.1.2 Taxanes

4.1.2.1 Docetaxel and paclitaxel

The taxanes include the microtubule-targeting cytotoxic chemotherapy drugs docetaxel and paclitaxel which were originally derived from the evergreen conifer Yew tree (Figure 20).

Docetaxel is a semi-synthetic taxane derived from the needles of the European yew tree (*Taxus baccata*). It achieves high intracellular concentrations with a long cell residence time and has been shown to disrupt the cellular microtubule network which is essential for normal cell function. The foremost cytotoxic activity of docetaxel is based on tubulin stabilisation and subsequent cell cycle arrest. Cell death by apoptosis, cell lysis, and the inhibition of angiogenesis has also been shown (174).

Docetaxel is an antineoplastic agent which has many solid-tumour therapeutic indications including breast cancer, non-small cell lung cancer (NSCLC), prostate cancer, gastric adenocarcinoma, as well as, head and neck cancer. *In vitro*, docetaxel has demonstrated more potent antimicrotubule activity than its taxane counterpart paclitaxel (174).

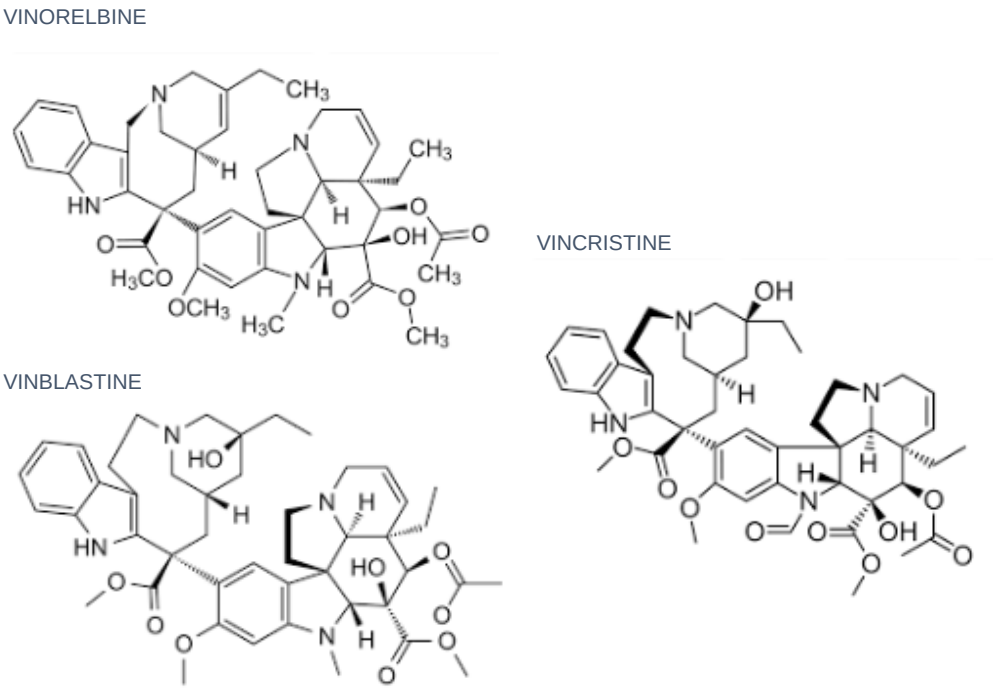

Figure 19. Chemical structures of the vinca alkaloids used in this work. *Vinorelbine (left, top), vincristine (right, middle), and vinblastine (left, bottom).*

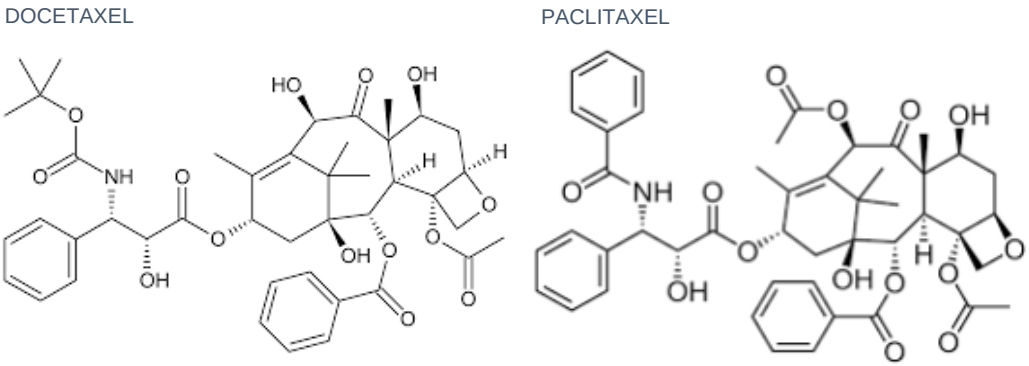

Figure 20. Chemical structures of the taxanes used in this work. *Docetaxel (left) and paclitaxel (right).*

Paclitaxel, a white crystalline powder, was isolated from the bark of the Pacific Yew tree (*Taxus brevifolia*). Its low solubility is a major limitation (~0.4 µg/mL) and, thus, paclitaxel is formulated in organic solvents of polyoxyethylated castor oil (Cremophor EL) and dehydrated ethanol ("Taxol") which carry their own clinical risks (e.g. hypersensitivity).

Similarly to docetaxel, paclitaxel also promotes the assembly of microtubules from tubulin dimers and stabilises microtubules by preventing depolymerisation. This stability disrupts microtubule function and induces subsequent downstream events which leads to cell death.

Its therapeutic indications include carcinoma of the ovary, breast, and lung (NSCLC) (175). Interestingly, the "nano" formulation Abraxane® utilises paclitaxel and albumin-bound nanoparticles (~130 nm) and is approved (FDA, 2005) for the treatment of metastatic breast cancer. Some advantages have been observed including reduced toxicity compared to the Taxol formulation (176).

4.1.3 Antimetabolites

4.1.3.1 Gemcitabine and capecitabine

The antimetabolite pharmacotherapeutic drug class includes the antineoplastic agents' gemcitabine and capecitabine which are both pyrimidine analogues and prodrugs.

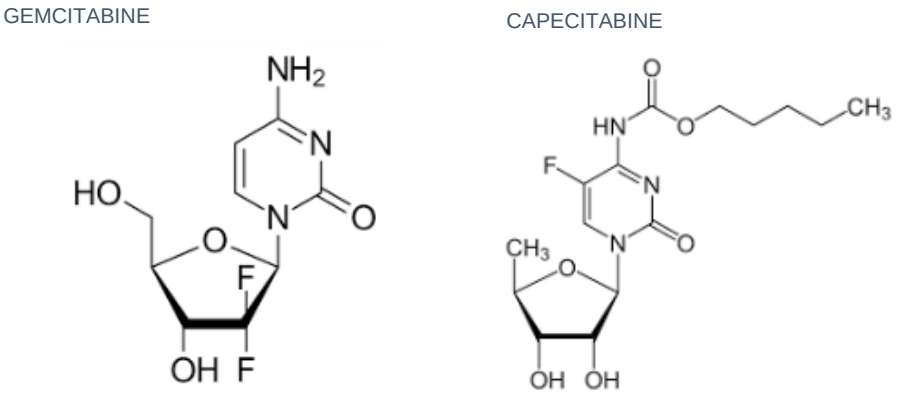

Figure 21. Chemical structures of the antimetabolite drugs used in the present work. *Gemcitabine (left) and capecitabine (right).*

Gemcitabine (2',2'-difluorodeoxycytidine) is a deoxycytidine analogue with broad activity in a variety of solid tumours (177). A pyrimidine antimetabolite, it is metabolised intracellularly, first to its monophosphate form before further phosphorylation to its therapeutically-active metabolites (diphosphate and triphosphate) by nucleoside kinase. Gemcitabine is subsequently incorporated into DNA and, following this nucleoside addition, further DNA synthesis is essentially completely inhibited (masked chain termination). Consequently, apoptotic cell death is induced as DNA polymerase cannot eliminate gemcitabine.

Gemcitabine is typically indicated for the treatment of metastatic cancers including those of the bladder, breast, and pancreas, and sometimes in combination with other chemotherapeutic agents. Gemcitabine enters the cell cytoplasm via a carrier-mediated nucleoside transport (177).

Capecitabine is a non-cytotoxic fluoro-pyrimidine prodrug which functions as a precursor of the cytotoxic moiety 5-fluorouracil (5-FU). The active drug is achieved *via* capecitabine activation by several catalytic enzymatic steps; the last of which involves the tumour-favoured enzyme thymidine phosphorylase. The sequence of capecitabine to 5-FU biotransformation therefore leads to higher concentrations within tumour tissues.

5-Fluorouracil (5-FU) is a commonly used in treating various solid tumours including those of the head and neck, breast, and pancreas (178). Its primary cytotoxic action results from its antimetabolite action of being incorporated into replicating RNA. This inhibits RNA and protein synthesis and also leads to the depletion of thymidine.

4.1.4 Glycopeptide antibiotic

4.1.4.1 Bleomycin

Bleomycin was the only agent investigated from the glycopeptide drug class. Despite it not featuring prominently in the clinical treatment guidelines for breast and pancreatic cancer, it *does* feature prominently in PCI therapy (53). Moreover, bleomycin is so-far the only chemotherapeutic agent to be tested in humans as part of a PCI regimen (47).

BLEOMYCIN

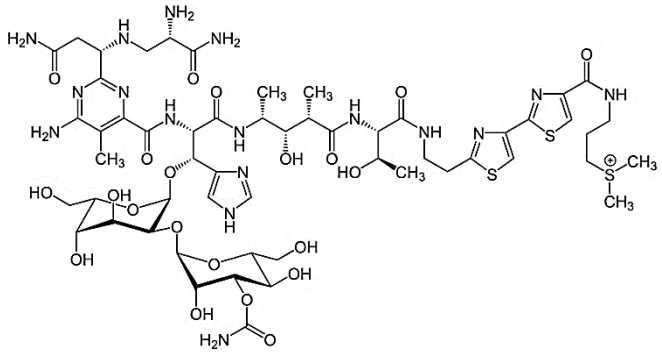

Figure 22. Chemical structure of bleomycin. *A glycopeptide antibiotic natural product isolated from the Gram-positive bacteria Streptomyces verticillus.*

Bleomycin is a water-soluble glycopeptide with cytotoxic activity against bacteria and eukaryotic cells. Its mechanism of action involves single- and double-strand scission of DNA

which leads to the subsequent inhibition of DNA synthesis, of cell division, and ultimately of tumour growth.

The therapeutic indications of bleomycin include solid and haematological malignancies such as squamous cell carcinoma of the head and neck, testicular cancer, and Hodgkin's disease. It is typically administered parenterally but local injection directly into the tumour may occasionally be indicated (73). Bleomycin is rapidly distributed in bodily tissues with highest concentrations achieved in the skin, lungs, and lymph nodes with low concentrations seen in bone marrow. Pulmonary fibrosis can result from bleomycin therapy.

4.2 Results

Before preceding to photochemical treatments, it was first pertinent to assess the performance of the new PCI drug candidates as standalone therapies within the 3D *in vitro* model. MDA-MB-231 and MCF-7 human breast cancer cells were cultured in 3D collagen hydrogels and exposed to various concentrations (0.5-250,000 nM) of chemotherapeutic compounds from several different drug classes. Following 18 h of drug exposure, cellular viability was then measured at 48 h and 72 h time-points. The performance of these compounds as standalone therapies serve as baseline experiments to further pursue protocols involving photochemical treatment.

4.2.1 Control cell viability

MDA-MB-231 and MCF-7 human breast cancer cells were cultured in 3D collagen hydrogels and their negative/no treatment control (henceforth referred to as 'control') cellular viability determined at the end of the two experimentation protocols (48 h and 72 h) using a cell viability assay that measures metabolic activity via ATP quantification.

4.2.1.1 MDA-MB-231 & MCF-7 cells – 48 h vs 72 h

Figure 23 displays that the MDA-MB-231 48 h control group had a higher viability (RLU; Mean ± Standard Error [SE]) than the 72 h control group; however, this difference was found *not* to be statistically significant ($p = 0.490$). With regard to MCF-7 control viability, Figure 23 shows that the 48 h group also had a higher viability than the 72 h group; however, once again, this difference was *not* statistically significant ($p = 0.123$).

Upon comparison of MDA-MB-231 and MCF-7 cells at the 48 h endpoint, a significant ($p < 0.001$) difference in control viability was observed (Figure 23). Furthermore, MDA-MB-231 control cells had around 1.5-fold higher overall viability (RLU; mean ± SE) than MCF-7 cells at the end of the 48 h experimentation period.

Pertaining to the 72 h experimental protocol, a significant increase ($p = 0.001$) in control cell viability was observed for MDA-MB-231 cells versus MCF-7 cells (Figure 23). More specifically, MDA-MB-231 control cells had around a 2-fold higher overall viability (RLU; mean ± SE) than MCF-7 cells at the end of the 72 h experimentation period.

4.2.1.2 Results summary

In summary, MDA-MB-231 control cells have a higher overall viability (RLU; mean ± SE) than MCF-7 cells at the end of both 48 h and 72 h experimentation protocols (Figure 23). However, when considering each cell line separately, there was no statistically significant difference in cell viability between their 48 h and 72 h experimental groups.

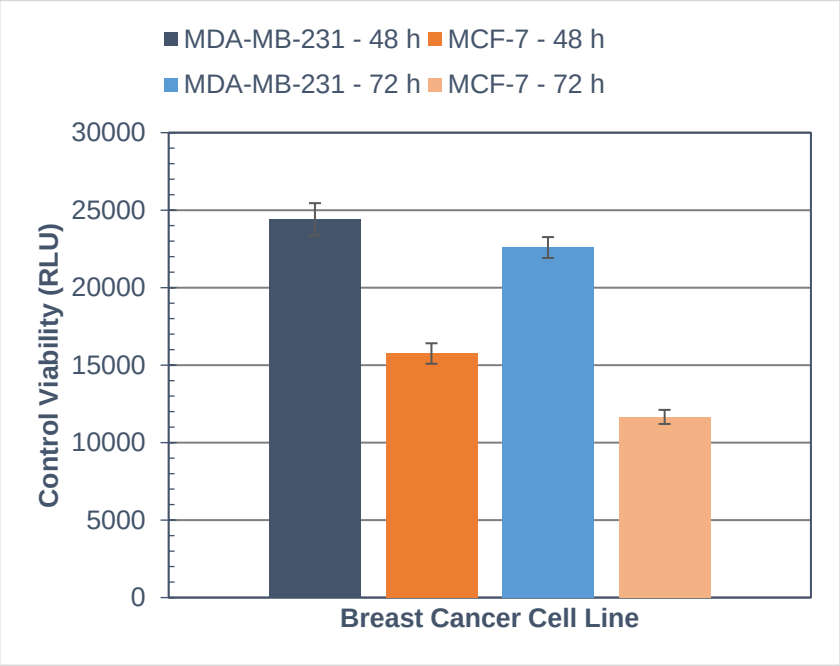

Figure 23. Summary of variation in breast cancer cell line control viability in 3D collagen hydrogels*. Cellular viability (Relative Light Units [RLU]) of MDA-MB-231 and MCF-7 breast cancer controls (untreated cells).*

4.2.2 Chemotherapy cytotoxicity

MDA-MB-231 and MCF-7 human breast cancer cells were cultured in 3D collagen hydrogels and exposed to various chemotherapy treatments. Many of these chemotherapeutic agents are clinically indicated for breast cancer treatment and are found in four broad therapeutic drug classes: (i) glycopeptide antibiotics (bleomycin – which is also a key chemotherapeutic for use in PCI studies (53)); (ii) vinca alkaloids (vinorelbine; vincristine; vinblastine); (iii) taxanes (paclitaxel; docetaxel); and, (iv) anti-metabolites (gemcitabine; capecitabine). Treatment effects were determined at both 48 h and 72 h endpoints (for a more detailed description of treatment sequence, please refer to Figure 15 within Chapter 3).

NB. The 48 h and 72 h time-points outlined here match the 48 h and 72 h endpoints used in later light-treatment experiments (where they are designated 48 h and 72 h "post-illumination"). More specifically, the sequence and timing of chemotherapeutic administration, removal, and wash phases, etc., matches exactly that of the later PCI experiments, although, here, the photosensitiser administration and red light irradiation elements of PCI treatment are negated. Cytotoxicity experiments are subsequently reported as percentage of their respective controls (% Control) rather than their raw RLU values which are less useful when attempting to ascertain treatment effects.

4.2.1.1 Bleomycin

4.2.1.1.1 MDA-MB-231 cells

First of the chosen chemotherapy drugs to be tested in the 3D *in vitro* breast cancer models was the glycopeptide antibiotic and archetypical PCI drug bleomycin. The effect of bleomycin chemotherapy (at various concentrations from 0.5-250,000 nM) on the triple-negative MDA-MB-231 breast cancer cell line was determined at 48 h and 72 h time-points and is shown in Figure 24. Here, a significant difference ($p = 0.023$) in MDA-MB-231 cell viability reduction was observed between the 48 h and 72 h experimental groups. In addition, bleomycin concentration had a significant effect ($p < 0.001$) on the cell viability reduction within each experimental group.

Pertaining to the *potency* of bleomycin therapy within this 3D *in vitro* model, the IC_{50} of bleomycin was found to be 12,500 nM and 2,250 nM for 48 h and 72 h groups, respectively. Moreover, the 72 h group achieved greater treatment potency at all of the concentrations tested. With regards to treatment *efficacy,* cellular viability at the maximum tested concentration of 250,000 nM (E_{max}) was found to reduce MDA-MB-231 cell viability to 16% (±1%) and 16% (±2%) for 48 h and 72 h, respectively.

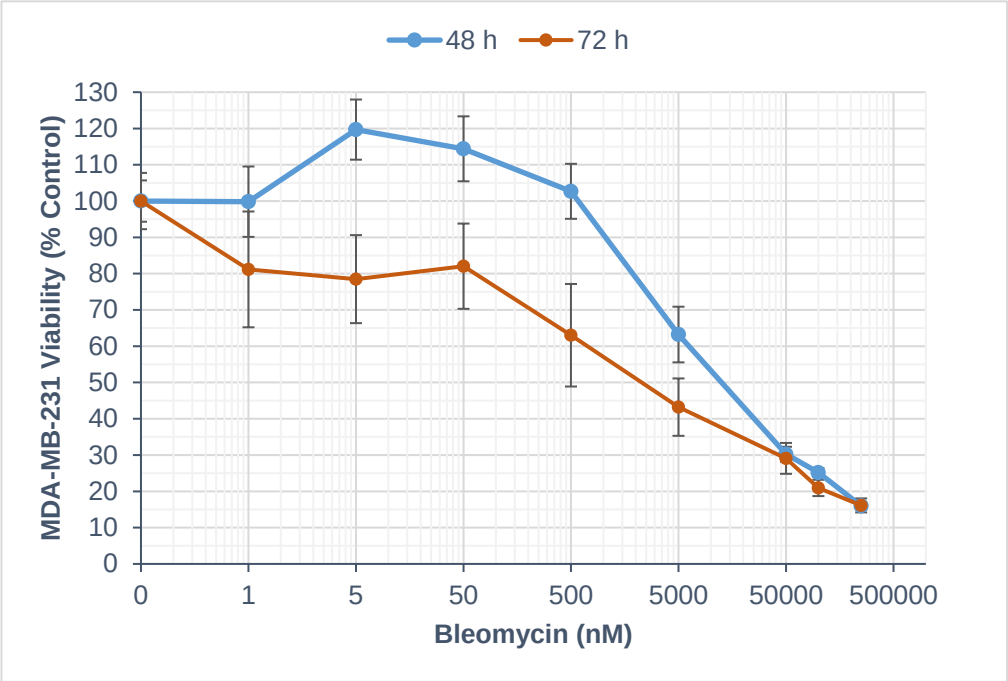

Figure 24. Reduction of MDA-MB-231 breast cancer cell viability in 3D collagen hydrogels after exposure to bleomycin chemotherapy*. Relative cell viability (% Control) of MDA-MB-231 cells following 18 h incubation with bleomycin (0.5-250,000 nM).*

4.2.1.1.2 MCF-7 cells

With regards to the oestrogen-receptor positive MCF-7 cell line, cell viability following bleomycin treatment at various concentrations (0.5-250,000 nM) and measured at 48 h and 72 h time-points is shown in Figure 25.

Here, a significant difference ($p = 0.002$) in MCF-7 cell viability reduction between the 48 h and 72 h groups was observed. Furthermore, bleomycin concentration had a significant effect ($p < 0.001$) on cell viability reduction within each experimental group.

With regards to treatment potency and efficacy, the IC_{50} of bleomycin was estimated to be 700 nM and 3 nM for 48 h and 72 h groups, respectively. Moreover, the 72 h group

generally achieved a greater treatment potency at all of the concentrations tested. In addition, it was found that the maximum tested concentration of 250,000 nM reduced cell viability to 10% (±1%) and 13% (±1%) for 48 h and 72 h, respectively.

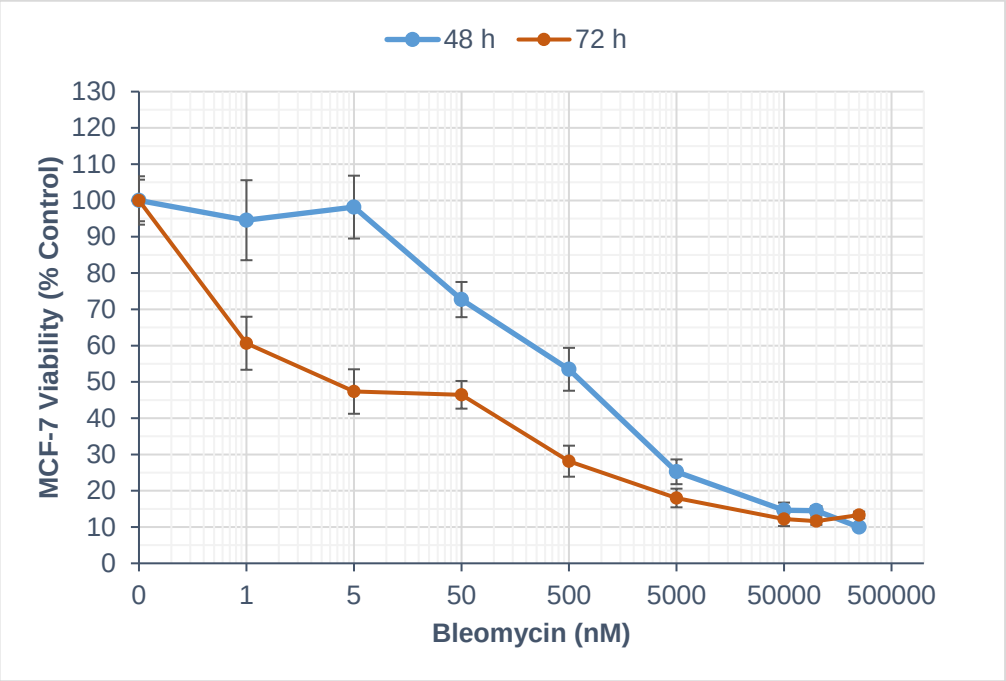

Figure 25. Reduction of MCF-7 breast cancer cell viability in 3D collagen hydrogels after exposure to bleomycin chemotherapy*. Relative cell viability (% Control) of MCF-7 cells following 18 h incubation with bleomycin (0.5-250,000 nM).*

4.2.1.2 Vinca Alkaloids

4.2.1.2.1 Vinorelbine

4.2.1.2.1.1 MDA-MB-231 cells

The first of the "new" potential PCI candidates tested in the 3D *in vitro* breast cancer model was the vinca alkaloid vinorelbine. Figure 26 displays the cell viability of MDA-MB-231 breast cancer cells following vinorelbine treatment at various concentrations (0.5-250,000 nM) measured both at 48 h and 72 h time-points.

Here, a significant difference ($p < 0.001$) in MDA-MB-231 cell viability reduction was observed between the 48 h and 72 h experimental groups. Vinorelbine concentration had a significant effect ($p < 0.001$) on cell viability reduction within each experimental group.

The IC_{50} of vinorelbine therapy was found to be 100 nM and 0.35 nM for 48 h and 72 h experimental groups, respectively. Furthermore, a greater treatment potency was observed at all of the tested concentrations for the 72 h group. It was also observed that both experimental groups saw a characteristic peak in MDA-MB-231 cell viability between 5,000-50,000 nM. In addition, cellular viability following treatment at the maximum tested concentration of 250,000 nM was found to be 0% of control in both 48 h and 72 h experimental groups.

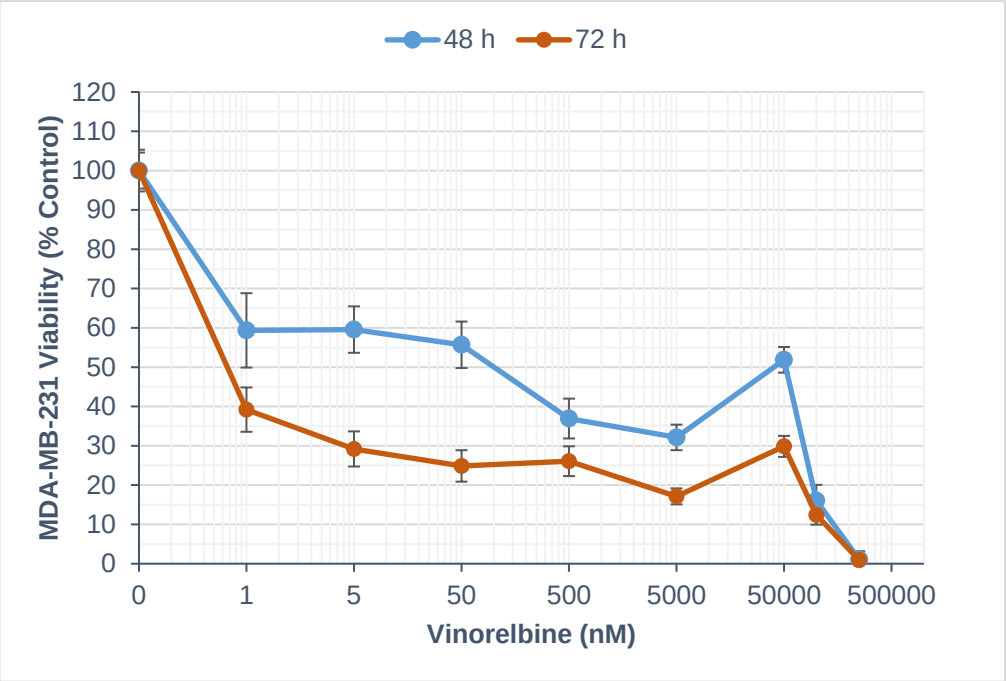

Figure 26. Reduction of MDA-MB-231 breast cancer cell viability in 3D collagen hydrogels after exposure to vinorelbine chemotherapy*. Relative cell viability (% Control) of MDA-MB-231 cells following 18 h incubation with vinorelbine (0.5-250,000 nM).*

4.2.1.2.1.2 MCF-7 cells

Vinorelbine treatment at various concentrations (0.5-250,000 nM) with endpoint measurement at 48 h and 72 h time-points, is shown in Figure 27. Here, it was observed that MCF-7 cell viability reduction was *not* significantly different ($p = 0.072$) between 48 h and 72 h groups despite the increased treatment potency seen in the 72 h group. In addition, vinorelbine concentration was found to have a significant effect ($p < 0.001$) on cell viability reduction within each experimental group.

With regards to treatment potency, the IC_{50} of vinorelbine was determined to be 7.5 nM and 0.35 nM for the 48 h and 72 h groups, respectively. At the maximum tested concentration of 250,000 nM, MCF-7 cell viability was observed to be 0% of control in both 48 h and 72 h experimental groups.

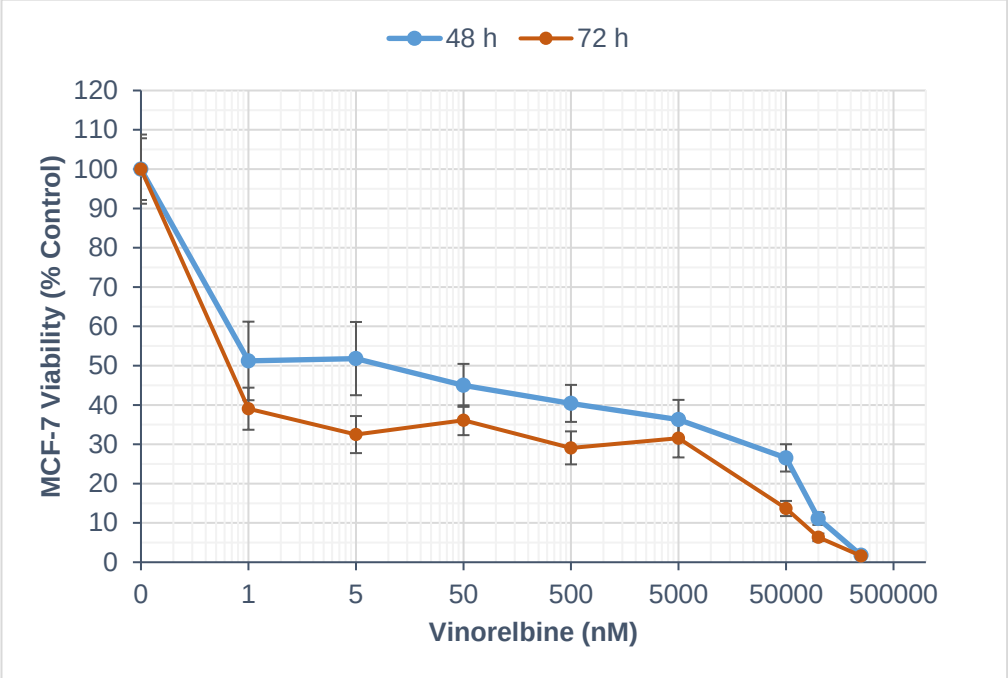

Figure 27. Reduction of MCF-7 breast cancer cell viability in 3D collagen hydrogels after exposure to vinorelbine chemotherapy. *Relative cell viability (% Control) of MCF-7 cells following 18 h incubation with vinorelbine (0.5-250,000 nM).*

4.2.1.2.2 Vincristine

4.2.1.2.2.1 MDA-MB-231 cells

The second chemotherapy drug from the vinca alkaloid class to be tested in the 3D *in vitro* model was vincristine. Here, the same range of treatment concentrations (0.5-250,000 nM) were utilised as with previous experiments and their effect on MDA-MB-231 cell viability determined after 48 h and 72 h time-points (Figure 28).

These experiments saw a significant difference (p = 0.001) in MDA-MB-231 cell viability reduction between the 48 h and 72 h groups. Moreover, vincristine concentration was found to have a significant effect ($p < 0.001$) on cell viability reduction within each experimental group.

The IC_{50} of vincristine was found to be 1,500 nM and 0.30 nM for 48 h and 72 h groups, respectively. In addition, a notable increase in MDA-MB-231 cell viability was observed in both experimental groups between 5,000-250,000 nM; with a particularly steep increase seen between 50,000-250,000 nM in the 72 h group. With regards to vincristine treatment efficacy, the maximum tested concentration of 250,000 nM was found to reduce cell viability to 59% (±7%) and 52% (±10%) for 48 h and 72 h groups, respectively.

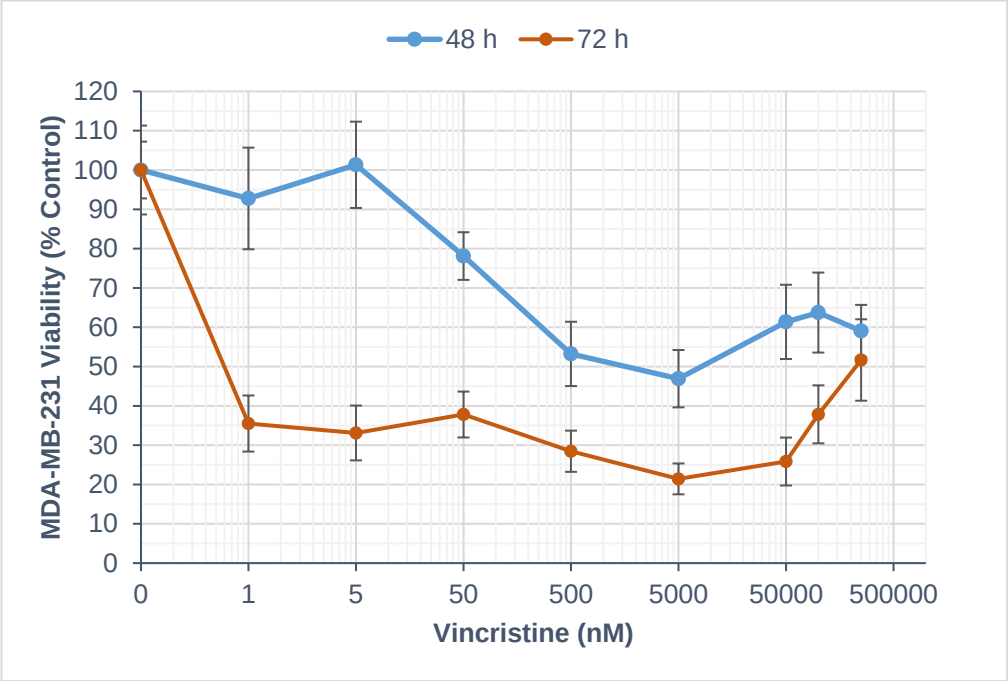

Figure 28. Reduction of MDA-MB-231 breast cancer cell viability in 3D collagen hydrogels after exposure to vincristine chemotherapy*. Relative cell viability (% Control) of MDA-MB-231 cells following 18 h incubation with vincristine (0.5-250,000 nM).*

4.2.1.2.2.2 MCF-7 cells

The effect on MCF-7 cell viability of vincristine treatment at various concentrations (0.5-250,000 nM) after 48 h and 72 h is shown in Figure 29.

Here, a non-significant difference (p = 0.078) in MCF-7 cell viability reduction was observed between the 48 h and 72 h experimental protocols despite the increased treatment potency seen in the 72 h group. Furthermore, vincristine concentration had a significant effect (p < 0.001) on cell viability reduction within each experimental group.

The IC_{50} of vincristine was estimated to be 2.25 nM and 0.35 nM for 48 h and 72 h groups, respectively. At the maximum tested concentration of 250,000 nM, MCF-7 cell viability was reduced to 18% (±2%) and 15% (±2%) after 48 h and 72 h, respectively.

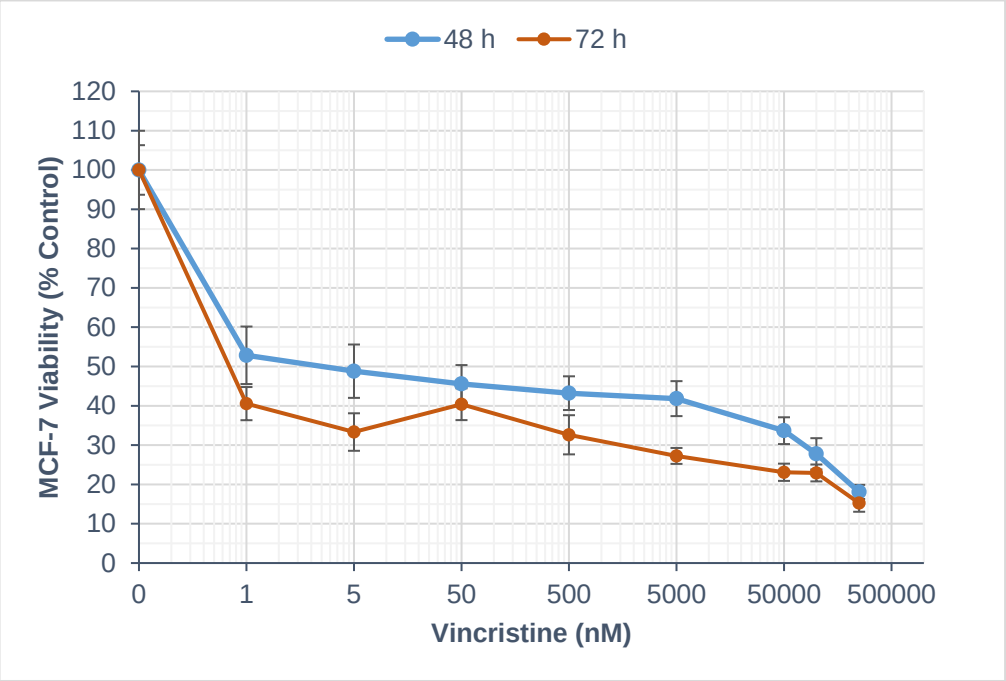

Figure 29. Reduction of MCF-7 breast cancer cell viability in 3D collagen hydrogels after exposure to vincristine chemotherapy*. Relative cell viability (% Control) of MCF-7 cells following 18 h incubation with vincristine (0.5-250,000 nM).*

4.2.1.2.3 Vinblastine

4.2.1.2.3.1 MDA-MB-231 cells

Vinblastine was the third chemotherapy drug to be tested from the vinca alkaloid class – and fourth drug overall. The viability of MDA-MB-231 cells following vinblastine treatment at various concentrations (0.5-250,000 nM) was determined at 48 h and 72 h time-points (Figure 30).

From these experiments, it was determined that there was *not* a significant difference (p = 0.139) in MDA-MB-231 cell viability reduction between the 48 h and 72 h experimental groups. In addition, vinblastine concentration had a significant effect (p < 0.001) on cell viability reduction within each experimental group.

The IC_{50} of vinblastine was estimated to be 75,000 nM and 85 nM for the 48 h and 72 h groups, respectively. At the maximum tested concentration of 250,000 nM, vinblastine

treatment was found to be maximally-efficacious in both 48 h and 72 h experimental groups given that MDA-MB-231 cell viability was reduced to 0% of control.

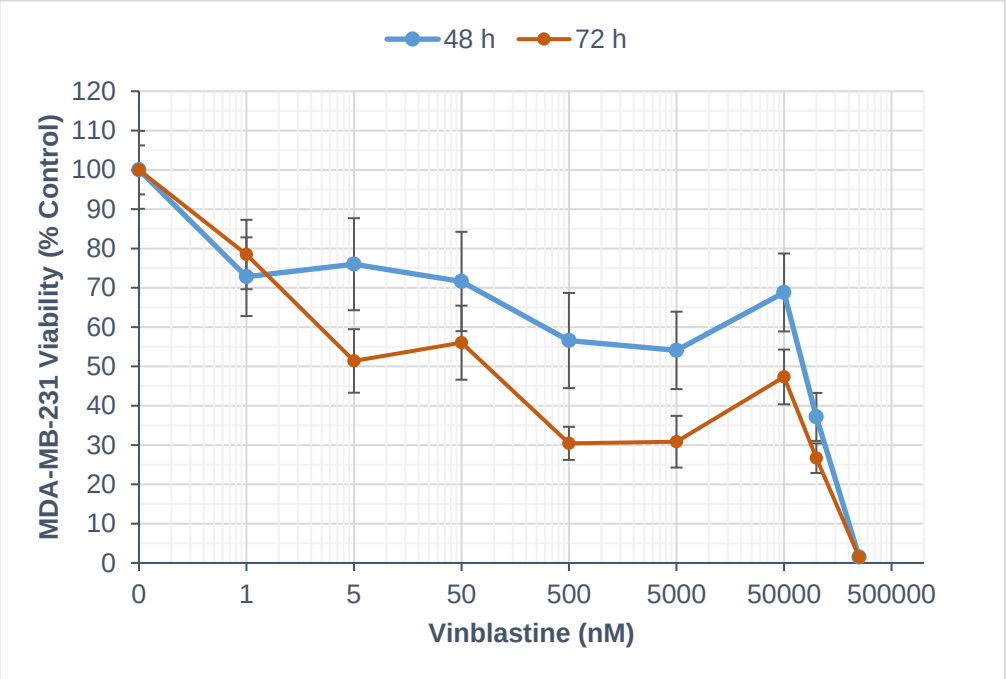

Figure 30. Reduction of MDA-MB-231 breast cancer cell viability in 3D collagen hydrogels after exposure to vinblastine chemotherapy*. Relative cell viability (% Control) of MDA-MB-231 cells following 18 h incubation with vinblastine (0.5-250,000 nM).*

4.2.1.2.3.2 MCF-7 cells

The effect of vinblastine chemotherapy (0.5-250,000 nM) on MCF-7 cells is displayed in Figure 31 following viability measurements at 48 h and 72 h time-points.

Here, a significant difference (p =< 0.001) in MCF-7 cell viability reduction was observed between the 48 h and 72 h groups. In addition, vinblastine concentration had a significant effect (p < 0.001) on cell viability reduction within each experimental group.

Pertaining to chemotherapy potency at these different time-points, the IC_{50} of vinblastine was found to be 750 nM and 0.325 nM for 48 h and 72 h groups, respectively. At the maximum tested concentration of 250,000 nM, vinblastine was maximally-efficacious in both 48 h and 72 h experimental groups given that chemotherapy reduced MCF-7 cell viability to 0% of control.

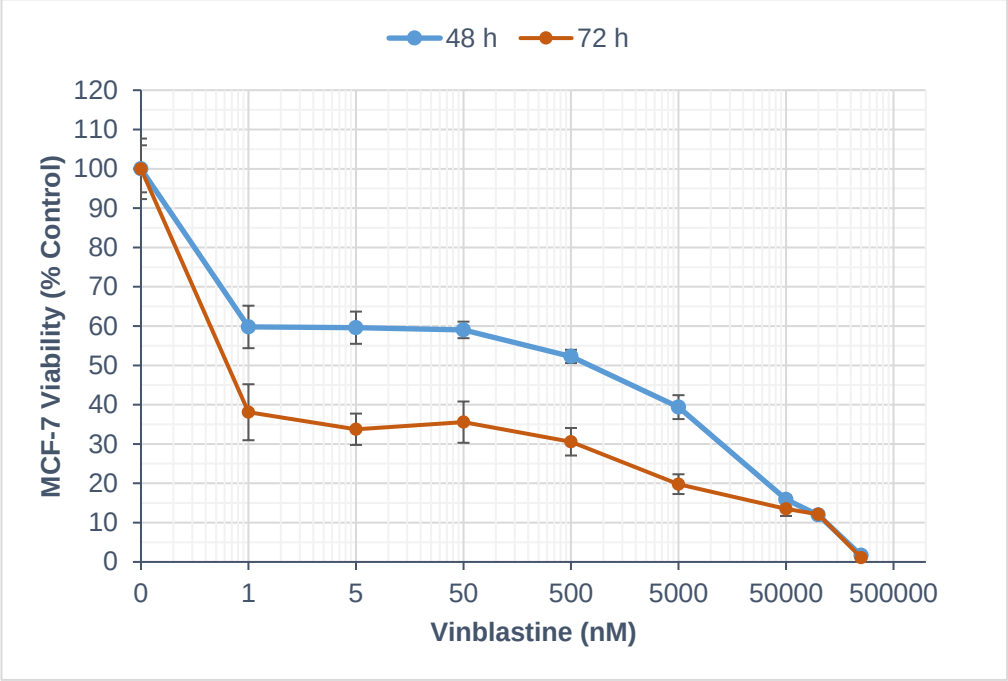

Figure 31. Reduction of MCF-7 breast cancer cell viability in 3D collagen hydrogels after exposure to vinblastine chemotherapy*. Relative cell viability (% Control) of MCF-7 cells following 18 h incubation with vinblastine (0.5-250,000 nM).*

4.2.1.3 Taxanes

4.2.1.3.1 Docetaxel

4.2.1.3.1.1 MDA-MB-231 cells

The next major group of chemotherapeutics to be investigated in the 3D *in vitro* breast cancer models were the taxanes. Firstly, docetaxel was to be tested and Figure 32 displays MDA-MB-231 cell viability following docetaxel chemotherapy treatment at various concentrations (0.5-250,000 nM) measured at 48 h and 72 h time-points.

Here, there was *not* a significant difference (p = 0.877) in MDA-MB-231 cell viability reduction observed between the 48 h and 72 h groups. Furthermore, docetaxel concentration was seen to have a significant effect (p < 0.001) on cell viability reduction within each experimental group.

With regard to chemotherapeutic potency, the IC_{50} of docetaxel was estimated to be 35,000 nM and was 22,500 nM for 48 h and 72 h groups, respectively. At the highest tested concentration of 250,000 nM, docetaxel was maximally-efficacious in both 48 h and 72 h experimental groups given its reduction of MDA-MB-231 cell viability to 0% of control.

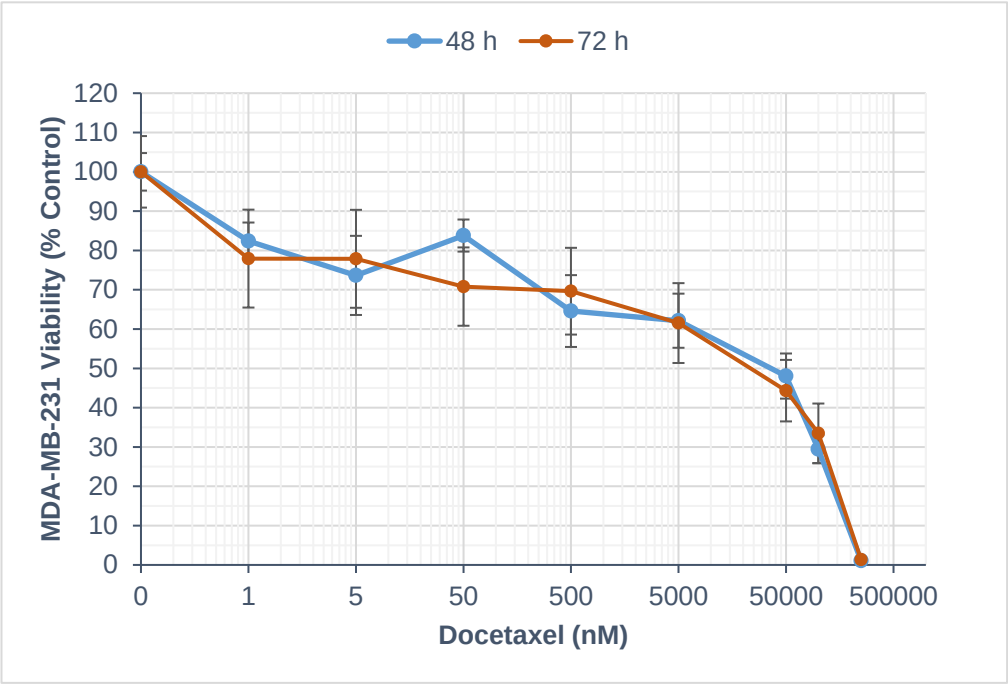

Figure 32. Reduction of MDA-MB-231 breast cancer cell viability in 3D collagen hydrogels after exposure to docetaxel chemotherapy*. Relative cell viability (% Control) of MDA-MB-231 cells following 18 h incubation with docetaxel (0.5-250,000 nM).*

4.2.1.3.1.2 MCF-7 cells

The MCF-7 cell line was also exposed to docetaxel chemotherapy at various concentrations from 0.5-250,000 nM and its cytotoxic effects measured at 48 h and 72 h time-points (as shown in Figure 33).

Here, a significant difference (p = 0.011) in MCF-7 cell viability reduction *was* observed between the 48 h and 72 h groups. Furthermore, docetaxel concentration had a significant effect ($p < 0.001$) on cell viability reduction within each experimental group.

The IC_{50} of docetaxel was determined to be 0.35 nM and 2,000 nM for 48 h and 72 h groups, respectively. Thus, the IC_{50} of paclitaxel was considerably lower in the 48 h group than the 72 h group. Pertaining to treatment efficacy at the maximum tested concentration of 250,000 nM, docetaxel chemotherapy reduced cell viability to 11% (±4%) and 9% (±2%) for 48 h and 72 h groups, respectively.

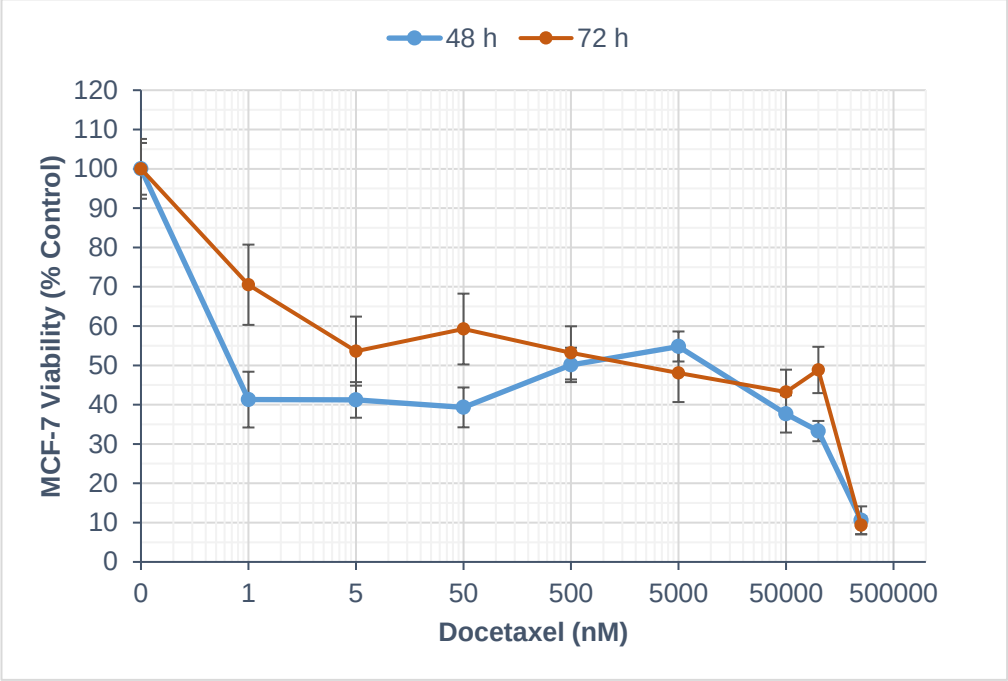

Figure 33. Reduction of MCF-7 breast cancer cell viability in 3D collagen hydrogels after exposure to docetaxel chemotherapy*. Relative cell viability (% Control) of MCF-7 cells following 18 h incubation with docetaxel (0.5-250,000 nM).*

4.2.1.3.2 Paclitaxel

4.2.1.3.2.1 MDA-MB-231 cells

The next taxane chemotherapeutic to be tried was paclitaxel which was tested at the same range of concentrations (0.5-250,000 nM) and measured at 48 h and 72 h time-points (as shown in Figure 34), as with previous experiments.

Here, there was *not* a significant difference ($p = 0.432$) in MDA-MB-231 cell viability reduction found between the 48 h and 72 h groups. It was also observed that chemotherapy had a greater potency at several concentrations (50-5,000 nM) in the 48 h group. In addition, paclitaxel concentration *did* have a significant effect ($p < 0.001$) on cell viability reduction within each experimental group.

The IC_{50} of paclitaxel was determined as 110,000 nM and 70,000 nM for 48 h and 72 h groups, respectively. With regards to treatment efficacy at the maximum tested concentration of 250,000 nM, cell viability was reduced to 27% (±2%) and 12% (±2%) for 48 h and 72 h groups, respectively.

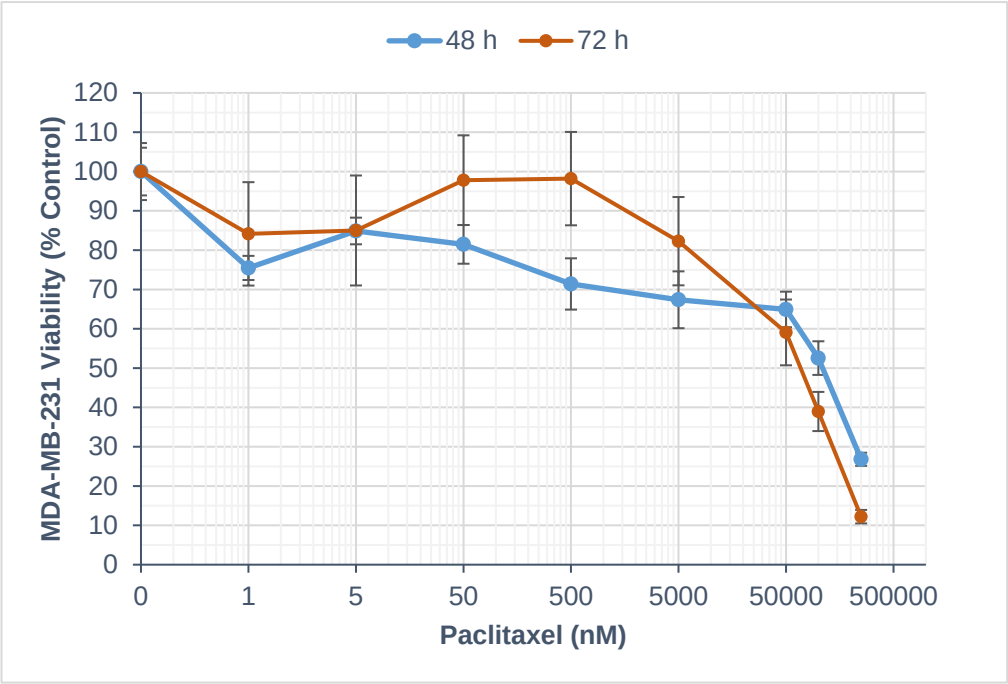

Figure 34. Reduction of MDA-MB-231 breast cancer cell viability in 3D collagen hydrogels after exposure to paclitaxel chemotherapy*. Relative cell viability (% Control) of MDA-MB-231 cells following 18 h incubation with paclitaxel (0.5-250,000 nM).*

4.2.1.3.2.2 MCF-7 cells

Paclitaxel chemotherapy (0.5-250,000 nM) was then tested in the MCF-7 cell line at 48 h and 72 h time-points (as shown in Figure 35).

In these experiments, a significant difference (p = 0.003) in MCF-7 cell viability reduction was observed between the 48 h and 72 h groups. Furthermore, it was determined that paclitaxel concentration had a significant effect ($p < 0.001$) on cell viability reduction within each experimental group.

Pertaining to chemotherapeutic potency, the IC_{50} of paclitaxel was estimated to be 0.75 nM and 7,500 nM for 48 h and 72 h groups, respectively. Thus, the IC_{50} of paclitaxel was considerably lower in the 48 h group than the 72 h group. It was also observed that the 48 h group achieved a greater cell viability reduction (and with less variance) across all concentrations versus the 72 h group. In addition, and with regards to treatment efficacy, cell viability was reduced to 28% (±2%) and 32% (±5%) for 48 h and 72 h groups, respectively, at the maximum tested concentration of 250,000 nM.

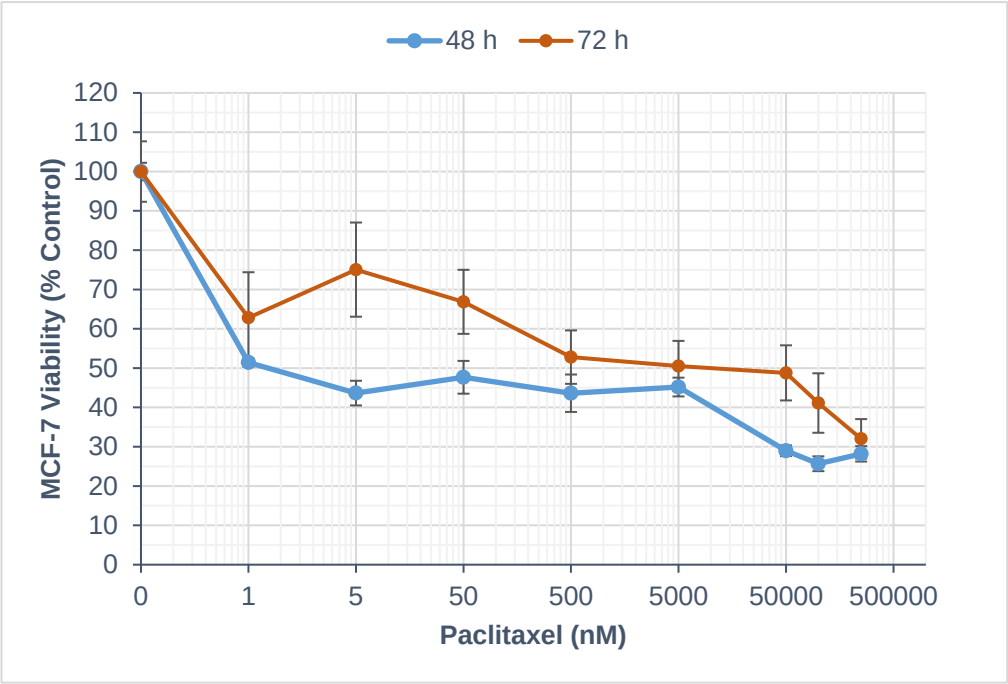

Figure 35. Reduction of MCF-7 breast cancer cell viability in 3D collagen hydrogels after exposure to paclitaxel chemotherapy*. Relative cell viability (% Control) of MCF-7 cells following 18 h incubation with paclitaxel (0.5-250,000 nM).*

4.2.1.4 Anti-metabolites

4.2.1.4.1 Gemcitabine

4.2.1.4.1.1 MDA-MB-231 cells

Following on from the cytotoxic experiments involving the glycopeptide antibiotic bleomycin, vinca alkaloids, and taxanes, the last chemotherapeutic drug class from which drugs would be tested in the 3D *in vitro* breast cancer models was the antimetabolites. To begin with, gemcitabine, and its cytotoxic effects (0.5-250,000 nM) were measured at 48 h and 72 h time-points (as shown in Figure 36).

These cytotoxic experiments exhibited a significant difference (p = 0.001) in MDA-MB-231 cell viability reduction between the 48 h and 72 h groups. Furthermore, gemcitabine concentration had a significant effect (p < 0.001) on cell viability reduction within each experimental group.

The IC_{50} of gemcitabine was *not attained* for the 48 h group and was 12.5 nM for 72 h group, respectively. Moreover, gemcitabine chemotherapy was observed to be more potent across most concentrations in the 72 h group when compared with the 48 h group. At the

maximum tested concentration of 250,000 nM, gemcitabine chemotherapy reduced cell viability to 56% (±6%) and 38% (±4%) for 48 h and 72 h groups, respectively.

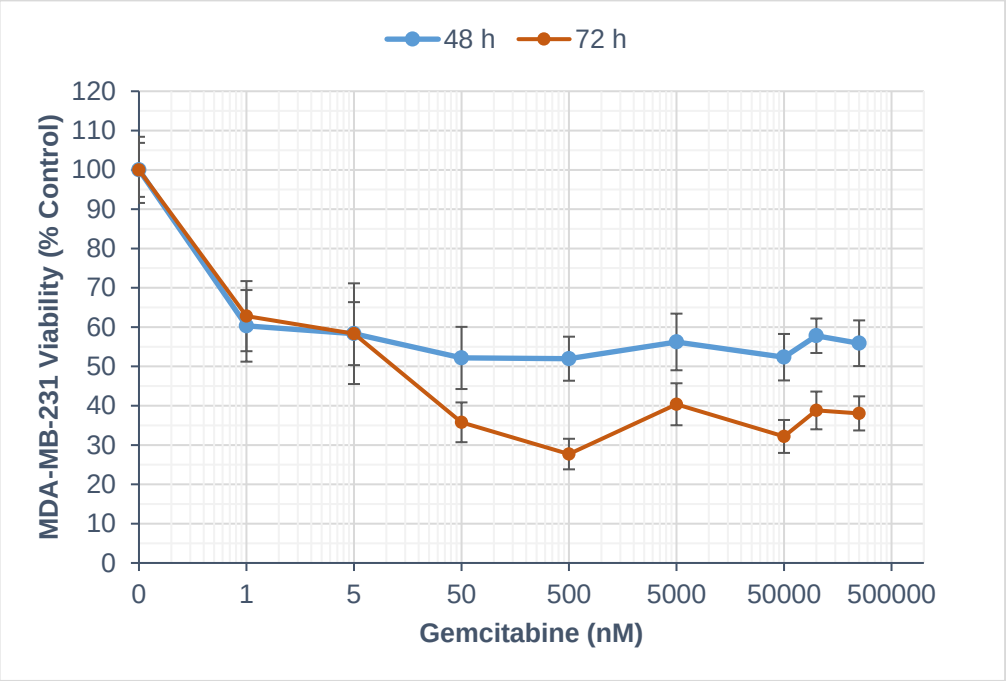

Figure 36. Reduction of MDA-MB-231 breast cancer cell viability in 3D collagen hydrogels after exposure to gemcitabine chemotherapy*. Relative cell viability (% Control) of MDA-MB-231 cells following 18 h incubation with gemcitabine (0.5-250,000 nM).*

4.2.1.4.1.2 MCF-7 cells

Gemcitabine chemotherapy was then investigated in the MCF-7 cell line at the same range of concentrations (0.5-250,000 nM) and with end-point measurements at 48 h and 72 h (shown in Figure 37).

Here, a significant difference ($p < 0.001$) in MCF-7 cell viability reduction *was* observed between the 48 h and 72 h groups. In addition, gemcitabine concentration had a significant effect ($p < 0.001$) on cell viability reduction within each experimental group.

With regards to gemcitabine potency, the IC_{50} of gemcitabine was found to be 40 nM and 0.35 nM for 48 h and 72 h groups, respectively. At the highest tested concentration of 250,000 nM, gemcitabine chemotherapy reduced MCF-7 cell viability to 52% (±5%) and 32% (±4%) for 48 h and 72 h groups, respectively.

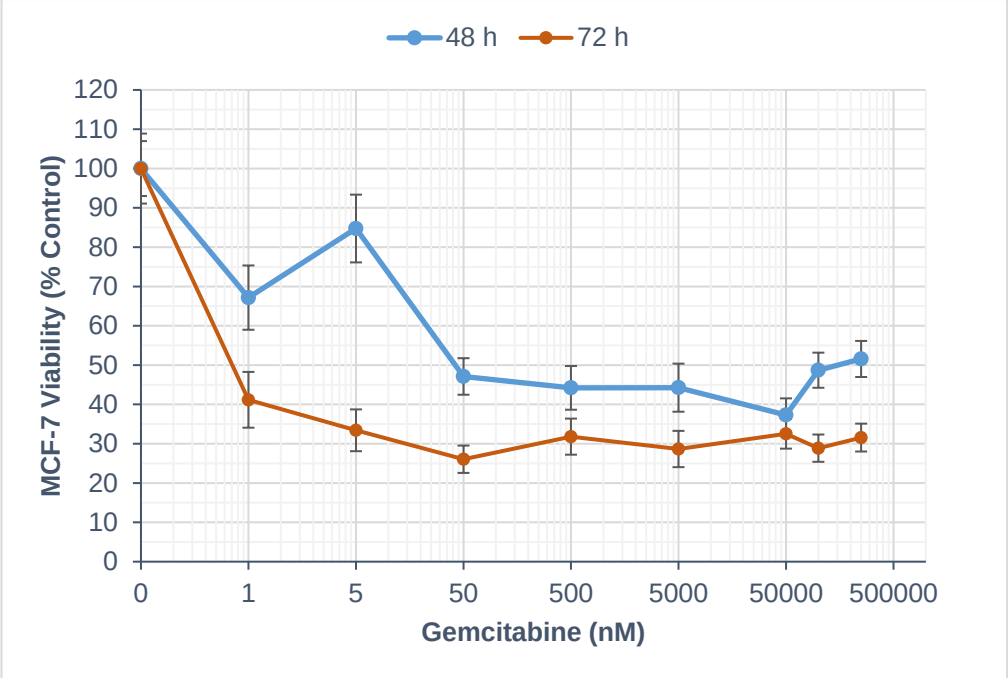

Figure 37. Reduction of MCF-7 breast cancer cell viability in 3D collagen hydrogels after exposure to gemcitabine chemotherapy*. Relative cell viability (% Control) of MCF-7 cells following 18 h incubation with gemcitabine (0.5-250,000 nM).*

4.2.1.4.2 Capecitabine

4.2.1.4.2.1 MDA-MB-231 cells

Capecitabine was the second antimetabolite and final chemotherapeutic drug to be investigated in the 3D *in vitro* breast cancer models. The cytotoxicity of capecitabine (0.5-250,000 nM) on MDA-MB-231 cells with end-point measurements at 48 h and 72 h is shown in Figure 38.

These experiments did *not* demonstrate a significant difference (p = 0.484) in MDA-MB-231 cell viability reduction between 48 h and 72 h groups. Furthermore, capecitabine concentration did *not* have a significant effect (p = 0.682) on cell viability reduction within either experimental group.

With regards to chemotherapeutic potency, the IC_{50} was *not attained* for either 48 h or 72 h groups for capecitabine. At the maximum tested concentration of 250,000 nM, MDA-MB-231 cell viability was reduced to 93% (±9%) and 90% (±13%) for 48 h and 72 h groups, respectively.

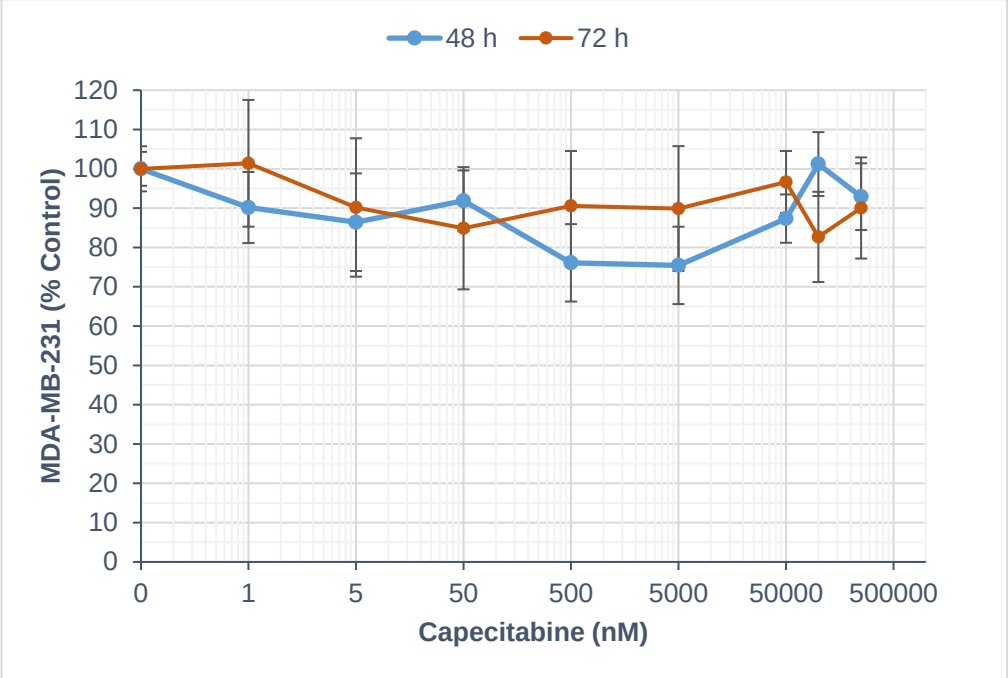

Figure 38. Reduction of MDA-MB-231 breast cancer cell viability in 3D collagen hydrogels after exposure to capecitabine chemotherapy*. Relative cell viability (% Control) of MDA-MB-231 cells following 18 h incubation with capecitabine (0.5-250,000 nM).*

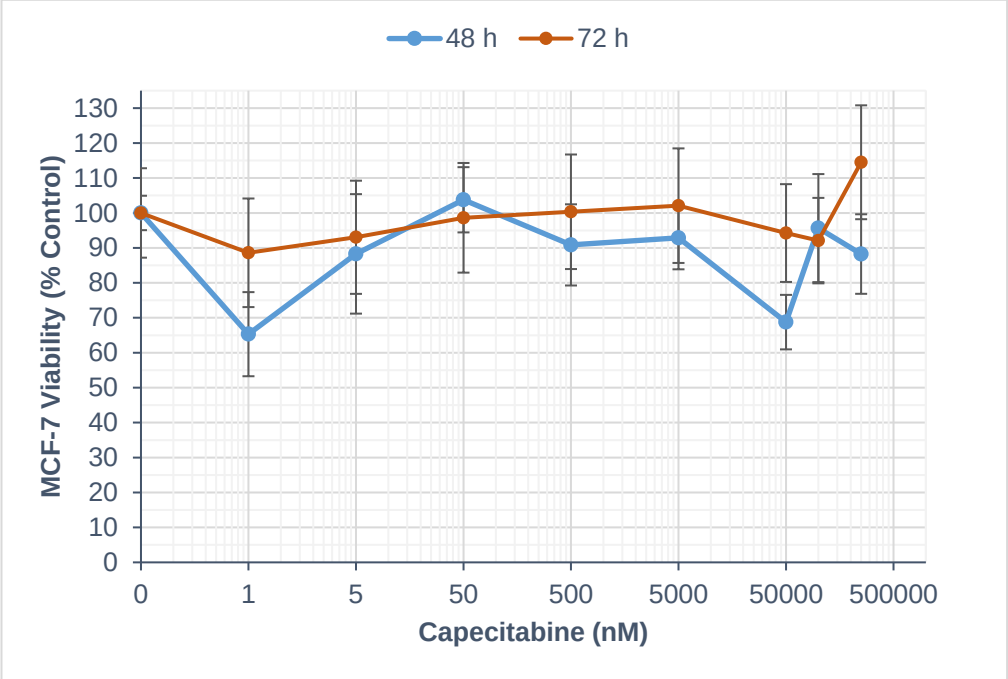

Figure 39. Reduction of MCF-7 breast cancer cell viability in 3D collagen hydrogels after exposure to capecitabine chemotherapy*. Relative cell viability (% Control) of MCF-7 cells following 18 h incubation with capecitabine (0.5-250,000 nM).*

4.2.1.4.2.2 MCF-7 cells

Next, MCF-7 cells were exposed to capecitabine chemotherapy at various concentrations from 0.5-250,000 nM and cell viability measured at 48 h and 72 h time-points (as shown in Figure 39).

Here, there was *not* a significant difference ($p = 0.245$) in MCF-7 cell viability reduction observed between the 48 h and 72 h groups. Moreover, capecitabine concentration did *not* have a significant effect ($p = 0.232$) on cell viability reduction within each experimental group.

The IC_{50} of capecitabine was *not attained* for either 48 h or 72 h groups. Pertaining to treatment efficacy at the highest tested concentration of 250,000 nM, cell viability was determined to be 88% (±11%) and 115% (±16%) for 48 h and 72 h groups, respectively.

4.2.3 Results Summary

4.2.3.1 IC_{50} and E_{max}

In summary, key treatment effects (IC_{50}; E_{max}) were identified from the chemotherapy cytotoxicity profiles for each drug for both 48 h and 72 h time-points (Table 2). Namely, the treatment IC_{50} (indicative of drug *potency*), which is defined as the concentration of drug at which response is half (50%) its theoretical maximum (which is 0%); whereby the E_{max} (indicative of drug *efficacy*), is the value of cell viability at the maximum drug concentration tested (here, 250,000 nM).

4.2.3.2 Maximum Drug Potency and Efficacy

The most potent drugs against MDA-MB-231 cells were vinorelbine and vincristine for the 48 h and 72 h protocols, respectively (as shown in Table 3). The most efficacious chemotherapy drugs against MDA-MB-231 cells were vinorelbine, vinblastine, and docetaxel for both 48 h and 72 h experimental groups.

Pertaining to the MCF-7 cell line, the most potent chemotherapy drugs were docetaxel and vinblastine for the 48 h and 72 h protocols, respectively (Table 3). The most efficacious chemotherapy drugs against MCF-7 cells were vinorelbine, and vinblastine for both 48 h and 72 h experimental groups.

Table 2. Summary of IC_{50} and E_{max} values from various treatment conditions on MDA-MB-231 and MCF-7 human breast cancer cells in 3D collagen hydrogels.

Cell line & Characteristics	Chemotherapy Drug Class	Chemotherapy Drug	Endpoint (h)	IC_{50} (nM)	E_{max} (% C [±SE])
MDA-MB-231: human breast adenocarcinoma of metastatic origin; triple negative; basal B; claudin low; invasive; tumorigenic	Glycopeptides	Bleomycin	48	12,500	16 (±1)
	Vinca alkaloids	Vinorelbine		100	0 (±0.2)
		Vincristine		1,500	59 (±7)
		Vinblastine		75,000	0 (±0.3)
	Taxanes	Docetaxel		35,000	0 (±0.2)
		Paclitaxel		110,000	27 (±2)
	Antimetabolites	Gemcitabine		-	56 (±6)
		Capecitabine		-	93 (±9)
	Glycopeptides	Bleomycin	72	2,250	16 (±2)
	Vinca alkaloids	Vinorelbine		0.35	0 (±0.2)
		Vincristine		0.30	52 (±10)
		Vinblastine		85	0 (±0.3)
	Taxanes	Docetaxel		22,500	0 (±0.3)
		Paclitaxel		70,000	12 (±2)
	Antimetabolites	Gemcitabine		12.5	38 (±4)
		Capecitabine		-	90 (±13)
MCF-7: human breast adenocarcinoma of metastatic origin; oestrogen receptor+; luminal A	Glycopeptides	Bleomycin	48	700	10 (±1)
	Vinca alkaloids	Vinorelbine		7.5	0 (±0.1)
		Vincristine		2.25	18 (±2)
		Vinblastine		750	0 (±0.3)
	Taxanes	Docetaxel		0.35	11 (±4)
		Paclitaxel		0.75	28 (±2)
	Antimetabolites	Gemcitabine		40	52 (±5)
		Capecitabine		-	88 (±11)
	Glycopeptides	Bleomycin	72	3	13 (±1)
	Vinca alkaloids	Vinorelbine		0.35	0 (±0.1)
		Vincristine		0.35	15 (±2)
		Vinblastine		0.325	0 (±0.3)
	Taxanes	Docetaxel		2,000	9 (±2)
		Paclitaxel		7,500	32 (±5)
	Antimetabolites	Gemcitabine		0.35	32 (±4)
		Capecitabine		-	115 (±16)

***Table 3.** Summary of the most potent and efficacious chemotherapy treatments on MDA-MB-231 and MCF-7 human breast cancer cells in 3D collagen hydrogels.*

Cell line	Most Potent				Most Efficacious			
	48 h		72 h		48 h		72 h	
	Drug Class	Drug	Drug Class	Drug	Drug Class	Drug	Drug Class	Drug
MDA-MB-231	Vinca alkaloids	Vinorelbine	Vinca alkaloids	Vincristine	Vinca alkaloids	Vinorelbine	Vinca alkaloids	Vinorelbine
					Vinca alkaloids	Vinblastine	Vinca alkaloids	Vinblastine
					Taxanes	Docetaxel	Taxanes	Docetaxel
MCF-7	Taxanes	Docetaxel	Vinca alkaloids	Vinblastine	Vinca alkaloids	Vinorelbine	Vinca alkaloids	Vinorelbine
					Vinca alkaloids	Vinblastine	Vinca alkaloids	Vinblastine

4.3 Discussion

In total, eight chemotherapy drugs were evaluated for their activity against two human breast cancer cell lines (MCF-7 and MDA-MB-231 (93,100)) within a 3D collagen type I *in vitro* model. This activity was ascertained by means of a luminescence assay (CellTiter-Glo®) that measures ATP activity (i.e. metabolic activity) – the amount of ATP is directly proportional to the number of viable cells present in culture and is, thus, a biomarker for cell viability (165). Importantly, previous studies have utilised this assay in order to report cytotoxicity evaluations with breast cancer cells in this kind of *anchorage-dependent* 3D model (119).

The two human breast cancer cell lines were chosen for several reasons including their differing molecular characteristics, responses to chemotherapy, and prognosis at the clinical level. Broadly-speaking, each respective cell line represents a breast cancer subtype which, clinically, retain very different clinical behaviours and available treatment options.

The MCF-7 cell line is representative of *luminal A* breast cancer and has the following characteristic biological properties: oestrogen receptor-positive (ER+), progesterone receptor-negative (PR-), human epidermal growth factor receptor-negative (HER-). In general, luminal A breast carcinomas are Ki67 low (a proliferation marker), responsive to endocrine therapy (as the oestrogen receptor is a therapeutic target; e.g. tamoxifen), and are responsive to chemotherapy (100).

By contrast, the MDA-MB-231 cell line is representative of triple-negative breast cancer (TNBC) as it lacks all three of the aforementioned receptors (ER, PR, and HER2) – all of which are recognised therapeutic targets. Due to the lack of a recognised therapeutic target, triple-negative disease is more difficult to treat, more biologically aggressive, and is often associated with a poor prognosis (100). More specifically, MDA-MB-231 cells are categorised as a *claudin-low* breast cancer which, along with the *basal* subtype, make up the triple-negative breast cancer classifications. In fact, MDA-MB-231 cells were initially clustered with the basal subtype due to their triple-negative phenotype but were recently found (along with some other breast cell lines) to retain unique features sufficient enough to warrant reclassification (179). Other general features of claudin-low breast carcinomas include low

Ki67, E-cadherin, claudin-4, claudin-4 and claudin-7; with an intermediate response to chemotherapy (100).

In relation to cellular responses to chemotherapy, MDA-MB-231 cells were indeed much more resistant to cytotoxic drug treatment than were MCF-7 cells (Table 2). For example, with regard to those chemotherapeutic agents that were tested and explicitly cited as recommended treatments for advanced breast cancer in the clinical setting (namely: docetaxel, vinorelbine, capecitabine), the IC_{50} value of docetaxel was 100,000-fold (48 h) and 11-fold (72 h) less potent, and vinorelbine was 13-fold less potent (48 h) and equipotent (72 h) in MDA-MB-231 cells versus MCF-7 cells, respectively. Capecitabine was seen to perform poorly in both breast cancer cell lines and did not achieve an IC_{50} at either 48 h or 72 h time-points. One potential reason for this could be that this small, water-soluble drug preferred to accumulate within the ECM provided by the 3D hydrogel structure.

Interestingly, *in vitro* models of TNBC (and patient samples) have demonstrated elevated metabolic activity versus ER+ breast cancer cell lines (180); and this activity has been correlated with therapeutic resistance (181). This was also borne out by our data upon consideration of the aforementioned IC_{50} values and the fact that untreated control MDA-MB-231 cells were seen to have a significantly ($p \leq 0.001$) higher viability compared to their MCF-7 counterparts at both 48 h and 72 h time-points (Figure 23). Nor was this increase likely due to a higher number of cells as population doubling times are specified to be 38 h and 29 h for MDA-MB-231 and MCF-7 cells, respectively (182,183). A small caveat being that our data was derived from cells grown in 3D culture so changes in these times are theoretically possible. Notwithstanding, recent evidence indicates that TNBC metabolic characteristics such as high glycolytic flux are associated with therapeutic resistance; including resistance to small molecule chemotherapy drugs such as doxorubicin (184).

Another interesting observation was that all three vinca alkaloids (vinorelbine, vincristine, and vinblastine) were each seen to exhibit a distinct ‘peak’ of increased cell viability in MDA-MB-231 cells, beginning at the same concentration of 5,000 nM in both 48 h and 72 h experimental conditions (Figure 26, Figure 28, Figure 30). With regard to vinorelbine and vinblastine (Figure 26, Figure 30), specifically, cell viability increases were observed between

the drug concentrations of 5,000-50,000 nM, before rapidly decreasing again. However, with vincristine (Figure 28), MDA-MB-231 cell viability did not recover to any great extent (48 h) and, in fact, began to increase at an even greater rate after 50,000 nM in the 72 h group. This meant that, despite a 500,000-fold increase in concentration, the highest-tested vincristine concentration (250,000 nM) achieved a 1.4-fold weaker cytotoxic effect than the lowest-tested vincristine concentration (0.5 nM) (MDA-MB-231 viability: 52% [±10%] and 36% [±7%] for 250,000 nM and 0.5 nM, respectively).

Here, it is possible that the collagen ECM might have absorbed some of the drugs at high concentrations although this activity was only observed specifically with the vinca alkaloid drug class and in the MDA-MB-231 cell line. Alternatively, this phenomenon is possibly suggestive of some kind of saturable process of cellular entry for these agents. However, counter to this, it has been posited elsewhere that vinca alkaloid transport into the cell is predominantly influenced by non-saturable, temperature-independent mechanisms akin to simple diffusion (185). Although, notably, the *in vitro* studies cited here were all early experiments preformed in monolayer culture. It is therefore possible that the altered cellular spatial arrangement, cell-cell and cell-matrix interactions afforded by 3D culture, has altered drug uptake or directed drug uptake processes more toward saturable, energy-dependent and temperature-dependent transport processes. Moreover, each vinca agent exhibits different physicochemical properties (e.g. lipophilicity) which, as previously introduced, can also greatly influence the cellular uptake and deposition of the drug. Furthermore, the increased uptake of the drug by *active* processes could eventually lead to its increased accumulation, sequestration, and degradation within endo/lysosomal compartments which could, ultimately, reduce drug efficacy.

Alternatively, the comparatively poor performance of vincristine could result from the fact that 3D-cultured cells are associated with a higher expression of the drug-metabolising enzyme CYP3A4 (186). All of the vinca alkaloids tested in the present study are a substrate of this cytochrome P450 enzyme (185). Crucially, in contrast to vincristine, both vinorelbine and vinblastine are metabolised by CYP3A4 to metabolites that are *more* potent than the parent compounds. It is therefore possible that between 5,000-50,000 nM there was some key disruption in the balance of active/inactive metabolites and drug metabolism, more

generally. Indeed, it is likely that there was a concomitant interplay between both drug uptake and drug metabolism processes which contributed to these interesting features of the respective dose-response profiles.

The taxanes also exhibited comparatively unusual behaviour in the MCF-7 cell line in that their 48 h cytotoxicity was generally greater than their 72 h effect. This could indicate that cells may have been relatively senescent at 48 h before then “reigniting” again and becoming more-viable and multiplying. For example, this behaviour has been observed in MCF-7 cells following treatment with another microtubule-targeting agent (187). Similarly, the cited study only observed this effect in MCF-7 breast cancer cells and not in the cervical carcinoma HeLa cell line that was also tested.

In general, the vinca alkaloids performed very well in all of the conditions and cell lines that were evaluated. Furthermore, the most potent and efficacious drugs in each experimental group (48 h and 72 h), for each breast cancer cell line, aligned very well with the drugs recommended in the clinical setting for advanced breast cancer; in particular, vinorelbine and docetaxel.

Chapter 5: Light Treatments in Breast Cancer

5. Evaluation of Light Treatments in a 3D Model of Breast Cancer *In Vitro*

5.1 Introduction

With regard to *in vitro* PCI investigations with clinically-approved chemotherapeutics, bleomycin has emerged as exceptional candidate for PCI delivery. Although, of the PCI studies published to date, the majority have utilised macromolecular toxins (e.g. gelonin) of seemingly ever-increasing complexity (53). Comparatively few studies have investigated small molecule anticancer chemotherapy drugs; so, one of the primary aims of this work was to redress this.

Following the evaluation of treatment effects from chemotherapy drugs as standalone agents in 3D-cultured breast cancer cells, photochemical treatments were then employed in order to ascertain treatment primacy. This chapter utilises the same chemotherapy drugs as the previous chapter although, here, they are administered as part of a PCI regimen. The same two models of human breast cancer were also employed here. Namely, 3D-cultured MDA-MB-231 TNBC cells and MCF-7 ER+ cells. Each of these types of breast cancer retain different clinical characteristics and, accordingly, have different treatment options and different prognoses.

The chosen photosensitiser (PS) for photochemical studies – aluminium(III) phthalocyanine chloride disulphonic acid, adjacent isomer ($AlPcS_{2a}$) – has previously been used effectively in numerous light treatment studies involving both PDT and PCI therapy in cancer cells (2,19,53). Furthermore, $AlPcS_{2a}$ has been safely used in the clinic as part of a mixed $AlPcS_{2n}$ formulation of tetra- and di-sulphonated derivatives (Photosense®).

First, PDT experiments were conducted and involved $AlPcS_{2a}$ addition to 3D-cultured MDA-MB-231 and MCF-7 cells at various concentrations (0.1-100,000 nM) for 18 h and then exposed to various light doses (660 nm; 0-4 min at 2.0 mW; total light dose/energy density: 0.0-0.48 J/cm^2) before measuring cell viability 48 h post-illumination.

Once PDT parameters had been established, PCI experiments were subsequently undertaken. Photochemical internalisation experimental procedures closely mirrored those

established in the prior evaluation of chemotherapy performance except with the necessary additional steps of $AlPcS_{2a}$ incubation and light irradiation (Figure 16). Specifically, MDA-MB-231 and MCF-7 human breast cancer cells were cultured in 3D collagen hydrogels and exposed to various concentrations (0.5-250,000 nM) of the same range of chemotherapeutic compounds previously tested as standalone agents. However, here, $AlPcS_{2a}$ was co-incubated with each chemotherapeutic for 18 h before light irradiation for 1 min (660 nm; light dose/energy density: 0.12 J/cm^2) and cellular viability measured at 48 h post-illumination.

Then, following these extensive investigations, PCI-drug combinations of therapeutic interest were identified and taken forward to subsequent work involving PCI regimen and model variations (and later, formulation techniques). A second, alternative PCI regimen was investigated for selective chemotherapy drugs which included important sequence changes including chemotherapeutic addition immediately *after* light treatment (that is, a “light-before” regimen). In addition to this, experiments were performed with 3D model parameter variations (namely, hydrogel stiffness and hydrogel volume) with the resulting effects on cytotoxic treatment ascertained.

5.2 Photodynamic therapy (PDT)

5.2.1 $AlPcS_{2a}$

Both human breast cancer cell lines were cultured in 3D and incubated with various $AlPcS_{2a}$ concentrations (0.1-100,000 nM) for 18 h and then exposed to various light doses (660 nm; 1-4 min at 2.0 mW; total light dose/energy density: 0.12-0.48 J/cm^2), as well as, no treatment light before having cell viability endpoint measurements 48 h post-illumination. The inherent cytotoxicity of the PS is known as the ‘dark toxicity’; that is, its cytotoxicity at a given concentration in the absence of light treatment.

5.2.1.1 MDA-MB-231 cells

First, 3D-cultured MDA-MB-231 TNBC cells were exposed to PDT therapy. From these experiments, a significant difference (p = 0.001) in MDA-MB-231 viability reduction *was* observed between the different PDT light dose experimental groups (Figure 40 and Figure

41). Furthermore, the concentration of the $AlPcS_{2a}$ had a significant effect ($p < 0.001$) on cell viability reduction within each experimental group except for dark toxicity ($p = 0.250$).

With regard to PDT potency, $AlPcS_{2a}$ IC_{50} values were *not attained*, 2,800 nM, 2,400 nM, and 325 nM for dark toxicity (0 min), 1 min, 2 min, and 4 min groups, respectively. Pertaining to PDT efficacy at the maximum tested concentration of 100,000 nM, PDT reduced MDA-MB-231 cell viability to 86% (±3%), 27% (±6%), 2% (±1%) and 0% (±0.1%) for the dark toxicity, 1 min, 2 min, and 4 min groups, respectively.

5.2.1.2 MCF-7 cells

Next, oestrogen-receptor positive MCF-7 cells were exposed to the same PDT treatments with effects, once again, measured at 48 h post-illumination. Here, there *was* a significant difference ($p < 0.001$) in MCF-7 viability reduction observed between the different light dose groups (as shown in Figure 42 and Figure 43). Furthermore, the concentration of the $AlPcS_{2a}$ had a significant effect ($p < 0.001$) on cell viability reduction within each experimental group except for dark toxicity ($p = 0.250$).

The IC_{50} values of the $AlPcS_{2a}$ were determined and were found to be *not attained*, 5,750 nM, 2,250 nM, and 275 nM for dark toxicity (0 min), 1 min, 2 min, and 4 min groups, respectively. At the maximum tested concentration of 100,000 nM, PDT reduced MCF-7 viability to 75% (±7%), 23% (±4%), 2% (±1%) and 0% (±0.2%) for the dark toxicity, 1 min, 2 min, and 4 min groups, respectively.

5.2.1.3 Dark toxicity

The dark toxicity of a photosensitiser provides some insight into the expected cellular cytotoxicity to those cells exposed to $AlPcS_{2a}$ but not exposed to light treatment – important when considering, for example, later off-target and adverse effects of systemically-administered drugs in patients.

Figure 40 and Figure 42 (plus, Figure 41 and Figure 43) show the dark toxicity of $AlPcS_{2a}$ in MDA-MB-231 and MCF-7 human breast cancer cells, respectively. Here, it was observed that there was *not* a significant difference ($p = 0.874$) in cell viability reduction between cell lines as a result of dark toxicity treatment. Moreover, $AlPcS_{2a}$ concentration did

not have a significant effect (p = 0.250) on cell viability reduction within each experimental group. With regards to treatment potency, $AlPcS_{2a}$ IC_{50} values were *not attained* in either cell line and the maximum tested concentration of 100,000 nM reduced cell viability to 86% (±3%) and 75% (±7%) for MDA-MB-231 and MCF-7 cell lines, respectively.

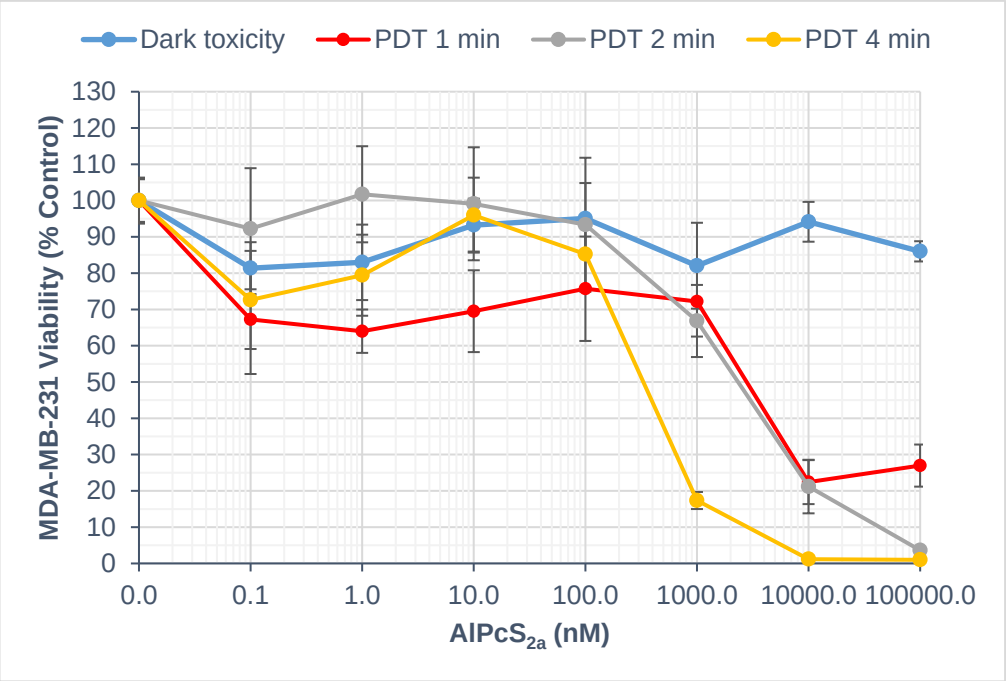

***Figure 40. Reduction of MDA-MB-231 breast cancer cell viability in 3D collagen hydrogels after $AlPcS_{2a}$ PDT exposure**. Relative cellular viability (% of control) of MDA-MB-231 breast cancer cells after PDT treatment at various $AlPcS_{2a}$ concentrations (0.1-100,000 nM).*

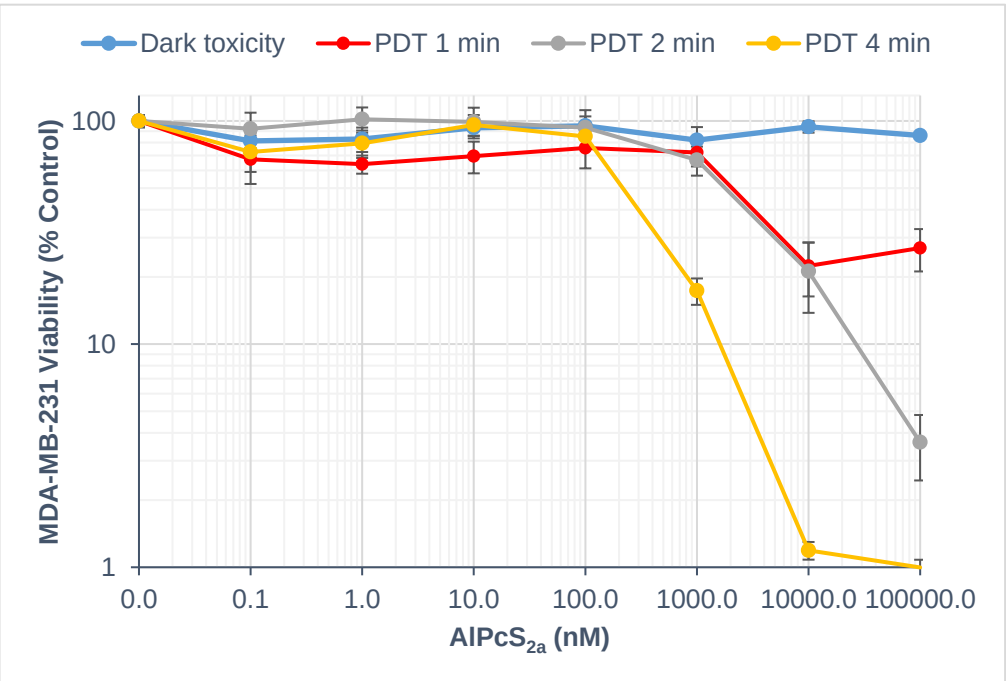

***Figure 41. Reduction of MDA-MB-231 breast cancer cell viability (log scale y-axis) in 3D collagen hydrogels after $AlPcS_{2a}$ PDT exposure**. Relative cellular viability (% of control presented on a log scale) of MDA-MB-231 breast cancer cells after PDT treatment at various $AlPcS_{2a}$ concentrations (0.1-100,000 nM) and light doses (0-4 min).*

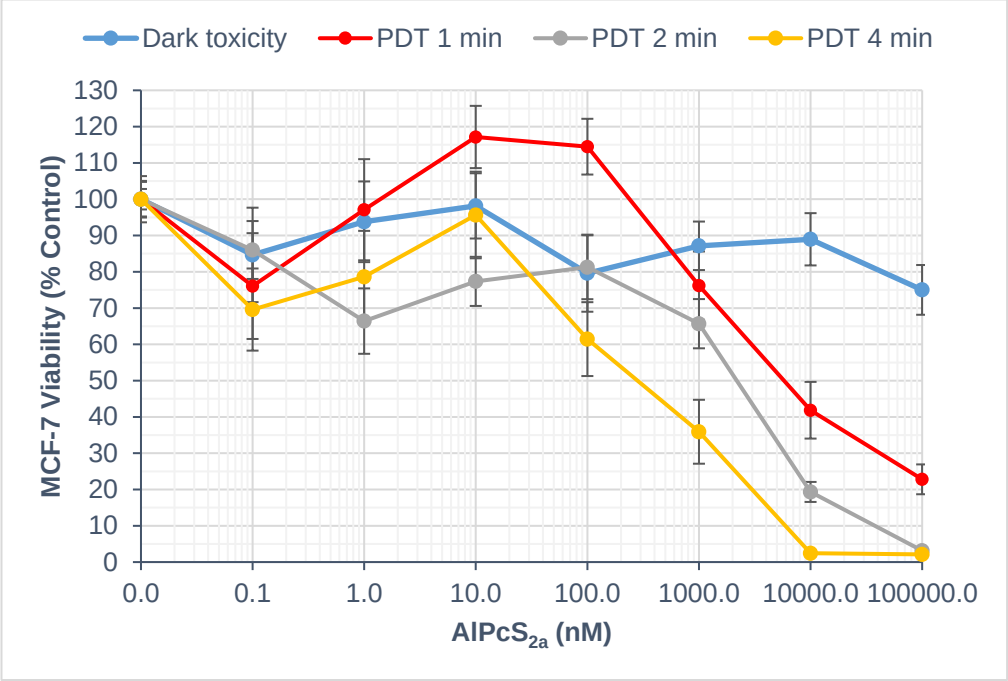

Figure 42. Reduction of MCF-7 breast cancer cell viability in 3D collagen hydrogels after $AlPcS_{2a}$ PDT exposure. *Relative cellular viability (% of control) of MCF-7 breast cancer cells after PDT treatment at various $AlPcS_{2a}$ concentrations (0.1-100,000 nM) and light doses (0-4 min).*

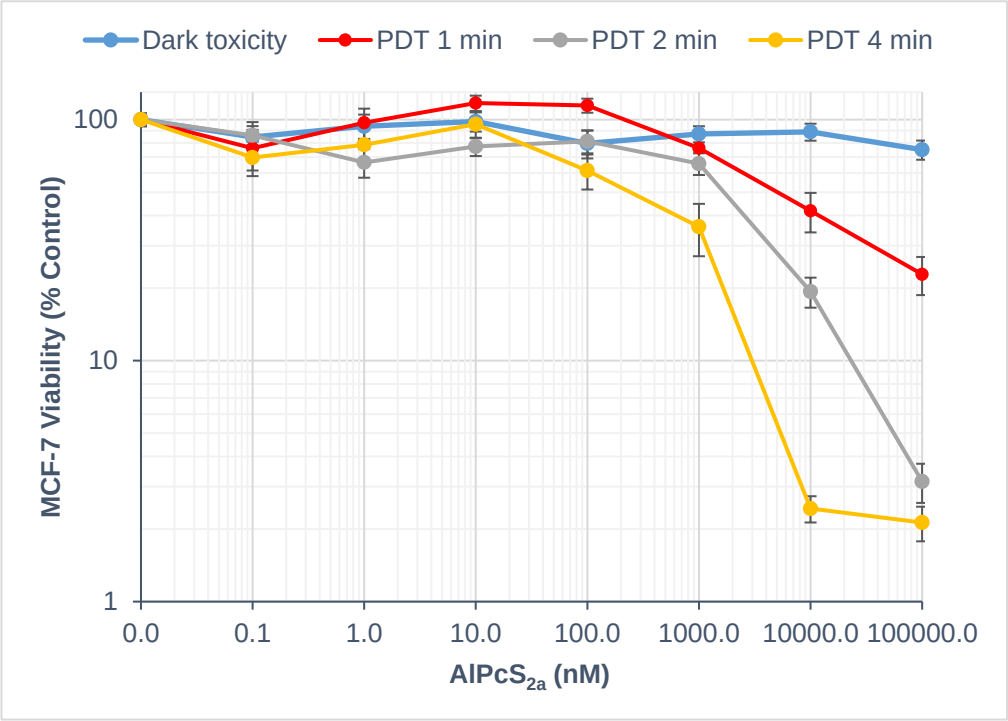

Figure 43. Reduction of MCF-7 breast cancer cell viability (log scale y-axis) in 3D collagen hydrogels after $AlPcS_{2a}$ PDT exposure. *Relative cellular viability (% of control presented on a log scale) of MCF-7 breast cancer cells after PDT treatment at various $AlPcS_{2a}$ concentrations (0.1-100,000 nM) and light doses (0-4 min).*

5.2.2 PDT 1 Minute

5.2.2.1 MDA-MB-231 cells vs MCF-7 cells

The PDT 1 minute treatment schedule was later taken forward to PCI studies for several reasons, including (but not limited to) the fact that the IC_{50} threshold *was* attained in both cell lines and that light fluence rates should be kept to a minimum.

Figure 40 and Figure 42 (plus, Figure 41 and Figure 43) also show the effect of PDT 1 minute treatment on MDA-MB-231 and MCF-7 cells. Here, it was observed that there *was* a significant difference ($p = 0.016$) in cell viability reduction between cell lines across the full range of concentrations tested (0.1-100,000 nM). Furthermore, $AlPcS_{2a}$ concentration had a significant effect ($p < 0.001$) on cell viability reduction within each experimental group.

The IC_{50} of $AlPcS_{2a}$ was estimated to be 2,800 nM and 5,750 nM for MDA-MB-231 and MCF-7 cell lines, respectively. At the highest tested concentration of 100,000 nM, PDT 1 min treatment reduced cell viability to 27% (±6%) and 23% (±4%) for MDA-MB-231 and MCF-7 cell lines, respectively.

5.2.3 $AlPcS_{2a}$ PDT Concentrations for Future PCI Studies

The dose of the photochemical ("PDT") component used in PCI studies appears to vary quite significantly. However, cytotoxic levels of around 15-50% from the PDT component appear most common (168,188). Due to 3D models having previously been shown to impact upon cytotoxicity, PDT doses were set toward the high end of this range in order to give PCI the highest probability of improving treatment outcomes.

On the basis of the PDT experiments carried out thus far, this would limit the range of $AlPcS_{2a}$ concentrations eligible to be taken forward to future PCI studies to all but the highest three tested concentrations (1,000 nM, 10,000 nM, & 100,000 nM; Figure 44). Subsequently, statistical analysis was performed and it was determined that there was *not* a significant difference ($p = 0.444$) in cell viability reduction at these concentrations between each cell line as a result of PDT 1 min treatment. In addition, $AlPcS_{2a}$ concentration *did* have a significant effect ($p < 0.001$) on cell viability reduction within each experimental group (i.e. cell line).

As shown previously in the present study, photosensitiser ($AlPcS_{2a}$) IC_{50} values were 2,800 nM and 5,750 nM for MDA-MB-231 and MCF-7 cell lines, respectively, and at the maximum tested concentration of 100,000 nM, PDT 1 min treatment reduced cell viability to 27% (±6%) and 23% (±4%) for MDA-MB-231 and MCF-7 cell lines, respectively.

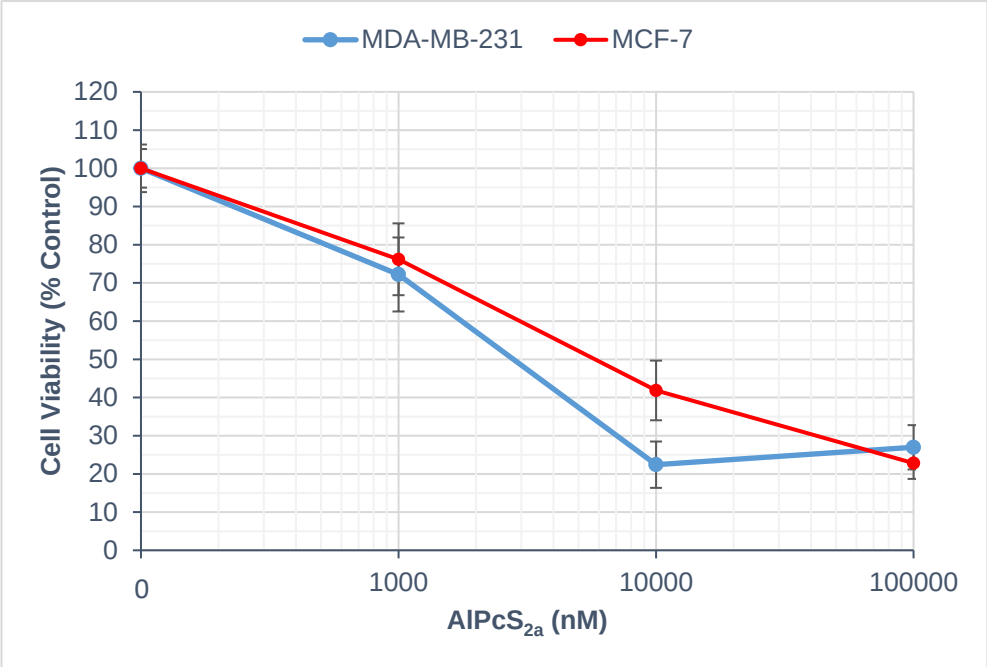

Figure 44. Reduction in MDA-MB-231 and MCF-7 breast cancer cell viability in 3D collagen hydrogels after $AlPcS_{2a}$ PDT treatment for 1 minute at concentrations for PCI studies. *Relative cellular viability (% of control) of MDA-MB-231 and MCF-7 breast cancer cells after $AlPcS_{2a}$ PDT treatment at 1,000 nM, 10,000 nM, and 100,000 nM with 1 min light irradiation.*

5.3 Photochemical Internalisation (PCI)

5.3.1 Overview

Previous PDT experiments in this chapter outlined the therapeutic indices of $AlPcS_{2a}$ within the 3D *in vitro* breast cancer models. This knowledge was then combined with information pertaining to $AlPcS_{2a}$ concentrations and PDT doses that have previously been reported in the PCI literature (189) in order to arrive at an appropriate $AlPcS_{2a}$ concentration and PDT dose for the present PCI studies. This PDT component was then combined (at a fixed dose) with the chemotherapeutic agents outlined in Chapter 4 (which were administered at various concentrations from 0.5-250,000 nM).

More specifically, MDA-MB-231 and MCF-7 human breast cancer cells were cultured in 3D collagen hydrogels and co-incubated with chemotherapy drugs at various concentrations (0.5-250,000 nM) and $AlPcS_{2a}$ 5 µg/mL (~6,800 nM) for 18 h before exposure to 1 min light

irradiation (660 nm; 1 min at 2.0 mW; total light dose/energy density: 0.12 J/cm^2). Cell viability was then measured at 48 h post-illumination. This PCI protocol constitutes the "conventional" PCI regimen. NB. Here, in order to allow for the full elucidation of any therapeutic benefit from PCI, treatment potency values are reported as the IC_{70} (wherever possible) due to the aforementioned fact that the PDT element was targeted to achieve around the $IC_{50\text{-}65}$. However, it should be noted that the PDT "$IC_{50\text{-}65}$" dose being carried forward to PCI experiments (as determined from Figure 44), was actually achieved as a standalone therapy. It is possible, therefore, that the co-incubation of PS and chemotherapy drug(s) during PCI experimentation could have some bearing on this PDT effect.

5.3.2 Red Light

Prior to commencing PCI studies, it was first important to ascertain whether any significant interaction existed between cancer cell viability and the red light dosage to be used (660 nm; 1 min at 2.0 mW; total light dose/energy density: 0.12 J/cm^2). More specifically, it was tested whether the red light dosage resulted in a significant *increase* in cancer cell viability which could be indicative of stimulating cell growth (190).

5.3.2.1 MDA-MB-231 cells vs MCF-7 cells

Below, the cell viabilities of both breast cancer cell lines are shown (Figure 45) following exposure to treatment with red light and compared to their respective controls. These experiments demonstrated that there was *not* a significant difference in cell viability between control and red light experimental groups for both MDA-MB-231 (p = 0.866) and MCF-7 (p = 0.991) cell lines.

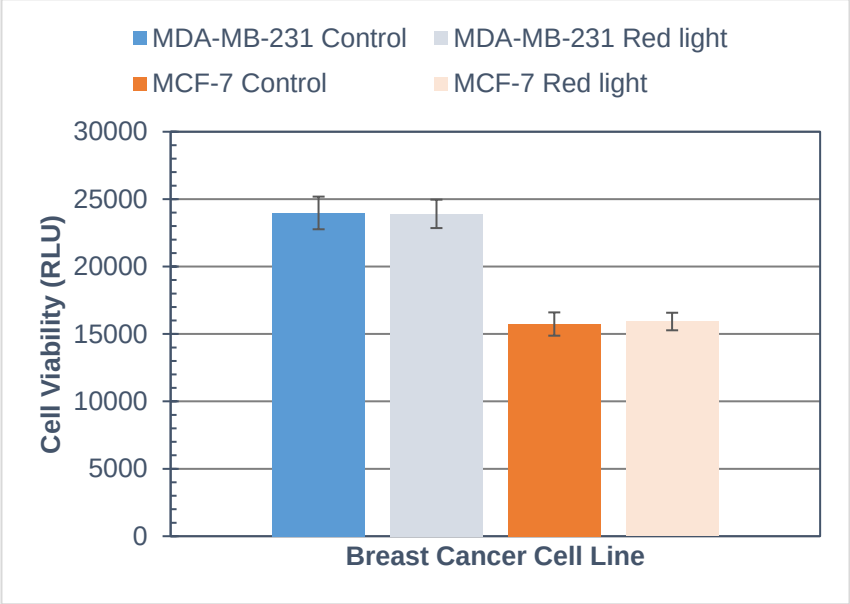

***Figure 45. Breast cancer cell line viability in 3D collagen hydrogels after exposure to red** light. Cellular viability (Relative Light Units [RLU]) of MDA-MB-231 and MCF-7 breast cancer cells after exposure to red light.*

5.3.3 Bleomycin

5.3.3.1 Chemotherapy vs PCI

5.3.3.1.1 MDA-MB-231 cells

PCI experimentation began with the investigation of the model PCI chemotherapeutic drug bleomycin. The bleomycin-PCI dose-response profile was then compared with the performance of its bleomycin chemotherapy counterpart experiment (as shown in Figure 46). These experiments saw a significant difference ($p = 0.049$) in cell viability reduction between chemotherapy and PCI experimental groups. Furthermore, the concentration of bleomycin had a significant effect ($p < 0.001$) on cell viability reduction within each experimental group.

The $AlPcS_{2a}$ (5 µg/mL) PDT control conducted alongside these PCI experiments reduced cell viability to 76% (±6%). With regard to PCI treatment potency, the IC_{70} of bleomycin was found to be 50,000 nM for the chemotherapy group and 27,500 nM for the PCI group, respectively. This represents a 1.8-fold reduction in IC_{70} value in favour of the PCI group. With regard to treatment efficacy at the highest tested concentration of 250,000 nM, cell viability was reduced to 16% (±1%) and 6% (±0%) for chemotherapy and PCI groups, respectively. This represents a 2.7-fold increase in treatment efficacy at 250,000 nM for the

PCI group. In addition, a notable increase in cell viability was observed at low bleomycin concentrations between approximately 0.5-50 nM in both treatment groups.

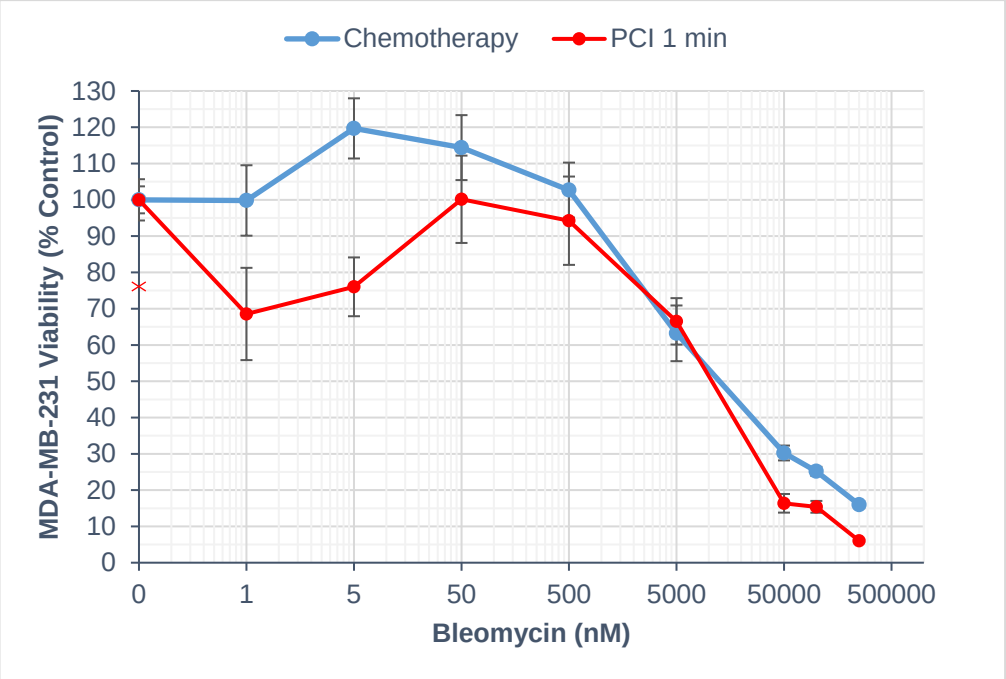

Figure 46. Reduction in MDA-MB-231 breast cancer cell viability in 3D collagen hydrogels after bleomycin chemotherapy and bleomycin PCI*. Relative cellular viability (% of control) of MDA-MB-231 cells after chemotherapy and PCI treatment at various bleomycin concentrations (0.5-250,000 nM).*

5.3.3.1.2 MCF-7 cells

Next, MCF-7 cells were exposed to bleomycin-PCI and treatment effects compared with bleomycin chemotherapy (as shown in Figure 47). Here, a significant difference ($p < 0.001$) in cell viability reduction was observed between chemotherapy and PCI experimental groups. Furthermore, the concentration of bleomycin had a significant effect ($p < 0.001$) on cell viability reduction within each experimental group.

The $AlPcS_{2a}$ (5 µg/mL) PDT control conducted alongside these PCI experiments reduced cell viability to 68% (±4%). The IC_{70} of the bleomycin treatments was estimated to be 3,500 nM for the chemotherapy group and 750 nM for the PCI group, respectively. This represents a 4.7-fold reduction in IC_{70} in favour of PCI. Pertaining to treatment efficacy at the highest tested concentration of 250,000 nM, cell viability was reduced to 10% (±1%) and 5% (±0%) for chemotherapy and PCI groups, respectively. This signifies a 2-fold increase in treatment efficacy at 250,000 nM for the PCI group.

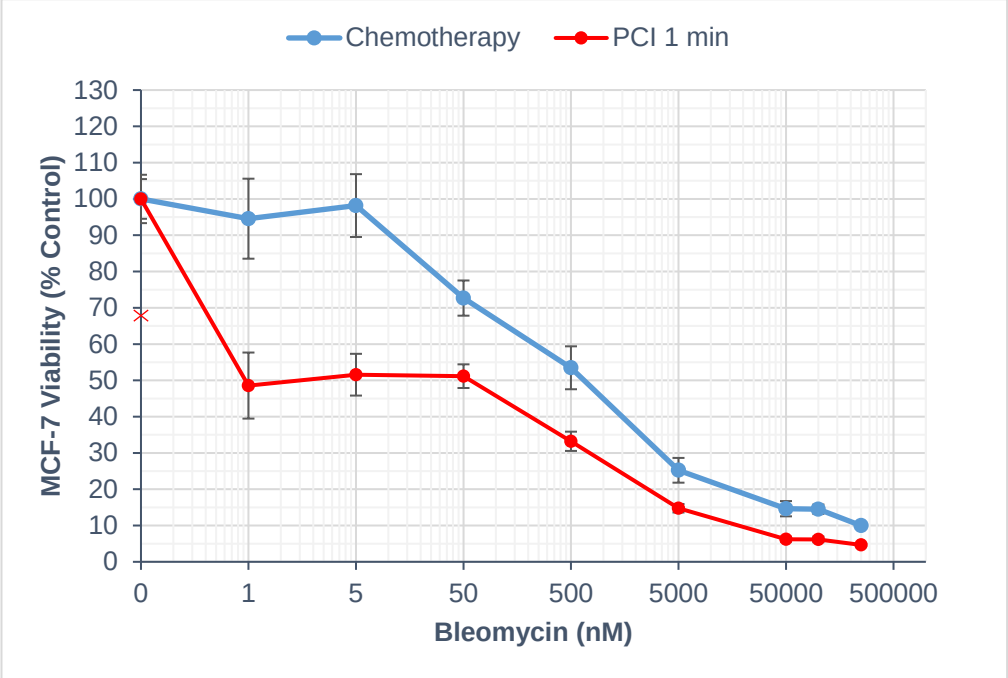

Figure 47. Reduction in MCF-7 breast cancer cell viability in 3D collagen hydrogels after bleomycin chemotherapy and bleomycin PCI*. Relative cellular viability (% of control) of MCF-7 cells after chemotherapy and PCI treatment at various bleomycin concentrations (0.5-250,000 nM).*

5.3.3.1.3 Bleomycin PCI – MDA-MB-231 cells vs MCF-7 cells

Further elucidation as to the full therapeutic effect of bleomycin-PCI can be provided by comparison between the two different breast cancer cell lines (as shown by Figure 48). Here, it was observed that there *was* a significant difference ($p < 0.001$) in cell viability reduction achieved by bleomycin-PCI between the MDA-MB-231 and MCF-7 cell lines.

It can be seen from Figure 48 that bleomycin-PCI treatment combinations were more potent against MCF-7 cells than MDA-MB-231 cells across all of the concentrations tested from 0.5-250,000 nM. Bleomycin-PCI treatment IC_{70} values were found to be 27,500 nM and 750 nM for MDA-MB-231 and MCF-7 cells, respectively, which represents a 37-fold reduction in the IC_{70} value in the MCF-7 cell line. With regards to efficacy at the highest tested concentration of 250,000 nM, bleomycin-PCI reduced cell viability to 6% (±0%) and 5% (±0%) in MDA-MB-231 and MCF-7 cells, respectively. This represents a 1.2-fold increase in efficacy in MCF-7 cells.

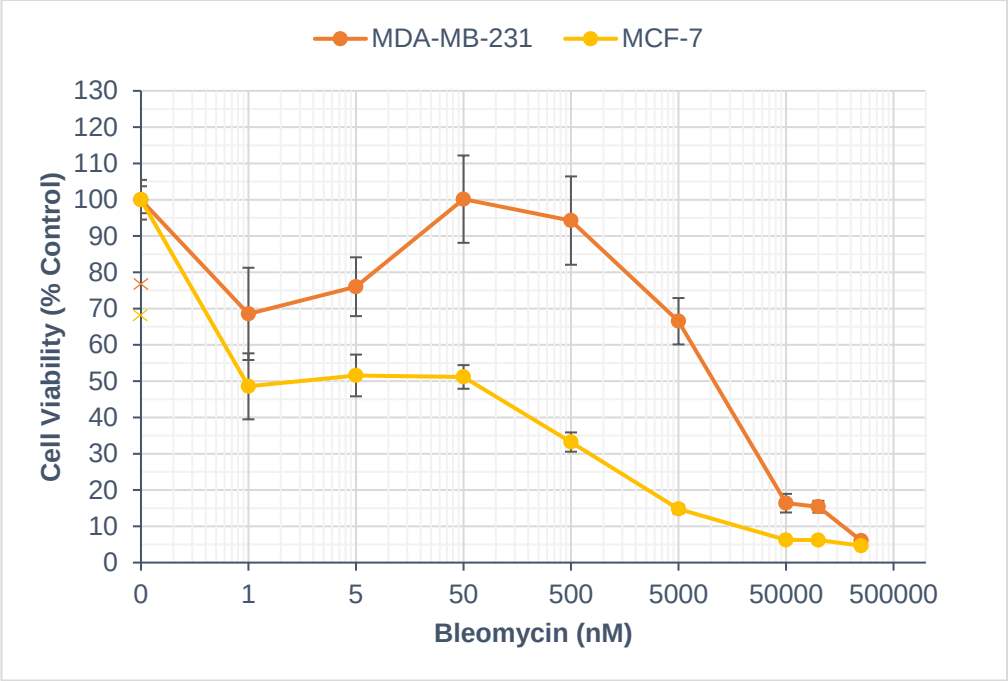

Figure 48. Reduction in breast cancer cell viability in 3D collagen hydrogels after bleomycin PCI*. Relative cellular viability (% of control) of MDA-MB-231 and MCF-7 cells after PCI treatment at various bleomycin concentrations (0.5-250,000 nM).*

5.3.3.1.4 Bleomycin PCI - Treatment Synergy

In order to realise the full benefit (or otherwise) of PCI treatment, it is necessary to compare the therapeutic effect of the combined chemotherapeutic and PDT components (that is, in PCI treatment) to their effects as individual, standalone therapies. Thus, it is necessary to calculate the treatment synergy (167–169). Synergy is achieved when the combination of two individual treatment components together produces an effect greater than merely the sum of the two components added together. Synergy is signified by: $\alpha > 1$; an additive effect by: $\alpha = 1$; antagonism $\alpha < 1$ - *please refer to Chapter 3 for the full equation*.

The synergy plot below (Figure 49) shows that 63% of bleomycin-PCI combinations were synergistic for the MDA-MB-231 cell line and the highest α value achieved was 2.1 (±0.1) at 250,000 nM. Pertaining to the MCF-7 cell line, 88% of bleomycin-PCI combinations were synergistic and the joint-highest α value achieved was 2.1 (±0.6) at 50,000 nM and 100,000 nM.

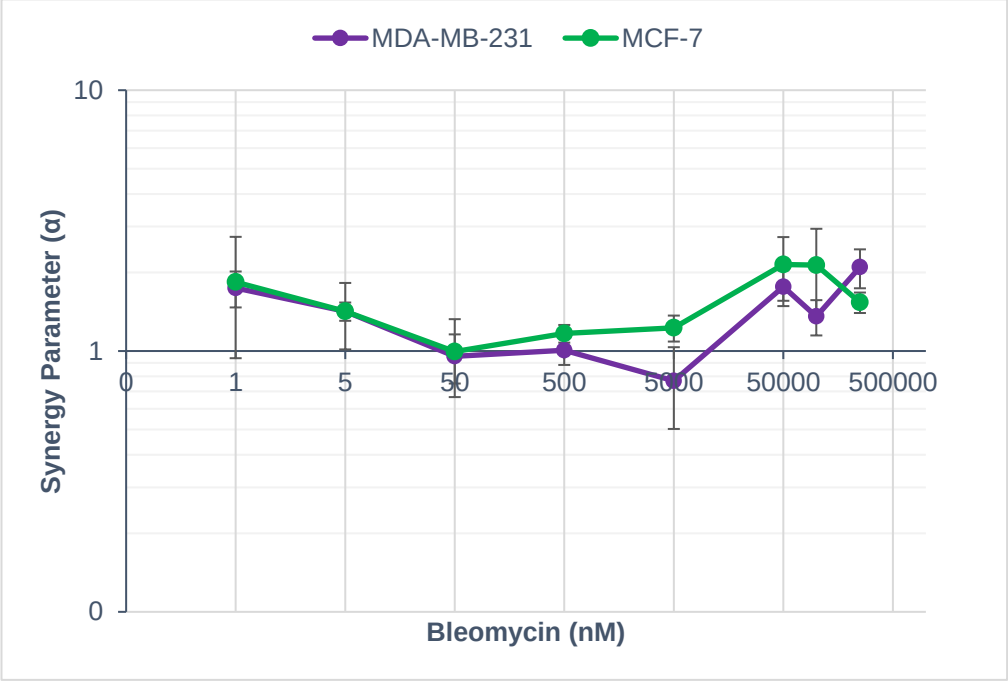

Figure 49. Synergy plot for bleomycin-PCI combinations in MDA-MB-231 and MCF-7 breast cancer cells. *Synergy (α) was calculated from the individual cell viability results (specifically, survival/viability fraction) obtained for each respective treatment condition chemotherapy, PDT, and PCI.*

5.3.4 Vinca alkaloids

5.3.4.1 Vinorelbine Chemotherapy vs Vinorelbine PCI

5.3.4.1.1 MDA-MB-231 cells

The first of the "new" PCI drug candidates to be evaluated in the 3D *in vitro* breast cancer models was the vinca alkaloid vinorelbine which is clinically-indicated and recommended by NICE for the treatment of advanced/metastatic breast cancer (147). Vinorelbine-PCI was performed at various concentrations (0.5-250,000 nM) and the results are plotted alongside vinorelbine chemotherapy in Figure 50. Here, it was determined that there *was* a significant difference ($p = 0.021$) in cell viability reduction between chemotherapy and PCI experimental groups. Furthermore, vinorelbine concentration had a significant effect ($p < 0.001$) on cell viability reduction within each experimental group.

The $AlPcS_{2a}$ (5 µg/mL) PDT control conducted alongside these PCI experiments reduced cell viability to 59% (±6%). With regard to treatment potency, IC_{70} values were estimated to be 75,000 nM and 275 nM for chemotherapy and PCI treatment groups, respectively. This represents a 273-fold reduction in IC_{70} value for the PCI group. There was

also a notable 'peak' in cell viability between 5,000-50,000 nM in both treatment groups which, incidentally, took cell viability back above the IC_{70} in the PCI group before it decreased rapidly again between 50,000-100,000 nM. At the maximum tested concentration of 250,000 nM, vinorelbine treatment reduced cell viability to 0% of control in both chemotherapy and PCI groups, respectively.

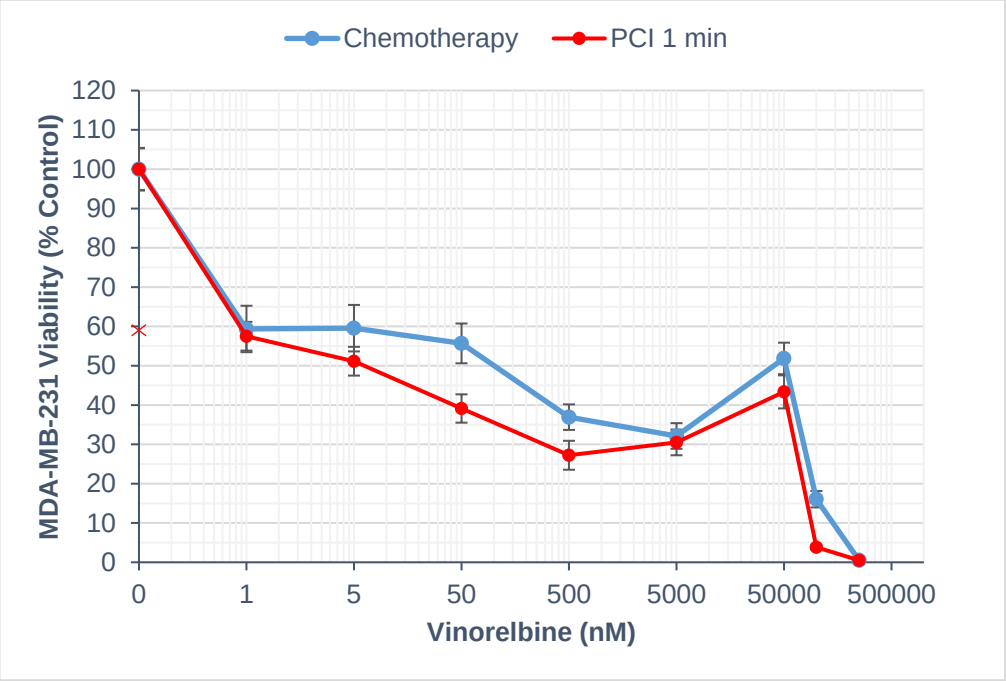

Figure 50. Reduction in MDA-MB-231 breast cancer cell viability in 3D collagen hydrogels after vinorelbine chemotherapy and vinorelbine PCI. *Relative cellular viability (% of control) of MDA-MB-231 cells after chemotherapy and PCI treatment at various vinorelbine concentrations (0.5-250,000 nM).*

5.3.4.1.2 MCF-7 cells

Vinorelbine-PCI was then evaluated in MCF-7 cells and compared to its chemotherapy counterpart (as shown in Figure 51). Here, there *was* a significant difference ($p = 0.008$) in cell viability reduction observed between chemotherapy and PCI experimental groups. Furthermore, vinorelbine concentration had a significant effect ($p < 0.001$) on cell viability reduction within each experimental group.

The $AlPcS_{2a}$ (5 µg/mL) PDT control conducted alongside these PCI experiments reduced cell viability to 45% (±7%). With regard to treatment potency, IC_{70} values were estimated to be 20,000 nM and 5 nM for chemotherapy and PCI treatment groups, respectively. This represents a 4,000-fold reduction in IC_{70} value for PCI therapy. At the

maximum tested concentration of 250,000 nM, both chemotherapy and PCI treatment reduced cell viability to 0% of control.

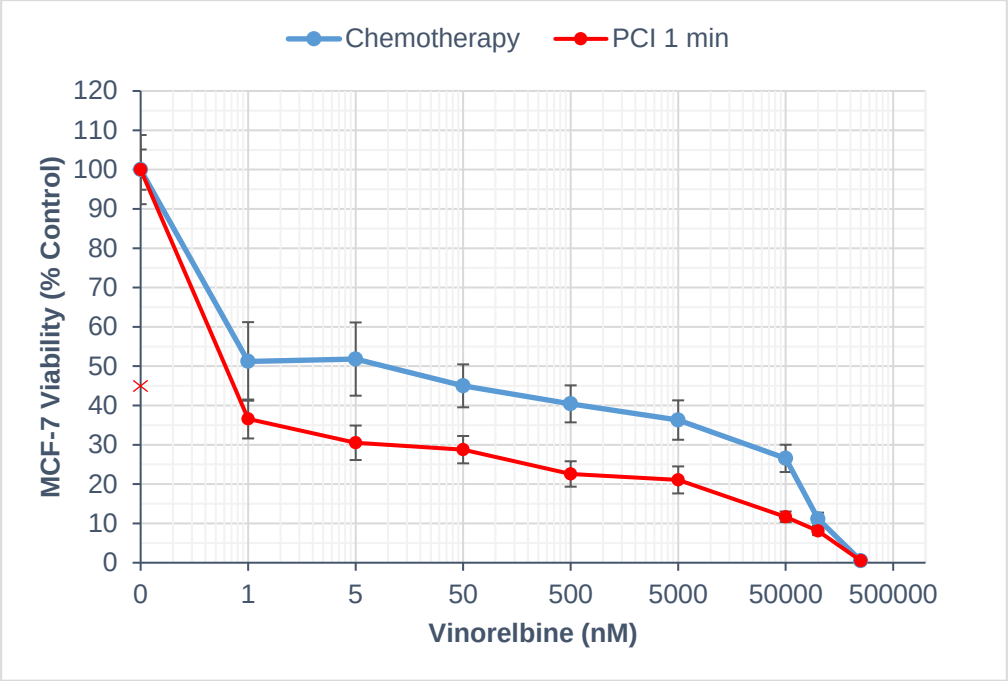

Figure 51. Reduction in MCF-7 breast cancer cell viability in 3D collagen hydrogels after vinorelbine chemotherapy and vinorelbine PCI*. Relative cellular viability (% of control) of MCF-7 cells after chemotherapy and PCI treatment at various vinorelbine concentrations (0.5-250,000 nM).*

5.3.4.1.3 Vinorelbine PCI – MDA-MB-231 cells vs MCF-7 cells

Below, Figure 52 shows a comparison of vinorelbine-PCI 1 min treatment in both MDA-MB-231 and MCF-7 breast cancer cells. Here, treatment effects were found to be significantly different (p = 0.001) between MDA-MB-231 and MCF-7 cell lines.

In general, vinorelbine-PCI treatment combinations were more potent against MCF-7 cells than MDA-MB-231 cells across all tested concentrations. In addition, the IC_{70} of each treatment was determined to be 275 nM and 5 nM for MDA-MB-231 and MCF-7 cells, respectively. This represents a 55-fold reduction in IC_{70} value for MCF-7 cells. Pertaining to treatment efficacy at the maximum tested concentration of 250,000 nM, cell viability was reduced to 0% of control in both cell lines.

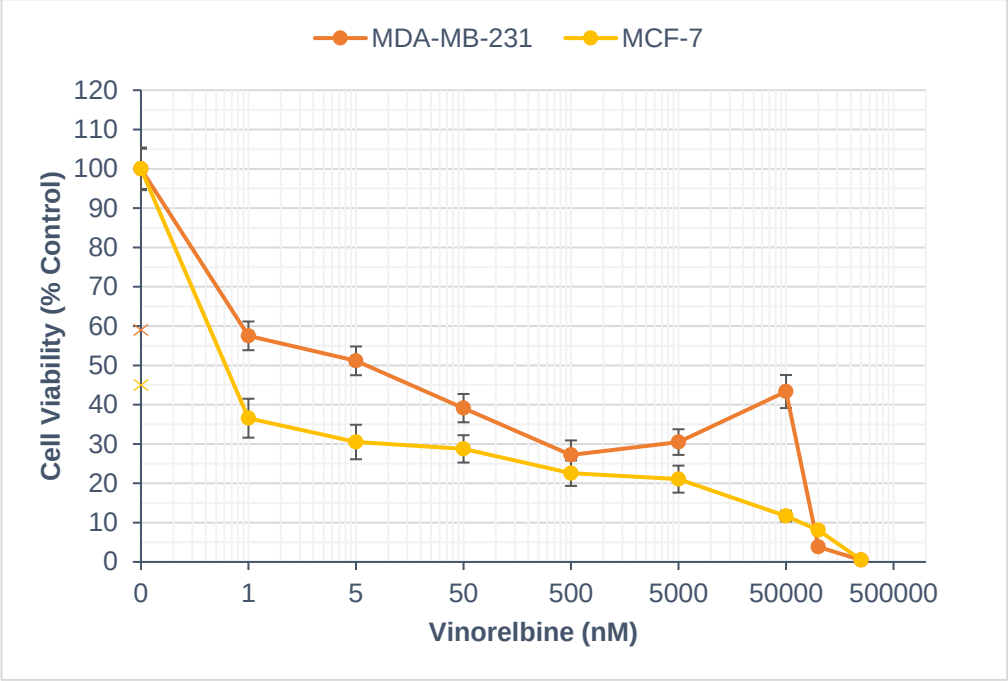

Figure 52. Reduction in breast cancer cell viability in 3D collagen hydrogels after vinorelbine PCI*. Relative cellular viability (% of control) of MDA-MB-231 and MCF-7 cells after PCI treatment at various vinorelbine concentrations (0.5-250,000 nM).*

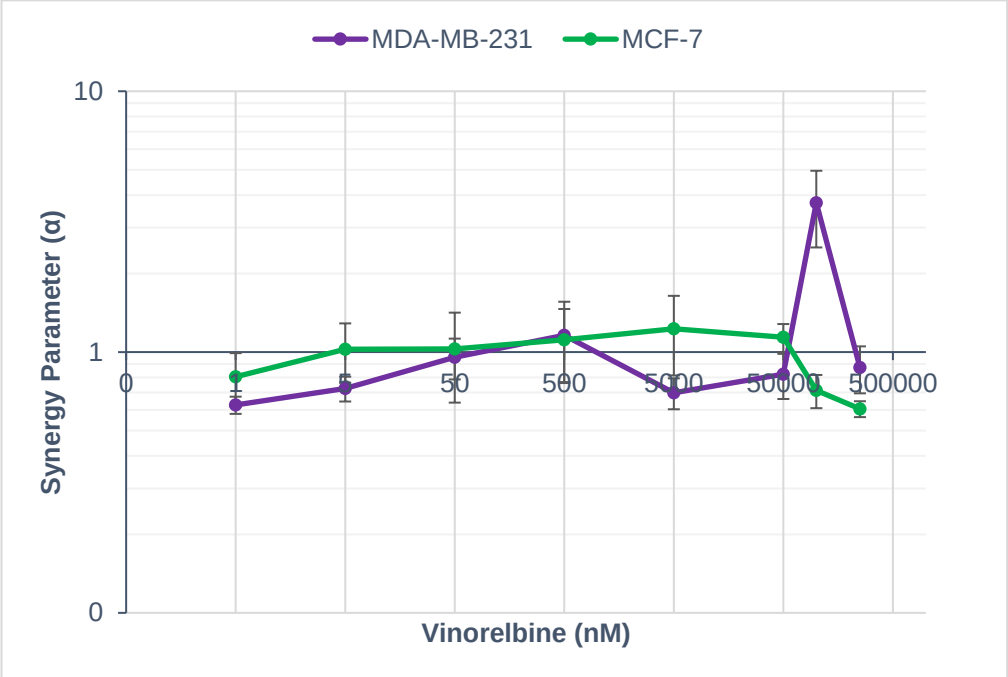

Figure 53. Synergy plot for vinorelbine-PCI combinations in MDA-MB-231 and MCF-7 breast cancer cells*. Synergy (α) was calculated from the individual cell viability results (specifically, survival/viability fraction) obtained for each respective treatment condition: chemotherapy, PDT, and PCI.*

5.3.4.1.4 Vinorelbine PCI – Treatment Synergy

Treatment synergy for vinorelbine-PCI combinations was observed in both MDA-MB-231 and MCF-7 cell lines (as shown in Figure 53). More specifically, it was observed that 25% of

vinorelbine-PCI combinations were synergistic in the MDA-MB-231 cell line and that the highest *α* value achieved was 3.7 (±1.2) at 100,000 nM. Pertaining to the MCF-7 cell line, it was determined that 38% of vinorelbine-PCI combinations were synergistic and that the highest *α* value achieved was 1.2 (±0.4) at 5,000 nM.

5.3.4.1.2 Vincristine Chemotherapy vs Vincristine PCI

5.3.4.1.2.1 MDA-MB-231 cells

The second chemotherapy drug from the vinca alkaloid class to be evaluated for PCI delivery was vincristine. For comparative purposes, vincristine-PCI results were plotted against vincristine chemotherapy (as shown in Figure 54) and there *was* a significant difference ($p < 0.001$) in cell viability reduction observed between chemotherapy and PCI experimental groups. Furthermore, vincristine concentration had a significant effect ($p < 0.001$) on cell viability reduction within each experimental group.

The $AlPcS_{2a}$ (5 µg/mL) PDT control conducted alongside these PCI experiments reduced cell viability to 53% (±4%). Concerning treatment potency, IC_{70} values were determined as being *not attained* for the chemotherapy group and 0.45 nM for the PCI group, respectively. The IC_{50} of each treatment was 1,500 nM for the chemotherapy group and 0.25 nM for the PCI group which represents a 6,000-fold reduction in IC_{50} value in favour of PCI. Pertaining to the PCI group, particularly, cell viability reduced rapidly at very low vincristine concentrations and remained at around this level at all other concentrations. At the maximum tested concentration of 250,000 nM, cell viability was reduced to 59% (±7%) and 21% (±4%) for chemotherapy and PCI groups, respectively. Thus, the respective treatment E_{max} values indicate that PCI was 2.8-fold more effective in reducing cell viability at 250,000 nM.

5.3.4.1.2.2 MCF-7 cells

Vincristine-PCI was then performed on MCF-7 cells and treatment effects compared with vincristine chemotherapy (as shown in Figure 55). From this data, it was determined that there *was* a significant difference ($p < 0.001$) in MCF-7 cell viability reduction between chemotherapy and PCI experimental groups. Furthermore, vincristine concentration had a significant effect ($p < 0.001$) on cell viability reduction within each experimental group.

The $AlPcS_{2a}$ (5 µg/mL) PDT control conducted alongside these PCI experiments reduced cell viability to 57% (±6%). With regard to treatment potency, the IC_{70} of each treatment was 75,000 nM for the chemotherapy group and was 0.425 nM for the PCI group, respectively. This represents a 176,470-fold reduction in IC_{70} in favour of PCI. With regard to treatment efficacy at the maximum tested concentration of 250,000 nM, cell viability was reduced to 18% (±2%) and 10% (±1%) for chemotherapy and PCI groups, respectively. Thus, given the respective E_{max} values, PCI was found to be 1.8-fold more effective in reducing cell viability at 250,000 nM.

5.3.4.1.2.3 Vincristine PCI – MDA-MB-231 cell vs MCF-7 cells

The performance of vincristine-PCI in each breast cancer cell line is shown below in Figure 56. Statistical analysis was then performed and it was determined that there was *not* a significant difference (p = 0.052) in cell viability reduction by vincristine-PCI between MDA-MB-231 and MCF-7 cell lines.

In general, however, vincristine-PCI treatment combinations were more potent against MCF-7 cells than MDA-MB-231 cells especially at the higher concentrations that were tested. In relation to treatment potency, treatment IC_{70} values were 0.45 nM and 0.40 nM for MDA-MB-231 and MCF-7 cells, respectively. This essentially represents an equipotent IC_{70} for vincristine-PCI in both cell lines. Concerning treatment efficacy at the maximum tested concentration of 250,000 nM, cell viability was reduced to 21% (±4%) and 10% (±1%) in MDA-MB-231 and MCF-7 cells, respectively. This represents around a 2-fold increase in efficacy in the MCF-7 cell line at 250,000 nM.

5.3.4.1.2.4 Vincristine PCI – Treatment synergy

The synergy plot relating to vincristine-PCI is shown below in Figure 57. From this, it can be observed that 100% of vincristine-PCI combinations were synergistic in the MDA-MB-231 cell line and that the highest α value achieved was 3.0 (±0.4) at 5 nM. Pertaining to the MCF-7 cell line, 100% of vincristine-PCI combinations were also synergistic here and the joint-highest α value achieved was 2.6 (±0.7) at 50,000 nM and 100,000 nM.

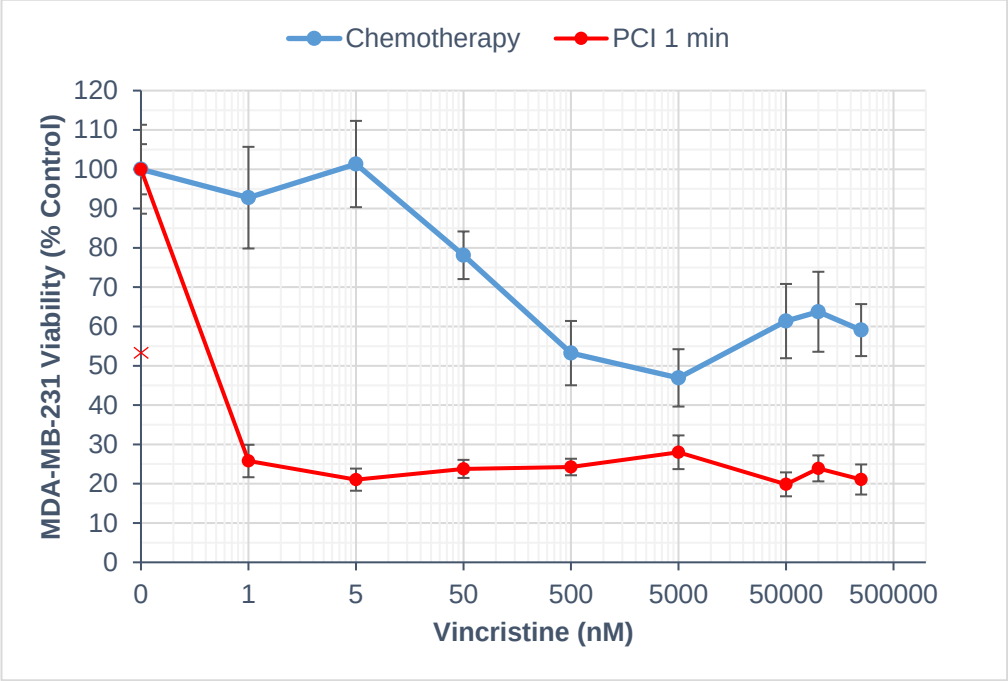

Figure 54. Reduction in MDA-MB-231 breast cancer cell viability in 3D collagen hydrogels after vincristine chemotherapy and vincristine PCI. *Relative cellular viability (% of control) of MDA-MB-231 cells after chemotherapy and PCI treatment at various vincristine concentrations (0.5-250,000 nM).*

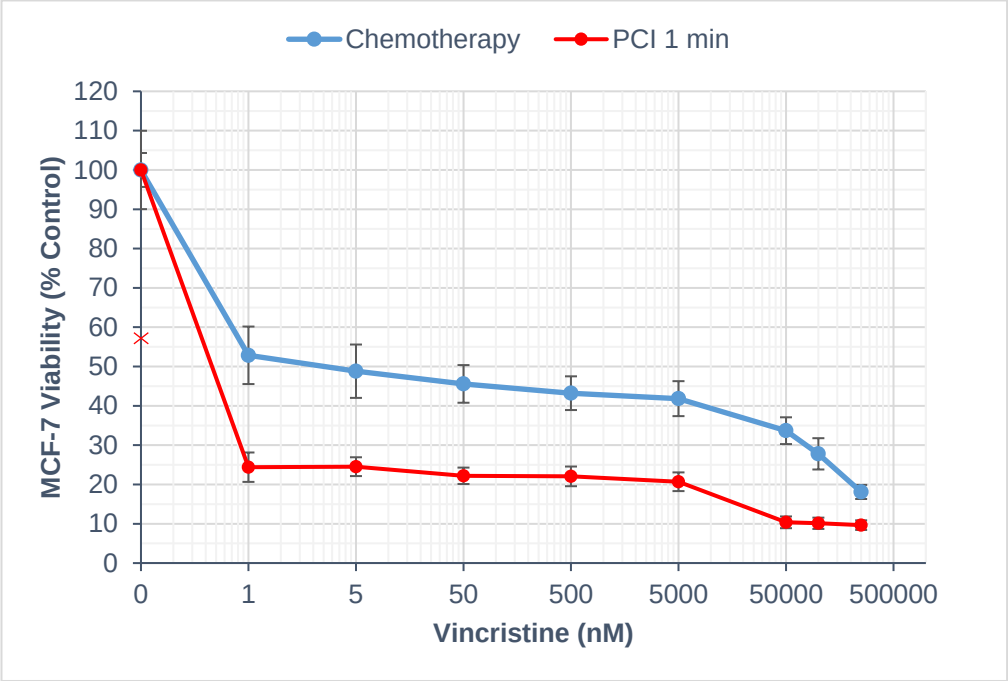

Figure 55. Reduction in MCF-7 breast cancer cell viability in 3D collagen hydrogels after vincristine chemotherapy and vincristine PCI*. Relative cellular viability (% of control) of MCF-7 cells after chemotherapy and PCI treatment at various vincristine concentrations (0.5-250,000 nM).*

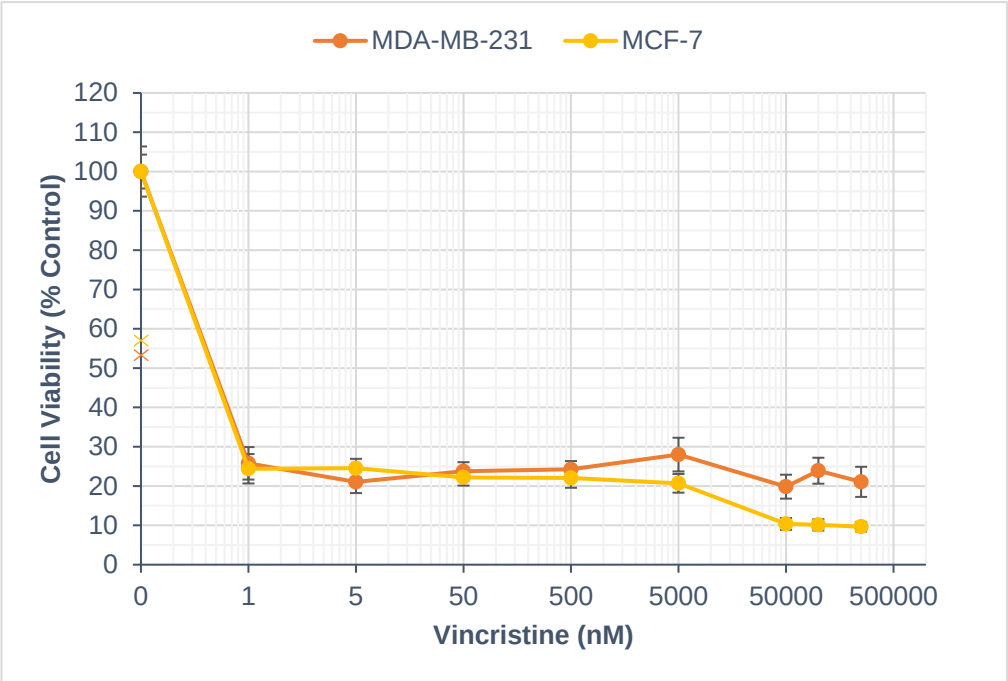

Figure 56. Reduction in breast cancer cell viability in 3D collagen hydrogels after vincristine PCI*. Relative cellular viability (% of control) of MDA-MB-231 and MCF-7 cells after PCI treatment at various vincristine concentrations (0.5-250,000 nM).*

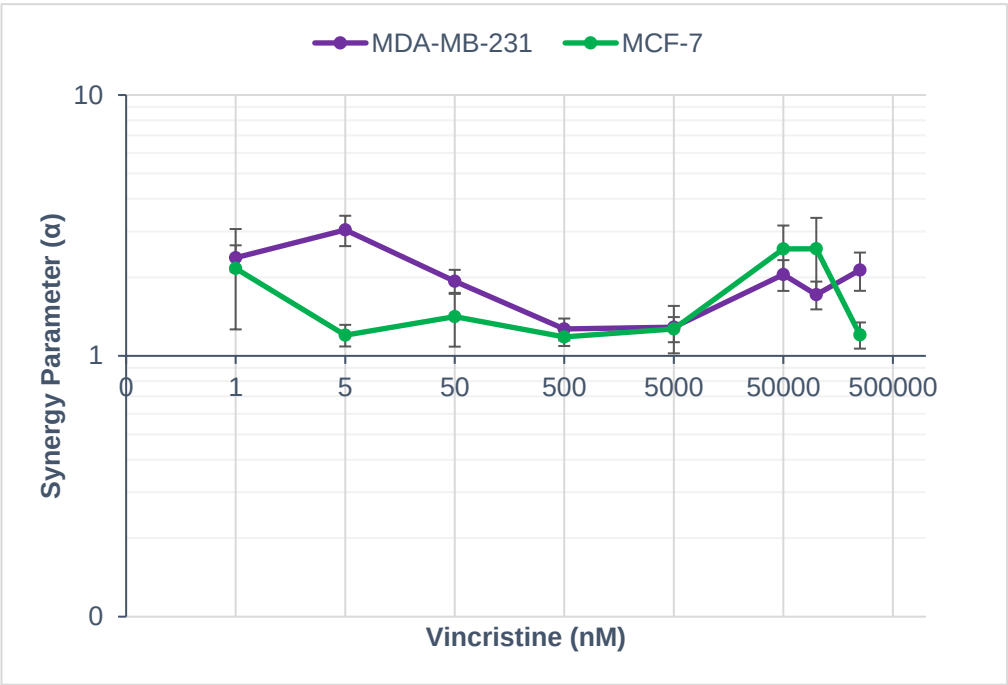

Figure 57. Synergy plot for vincristine-PCI combinations in MDA-MB-231 and MCF-7 breast cancer cells*. Synergy (α) was calculated from the individual cell viability results (specifically, survival/viability fraction) obtained for each respective treatment condition: chemotherapy, PDT, & PCI.*

5.3.4.1.3 Vinblastine Chemotherapy vs Vinblastine PCI

5.3.4.1.3.1 MDA-MB-231 cells

The third (and final) vinca alkaloid to be evaluated for PCI delivery was vinblastine. Figure 58 shows the dose-response profile of the vinblastine-PCI combinations alongside vinblastine

chemotherapy. These treatment groups were seen to differ significantly (p = 0.022) in their reduction of cell viability. Furthermore, vinblastine concentration had a significant effect (p < 0.001) on cell viability reduction within each experimental group.

The $AlPcS_{2a}$ (5 µg/mL) PDT control conducted alongside these PCI experiments reduced cell viability to 57% (±5%). In relation to treatment potency, the IC_{70} of each treatment was 150,000 nM for the chemotherapy group and 80,000 nM for the PCI group, respectively. This represents a 1.9-fold reduction in IC_{70} value for the PCI group. With regards to treatment efficacy at the highest tested concentration of 250,000 nM, cell viability was reduced to 0% of control in both chemotherapy and PCI groups, respectively. There was also a notable increase in cell viability between 5,000-50,000 nM in both treatment groups.

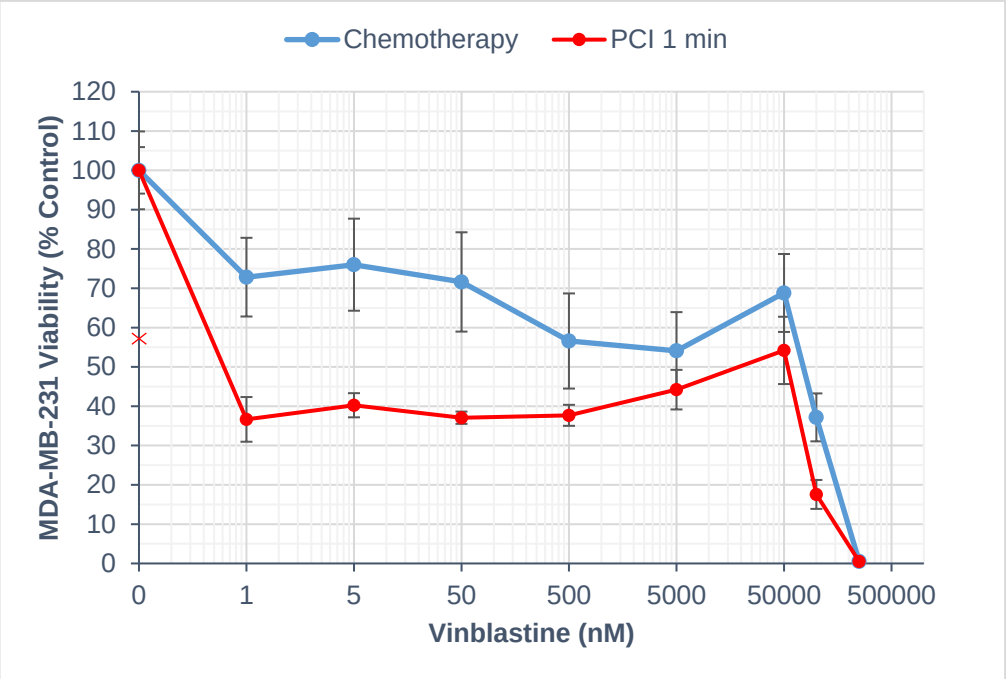

Figure 58. Reduction in MDA-MB-231 breast cancer cell viability in 3D collagen hydrogels after vinblastine chemotherapy and vinblastine PCI. *Relative cellular viability (% of control) of MDA-MB-231 cells after chemotherapy and PCI treatment at various vinblastine concentrations (0.5-250,000 nM).*

5.3.4.1.3.2 MCF-7 cells

Vinblastine-PCI was then administered to MCF-7 cells. From these experiments (Figure 59), it was determined that there *was* a significant difference (p < 0.001) in cell viability reduction between chemotherapy and PCI experimental groups. Furthermore, vinblastine concentration

was found to have a significant effect ($p < 0.001$) on cell viability reduction within each experimental group.

The $AlPcS_{2a}$ (5 µg/mL) PDT control conducted alongside these PCI experiments reduced cell viability to 66% (±4%). Pertaining to treatment potency, the IC_{70} for each treatment was estimated to be 12,500 nM for the chemotherapy group and 12.5 nM for the PCI group, respectively. This represents a 1000-fold reduction in IC_{70} in favour of the PCI group. With regard to treatment efficacy at the highest tested concentration of 250,000 nM (E_{max}), cell viability was found to be reduced to 0% of control in both treatment groups.

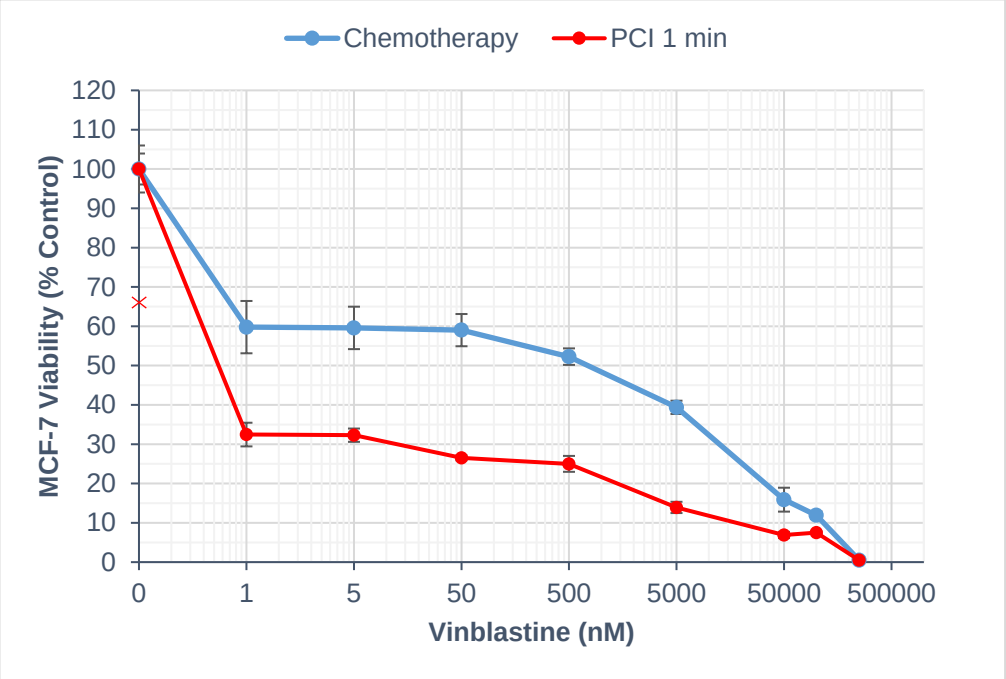

Figure 59. Reduction in MCF-7 breast cancer cell viability in 3D collagen hydrogels after vinblastine chemotherapy and vinblastine PCI. *Relative cellular viability (% of control) of MCF-7 cells after chemotherapy and PCI treatment at various vinblastine concentrations (0.5-250,000 nM).*

5.3.4.1.3.3 Vinblastine PCI – MDA-MB-231 cells vs MCF-7 cells

The cytotoxicity of vinblastine-PCI treatment was then compared across the two breast cancer cells lines as shown in Figure 60. Here, it was observed that there *was* a significant difference ($p < 0.001$) in cell viability reduction by vinblastine-PCI between MDA-MB-231 and MCF-7 cell lines.

Upon observation of Figure 60, it can be determined that vinblastine-PCI combinations were more potent against MCF-7 cells than MDA-MB-231 cells at all tested concentrations. Moreover, the IC_{70} of vinblastine-PCI was estimated to be 80,000 nM and

12.5 nM for MDA-MB-231 and MCF-7 cells, respectively, which represents a 6,400-fold reduction in IC_{70} in favour of the MCF-7 cell line. At the highest tested concentration of 250,000 nM, vinblastine-PCI was found to be maximally-effective in both MDA-MB-231 and MCF-7 cell lines as cell viability was reduced to 0% of control.

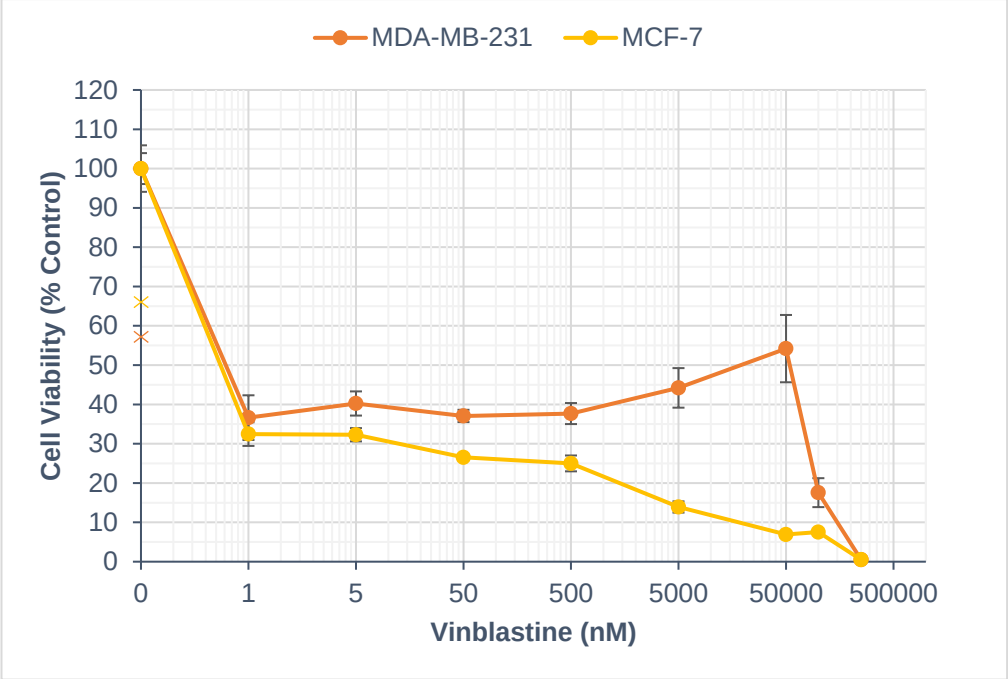

Figure 60. Reduction in breast cancer cell viability in 3D collagen hydrogels after vinblastine PCI*. Relative cellular viability (% of control) of MDA-MB-231 and MCF-7 cells after PCI treatment at various vinblastine concentrations (0.5-250,000 nM).*

5.3.4.1.3.3 Vinblastine PCI – Treatment synergy

Synergy calculations were then performed after collating the PCT, PDT, and chemotherapy data and the synergy plot is shown in Figure 61. It can be seen from this figure that 63% of vinblastine-PCI combinations were synergistic against the MDA-MB-231 cell line and that the highest α value achieved was 1.6 (±0.2) at 100,000 nM. Pertaining to the MCF-7 cell line, it can be seen that 88% of vinblastine-PCI combinations were synergistic and that the highest α value achieved was 2.0 (±0.2) at 5,000 nM.

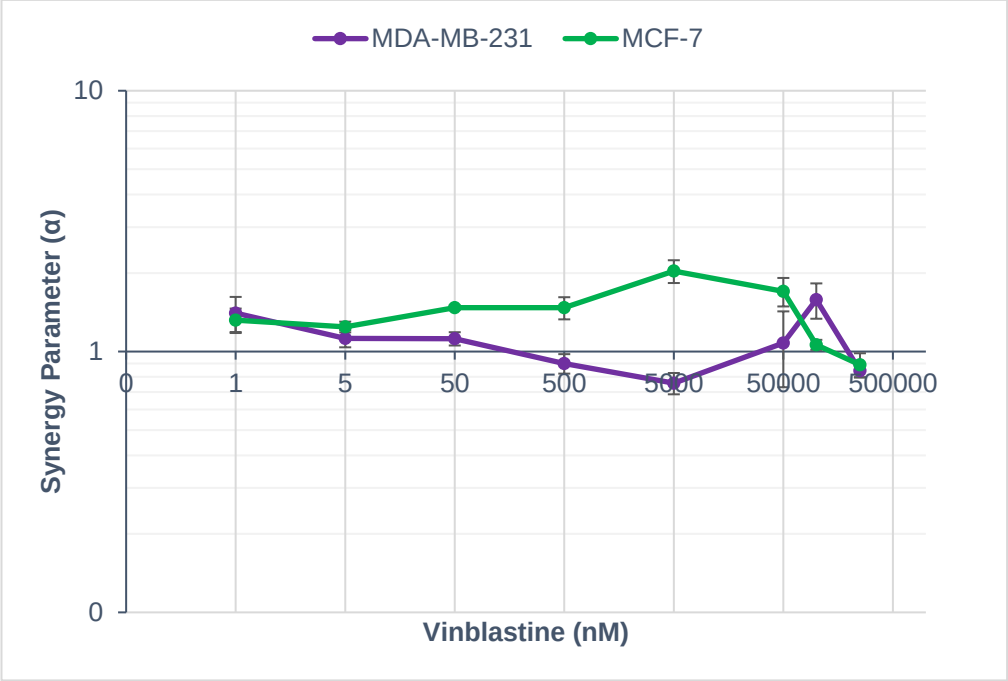

Figure 61. Synergy plot for vinblastine-PCI combinations in MDA-MB-231 and MCF-7 breast cancer cells. *Synergy (α) was calculated from the individual cell viability results (specifically, survival/viability fraction) obtained for each respective treatment condition: chemotherapy, PDT, and PCI.*

5.3.5 Taxanes

5.3.5.1 Docetaxel Chemotherapy vs Docetaxel PCI

5.3.5.1.1 MDA-MB-231 cells

Following PCI investigations with the glycopeptide bleomycin and the vinca alkaloids (vinorelbine, vincristine, vinblastine), the taxanes were the next therapeutic drug class to be tested. Firstly, docetaxel, which is clinically-indicated for breast cancer treatment and specifically recommended as a first-line monotherapy by NICE (subject to certain specific clinical considerations) in advanced/metastatic breast cancer (147).

Docetaxel-PCI and docetaxel chemotherapy are shown in Figure 62. From these experiments, it was determined that there was *not* a significant difference ($p = 0.095$) in cell viability reduction between chemotherapy and PCI experimental groups. In addition, docetaxel concentration had a significant effect ($p < 0.001$) on cell viability reduction within each experimental group.

The $AlPcS_{2a}$ (5 µg/mL) PDT control conducted alongside these PCI experiments reduced cell viability to 83% (±10%). With regard to treatment potency, the IC_{70} of docetaxel

chemotherapy and docetaxel-PCI was determined to be 100,000 nM for both treatment groups, respectively. There was also a notable 'peak' in MDA-MB-231 cell viability between 50-500 nM. At the highest tested concentration of 250,000 nM, cell viability was reduced to 0% of control for both chemotherapy and PCI groups, respectively.

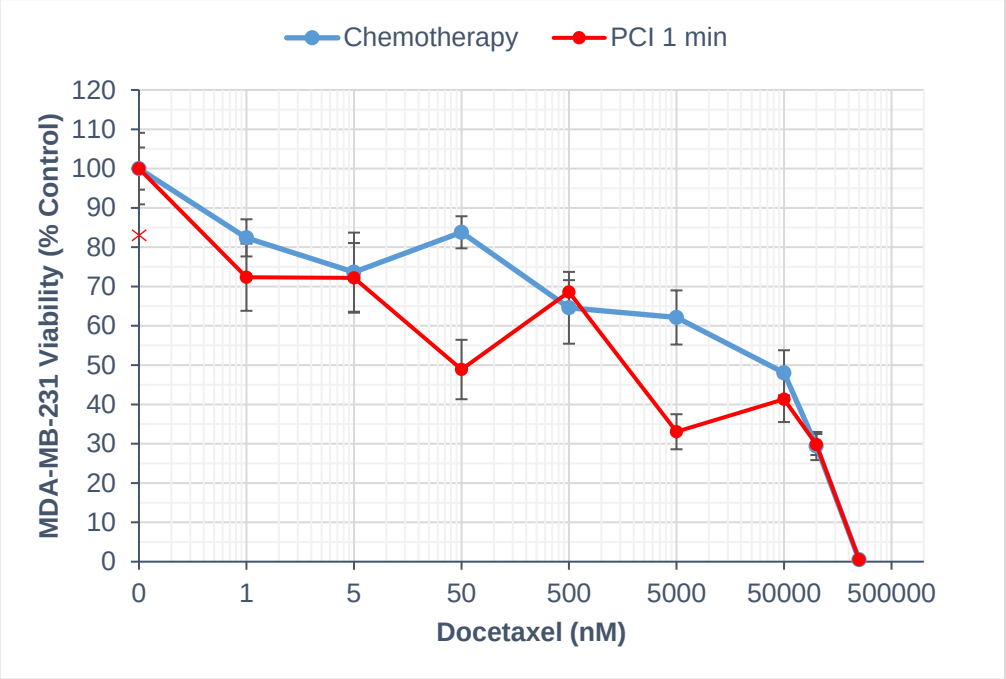

Figure 62. Reduction in MDA-MB-231 breast cancer cell viability in 3D collagen hydrogels after docetaxel chemotherapy and docetaxel PCI*. Relative cellular viability (% of control) of MDA-MB-231 cells after chemotherapy and PCI treatment at various docetaxel concentrations (0.5-250,000 nM).*

5.3.5.1.2 MCF-7 cells

Following docetaxel-PCI administration to MDA-MB-231 cells, the same treatment combinations were applied to MCF-7 cells. Comparing docetaxel chemotherapy and docetaxel-PCI, Figure 63 shows that there *was* a significant difference (p = 0.002) in cell viability reduction between chemotherapy and PCI experimental groups. Furthermore, docetaxel concentration had a significant effect (p < 0.001) on cell viability reduction within each experimental group.

The $AlPcS_{2a}$ (5 µg/mL) PDT control conducted alongside these PCI experiments reduced cell viability to 69% (±7%). In relation to treatment potency, the IC_{70} values were 112,500 nM and 1,250 nM for the chemotherapy and PCI groups, respectively, which represents a 90-fold reduction in IC_{70} in favour of PCI. In addition, at the highest tested

concentration of 250,000 nM, cell viability was reduced to 11% (±4%; ±3%) for the chemotherapy and PCI groups, respectively.

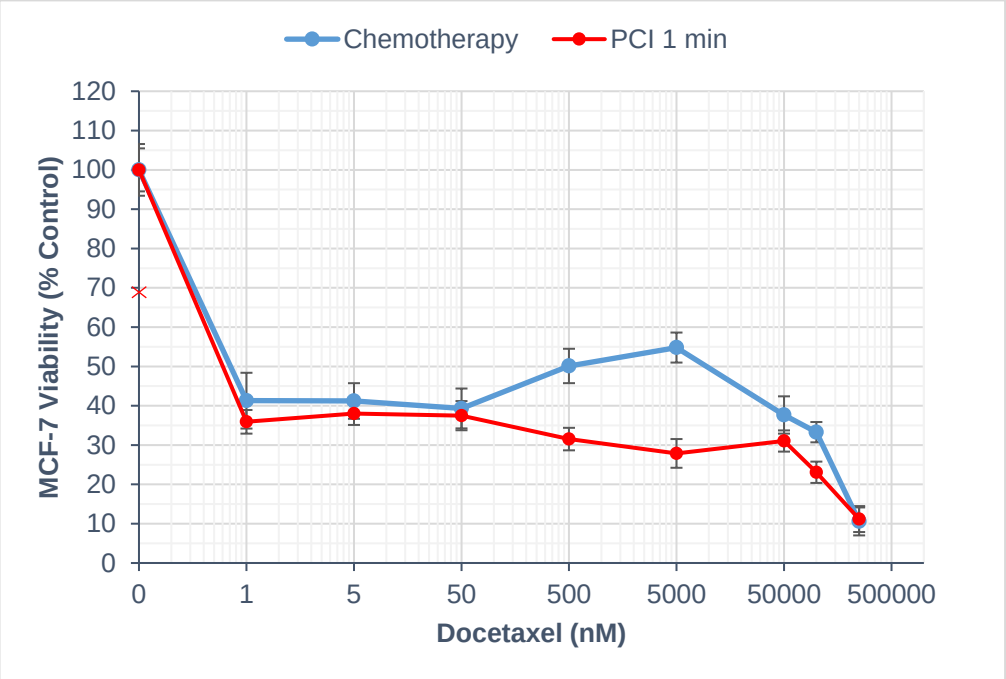

Figure 63. Reduction in MCF-7 breast cancer cell viability in 3D collagen hydrogels after docetaxel chemotherapy and docetaxel PCI*. Relative cellular viability (% of control) of MCF-7 cells after chemotherapy and PCI treatment at various docetaxel concentrations (0.5-250,000 nM).*

5.3.5.1.2 Docetaxel PCI – MDA-MB-231 cells vs MCF-7 cells

Docetaxel-PCI treatment effects were then compared between cell lines and Figure 64 shows that there *was* a significant difference ($p = 0.001$) in cell viability reduction between MDA-MB-231 and MCF-7 cell lines.

Moreover, docetaxel-PCI treatment combinations were generally more potent against MCF-7 cells than MDA-MB-231 cells across the concentrations tested (0.5-250,000 nM). Pertaining to treatment potency, the IC_{70} values were estimated to be 100,000 nM and 1,250 nM for MDA-MB-231 and MCF-7 cells, respectively. This represents an 18-fold reduction in IC_{70} value for docetaxel-PCI in the MCF-7 cell line. In relation to maximum treatment efficacy (E_{max}), cell viability was reduced to 0% (±0%) and 11% (±3%) in MDA-MB-231 and MCF-7 cells, respectively. This represents an 11-fold increase in docetaxel-PCI efficacy in the MDA-MB-231 cell line at 250,000 nM.

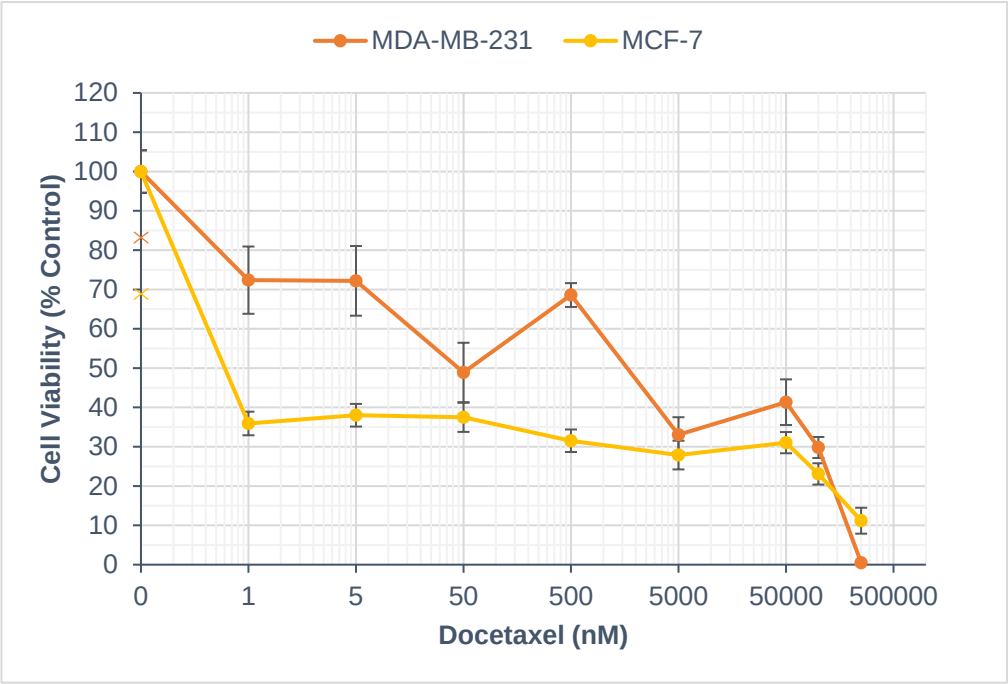

Figure 64. Reduction in breast cancer cell viability in 3D collagen hydrogels after docetaxel PCI*. Relative cellular viability (% of control) of MDA-MB-231 and MCF-7 cells after PCI treatment at various docetaxel concentrations (0.5-250,000 nM).*

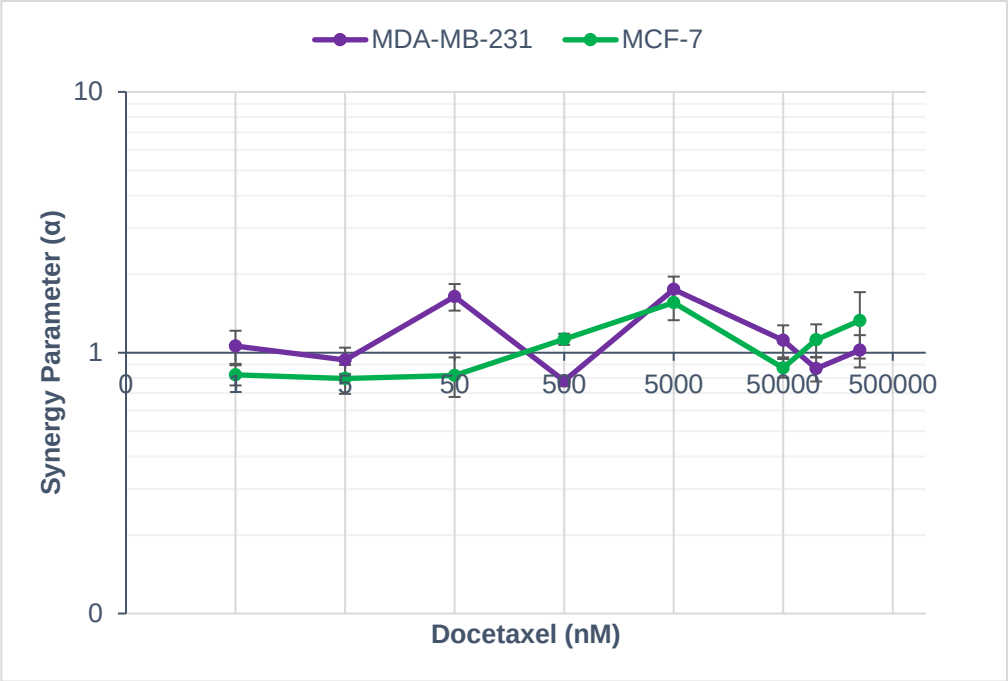

Figure 65. Synergy plot for docetaxel-PCI combinations in MDA-MB-231 and MCF-7 breast cancer cells*. Synergy (α) was calculated from the individual cell viability results (specifically, survival/viability fraction) obtained for each respective treatment condition: chemotherapy, PDT, and PCI.*

5.3.5.1.3 Docetaxel PCI – Treatment Synergy

Following synergy calculations (the synergy plot is shown in Figure 65), it was determined that 50% of docetaxel-PCI combinations were synergistic for the MDA-MB-231 cell line and that the highest *α* value achieved was 1.7 (±0.2) at 5,000 nM. In relation to the MCF-7 cell line,

50% of docetaxel-PCI combinations were synergistic and the highest *α* value achieved was 1.6 (±0.2) at 5,000 nM.

5.3.5.2 Paclitaxel Chemotherapy vs Paclitaxel PCI

5.3.5.2.1 MDA-MB-231 cells

The second taxane chemotherapeutic to be delivered via PCI was paclitaxel. Figure 66 compares paclitaxel chemotherapy and paclitaxel-PCI, and, following statistical analysis, it was determined that there *was* a significant difference ($p = 0.015$) in cell viability reduction between chemotherapy and PCI experimental groups. Furthermore, paclitaxel concentration had a significant effect ($p < 0.001$) on cell viability reduction within each experimental group.

The $AlPcS_{2a}$ (5 µg/mL) PDT control conducted alongside these PCI experiments reduced cell viability to 58% (±8%). The IC_{70} of the paclitaxel treatments were 225,000 nM for the chemotherapy group and 75,000 nM for the PCI group, respectively, which represents a 3-fold reduction in IC_{70} in favour of the PCI group. In relation to treatment efficacy at the maximum tested concentration of 250,000 nM, cell viability was reduced to 27% (±2%) and 6% (±1%) for the chemotherapy and PCI groups, respectively. This represents a 4.5-fold increase in treatment efficacy at 250,000 nM for the PCI group.

5.3.5.2.2 MCF-7 cells

Next, paclitaxel-PCI was performed on the MCF-7 cell line. As shown in Figure 67, there *was* a significant difference ($p = 0.001$) in cell viability reduction observed between chemotherapy and PCI experimental groups. Furthermore, paclitaxel concentration had a significant effect ($p < 0.001$) on cell viability reduction within each experimental group.

The $AlPcS_{2a}$ (5 µg/mL) PDT control conducted alongside these PCI experiments reduced cell viability to 53% (±6%). With regard to treatment potency, the IC_{70} was found to be 42,500 nM and 4,250 nM for the chemotherapy and PCI groups, respectively. This represents a 10-fold reduction in IC_{70} value for the PCI group. Pertaining to treatment efficacy at the highest tested concentration of 250,000 nM, cell viability was reduced to 28% (±2%) and 17% (±2%) for the chemotherapy and PCI groups, respectively. These E_{max} values represent a 1.6-fold increase in treatment efficacy at 250,000 nM for PCI.

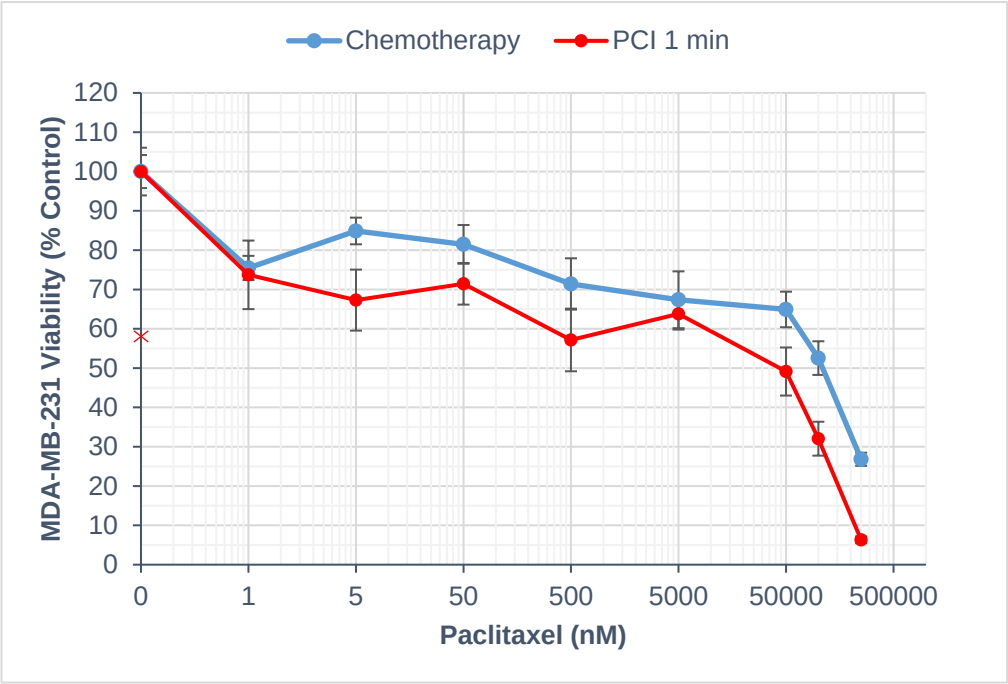

Figure 66. Reduction in MDA-MB-231 breast cancer cell viability in 3D collagen hydrogels after paclitaxel chemotherapy and paclitaxel PCI. *Relative cellular viability (% of control) of MDA-MB-231 cells after chemotherapy and PCI treatment at various paclitaxel concentrations (0.5-250,000 nM).*

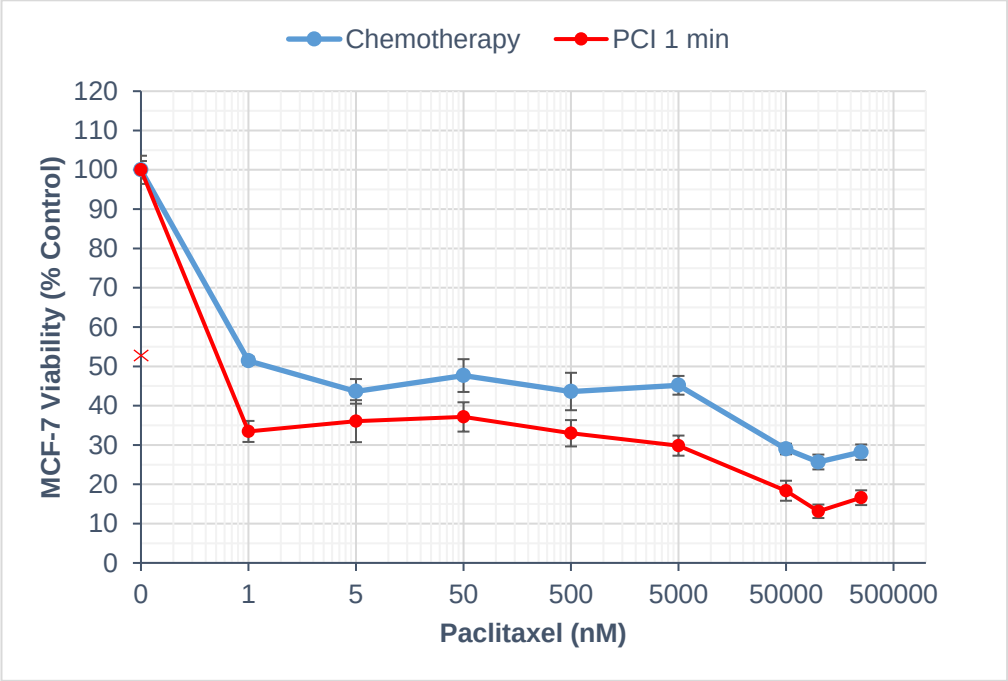

Figure 67. Reduction in MCF-7 breast cancer cell viability in 3D collagen hydrogels after paclitaxel chemotherapy and paclitaxel PCI*. Relative cellular viability (% of control) of MCF-7 cells after chemotherapy and PCI treatment at various paclitaxel concentrations (0.5-250,000 nM).*

5.3.5.2.3 Paclitaxel PCI – MDA-MB-231 cells vs MCF-7 cells

The cytotoxic effect of paclitaxel-PCI was then compared between MDA-MB-231 and MCF-7 cell lines. This comparison is shown in Figure 68 where there *was* a significant difference ($p < 0.001$) in cell viability reduction observed between the MDA-MB-231 and MCF-7 cell lines.

It can also be seen from Figure 68 that paclitaxel-PCI treatment combinations were generally more potent against MCF-7 cells than MDA-MB-231 cells across the concentrations tested. The IC_{70} values of paclitaxel-PCI were estimated to be 75,000 nM and 4,250 nM for MDA-MB-231 and MCF-7 cells, respectively, which represents around an 18-fold reduction in IC_{70} for paclitaxel-PCI in MCF-7 cells. In addition, at the maximum tested concentration of 250,000 nM, cell viability was seen to be reduced to 6% (±1%) and 17% (±2%) in MDA-MB-231 and MCF-7 cells, respectively. This represents a 2.8-fold increase in paclitaxel-PCI efficacy in the MDA-MB-231 cell line at 250,000 nM.

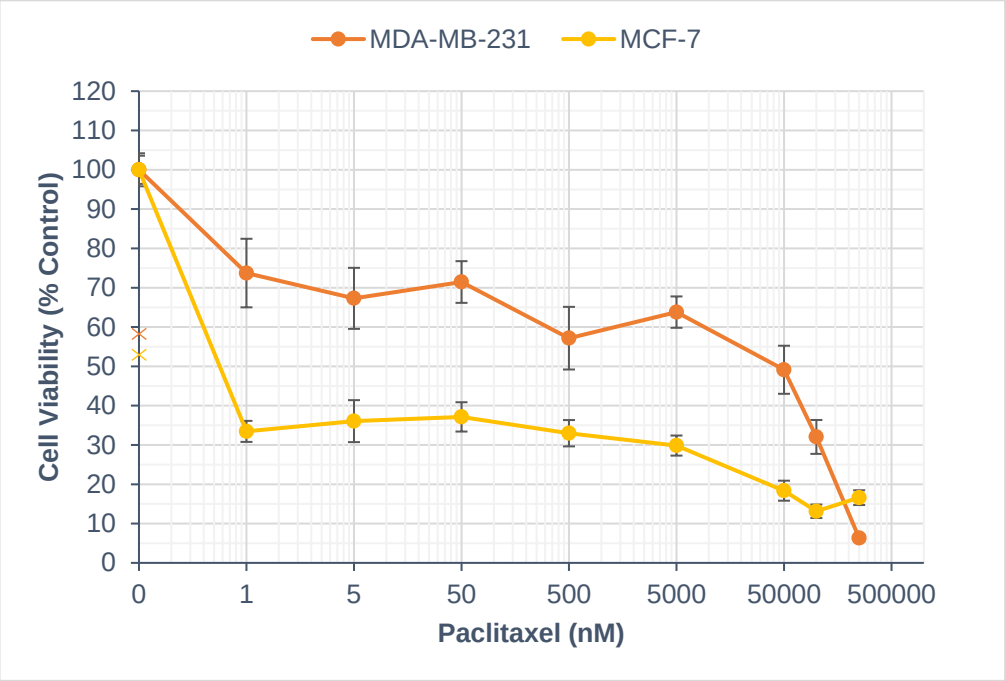

Figure 68. Reduction in breast cancer cell viability in 3D collagen hydrogels after paclitaxel PCI. *Relative cellular viability (% of control) of MDA-MB-231 and MCF-7 cells after PCI treatment at various paclitaxel concentrations (0.5-250,000 nM).*

5.3.5.2.3 Paclitaxel PCI – Treatment Synergy

Following treatment synergy calculations (the synergy plot for paclitaxel-PCI is shown in Figure 69), it was determined that 13% of paclitaxel-PCI combinations were synergistic for the MDA-MB-231 cell line and that the highest α value achieved was 2.9 (±0.5) at 250,000 nM. Pertaining to the MCF-7 cell line, it was observed that 25% of paclitaxel-PCI combinations were synergistic and the highest α value achieved was 1.2 (±0.2) at 100,000 nM.

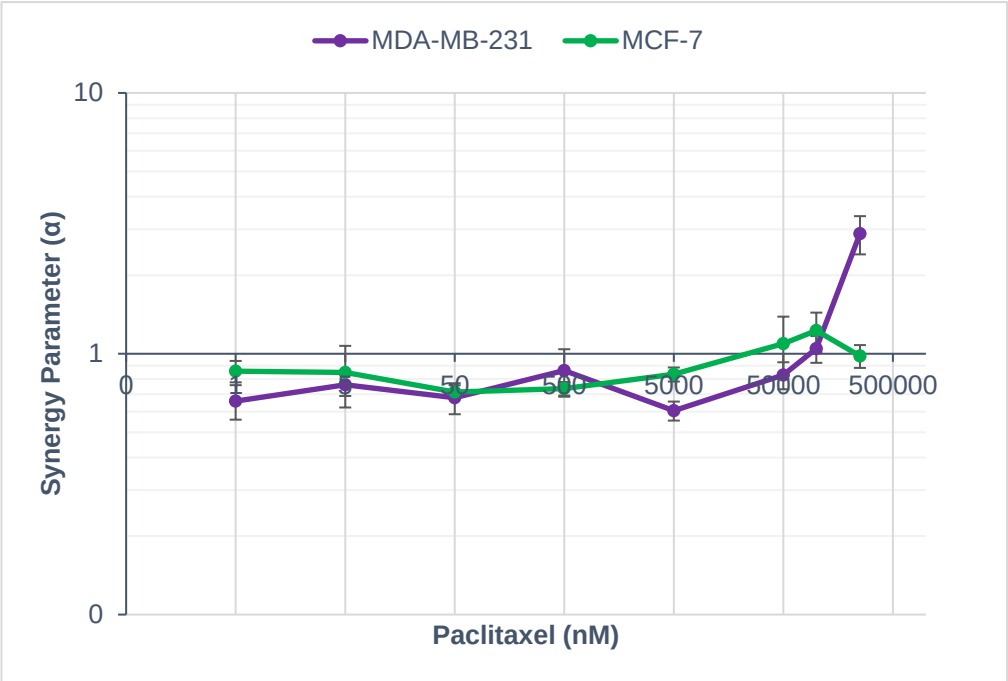

Figure 69. Synergy plot for paclitaxel-PCI combinations in MDA-MB-231 and MCF-7 breast cancer cells. *Synergy (α) was calculated from the individual cell viability results (specifically, survival/viability fraction) obtained for each respective treatment condition: chemotherapy, PDT, and PCI.*

5.3.6 Anti-metabolites

5.3.6.1 Gemcitabine Chemotherapy vs Gemcitabine PCI

5.3.6.1.1 MDA-MB-231 cells

The final chemotherapeutic drug class to be tested for compatibility with PCI was the antimetabolites and the first drug from this class was gemcitabine. Gemcitabine-PCI was performed on MDA-MB-231 cells and then compared with gemcitabine chemotherapy (as shown in Figure 70). Here, it was observed that there was *not* a significant difference (p = 0.245) in cell viability reduction between chemotherapy and PCI experimental groups. In addition, gemcitabine concentration had a significant effect ($p < 0.001$) on cell viability reduction within each experimental group.

The $AlPcS_{2a}$ (5 µg/mL) PDT control conducted alongside these PCI experiments reduced cell viability to 59% (±7%). With regard to treatment potency, the IC_{70} was *not attained* for either chemotherapy or PCI treatment groups. Subsequently, the IC_{50} of gemcitabine-PCI was determined to be 12.5 nM whereby gemcitabine chemotherapy did not attain the IC_{50}. Pertaining to treatment efficacy at the highest tested concentration of 250,000

nM, cell viability was reduced to 56% (±6%) and 40% (±5%) for chemotherapy and PCI groups, respectively. This represents a 1.4-fold increase in efficacy at 250,000 nM for the PCI treatment group.

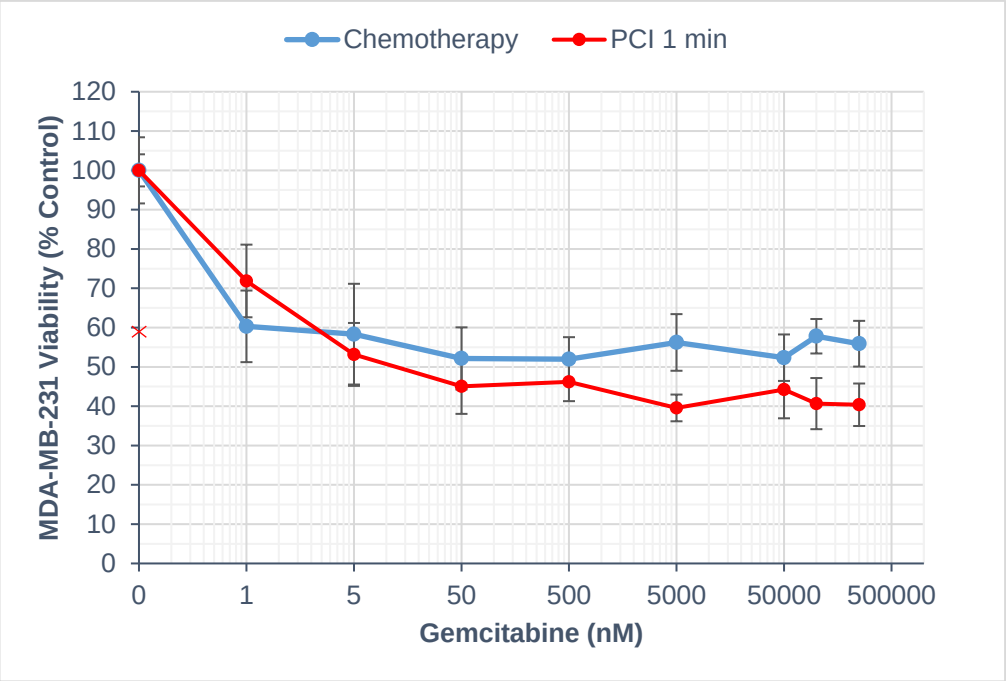

Figure 70. Reduction in MDA-MB-231 breast cancer cell viability in 3D collagen hydrogels after gemcitabine chemotherapy and gemcitabine PCI*. Relative cellular viability (% of control) of MDA-MB-231 cells after chemotherapy and PCI treatment at various gemcitabine concentrations (0.5-250,000 nM).*

5.3.6.1.2 MCF-7 cells

Gemcitabine-PCI was then performed on MCF-7 cells and was compared to gemcitabine chemotherapy in Figure 71. Here, it was determined that there was *not* a significant difference ($p = 0.580$) in cell viability reduction between chemotherapy and PCI experimental groups. In addition, gemcitabine concentration had a significant effect ($p < 0.001$) on cell viability reduction within each experimental group.

The $AlPcS_{2a}$ (5 µg/mL) PDT control conducted alongside these PCI experiments reduced cell viability to 85% (±5%). In relation to treatment potency, the IC_{70} was *not attained* for either chemotherapy or PCI treatment groups. Consequently, the IC_{50} of gemcitabine chemotherapy was estimated to be 40 nM whereby gemcitabine PCI achieved an IC_{50} of 20 nM – a 2-fold IC_{50} reduction in favour of PCI. At the maximum tested concentration of 250,000 nM, cell viability was seen to be reduced to 52% (±5%) and 43% (±3%) for chemotherapy and

PCI groups, respectively. These E_{max} values represent a 1.2-fold increase in efficacy at 250,000 nM for the PCI treatment group.

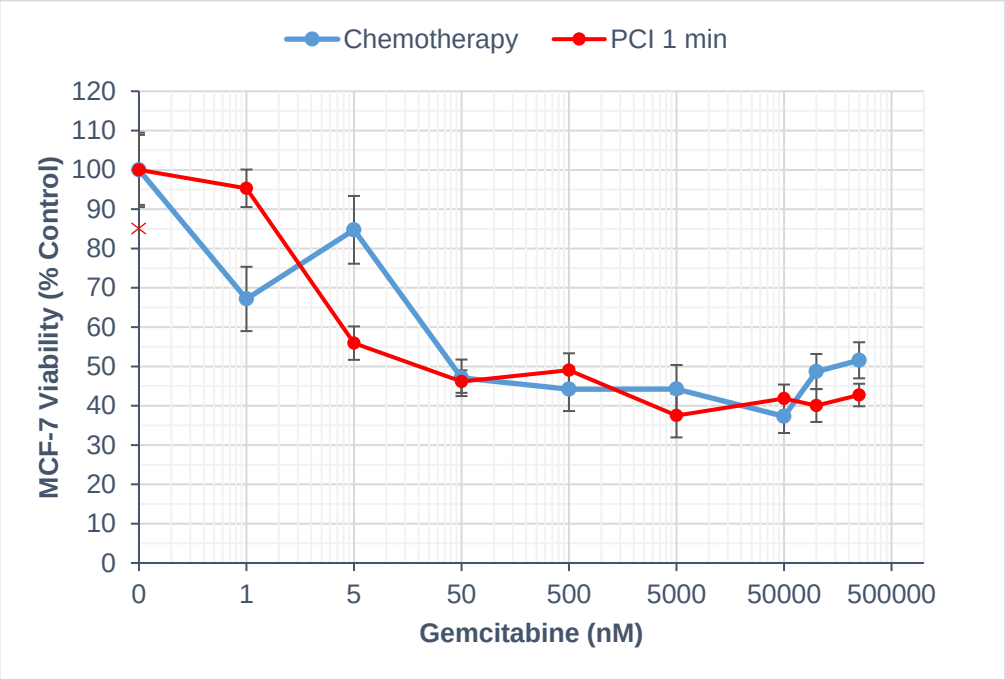

Figure 71. Reduction in MCF-7 breast cancer cell viability in 3D collagen hydrogels after gemcitabine chemotherapy and gemcitabine PCI*. Relative cellular viability (% of control) of MCF-7 cells after chemotherapy and PCI treatment at various gemcitabine concentrations (0.5-250,000 nM).*

5.3.6.1.3 Gemcitabine PCI – MDA-MB-231 cells vs MCF-7 cells

Upon comparison of gemcitabine-PCI performance in MDA-MB-231 and MCF-7 cells (shown in Figure 72), it was determined that there was *not* a statistically significant difference (p = 0.642) in cell viability reduction between MDA-MB-231 and MCF-7 cell lines.

Additionally, it can be seen from Figure 72 that gemcitabine-PCI treatment combinations were generally equipotent in each cell line across all of the concentrations tested. Although IC_{70} values were *not* attained, IC_{50} values were found to be 12 nM and 20 nM for MDA-MB-231 and MCF-7 cells, respectively. This represents a 1.7-fold reduction in IC_{50} value for gemcitabine-PCI in the MDA-MB-231 cell line. With regard to gemcitabine-PCI treatment efficacy, cell viability was reduced to 40% (±5%) and 43% (±3%) in MDA-MB-231 and MCF-7 cells, respectively, which represents an essentially equal E_{max} at 250,000 nM.

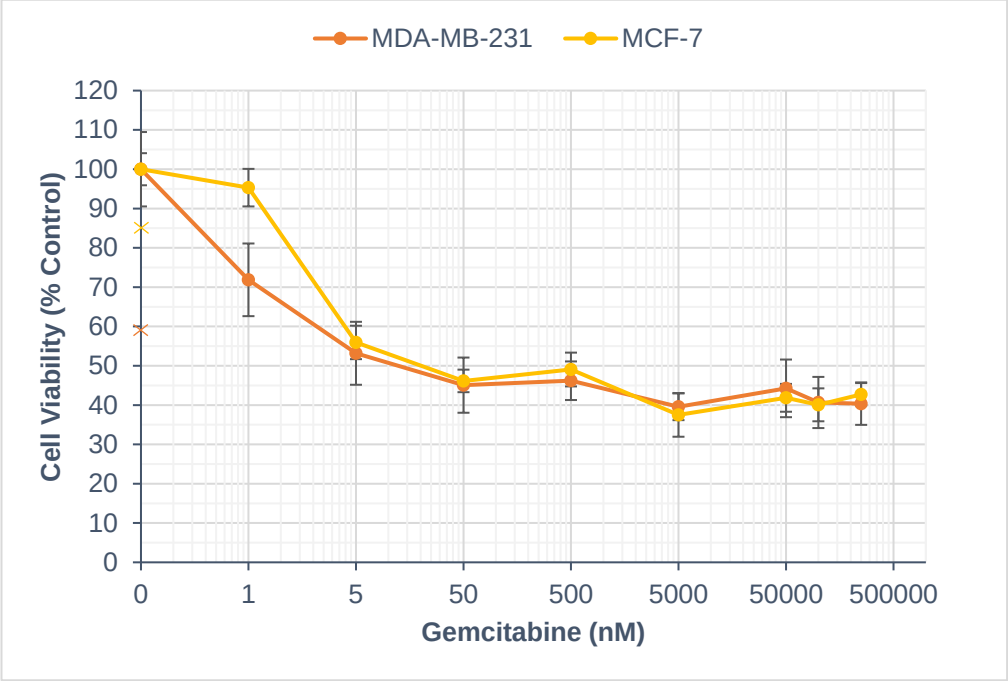

Figure 72. Reduction in breast cancer cell viability in 3D collagen hydrogels after gemcitabine PCI. *Relative cellular viability (% of control) of MDA-MB-231 and MCF-7 cells after PCI treatment at various gemcitabine concentrations (0.5-250,000 nM).*

5.3.6.1.3 Gemcitabine PCI – Treatment Synergy

Synergy calculations were then carried out and a synergy plot constructed for gemcitabine PCI (Figure 73). From this plot it can be seen that 25% of gemcitabine-PCI combinations were synergistic for the MDA-MB-231 cell line and the highest α value achieved was 1.2 (±0.1) at 100,000 nM. With regard to treatment synergy in the MCF-7 cell line, it can be seen that 50% of gemcitabine-PCI combinations were synergistic and the highest α value achieved was 1.4 (±0.2) at 5 nM.

5.3.6.2 Capecitabine Chemotherapy vs Capecitabine PCI

5.3.6.2.1 MDA-MB-231 cells

Following investigative PCI treatment with gemcitabine, the next antimetabolite drug to be considered was capecitabine. Figure 74 shows capecitabine-PCI alongside its capecitabine chemotherapy counterpart experiments. Here, it was found that there was *not* a significant difference (p = 0.308) in cell viability reduction between chemotherapy and PCI experimental groups. Moreover, capecitabine concentration did *not* have a significant effect (p = 0.362) on cell viability reduction within each experimental group.

The $AlPcS_{2a}$ (5 µg/mL) PDT control conducted alongside these PCI experiments reduced cell viability to 93% (±15%). Concerning the potency of capecitabine treatments, it can be seen in Figure 74 that neither the IC_{70} nor the IC_{50} were attained by chemotherapy or PCI treatment, respectively. In addition, at the maximum tested concentration of 250,000 nM, cell viability was seen to be 93% (±9%) and 86% (±10%) for chemotherapy and PCI groups, respectively.

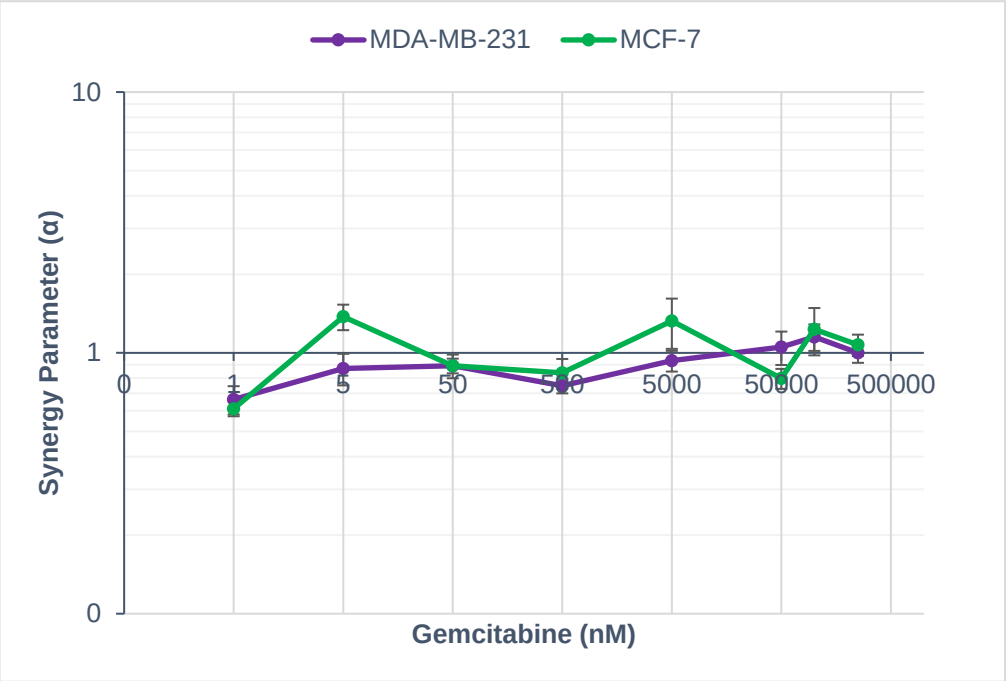

Figure 73. Synergy plot for gemcitabine-PCI combinations in MDA-MB-231 and MCF-7 breast cancer cells. *Synergy (α) was calculated from the individual cell viability results (specifically, survival/viability fraction) obtained for each respective treatment condition: chemotherapy, PDT, & PCI.*

5.3.6.2.2 MCF-7 cells

Capecitabine-PCI was then carried out in MCF-7 cells and is compared with capecitabine chemotherapy in Figure 75 below. Here, there *was* a significant difference ($p < 0.001$) in cell viability reduction observed between chemotherapy and PCI experimental groups. However, capecitabine concentration did *not* have a significant effect ($p = 0.001$) on cell viability reduction within each experimental group.

The $AlPcS_{2a}$ (5 µg/mL) PDT control conducted alongside these PCI experiments reduced cell viability to 47% (±6%). The IC_{70} was not attained by chemotherapy or PCI treatment. Capecitabine PCI achieved an IC_{50} at 5,000 nM. The maximum tested concentration (250,000 nM) reduced cell viability to 88% (±11%) and 48% (±7%) for

chemotherapy and PCI groups, respectively, which represents a 1.8-fold increase in treatment efficacy at 250,000 nM.

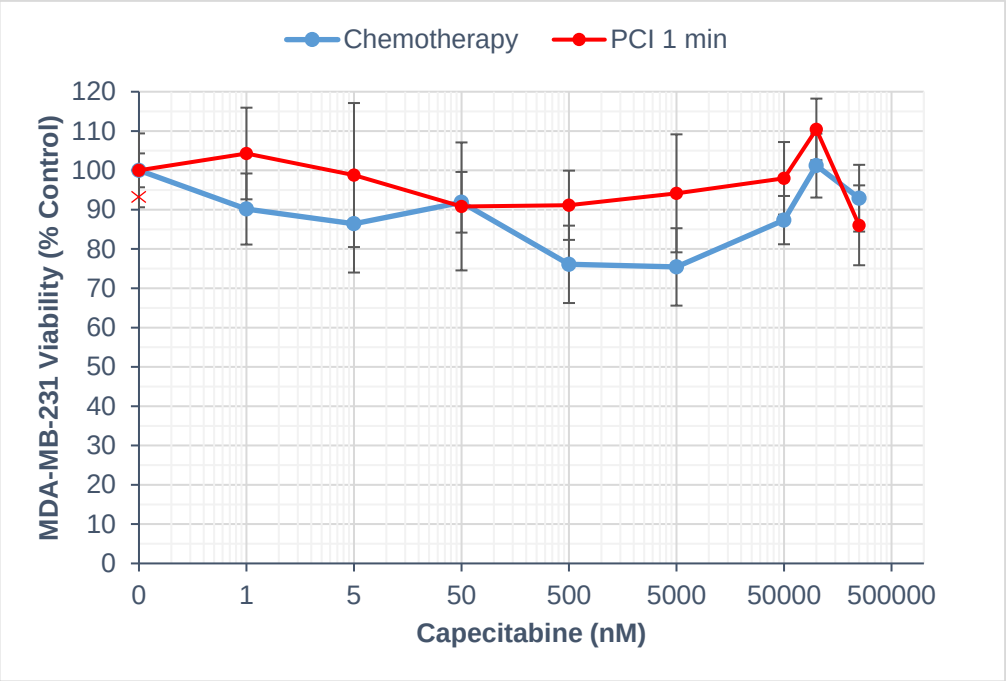

Figure 74. Reduction in MDA-MB-231 breast cancer cell viability in 3D collagen hydrogels after capecitabine chemotherapy and capecitabine PCI. *Relative cellular viability (% of control) of MDA-MB-231 cells after chemotherapy and PCI treatment at various capecitabine concentrations (0.5-250,000 nM).*

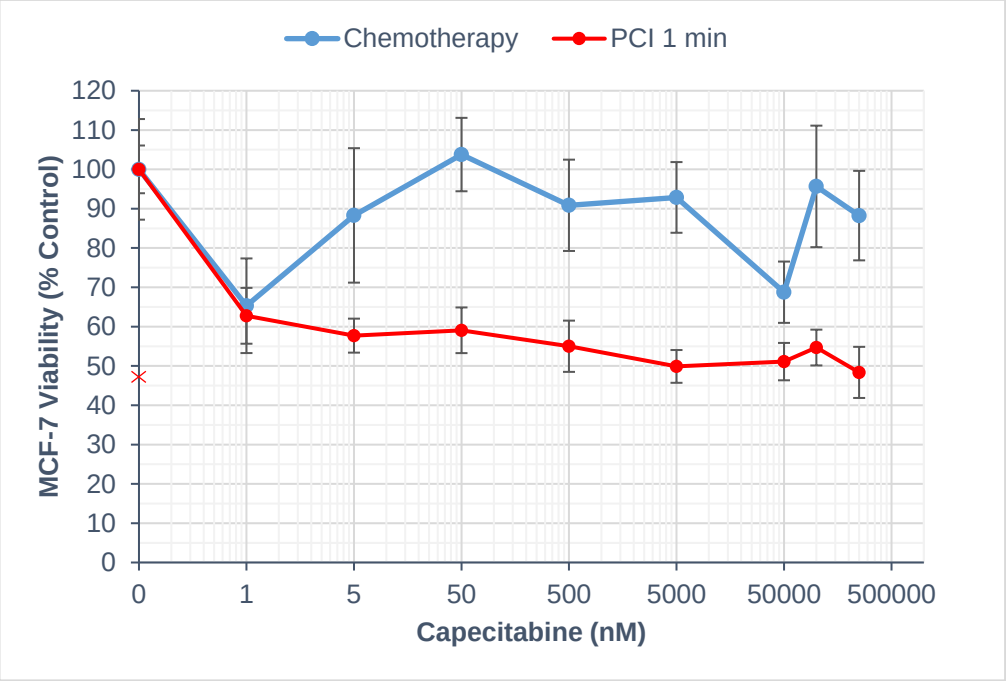

Figure 75. Reduction in MCF-7 breast cancer cell viability in 3D collagen hydrogels after capecitabine chemotherapy and capecitabine PCI. *Relative cellular viability (% of control) of MCF-7 cells after chemotherapy and PCI treatment at various capecitabine concentrations (0.5-250,000 nM).*

5.3.6.2.3 Capecitabine PCI – MDA-MB-231 cells vs MCF-7 cells

In Figure 76, the effect of capecitabine-PCI is shown for both MDA-MB-231 and MCF-7 cell lines. This comparison shows that there *was* a significant difference ($p < 0.001$) in cell viability reduction by capecitabine-PCI between MDA-MB-231 and MCF-7 cell lines.

Furthermore, capecitabine-PCI treatment combinations were seen to be more potent in the MCF-7 cell line across all tested concentrations. In relation to capecitabine-PCI, Figure 76 demonstrates that treatment IC_{70} values were *not* attained in either cell line but that an IC_{50} of 5,000 nM *was* achieved in MCF-7 cells. Pertaining to treatment efficacy at the maximum tested concentration of 250,000 nM, cell viability was reduced to 86% (±10%) and 48% (±7%) in MDA-MB-231 and MCF-7 cells, respectively. These E_{max} values represent a 1.8-fold increase in capecitabine-PCI efficacy in MCF-7 cells at the capecitabine concentration of 250,000 nM.

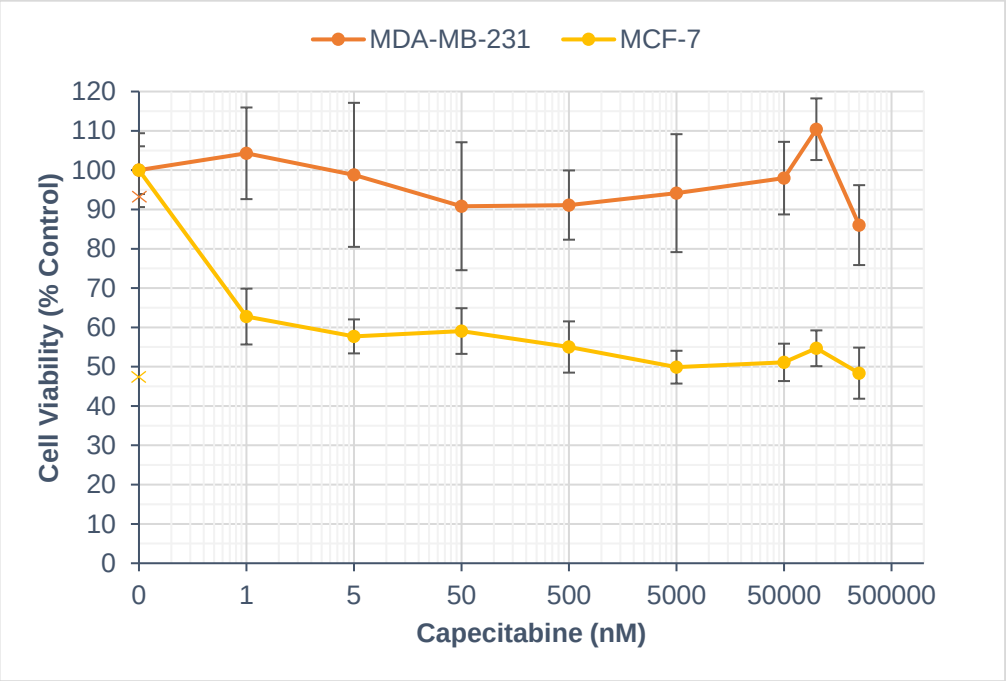

Figure 76. Reduction in breast cancer cell viability in 3D collagen hydrogels after capecitabine PCI. *Relative cellular viability (% of control) of MDA-MB-231 and MCF-7 cells after PCI treatment at various capecitabine concentrations (0.5-250,000 nM).*

5.3.6.2.4 Capecitabine PCI – Treatment Synergy

Capecitabine-PCI treatment synergy calculations were then performed (the synergy plot can be seen in Figure 77 below) and it was determined that 25% of capecitabine-PCI combinations were synergistic for the MDA-MB-231 cell line. Moreover, the joint-highest α value achieved

was 1.1 (±0.1) at 50 nM and 250,000 nM. With regard to treatment synergy in the MCF-7 cell line, here, 0% of capecitabine-PCI combinations were found to be synergistic.

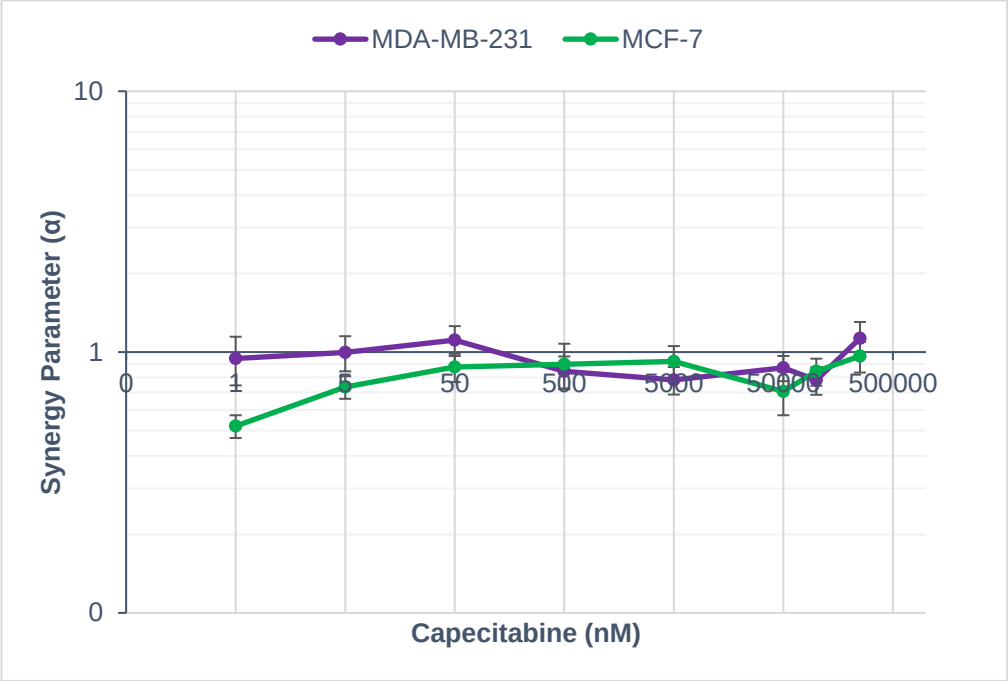

Figure 77. Synergy plot for capecitabine-PCI combinations in MDA-MB-231 and MCF-7 breast cancer cells. *Synergy (α) was calculated from the individual cell viability results (specifically, survival/viability fraction) obtained for each respective treatment condition: chemotherapy, PDT, & PCI.*

5.3.7 Chemotherapy in Combination

5.3.7.1 Gemcitabine & Paclitaxel Chemotherapy vs Gemcitabine & Paclitaxel PCI

5.3.7.1.1 MDA-MB-231 cells

Thus far, both chemotherapy and PCI investigations have been carried out in monotherapy with respect to the chemotherapeutic component. Next, the clinically-indicated (for advanced/metastatic breast cancer) chemotherapy combination of gemcitabine and paclitaxel (gemcitabine & paclitaxel) was tested in the 3D *in vitro* breast cancer models for its compatibility with PCI delivery (147). In Figure 78, gemcitabine & paclitaxel chemotherapy is compared with gemcitabine & paclitaxel PCI. Statistical analysis determined that there *was* a significant difference ($p < 0.001$) in cell viability reduction between chemotherapy and PCI experimental groups. Furthermore, gemcitabine & paclitaxel concentration had a significant effect ($p < 0.001$) on cell viability reduction within each experimental group.

The $AlPcS_{2a}$ (5 µg/mL) PDT control conducted alongside these PCI experiments reduced cell viability to 48% (±4%). In relation to the potency of combinatorial chemotherapy treatment, the IC_{70} was estimated to be 170,000 nM for the chemotherapy group and 37,500 nM for the PCI group, respectively. These values represent a 4.5-fold reduction in IC_{70} value in favour of PCI. In addition, at the maximum tested concentration of 250,000 nM, cell viability was reduced to 17% (±2%) and 1% (±0%) for the chemotherapy and PCI groups, respectively. This represents a 17-fold increase in treatment efficacy at 250,000 nM for the PCI group. There was also a notable increase in cell viability at low concentrations between 0.5-50 nM in the PCI group.

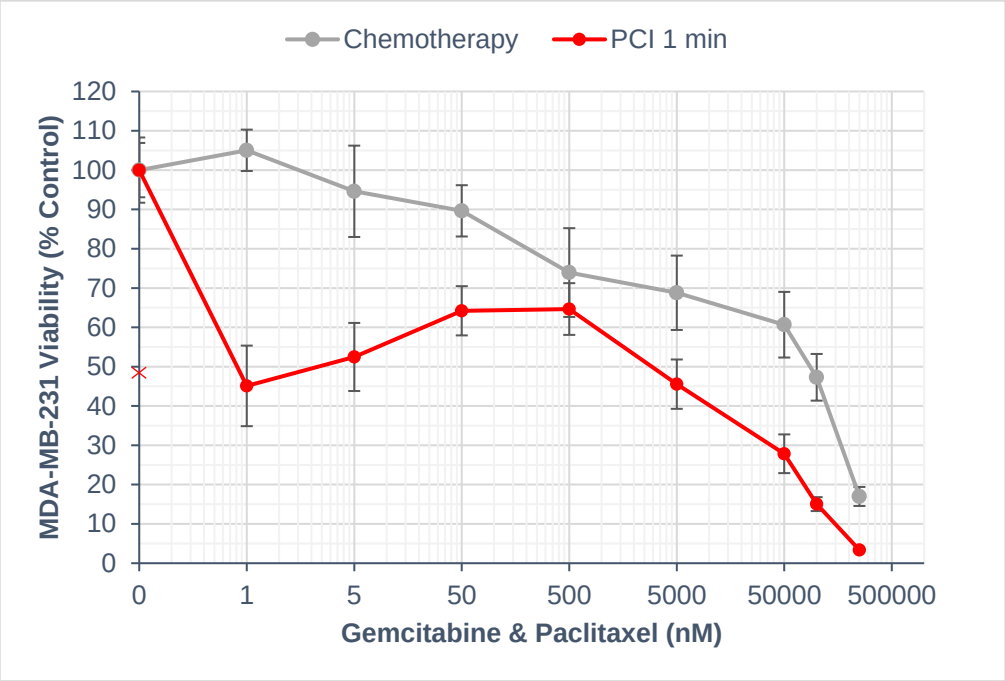

Figure 78. Reduction in MDA-MB-231 breast cancer cell viability in 3D collagen hydrogels after gemcitabine & paclitaxel dual chemotherapy and gemcitabine & paclitaxel PCI. *Relative cellular viability (% of control) of MDA-MB-231 cells after chemotherapy and PCI treatment at various gemcitabine & paclitaxel concentrations (0.5-250,000 nM).*

5.3.7.1.2 MCF-7 cells

Gemcitabine & paclitaxel chemotherapy and gemcitabine & paclitaxel PCI was then carried out in the MCF-7 cell line (as shown in Figure 79). Here, a significant difference ($p < 0.001$) in cell viability reduction *was* observed between chemotherapy and PCI treatment groups. Furthermore, gemcitabine & paclitaxel concentration had a significant effect ($p < 0.001$) on cell viability reduction within each experimental group.

The $AlPcS_{2a}$ (5 µg/mL) PDT control conducted alongside these PCI experiments reduced cell viability to 38% (±2%). With regard to treatment potency, the IC_{70} was determined as 26,000 nM for the chemotherapy group and 0.45 nM for the PCI group, respectively. This represents a 57,778-fold reduction in IC_{70} value in favour of the PCI group. At the maximum tested concentration of 250,000 nM, cell viability was reduced to 25% (±1%) and 10% (±1%) for the chemotherapy and PCI groups, respectively. This represents a 2.5-fold increase in treatment efficacy at 250,000 nM for the PCI group.

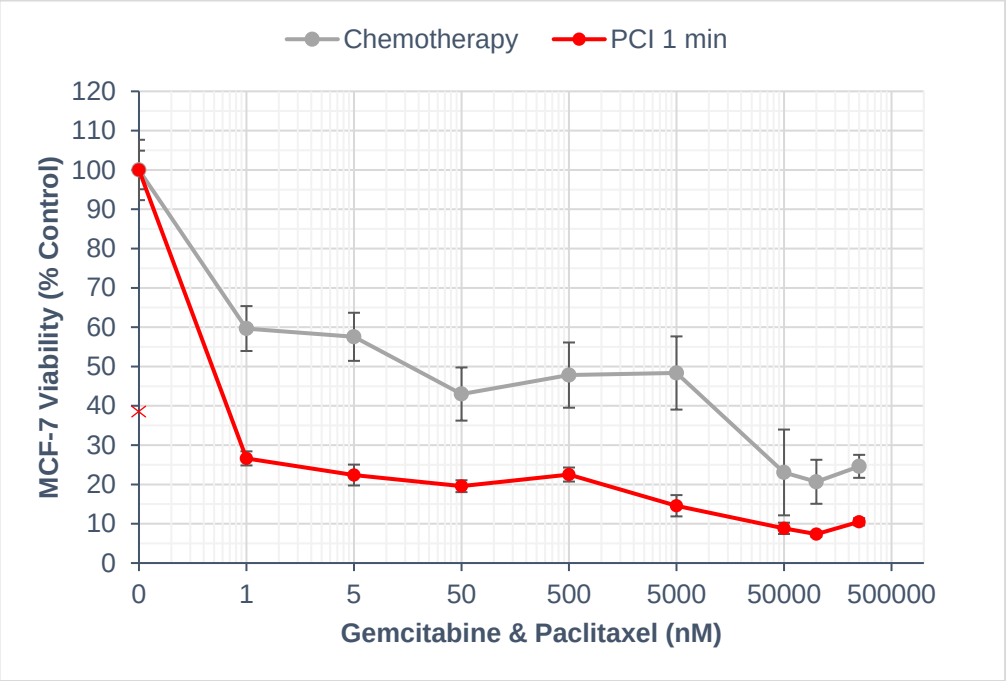

Figure 79. Reduction in MCF-7 breast cancer cell viability in 3D collagen hydrogels after gemcitabine & paclitaxel chemotherapy and gemcitabine & paclitaxel PCI*. Relative cellular viability (% of control) of MCF-7 cells after chemotherapy and PCI treatment at various gemcitabine & paclitaxel concentrations (0.5-250,000 nM).*

5.3.7.1.3 Gemcitabine & Paclitaxel PCI – MDA-MB-231 cells vs MCF-7 cells

Gemcitabine & paclitaxel PCI treatment was then compared between the breast cancer cell lines (as shown in Figure 80). From these experiments it was determined that there *was* a significant difference ($p < 0.001$) in cell viability reduction by gemcitabine & paclitaxel-PCI between MDA-MB-231 and MCF-7 cell lines.

In addition, gemcitabine & paclitaxel-PCI treatment combinations were generally more potent against MCF-7 cells than MDA-MB-231 cells across the various concentrations tested. With respect to treatment potency, the IC_{70} values were 37,500 nM and 0.45 nM for MDA-MB-231 and MCF-7 cells, respectively. This represents an 83,333-fold reduction in IC_{70} value for

gemcitabine & paclitaxel-PCI in the MCF-7 cell line. Pertaining to treatment efficacy at the maximum tested concentration of 250,000 nM, cell viability was seen to be reduced to 3% (±0%) and 10% (±1%) in MDA-MB-231 and MCF-7 cells, respectively. These E_{max} values represent a 3.3-fold increase in gemcitabine & paclitaxel-PCI efficacy in the MDA-MB-231 cell line at 250,000 nM.

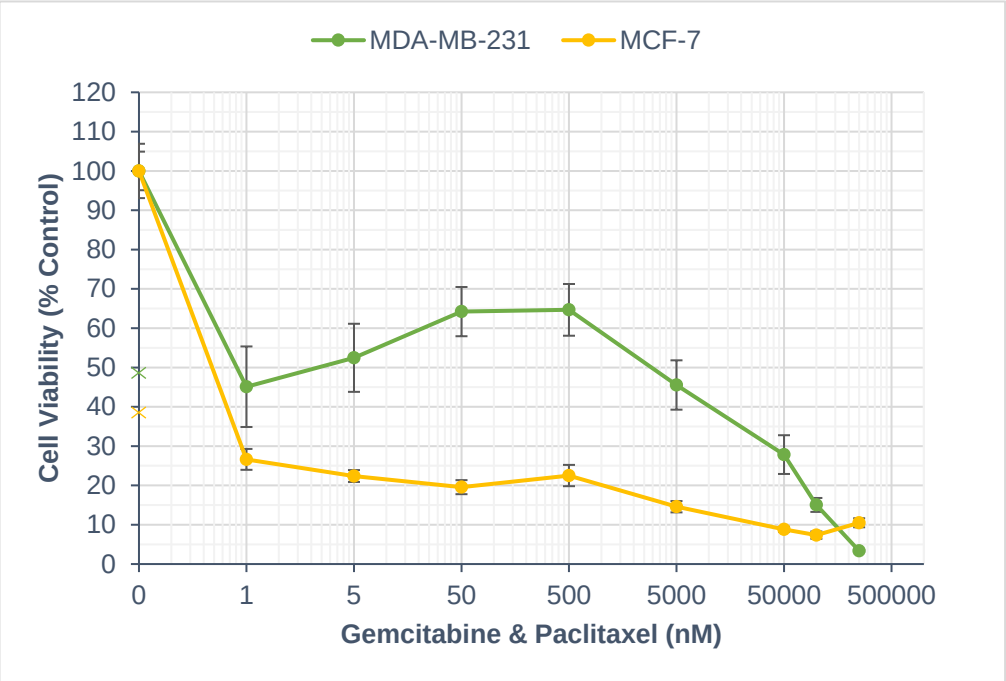

Figure 80. Reduction in breast cancer cell viability in 3D collagen hydrogels after gemcitabine & paclitaxel PCI*. Relative cellular viability (% of control) of MDA-MB-231 and MCF-7 cells after PCI treatment at various gemcitabine & paclitaxel concentrations (0.5-250,000 nM).*

5.3.7.1.4 Gemcitabine & Paclitaxel – Treatment Synergy

In relation to treatment synergy, firstly, the dual chemotherapy combination treatment (gemcitabine & paclitaxel) was compared with the two chemotherapy drugs as individual, standalone agents. This synergy plot can be seen in Figure 81 (*top*) and it demonstrates that 13% of gemcitabine & paclitaxel dual chemotherapy combinations were synergistic for the MDA-MB-231 cell line. Here, the highest α value achieved was 1.2 (±0.3) at 250,000 nM. Pertaining to treatment synergy in the MCF-7 cell line, it was found that 0% of gemcitabine & paclitaxel combinations were synergistic.

5.3.7.1.5 Gemcitabine & Paclitaxel PCI – Treatment Synergy

Next, treatment synergy was assessed between chemotherapy and PCI treatment groups, as shown in Figure 81 (*bottom*).

Here, it can be seen that 50% of gemcitabine & paclitaxel-PCI combinations were synergistic for the MDA-MB-231 cell line. Furthermore, that the highest *α* value achieved was 2.5 (±0.2) at 250,000 nM. Pertaining to synergy in the MCF-7 cell line, 25% of gemcitabine & paclitaxel-PCI combinations were synergistic and the highest *α* value achieved was 1.5 (±0.3) at 5,000 nM.

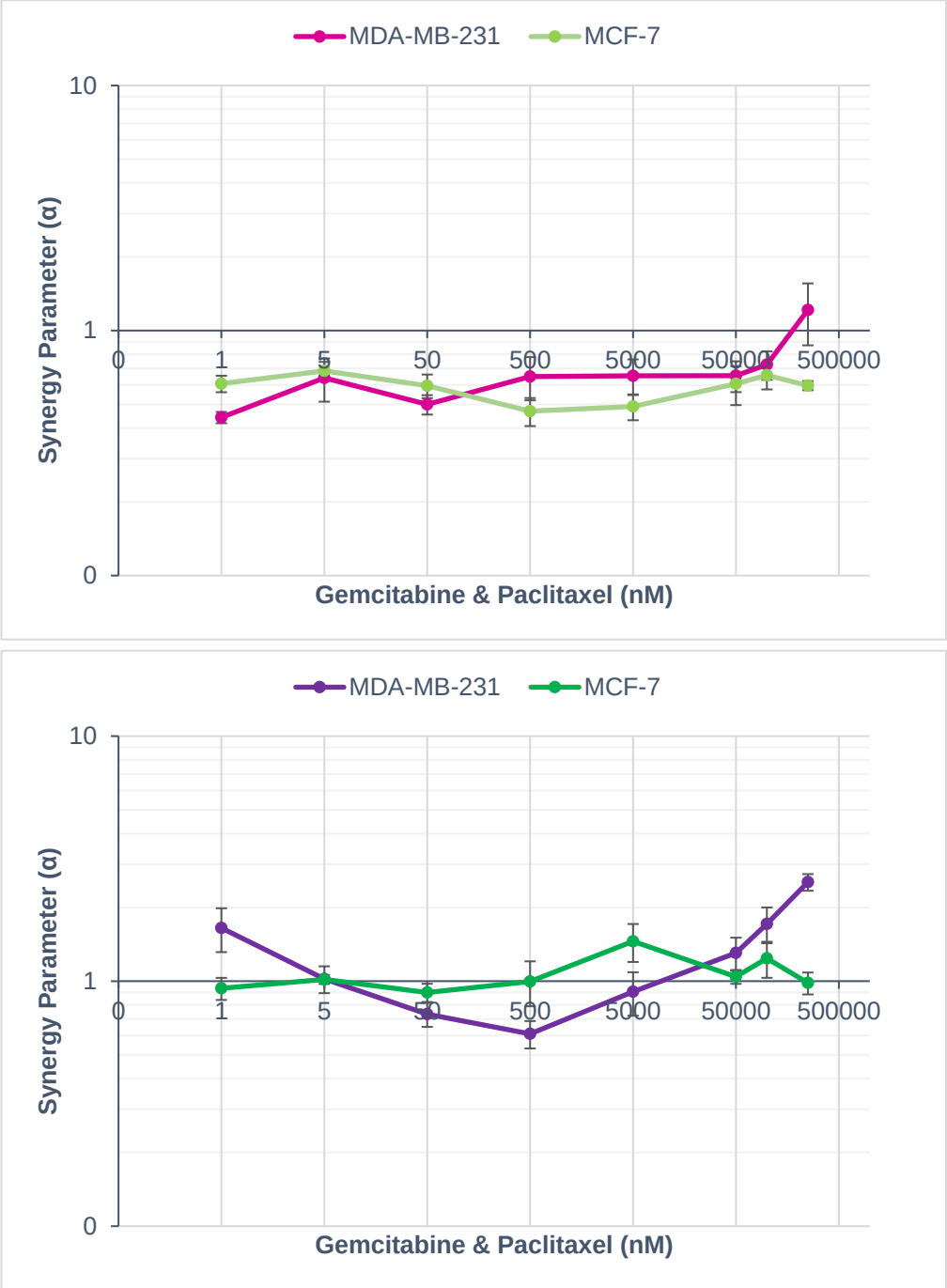

Figure 81. Synergy plot for gemcitabine & paclitaxel chemotherapy and PCI combinations in MDA-MB-231 and MCF-7 breast cancer cells*. Synergy (α) was calculated from the individual cell viability results (specifically, survival/viability fraction) obtained for each respective treatment.*

5.3.8 Chemotherapy & Lysosome Co-localisation

5.3.8.1 Vinblastine & Lysotracker

In order to determine whether the observed PCI-regimen improvements in treatment outcomes were actually the result of a *classical* PCI mechanism, fluorescence imaging was performed in MDA-MB-231 TNBC cells (Figure 82). Indeed, fluorescence imaging of fluorescent green BODIPY™-tagged vinblastine chemotherapy (*left* image; 10,000 nM) and fluorescent red Lysotracker™ (*centre* image; 75 nM) showed that there *was* a subcellular localisation of chemotherapy to lysosomal compartments – as demonstrated by the orange-yellow colour of the composite image (*right*).

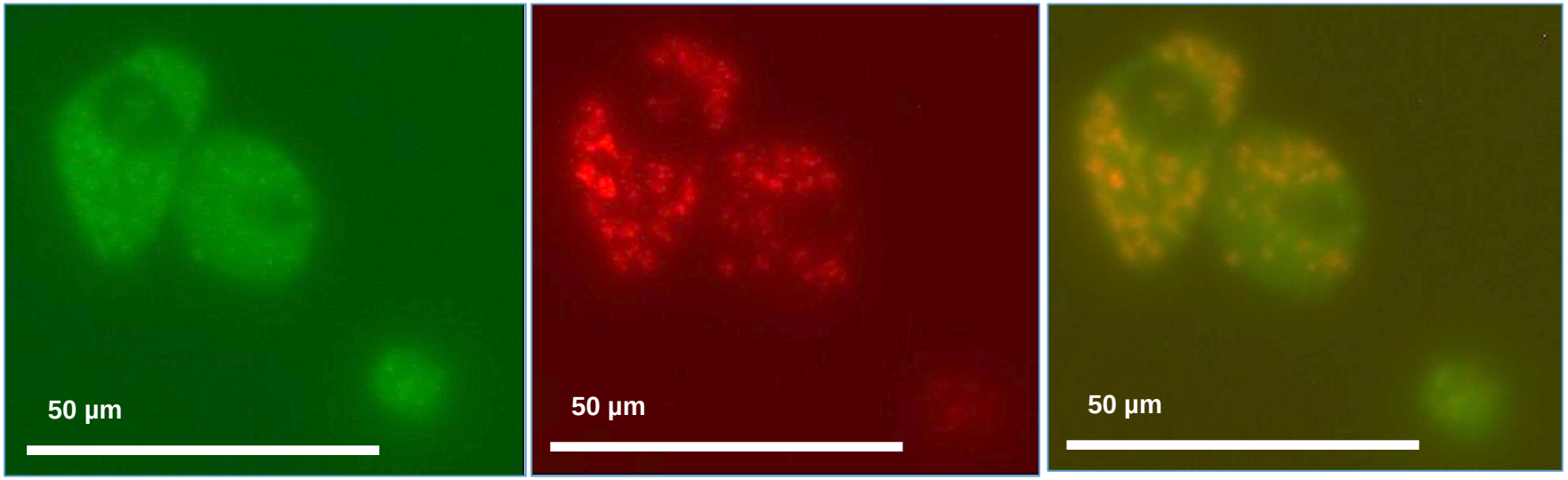

Figure 82. Co-localisation of chemotherapy and lysosome. *Fluorescence microscopy of MDA-MB-231 TNBC cells incubated (18 h) with: fluorescently-tagged vinblastine (left); and lysotracker red (centre). The right image is the two former images merged together showing chemotherapy-lysosome co-localisation. Scale bar shown as 50 µm.*

5.3.9 MDA-MB-231 Cell death

5.3.9.1 Live/dead imaging

In order to determine whether reduced cell viability was due to increased cell death, fluorescent live/dead imaging was conducted in MDA-MB-231 TNBC cells with vinblastine as a model small molecule chemotherapy drug. The *left* image of Figure 83 shows untreated control cells; the *right* image, cells after 18 h incubation with vinblastine (10,000 nM). Live cells (*green*) are shown with dead cells (*red*). Upon comparison of left and right images, it can be seen that dead cells are much more prevalent after just 18 h incubation with chemotherapy and that the morphology of live cells has altered from stellate to round. These experiments demonstrate that the decrease in cell viability resulting from the various chemotherapy and PCI treatments actually did correspond to cell *death*.

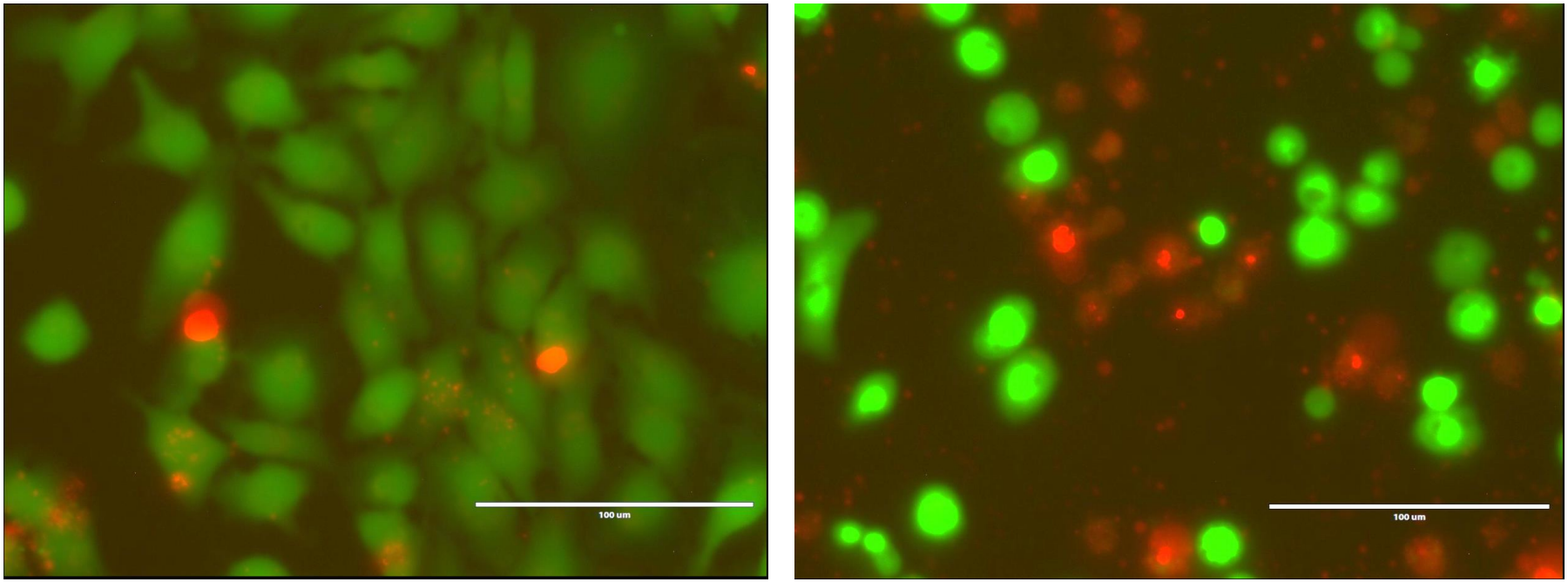

Figure 83. Change in MDA-MB-231 morphology and cell death after chemotherapy. *Fluorescent imaging of MDA-MB-231 cells showing control cells [Left] and cells treated [Right] with vinblastine chemotherapy (10,000 nM). Live cells (green) and dead cells (red) are displayed together. Scale bar shown is 100 µm.*

5.3.10 Results Summary

5.3.10.1 IC_{70} and E_{max}

The key treatment effects indicative of treatment potency and efficacy (IC_{70}; E_{max}) were identified from the chemotherapy and PCI cytotoxicity profiles for each drug and are summarised below (Table 4). Chemotherapy and PCI treatment effects were also compared against each other and, accordingly, the changes in potency and efficacy are also listed.

Table 4. Summary of IC_{70} and E_{max} values comparing the treatment effects of chemotherapy to PCI on MDA-MB-231 and MCF-7 human breast cancer cells in 3D collagen hydrogels.

Chemotherapy Drug	Treatment	IC_{70} (nM)				E_{max} (% Control [±SE])			
		MDA-MB-231	*Potency change (fold)*	*MCF-7*	*Potency change (fold)*	*MDA-MB-231*	*Efficacy change (fold)*	*MCF-7*	*Efficacy change (fold)*
Bleomycin	Chemotherapy	50,000	.	3,500	.	16 (±1)	.	10 (±1)	.
Vinorelbine		75,000	.	20,000	.	0 (±0)	≡	0 (±0)	≡
Vincristine		1,500 (IC_{50})	.	75,000	.	59 (±7)	.	18 (±2)	.
Vinblastine		150,000	.	12,500	.	0 (±0)	≡	0 (±0)	≡
Docetaxel		100,000	≡	112,500	.	0 (±0)	≡	11 (±4)	≡
Paclitaxel		225,000	.	42,500	.	27 (±2)	.	28 (±2)	.
Gemcitabine		n/a	n/a	40 (IC_{50})	.	56 (±6)	.	52 (±5)	.
Capecitabine		n/a	n/a	n/a	.	93 (±9)	.	88 (±11)	.
Gemcitabine & Paclitaxel		170,000	.	26,000	.	17 (±2)	.	25 (±1)	.
Bleomycin	PCI	27,500	+ 1.8	750	+ 4.7	6 (±0)	+ 2.7	5 (±0)	+ 2.0
Vinorelbine		275	+ 273	5	+ 4,000	0 (±0)	≡	0 (±0)	≡
Vincristine		0.25 (IC_{50})	+ 6,000 (IC_{50})	0.425	+176,470	21 (±4)	+ 2.8	10 (±1)	+ 1.8
Vinblastine		80,000	+ 1.9	12.5	+ 1,000	0 (±0)	≡	0 (±0)	≡
Docetaxel		100,000	≡	1,250	+ 90	0 (±0)	≡	11 (±3)	≡
Paclitaxel		75,000	+ 3.0	4,250	+ 10	6 (±1)	+ 4.5	17 (±2)	+ 1.6
Gemcitabine		12.5 (IC_{50})	n/a	20 (IC_{50})	+ 2.0	40 (±5)	+ 1.4	43 (±3)	+ 1.2
Capecitabine		n/a	n/a	5,000	n/a	86 (±10)	+ 1.1	48 (±7)	+ 1.8
Gemcitabine & Paclitaxel		37,500	+ 4.5	0.45	+ 57,778	1 (±0)	+ 17	10 (±1)	+ 2.5

5.3.10.2 Maximum Drug Potency and Efficacy

The most potent PCI-drug combination in MDA-MB-231 cells was PCI-vincristine (as shown in Table 5). The most efficacious PCI combinations were PCI-vinorelbine, PCI-vinblastine,

and PCI-docetaxel. With regard to the MCF-7 cell line, the most potent PCI-drug combination was also PCI-vincristine. The most efficacious PCI combinations against MCF-7 cells were PCI-vinorelbine, and PCI-vinblastine.

The majority of PCI-drug treatments were more potent in MCF-7 cells (Table 6) with the largest disparity between cell lines seen with PCI gemcitabine & paclitaxel (83,333-fold). By contrast, PCI efficacy favoured MDA-MB-231 cells; with PCI-docetaxel exhibiting an 11-fold increase.

Table 5. Summary of the most potent and efficacious chemotherapy and PCI treatments in MDA-MB-231 and MCF-7 human breast cancer cells in 3D collagen hydrogels.

Cell line	Most Potent (IC_{70})				Most Efficacious			
	Chemotherapy		PCI		Chemotherapy		PCI	
	Drug Class	Drug	Drug Class	Drug	Drug Class	Drug	Drug Class	Drug
MDA-MB-231	Glycopeptides	Bleomycin	Vinca alkaloids	Vincristine	Vinca alkaloids	Vinorelbine	Vinca alkaloids	Vinorelbine
					Vinca alkaloids	Vinblastine	Vinca alkaloids	Vinblastine
					Taxanes	Docetaxel	Taxanes	Docetaxel
MCF-7	Glycopeptides	Bleomycin	Vinca alkaloids	Vincristine	Vinca alkaloids	Vinorelbine	Vinca alkaloids	Vinorelbine
					Vinca alkaloids	Vinblastine	Vinca alkaloids	Vinblastine

Table 6. Summary of IC_{70} and E_{max} values comparing PCI treatment effects between MDA-MB-231 and MCF-7 human breast cancer cells in 3D collagen hydrogels.

Chemotherapy Drug	Treatment	IC_{70} (nM)				E_{max} (% Control [±SE])			
		MDA-MB-231	Potency change (fold)	MCF-7	Potency change (fold)	MDA-MB-231	Efficacy change (fold)	MCF-7	Efficacy change (fold)
Bleomycin	PCI	27,500	.	750	+ 37	6 (±0)	.	5 (±0)	+ 1.2
Vinorelbine		275	.	5	+ 55	0 (±0)	≡	0 (±0)	≡
Vincristine		0.45	.	0.40	+ 1.1	21 (±4)	.	10 (±1)	+ 2.0
Vinblastine		80,000	.	12.5	+ 6,400	0 (±0)	≡	0 (±0)	≡
Docetaxel		100,000	.	1,250	+ 18	0 (±0)	+ 11	11 (±3)	.
Paclitaxel		75,000	.	4,250	+ 18	6 (±1)	+ 2.8	17 (±2)	.
Gemcitabine		12 (IC_{50})	+ 1.7	20 (IC_{50})	.	40 (±5)	+ 1.1	43 (±3)	.
Capecitabine		n/a	n/a	5,000 (IC_{50})	n/a	86 (±10)	.	48 (±7)	+ 1.8
Gemcitabine & Paclitaxel		37,500	.	0.45	+ 83,333	3 (±0)	+ 3.3	10 (±1)	.

5.3.10.3 Treatment Synergy

Next, the key treatment effects pertaining to the treatment synergy achieved by PCI delivery was identified and is summarised below (Table 7). Specifically, the results obtained for the percentage of synergistic treatment combinations, the highest *α* values achieved and at which concentrations. In addition, the average *α* value achieved by synergistic combinations was calculated and is also reported. PCI-vincristine performed especially highly in this regard in both breast cancer cell lines with 100% synergy in PCI-drug combinations.

Table 7. Summary of treatment synergy from PCI treatment combinations on MDA-MB-231 and MCF-7 human breast cancer cells in 3D collagen hydrogels.

Chemotherapy Drug	Treatment	Synergy (α)							
		MDA-MB-231				MCF-7			
		Synergistic combinations (%) / Ave (α)		Highest α value	Conc. (nM)	Synergistic combinations (%) / Ave (α)		Highest α value	Conc. (nM)
Bleomycin	PCI	63	1.7 (±0.2)	2.1 (±0.1)	250,000	88	1.6 (±0.3)	2.1 (±0.6)	50,000 & 100,000
Vinorelbine		25	2.5 (±0.8)	3.7 (±1.2)	100,000	38	1.1 (±0.3)	1.2 (±0.4)	5,000
Vincristine		100	2.0 (±0.3)	3.0 (±0.4)	5	100	1.7 (±0.4)	2.6 (±0.7)	50,000 & 100,000
Vinblastine		63	1.3 (±0.2)	1.6 (±0.2)	100,000	88	1.5 (±0.1)	2.0 (±0.2)	5,000
Docetaxel		50	1.4 (±0.2)	1.7 (±0.2)	5,000	50	1.3 (±0.2)	1.6 (±0.2)	5,000
Paclitaxel		13	2.9 (±0.5)	2.9 (±0.5)	250,000	25	1.2 (±0.3)	1.2 (±0.2)	100,000
Gemcitabine		25	1.2 (±0.2)	1.2 (±0.1)	100,000	50	1.3 (±0.2)	1.4 (±0.2)	5
Capecitabine		25	1.1 (±0.1)	1.1 (±0.1)	50 & 250,000	0	n/a	n/a	n/a
Gemcitabine & Paclitaxel		50	1.8 (±0.3)	2.5 (±0.2)	250,000	25	1.4 (±0.3)	1.5 (±0.3)	250,000
Gemcitabine & Paclitaxel	Dual Chemotherapy	13	1.2 (±0.3)	1.2 (±0.3)	250,000	0	n/a	n/a	n/a

5.4 Chemotherapy & PCI Treatment Effects by Drug Class versus Bleomycin

5.4.1 Vinca alkaloids

5.4.1.1 MDA-MB-231 cells

5.4.1.1.1 Chemotherapy vs Bleomycin chemotherapy

Following the testing of clinically-important chemotherapy drugs both in the guise of standalone chemotherapy and as a part of a PCI regimen (and determining potential clinical benefits through, for example, synergy calculations), it was pertinent to compare the individual

agents both in the context of their respective drug classes and next to the model PCI chemotherapeutic drug bleomycin.

Below, Figure 84 displays the relative performance of vinca alkaloids and bleomycin chemotherapy against MDA-MB-231 triple-negative human breast adenocarcinoma cells. Here, it was observed that there *was* a significant difference ($p < 0.001$) in cell viability reduction between the various chemotherapy treatments.

More specifically, vinorelbine chemotherapy was generally the most potent against MDA-MB-231 cells across the various concentrations tested. Pertaining to treatment potency, Figure 84 shows that bleomycin chemotherapy achieved the lowest IC_{70} value of 50,000 nM, whereby vinorelbine achieved the lowest IC_{70} value of 75,000 nM for the vinca alkaloids. This represents a 1.5-fold reduction in favour of bleomycin chemotherapy. In relation to treatment efficacy at the highest tested concentration of 250,000 nM, the vinca alkaloids vinorelbine and vinblastine were maximally effective as they were found to reduce cell viability to 0% of control – a 16-fold increase in efficacy compared with bleomycin chemotherapy.

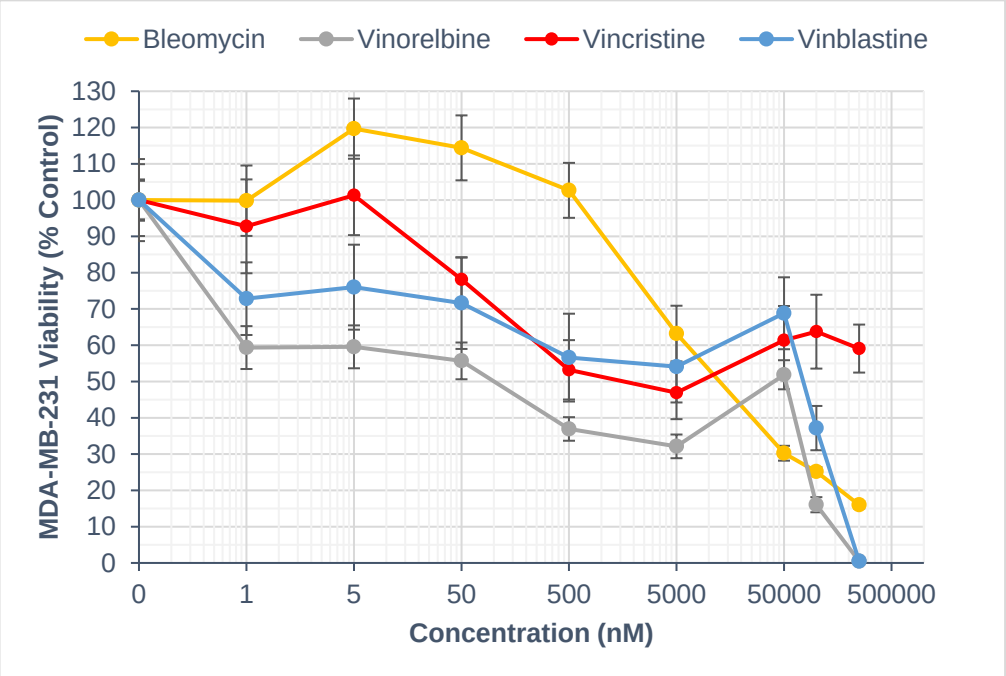

Figure 84. Reduction in MDA-MB-231 breast cancer cell viability in 3D collagen hydrogels after vinca alkaloid and bleomycin chemotherapy*. Relative cellular viability (% of control) of MDA-MB-231 cells after vinca alkaloids (vinorelbine; vincristine; vinblastine) and bleomycin chemotherapy at various concentrations (0.5-250,000 nM).*

5.4.1.1.2 PCI vs Bleomycin PCI

Next, comparisons were made between vinca alkaloids-PCI and bleomycin-PCI (as shown in Figure 85). Here, a significant difference ($p < 0.001$) in MDA-MB-231 cell viability reduction *was* observed between the various PCI treatments.

Furthermore, vincristine-PCI was generally more potent at lower drug concentrations and vinorelbine-PCI at the highest drug concentrations. With regard to the potency of the PCI treatments, vincristine-PCI achieved the lowest IC_{70} value of 0.45 nM whereby the model PCI drug bleomycin achieved an IC_{70} of 27,500 nM. These IC_{70} values represent a 61,111-fold reduction in favour of vincristine-PCI versus bleomycin-PCI. Vinorelbine-PCI and vinblastine-PCI were maximally effective at 250,000 nM as both treatment regimens reduced viability to 0% of control. By contrast, bleomycin-PCI reduced cell viability to 16% (±0%) which represents around a 16-fold decrease in efficacy for bleomycin-PCI.

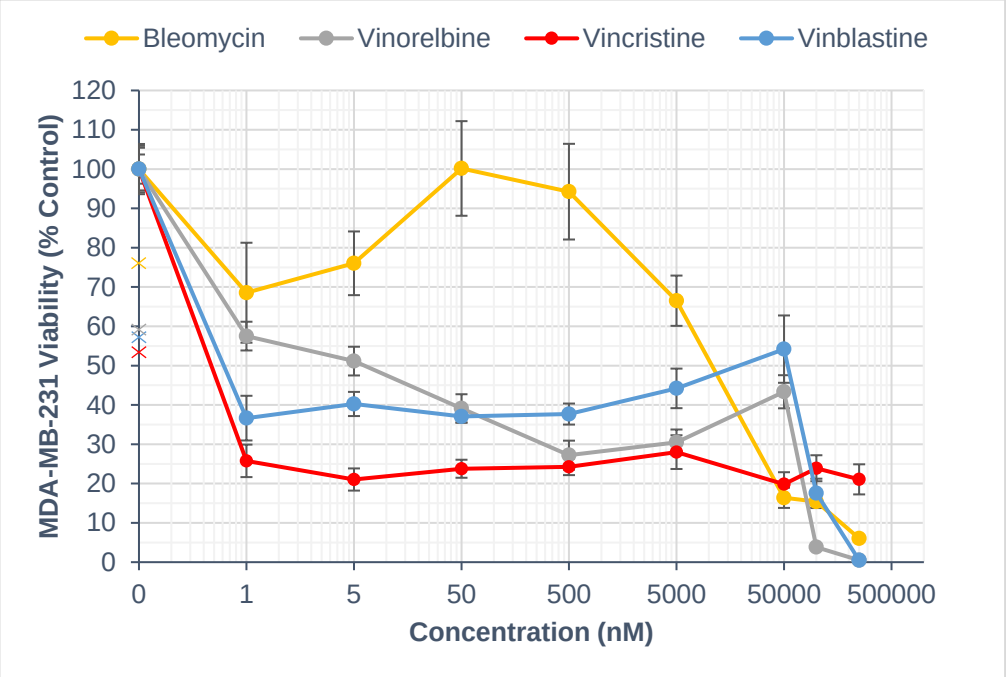

Figure 85. Reduction in MDA-MB-231 breast cancer cell viability in 3D collagen hydrogels after vinca alkaloid and bleomycin PCI. *Relative cellular viability (% of control) of MDA-MB-231 cells after vinca alkaloid (vinorelbine; vincristine; vinblastine) and bleomycin PCI at various concentrations (0.5-250,000 nM).*

5.4.1.1.3 Pooled Chemotherapy vs Pooled PCI

Next, results for each separate vinca alkaloid drug (vinorelbine, vincristine, and vinblastine) were pooled together for both chemotherapy and PCI treatments (as shown in Figure 86).

Here, a significant difference ($p < 0.001$) in MDA-MB-231 cell viability reduction *was* observed between pooled vinca alkaloid chemotherapy and pooled vinca alkaloid-PCI groups.

Moreover, vinca alkaloid-PCI was more potent than vinca alkaloid chemotherapy at all tested concentrations and achieved an IC_{70} of 350 nM. By way of comparison, vinca alkaloid chemotherapy achieved an IC_{70} of 150,000 nM which represents a 429-fold IC_{70} reduction in favour of PCI. At the maximum tested concentration of 250,000 nM, cell viability was reduced to 7% (±1%) by vinca alkaloid-PCI and to 20% (±1%) by vinca alkaloid chemotherapy which represents around a 3-fold increase in treatment efficacy in favour of PCI.

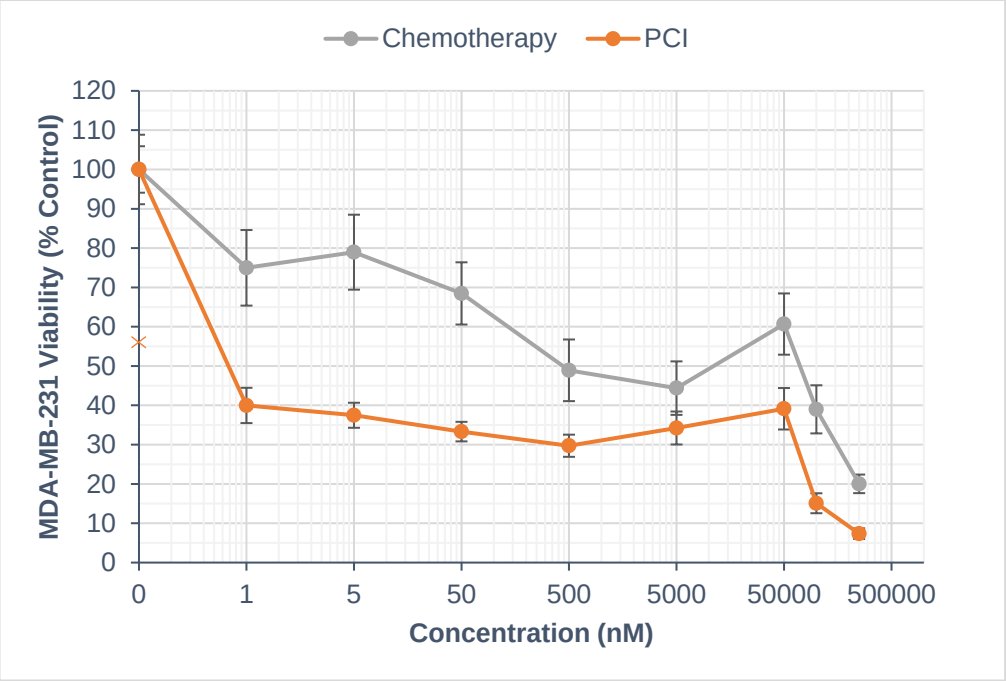

Figure 86. Reduction in MDA-MB-231 breast cancer cell viability in 3D collagen hydrogels after vinca alkaloid chemotherapy and vinca alkaloid PCI. *Relative cellular viability (% of control) of MDA-MB-231 cells after pooled (vinorelbine; vincristine; vinblastine) vinca alkaloid chemotherapy and pooled (vinorelbine; vincristine; vinblastine) vinca alkaloid PCI at various concentrations (0.5-250,000 nM).*

5.4.1.2 MCF-7 cells

5.4.1.2.1 Chemotherapy vs Bleomycin chemotherapy

The same treatment comparisons were then made for the MCF-7 oestrogen receptor-positive cell line beginning with the chemotherapy comparisons shown in Figure 87. Here, there *was*

a significant difference ($p < 0.001$) in MCF-7 cell viability reduction observed between the various chemotherapy treatments.

In general, vinorelbine chemotherapy was the most potent against MCF-7 cells across the various concentrations tested. It can also be seen in Figure 87 that bleomycin chemotherapy achieved the lowest IC_{70} of 3,500 nM whereby vinblastine achieved the lowest IC_{70} of the vinca alkaloids with 12,500 nM - a 3.6-fold reduction in favour of bleomycin chemotherapy. At the highest tested concentration of 250,000 nM, the vinca alkaloids vinorelbine and vinblastine were maximally effective given their reduction of cell viability to 0% of control. By contrast, bleomycin chemotherapy reduced cell viability to 10% (±1%) which represents around a 10-fold increase in treatment efficacy for vinorelbine and vinblastine chemotherapy.

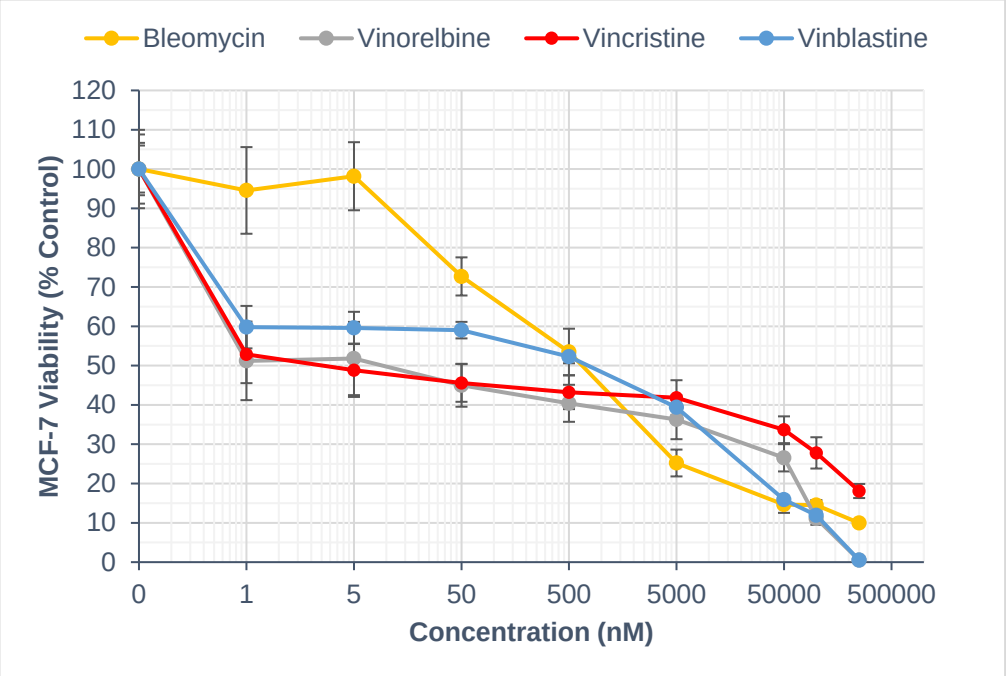

Figure 87. Reduction in MCF-7 breast cancer cell viability in 3D collagen hydrogels after vinca alkaloid and bleomycin chemotherapy*. Relative cellular viability (% of control) of MCF-7 cells after vinca alkaloid (vinorelbine; vincristine; vinblastine) and bleomycin chemotherapy at various concentrations (0.5-250,000 nM).*

5.4.1.2.2 PCI vs Bleomycin PCI

Comparisons between vinca alkaloid-PCI and bleomycin-PCI in MCF-7 cells is shown in Figure 88. Here, statistical analysis determined that there *was* a significant difference ($p < 0.001$) in cell viability reduction between the various PCI treatments.

In addition, vincristine-PCI was generally most potent at lower drug concentrations and vinblastine-PCI at higher drug concentrations. Furthermore, vincristine-PCI achieved the lowest IC_{70} value with 0.40 nM whereby PCI utilising the model drug bleomycin achieved an IC_{70} of 750 nM. This represents a 1,875-fold reduction in favour of vincristine-PCI. Pertaining to treatment efficacy, vinorelbine-PCI and vinblastine-PCI were maximally effective (that is, reduced cell viability to 0% of control) at the highest tested concentration of 250,000 nM whereby bleomycin-PCI reduced MCF-7 cell viability to 5% (±0%).

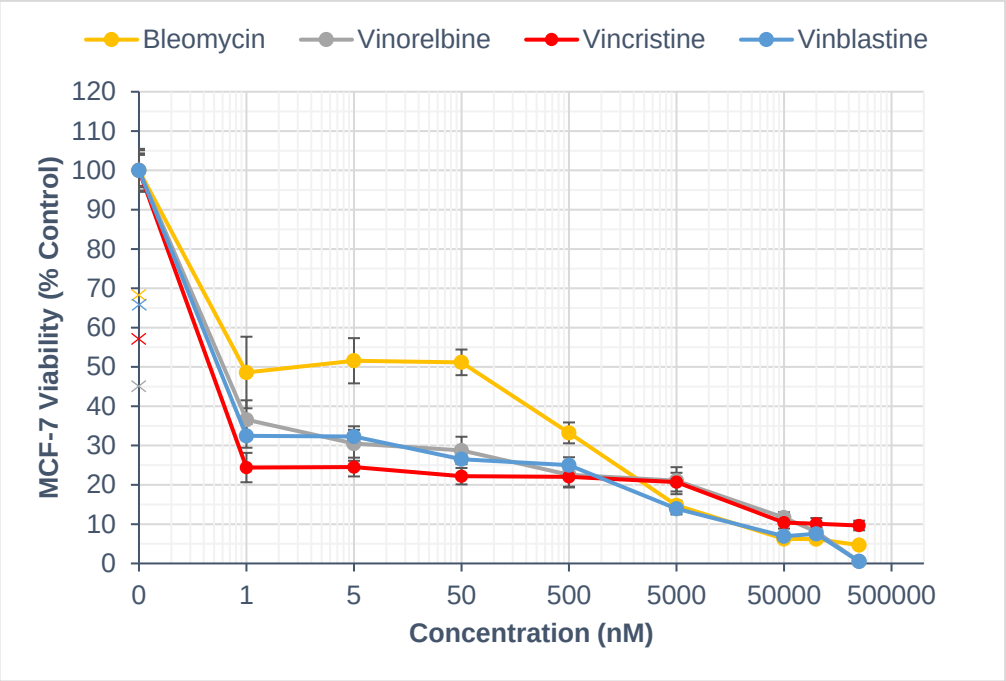

Figure 88. Reduction in MCF-7 breast cancer cell viability in 3D collagen hydrogels after vinca alkaloid and bleomycin PCI. *Relative cellular viability (% of control) of MCF-7 cells after vinca alkaloid (vinorelbine; vincristine; vinblastine) and bleomycin PCI at various concentrations (0.5-250,000 nM).*

5.4.1.2.3 Pooled Chemotherapy vs Pooled PCI

Chemotherapy and PCI treatment effect data from individual vinca alkaloid drugs (vinorelbine, vincristine, and vinblastine) was then pooled together as shown in Figure 89. Here, there *was* a significant difference ($p < 0.001$) in MCF-7 cell viability reduction observed between pooled vinca alkaloid chemotherapy and pooled vinca alkaloid PCI experimental groups.

Moreover, vinca alkaloid-PCI was more potent against 3D-cultured MCF-7 cancer cells than vinca alkaloid chemotherapy at all tested concentrations. In relation to IC_{70} values, vinca alkaloid-PCI achieved an IC_{70} of 1.5 nM whereby vinca alkaloid chemotherapy achieved

an IC_{70} of 22,500 nM. This represents a 15,000-fold reduction in favour of PCI treatment. At the maximum tested concentration of 250,000 nM, vinca alkaloid-PCI reduced cell viability to 4% (±1%) and vinca alkaloid chemotherapy to 6% (±1%) which represents a 1.5-fold increase in efficacy in favour of PCI.

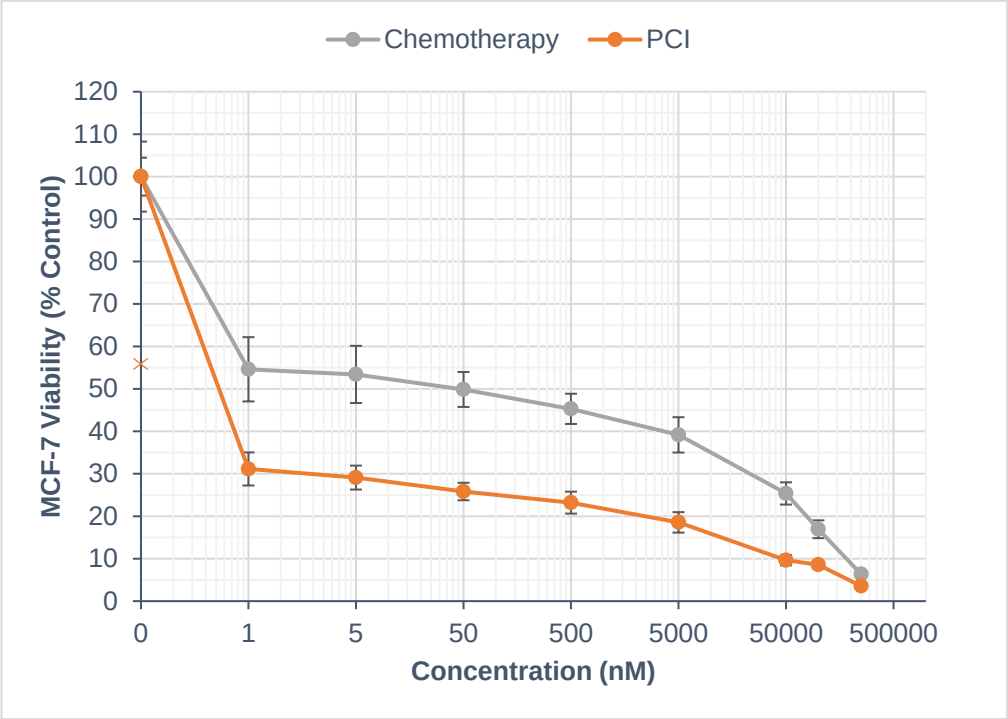

Figure 89. Reduction in MCF-7 breast cancer cell viability in 3D collagen hydrogels after vinca alkaloid chemotherapy and vinca alkaloid PCI*. Relative cellular viability (% of control) of MCF-7 cells after pooled (vinorelbine; vincristine; vinblastine) vinca alkaloid chemotherapy and pooled (vinorelbine; vincristine; vinblastine) vinca alkaloid PCI at various concentrations (0.5-250,000 nM).*

5.4.2 Taxanes

5.4.2.1 MDA-MB-231 cells

5.4.2.1.1 Chemotherapy vs Bleomycin

The next drug class to be considered and contrasted against bleomycin was the taxanes. The combined gemcitabine & paclitaxel regimen was also included for comparative purposes (as shown in Figure 90). This figure shows that there was a significant difference (p = 0.026) in MDA-MB-231 cell viability reduction between the various chemotherapy treatments.

In general, docetaxel chemotherapy was the most potent against MDA-MB-231 cells across the various concentrations tested. Additionally, bleomycin chemotherapy achieved the lowest IC_{70} value with 50,000 nM whereby docetaxel achieved the lowest IC_{70} of the taxanes

with 100,000 nM. These values represent a 2-fold IC_{70} reduction in favour of bleomycin chemotherapy. At the highest tested concentration of 250,000 nM, docetaxel chemotherapy was maximally effective in that it reduced cell viability to 0% of control and bleomycin chemotherapy reduced cell viability to 16% (±1%) – a 16-fold increase in efficacy for docetaxel.

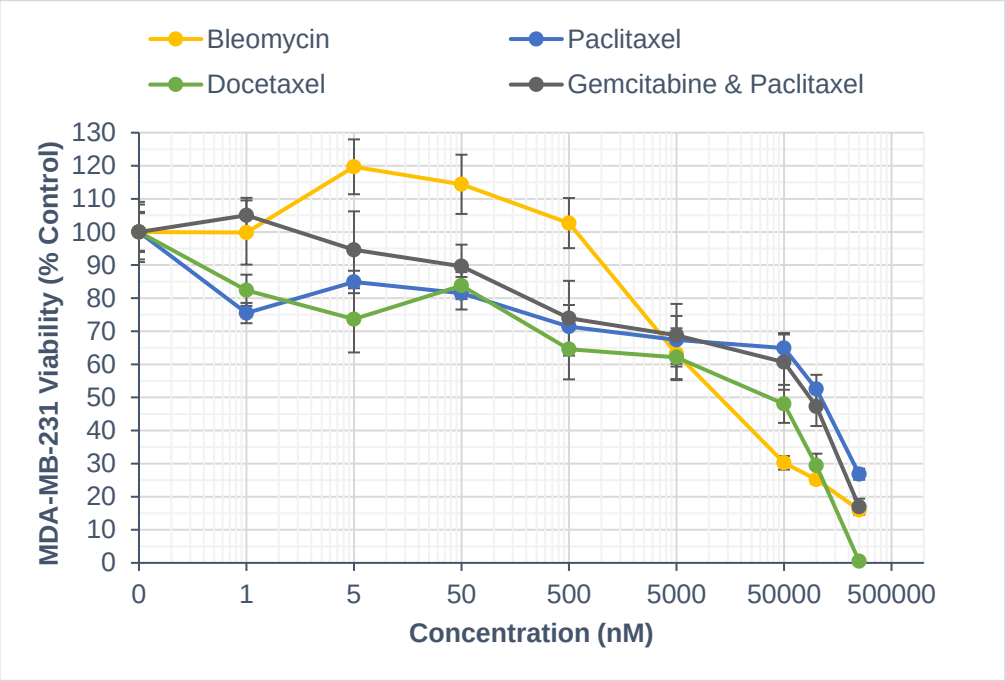

Figure 90. Reduction in MDA-MB-231 breast cancer cell viability in 3D collagen hydrogels after taxane and bleomycin chemotherapy*. Relative cellular viability (% of control) of MDA-MB-231 cells after taxane (paclitaxel; docetaxel), dual chemotherapy (gemcitabine & paclitaxel), and bleomycin chemotherapy at various concentrations (0.5-250,000 nM).*

5.4.2.1.2 PCI vs Bleomycin PCI

In relation to taxane-PCI as compared to bleomycin-PCI (shown in Figure 91), statistical analysis demonstrated that there *was* a significant difference ($p < 0.001$) in MDA-MB-231 cell viability reduction seen between the various PCI treatments.

Here, treatment potency and performance was generally seen to be mixed for these PCI combinations across the concentrations tested. In addition, Figure 91 shows that bleomycin-PCI achieved the lowest IC_{70} value with 27,500 nM, whereby the next-most potent PCI combination was the combined gemcitabine & paclitaxel-PCI regimen with an IC_{70} of 37,500 nM. This represents a 1.4-fold IC_{70} reduction in favour of bleomycin-PCI. Pertaining to treatment efficacy at 250,000 nM, docetaxel-PCI and gemcitabine & paclitaxel-PCI were

both maximally effective (that is, reducing cell viability to 0% of control) whereby bleomycin-PCI reduced viability to 6% (±0%) – a 6-fold decrease in efficacy for bleomycin-PCI.

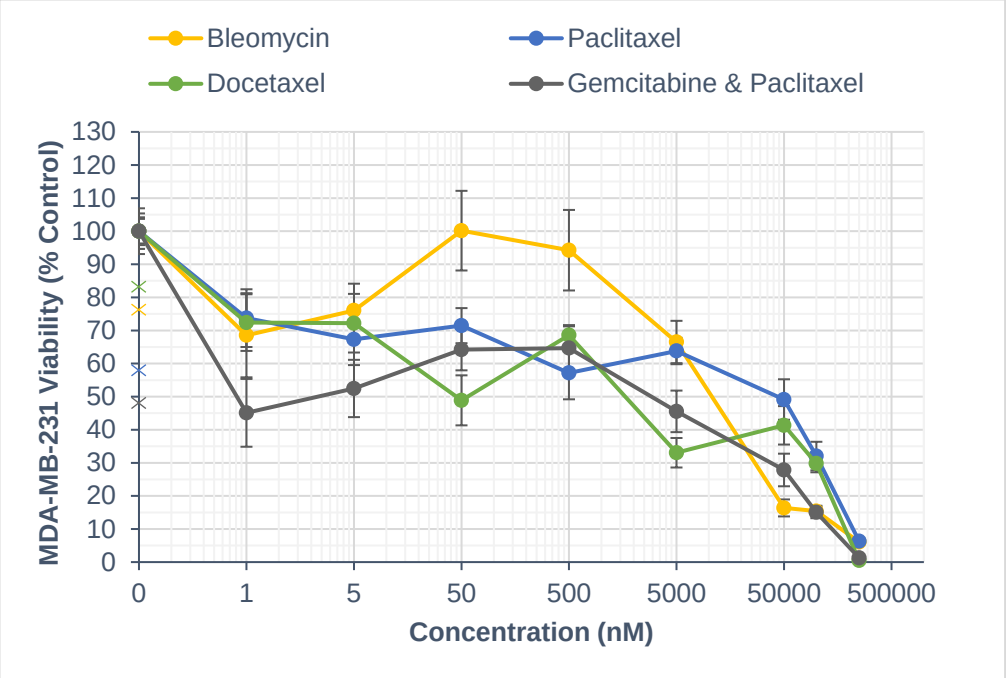

Figure 91. Reduction in MDA-MB-231 breast cancer cell viability in 3D collagen hydrogels after taxane and bleomycin PCI. *Relative cellular viability (% of control) of MDA-MB-231 cells after taxane (paclitaxel; docetaxel) PCI, gemcitabine & paclitaxel PCI, and bleomycin PCI at various concentrations (0.5-250,000 nM).*

5.4.2.1.3 Pooled Chemotherapy vs Pooled PCI

Respective taxane (docetaxel and paclitaxel) chemotherapy and PCI data are pooled together and compared (as shown in Figure 92). In these data, a significant difference (p = 0.005) in MDA-MB-231 cell viability reduction *was* observed between pooled taxane chemotherapy and pooled taxane-PCI groups.

Moreover, the cytotoxic effects of taxane-PCI was greater than that of taxane chemotherapy at all tested concentrations. With regard to treatment IC_{70}, taxane-PCI achieved an IC_{70} of 100,000 nM whereby taxane chemotherapy achieved an IC_{70} of 150,000 nM which represents a 1.5-fold reduction in favour of PCI. At the maximum tested concentration of 250,000 nM, taxane-PCI reduced viability to 3% (±1%) and taxane chemotherapy to 14% (±1%) which represents around a 5-fold increase in efficacy in favour of PCI.

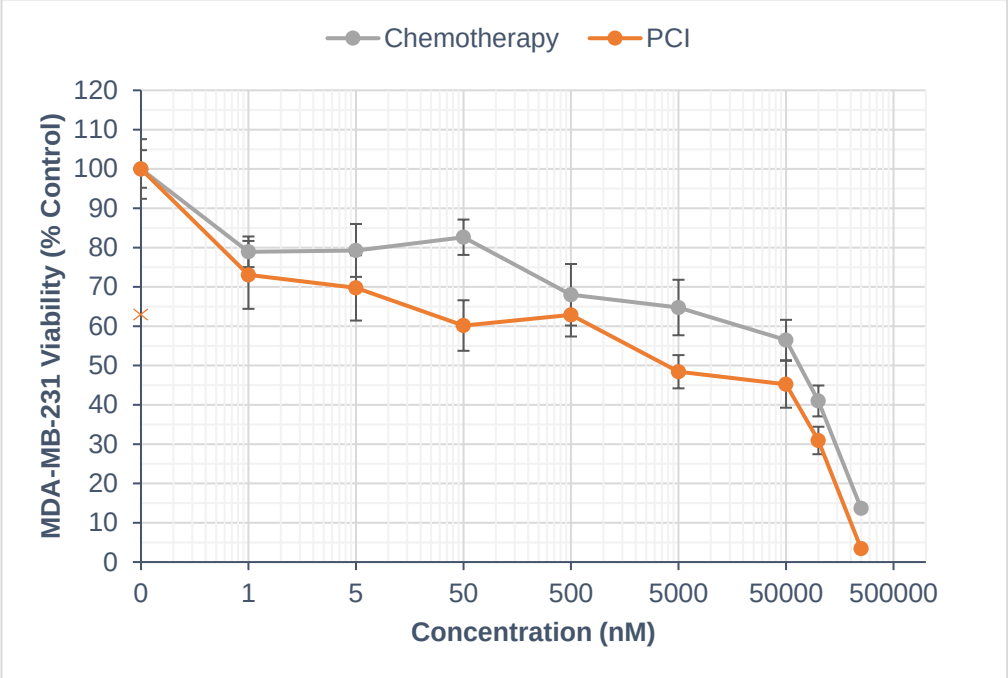

Figure 92. Reduction in MDA-MB-231 breast cancer cell viability in 3D collagen hydrogels after taxane chemotherapy and taxane PCI*. Relative cellular viability (% of control) of MDA-MB-231 cells after pooled (paclitaxel, docetaxel) taxane chemotherapy and pooled (paclitaxel, docetaxel) taxane PCI at various concentrations (0.5-250,000 nM).*

5.4.2.2 MCF-7 cells

5.4.2.2.1 Chemotherapy vs Bleomycin chemotherapy

Next, similar comparisons were made of the results achieved in the MCF-7 cell line. Figure 93 shows that there *was* a significant difference ($p < 0.001$) in MCF-7 cell viability reduction between the various chemotherapy treatments.

Moreover, docetaxel chemotherapy was generally the most potent against MCF-7 cells at low drug concentrations and then bleomycin chemotherapy at high drug concentrations. The IC_{70} of bleomycin chemotherapy was the lowest at 3,500 nM with the next-most potent of the taxane-containing chemotherapies being gemcitabine & paclitaxel with an IC_{70} of 26,000 nM. This signifies a 7.4-fold reduction in favour of bleomycin chemotherapy. At the highest tested concentration of 250,000 nM, bleomycin chemotherapy and docetaxel chemotherapy reduced cell viability to 10% (±1%) and 11% (±4%), respectively.

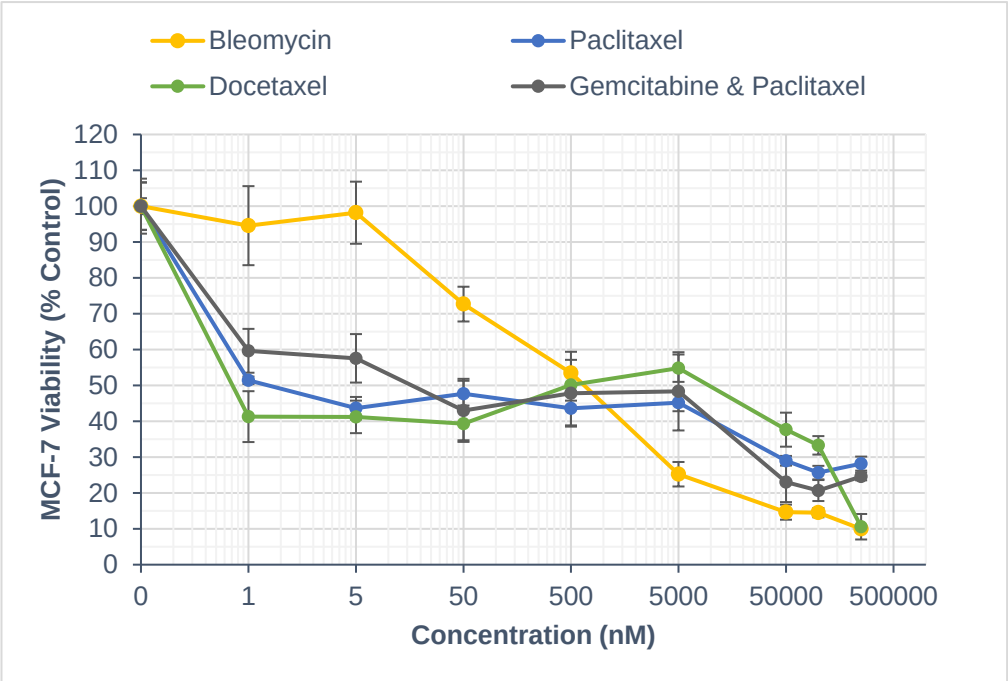

Figure 93. Reduction in MCF-7 breast cancer cell viability in 3D collagen hydrogels after taxane and bleomycin chemotherapy*. Relative cellular viability (% of control) of MCF-7 cells after taxane (paclitaxel; docetaxel), gemcitabine & paclitaxel, and bleomycin chemotherapy at various concentrations [0.5-250,000 nM]).*

5.4.2.2.2 PCI vs Bleomycin PCI

The treatment effects of the taxane-PCI regimens can be seen compared with bleomycin-PCI in Figure 94. Comparisons between these PCI treatments saw a significant difference ($p < 0.001$) in MCF-7 cell viability reduction between the various PCI treatments. In addition, gemcitabine & paclitaxel-PCI was generally the most potent treatment across the majority of concentrations tested. The gemcitabine & paclitaxel-PCI regimen achieved the lowest IC_{70} value with 0.45 nM whereby PCI utilising the model drug bleomycin achieved an IC_{70} of 750 nM. This difference represents a 1,667-fold reduction in favour of gemcitabine & paclitaxel-PCI. At the highest tested concentration of 250,000 nM, bleomycin-PCI achieved the highest efficacy by reducing cell viability to 5% (±0%) – a 2-fold increase in efficacy over gemcitabine & paclitaxel-PCI.

5.4.2.2.3 Pooled Chemotherapy vs Pooled PCI

Results from the individual (docetaxel and paclitaxel) taxane chemotherapy and PCI regimens were then pooled together for comparative purposes (as shown in Figure 95). Here, there

was a significant difference ($p < 0.001$) in MCF-7 cell viability reduction observed between pooled taxane chemotherapy and pooled taxane PCI treatment groups.

It can be seen from Figure 95 that taxane-PCI was more potent than taxane chemotherapy at all tested concentrations. Furthermore, taxane-PCI achieved an IC_{70} of 2,000 nM whereby taxane chemotherapy achieved an IC_{70} of 90,000 nM which represents a 45-fold reduction in favour of PCI. At the maximum tested concentration of 250,000 nM, taxane-PCI reduced viability to 14% (±3%) and taxane chemotherapy to 19% (±3%) which represents a 1.4-fold reduction in favour of PCI.

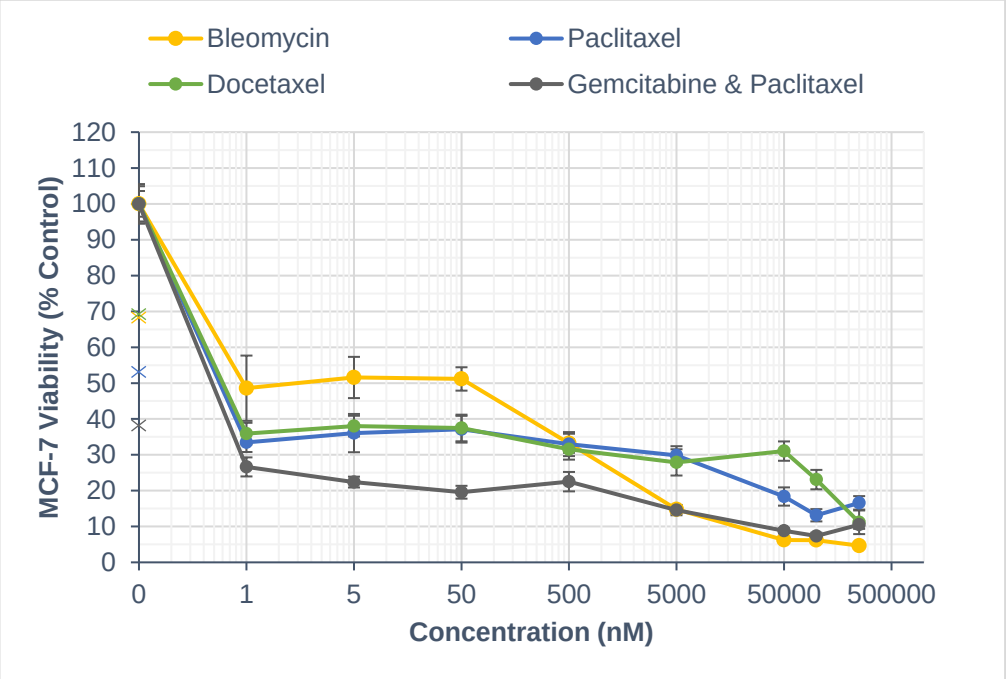

Figure 94. Reduction in MCF-7 breast cancer cell viability in 3D collagen hydrogels after taxane PCI and bleomycin PCI. *Relative cellular viability (% of control) of MCF-7 cells after taxane (paclitaxel, docetaxel) PCI, gemcitabine & paclitaxel PCI, and bleomycin PCI at various concentrations (0.5-250,000 nM).*

5.4.3 Antimetabolites

5.4.3.1 MDA-MB-231 cells

5.4.3.1.1 Chemotherapy vs Bleomycin chemotherapy

Following the comparisons of the cytotoxic profiles of the vinca alkaloids and the taxanes to bleomycin, the next chemotherapeutic drug class to be considered was the antimetabolites. Below, Figure 96 shows that there *was* a significant difference ($p < 0.001$) in MDA-MB-231 cell viability reduction observed between the various chemotherapy treatments.

Moreover, gemcitabine chemotherapy was generally the most potent against MDA-MB-231 cells at the low and middle drug concentrations tested (0.5-5,000 nM) with bleomycin becoming the most potent treatment at the highest concentrations tested (50,000-250,000 nM). In addition, it can also be observed from Figure 96 that bleomycin chemotherapy achieved the lowest IC_{70} with 50,000 nM whereby gemcitabine & paclitaxel achieved the next-lowest for the antimetabolite chemotherapies with an IC_{70} of 170,000 nM. This represents a 3.4-fold reduction in favour of bleomycin chemotherapy. At the highest tested concentration of 250,000 nM, bleomycin chemotherapy and gemcitabine & paclitaxel chemotherapy were essentially seen to be equipotent whereby cell viability was reduced to 16% (±1%) and 17% (±2%), respectively.

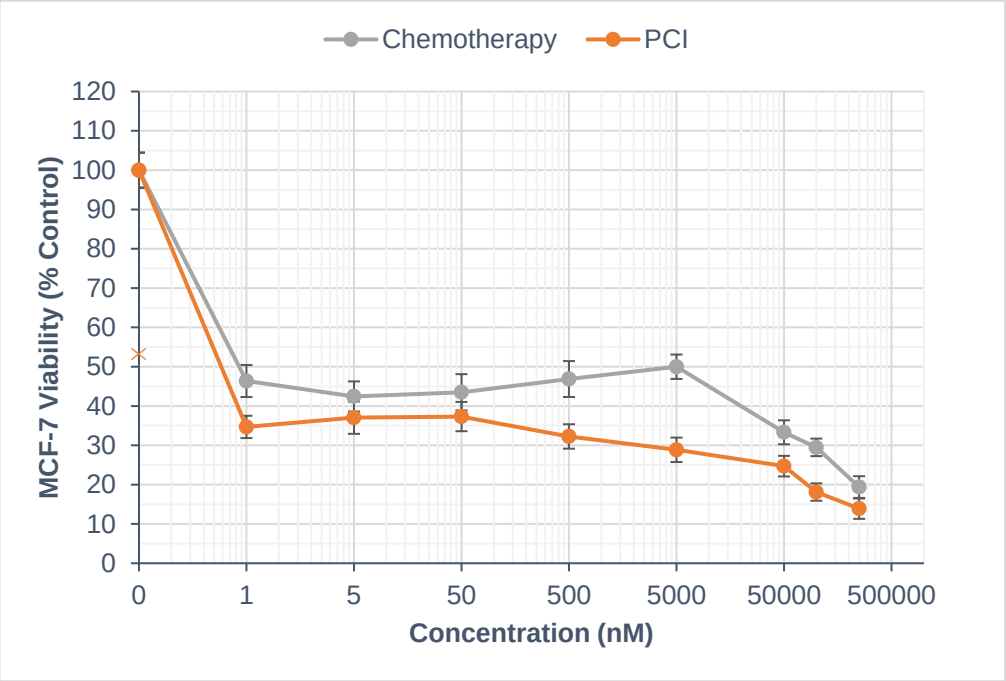

Figure 95. Reduction in MCF-7 breast cancer cell viability in 3D collagen hydrogels after taxane chemotherapy and taxane PCI*. Relative cellular viability (% of control) of MCF-7 cells after taxane pooled (paclitaxel, docetaxel) chemotherapy and pooled (paclitaxel, docetaxel) taxane PCI at various concentrations (0.5-250,000 nM).*

5.4.3.1.2 PCI vs Bleomycin PCI

Comparisons were then made between PCI experiments utilising the antimetabolite drugs and bleomycin (as shown in Figure 97). Here, it was demonstrated that there *was* a significant difference ($p < 0.001$) in MDA-MB-231 cell viability reduction observed between the various PCI treatments.

It can also be determined from Figure 97 that treatment potency was generally mixed for these PCI combinations across the range of concentrations tested. Furthermore, bleomycin-PCI achieved the lowest IC_{70} value of 27,500 nM whereby the next-most potent combination was gemcitabine & paclitaxel-PCI with an IC_{70} of 37,500 nM. This represents a 1.4-fold IC_{70} reduction in favour of bleomycin-PCI. Pertaining to treatment efficacy, gemcitabine & paclitaxel-PCI was found to be maximally-effective (that is, reduced cell viability to 0% of control) at the highest tested concentration of 250,000 nM whereby bleomycin-PCI reduced viability to 6% (±0%) – a 6-fold decrease in efficacy for bleomycin-PCI.

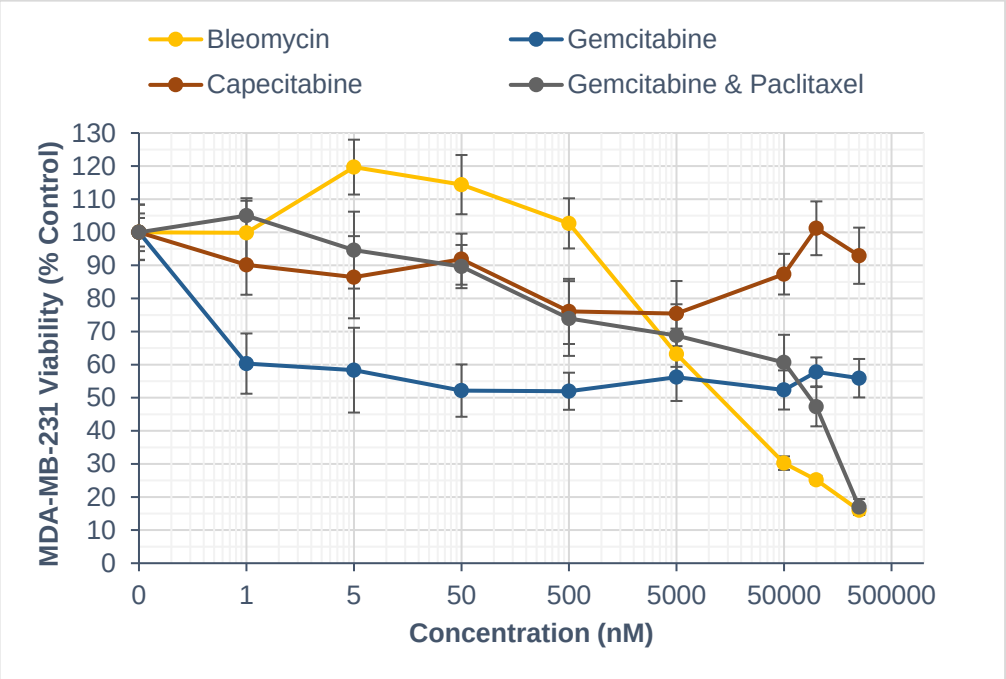

Figure 96. Reduction in MDA-MB-231 breast cancer cell viability in 3D collagen hydrogels after antimetabolite and bleomycin chemotherapy*. Relative cellular viability (% of control) of MDA-MB-231 cells after antimetabolite (gemcitabine, capecitabine), gemcitabine & paclitaxel, and bleomycin chemotherapy at various concentrations (0.5-250,000 nM).*

5.4.3.1.3 Pooled Chemotherapy vs Pooled PCI

In relation to treatment effects from the pooled results (gemcitabine and capecitabine) of the antimetabolite chemotherapy and antimetabolite-PCI, Figure 98 demonstrates that there was *not* a significant difference (p = 0.482) in MDA-MB-231 cell viability reduction observed between pooled antimetabolite chemotherapy and pooled antimetabolite PCI treatment groups.

In general, neither treatment group was more potent than the other across the various concentrations tested. Nor did either of the treatments achieve the IC_{70} or IC_{50} threshold. At the maximum tested concentration of 250,000 nM, antimetabolite-PCI reduced cell viability to 63% (±8%) and antimetabolite chemotherapy reduced viability to 74% (±7%) which represents a 1.2-fold increase in efficacy in favour of PCI treatment.

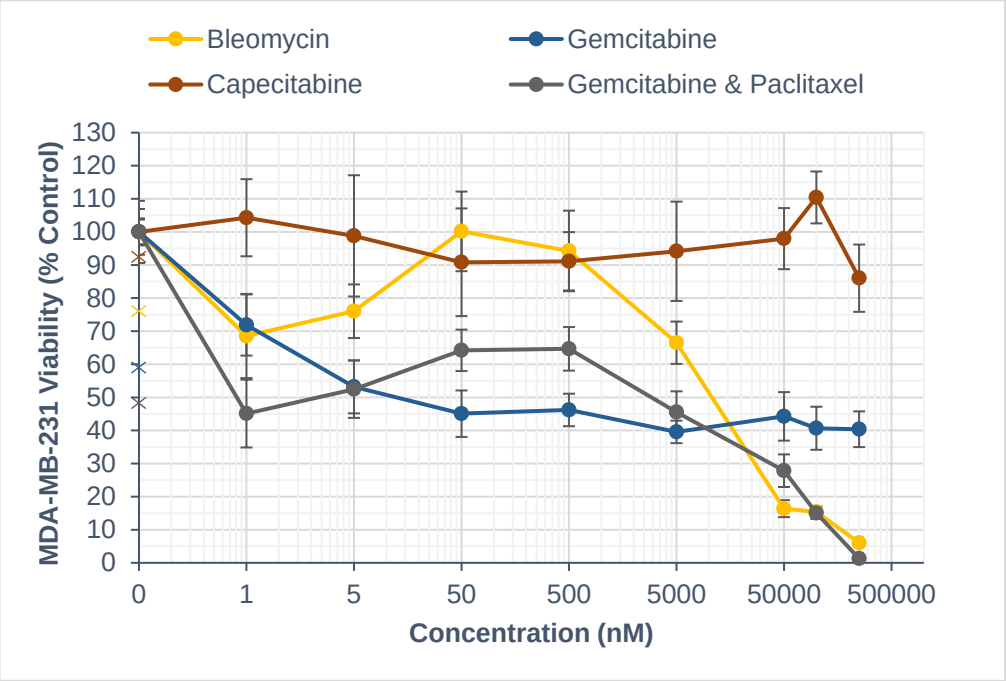

Figure 97. Reduction in MDA-MB-231 breast cancer cell viability in 3D collagen hydrogels after antimetabolite and bleomycin PCI*. Relative cellular viability (% of control) of MDA-MB-231 cells after antimetabolite (gemcitabine, capecitabine) PCI, gemcitabine & paclitaxel PCI, and bleomycin PCI at various concentrations (0.5-250,000 nM).*

5.4.3.1 MCF-7 cells

5.4.3.1.1 Chemotherapy vs Bleomycin chemotherapy

Antimetabolite comparisons were then made for chemotherapy experiments in MCF-7 cells (as seen in Figure 99). Here, there *was* a significant difference ($p < 0.001$) in MCF-7 cell viability reduction observed between the various chemotherapy treatments.

In addition, gemcitabine & paclitaxel chemotherapy was generally the most potent against MCF-7 cells at low concentrations and then bleomycin chemotherapy at high concentrations. It can also be determined from Figure 99 that bleomycin chemotherapy achieved the lowest IC_{70} of 3,500 nM whereby gemcitabine & paclitaxel chemotherapy achieved an IC_{70} of 26,000 nM for the antimetabolite-containing chemotherapies. This

signifies a 7.4-fold reduction in IC_{70} in favour of bleomycin chemotherapy. At the highest tested concentration of 250,000 nM bleomycin chemotherapy and gemcitabine & paclitaxel chemotherapy reduced cell viability to 10% (±1%) and 25% (±1%), respectively – 2.5-fold increase in efficacy for bleomycin chemotherapy.

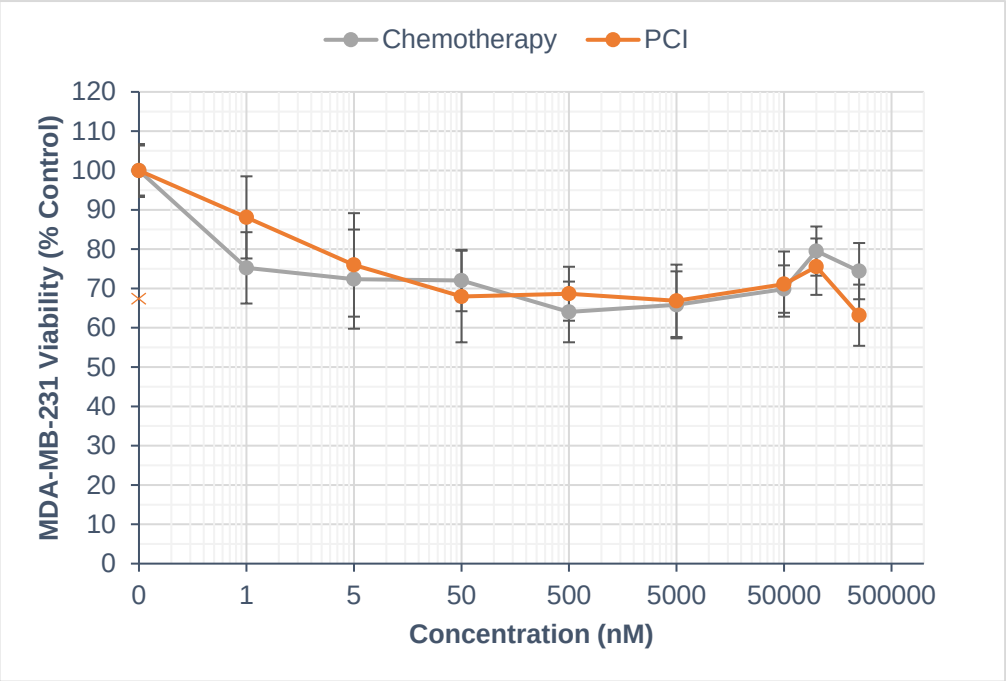

Figure 98. Reduction in MDA-MB-231 breast cancer cell viability in 3D collagen hydrogels after antimetabolite chemotherapy and antimetabolite PCI. *Relative cellular viability (% of control) of MDA-MB-231 cells after pooled (gemcitabine, capecitabine) antimetabolite chemotherapy and pooled (gemcitabine, capecitabine) antimetabolite PCI at various concentrations (0.5-250,000 nM).*

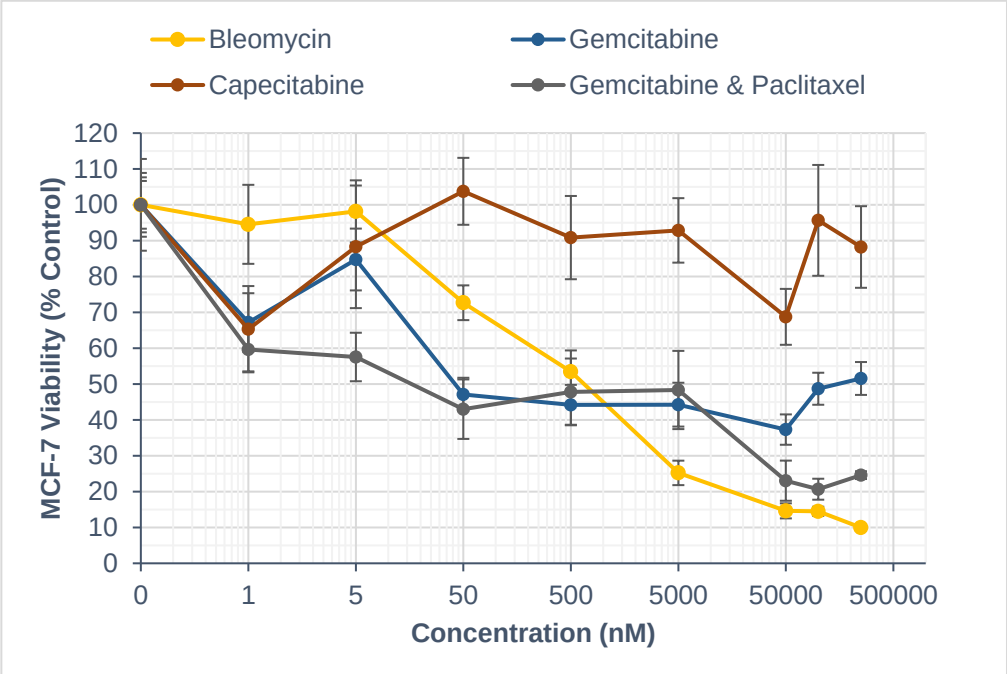

Figure 99. Reduction in MCF-7 breast cancer cell viability in 3D collagen hydrogels after antimetabolite and bleomycin chemotherapy*. Relative cellular viability (% of control) of MCF-7 cells after antimetabolite (gemcitabine, capecitabine), gemcitabine & paclitaxel, and bleomycin chemotherapy at various concentrations (0.5-250,000 nM).*

5.4.3.1.2 PCI vs Bleomycin PCI

PCI comparisons were then made (as shown in Figure 100) whereby a significant difference ($p < 0.001$) in MCF-7 cell viability reduction *was* observed between the various PCI treatments. Moreover, gemcitabine & paclitaxel-PCI was generally the most potent treatment across the majority of concentrations tested. With regard to treatment IC_{70}, gemcitabine & paclitaxel-PCI achieved the lowest IC_{70} value of 0.45 nM whereby PCI utilising the model drug bleomycin achieved an IC_{70} of 750 nM. This signifies a 1,667-fold IC_{70} reduction in favour of gemcitabine & paclitaxel-PCI. At the highest tested concentration of 250,000 nM, bleomycin-PCI achieved the highest efficacy by reducing cell viability to 5% (±0%) with gemcitabine & paclitaxel-PCI reducing cell viability to 10% (±1%) - a 2-fold efficacy increase for bleomycin-PCI.

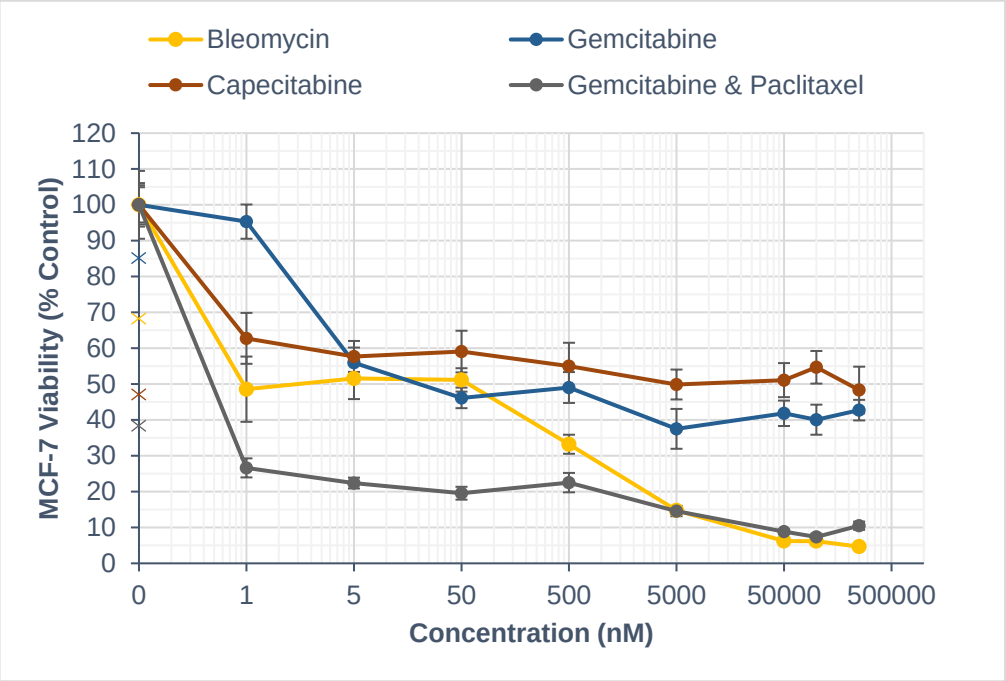

Figure 100. Reduction in MCF-7 breast cancer cell viability in 3D collagen hydrogels after antimetabolite PCI and bleomycin PCI. *Relative cellular viability (% of control) of MCF-7 cells after antimetabolite (gemcitabine, capecitabine) PCI, gemcitabine & paclitaxel PCI, and bleomycin PCI at various concentrations (0.5-250,000 nM).*

5.4.3.1.3 Pooled Chemotherapy vs Pooled PCI

The results from the respective chemotherapy and PCI antimetabolite experiments were then pooled together and compared (as seen in Figure 101). Figure 101 shows that there *was* a significant difference ($p = 0.005$) in MCF-7 cell viability reduction observed between pooled antimetabolite chemotherapy and pooled antimetabolite PCI treatment groups.

In general, PCI treatment was more potent than chemotherapy treatment across all of the various concentrations tested. Neither treatment achieved the IC_{70} although antimetabolite-PCI did achieve an IC_{50} of 875 nM. At the maximum tested concentration of 250,000 nM, antimetabolite-PCI reduced viability to 46% (±5%) and antimetabolite chemotherapy to 70% (±8%) which represents a 1.5-fold increase in efficacy in favour of PCI therapy.

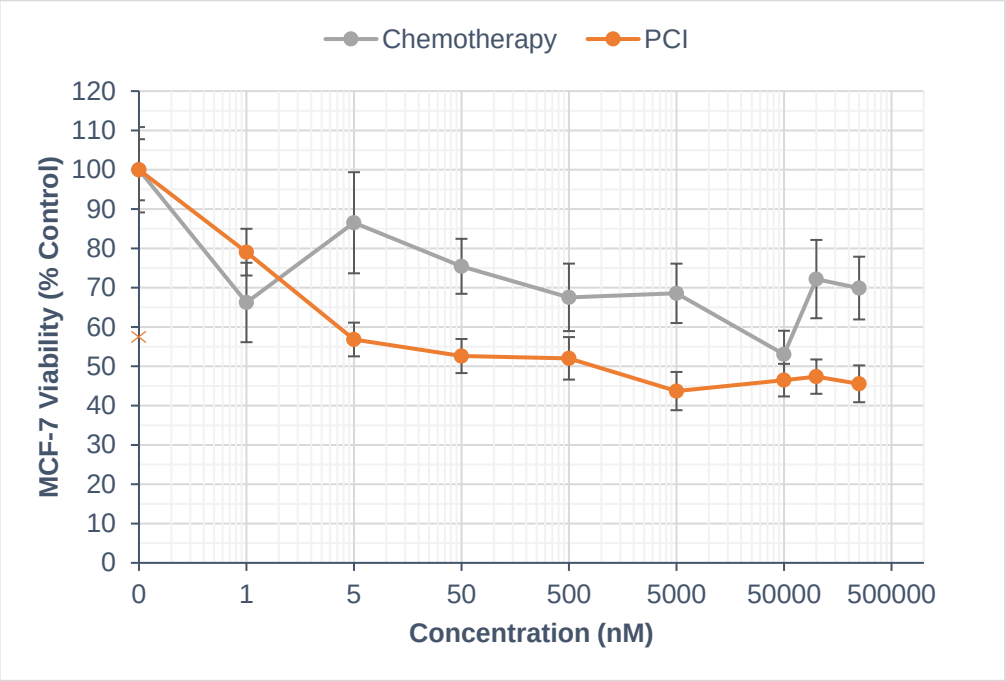

Figure 101. Reduction in MCF-7 breast cancer cell viability in 3D collagen hydrogels after antimetabolite chemotherapy and antimetabolite PCI. *Relative cellular viability (% of control) of MCF-7 cells after pooled (gemcitabine, capecitabine) antimetabolite chemotherapy and pooled (gemcitabine, capecitabine) antimetabolite PCI at various concentrations (0.5-250,000 nM).*

5.4.4 Results summary

5.4.4.1 IC_{70} and E_{max}

The key treatment effects indicative of treatment potency and efficacy (IC_{70}; E_{max}) were identified from the chemotherapy and PCI cytotoxicity profiles for each drug and were compared to the model PCI drug bleomycin (Table 8). Specifically, chemotherapy experiments were compared to bleomycin chemotherapy and PCI experiments compared to PCI-bleomycin.

Subsequently, the most potent and efficacious PCI combinations were identified from Table 8 and are summarised in Table 9.

Table 8. Summary of key chemotherapy and PCI treatment effects (IC_{70}; E_{max}) compared against bleomycin chemotherapy (chemotherapy) and bleomycin PCI (PCI).

Chemotherapy Drug	Treatment	IC_{70} (nM)				E_{max} (% Control [±SE])			
		MDA-MB-231	Potency change (fold)	MCF-7	Potency change (fold)	MDA-MB-231	Efficacy change (fold)	MCF-7	Efficacy change (fold)
Bleomycin	Chemotherapy	50,000	.	3,500	.	16 (±1)	.	10 (±1)	.
Vinorelbine		75,000	- 1.5	20,000	- 5.7	0 (±0)	+ 16	0 (±0)	+ 10
Vincristine		1,500 (IC_{50})	+ 8.3 (IC_{50})	75,000	- 21.4	59 (±7)	- 3.7	18 (±2)	- 1.8
Vinblastine		150,000	- 3.0	12,500	- 3.6	0 (±0)	+ 16	0 (±0)	+ 10
Paclitaxel		225,000	- 4.5	42,500	- 12.1	27 (±2)	- 1.7	28 (±2)	- 2.8
Docetaxel		100,000	- 2.0	112,500	- 32.1	0 (±0)	+ 16	11 (±4)	- 1.1
Gemcitabine		n/a	n/a	40 (IC_{50})	+18.8 (IC_{50})	56 (±6)	- 3.5	52 (±5)	- 5.2
Capecitabine		n/a	n/a	n/a	n/a	93 (±9)	- 5.8	88 (±11)	- 8.8
Gemcitabine & Paclitaxel		170,000	- 3.4	26,000	- 7.4	17 (±2)	- 1.1	25 (±1)	- 2.5
Bleomycin	PCI	27,500	.	750	.	6 (±0)	.	5 (±0)	.
Vinorelbine		275	+ 100	5	+ 150	0 (±0)	+ 6.0	0 (±0)	+ 5.0
Vincristine		0.45	+ 61,111	0.425	+ 1,765	21 (±4)	+ 3.5	10 (±1)	- 2.0
Vinblastine		80,000	- 2.9	12.5	+ 60	0 (±0)	+ 6.0	0 (±0)	+ 5.0
Paclitaxel		75,000	- 2.7	4,250	- 5.7	6 (±1)	≡	17 (±2)	- 3.4
Docetaxel		100,000	- 3.6	1,250	- 1.7	0 (±0)	+ 6.0	11 (±3)	- 2.2
Gemcitabine		12.5 (IC_{50})	+ 917 (IC_{50})	20 (IC_{50})	+ 550 (IC_{50})	40 (±5)	- 6.7	43 (±3)	- 8.6
Capecitabine		n/a	n/a	5,000 (IC_{50})	- 11,111 (IC_{50})	86 (±10)	- 14.3	48 (±7)	- 9.6
Gemcitabine & Paclitaxel		37,500	- 1.4	0.45	+ 1,667	1 (±0)	+ 6.0	10 (±1)	- 2.0

Table 9. Summary of the most potent and efficacious PCI treatment combinations when compared to the model PCI drug bleomycin.

Cell line	Bleomycin PCI as Comparator					
	Most Potent (IC_{70})			Most Efficacious		
	Drug Class	Drug	Potency change (fold)	Drug Class	Drug	Efficacy change (fold)
MDA-MB-231	Vinca alkaloids	Vincristine	+ 61,111	Vinca alkaloids	Vinorelbine	+ 6.0
				Vinca alkaloids	Vinblastine	
				Taxanes	Docetaxel	
				Combination	Gemcitabine & paclitaxel	
MCF-7	Vinca alkaloids	Vincristine	+ 1,765	Vinca alkaloids	Vinorelbine	+ 5.0
				Vinca alkaloids	Vinblastine	

5.5 PCI Treatment Effects by Pooled Drug Class versus Bleomycin-PCI

5.5.1 MDA-MB-231 cells

Below, Figure 102 shows the cytotoxic profiles of the PCI treatments collated by drug class and compared to bleomycin-PCI. Here, there *was* a significant difference ($p < 0.001$) in MCF-7 cell viability reduction observed between the various PCI treatments.

In general, vinca alkaloid-PCI was the most potent treatment across the range of concentrations tested. Furthermore, Figure 102 shows that vinca alkaloid-PCI achieved the lowest IC_{70} value of 350 nM whereby PCI utilising the model drug bleomycin achieved an IC_{70} of 27,500 nM. This signifies a 79-fold reduction in IC_{70} in favour of vinca alkaloid-PCI. At the highest tested concentration of 250,000 nM, vinca alkaloid-PCI and bleomycin-PCI were essentially equipotent in that both treatment groups reduced cell viability to 6% (±0%) and 7% (±1%). Taxane-PCI was seen to be the most effective at 250,000 nM given that this treatment reduced cell viability to 3% (±1%) – a 2-fold increase in efficacy versus the next-most efficacious group (vinca alkaloid-PCI).

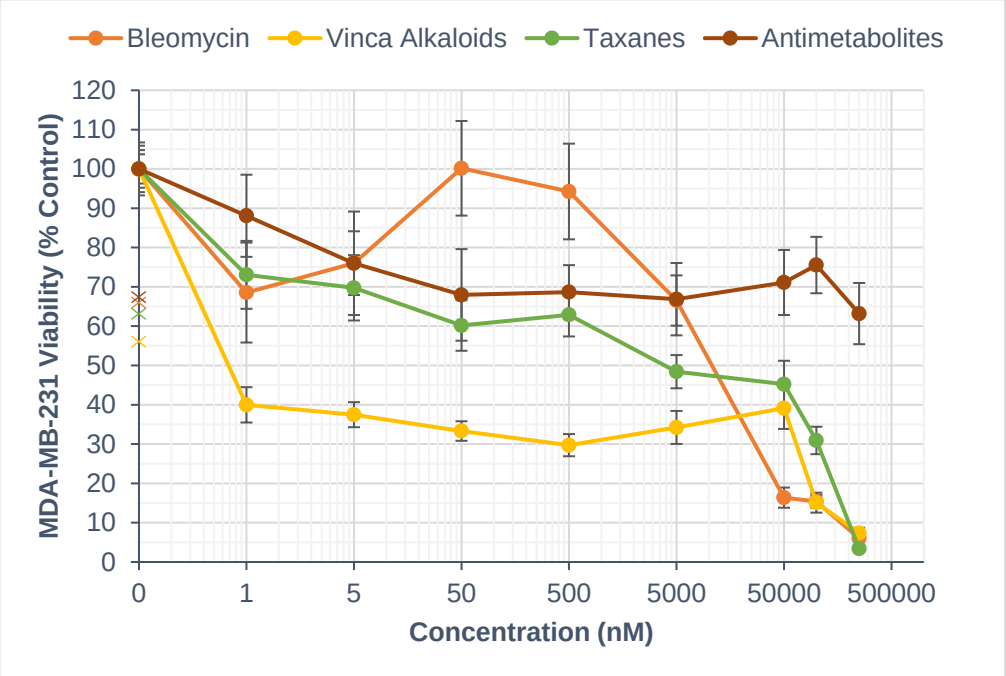

Figure 102. Reduction in MDA-MB-231 breast cancer cell viability in 3D collagen hydrogels after PCI with various drug classes. *Relative cellular viability (% of control) of MDA-MB-231 cells after pooled vinca alkaloid-PCI, taxane-PCI, antimetabolite-PCI, and bleomycin-PCI at various concentrations (0.5-250,000 nM).*

5.5.2 MCF-7 cells

Similar comparisons were also made of the PCI results in MCF-7 cells (as seen in Figure 103). Here, there *was* a significant difference ($p < 0.001$) in MCF-7 cell viability reduction observed between the various PCI treatments.

In general, vinca alkaloid-PCI was the most potent treatment across the low and middle drug concentrations (0.5-500 nM) and was essentially equipotent with bleomycin-PCI at higher drug concentrations (5,000-250,000 nM). It can also be seen from Figure 103 that vinca alkaloid-PCI achieved the lowest IC_{70} value of 1.5 nM whereby PCI utilising the model drug bleomycin achieved an IC_{70} of 750 nM. This signifies a 500-fold reduction in IC_{70} in favour of vinca alkaloid-PCI. At the highest tested concentration of 250,000 nM, vinca alkaloid-PCI and bleomycin-PCI were the most efficacious and were essentially equipotent in reducing cell viability to 4% (±1%) and 5% (±0%) – although this is still a 1.3-fold increase in efficacy for vinca alkaloid-PCI.

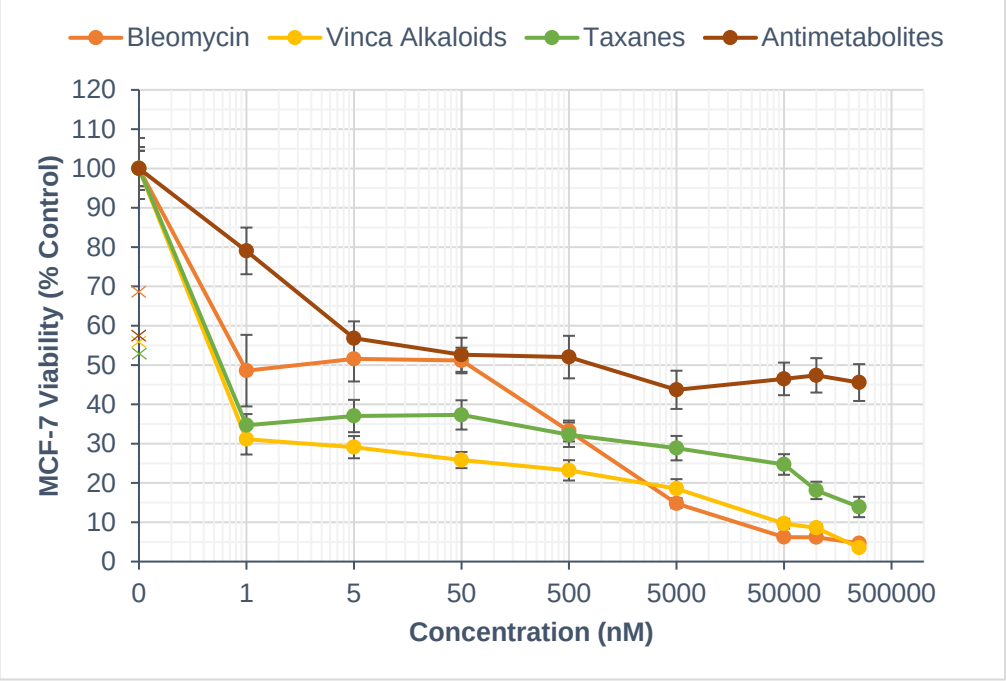

Figure 103. Reduction in MCF-7 breast cancer cell viability in 3D collagen hydrogels after PCI with various drug classes*. Relative cellular viability (% of control) of MCF-7 cells after pooled vinca alkaloid-PCI, taxane-PCI, antimetabolite-PCI, and bleomycin-PCI at various concentrations (0.5-250,000 nM).*

5.5.3 MDA-MB-231 cells vs MCF-7 cells

Following the identification of the most potent drug classes in each breast cancer cell line, Figure 104 shows them collated together for comparative purposes. Here, it can be seen that

there *was* a significant difference ($p = 0.001$) in cell viability reduction between the various PCI treatments.

In general, vinca alkaloid-PCI was more potent than bleomycin-PCI in both breast cancer cell lines across the majority of drug concentrations tested and also achieved lower IC_{70} values. In addition, all PCI treatments were broadly similarly efficacious at the maximum tested concentration of 250,000 nM. Pertaining to the MDA-MB-231 cell line, bleomycin-PCI was 1.2-fold more efficacious; whilst in the MCF-7 cell line vinca alkaloid-PCI was 1.3-fold more efficacious. There was also notable divergence in vinca alkaloid-PCI cytotoxicity between 500-50,000 nM when comparing MDA-MB-231 and MCF-7 cells.

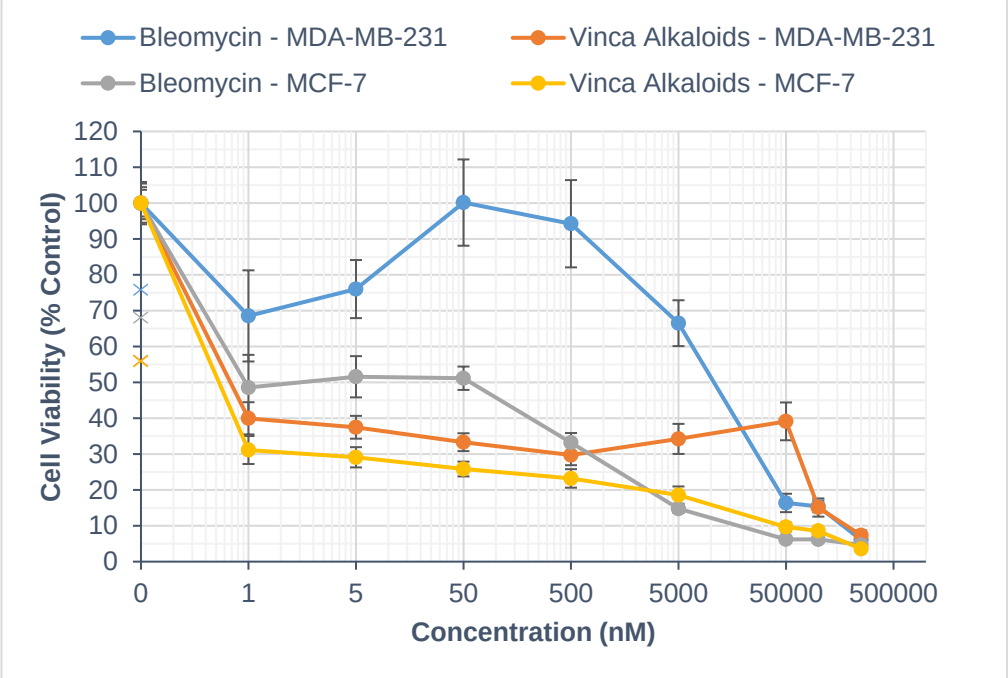

Figure 104. Reduction in breast cancer cell viability in 3D collagen hydrogels after PCI treatment with the most potent identified drug classes and bleomycin*. Relative cellular viability (% of control) of MDA-MB-231 and MCF-7 cells after pooled vinca alkaloid-PCI and bleomycin-PCI at various concentrations (0.5-250,000 nM).*

5.5.4 Results Summary

5.5.4.1 IC_{70} and E_{max}

The key treatment effects indicative of treatment potency and efficacy (IC_{70}; E_{max}) were identified from the PCI cytotoxicity profiles by drug class and compared to the model bleomycin-PCI regimen (Table 10).

Table 10. Summary of PCI treatment effects pooled by chemotherapeutic drug class and compared with bleomycin-PCI.

Chemotherapy Drug	Treatment	IC_{70} (nM)				E_{max} (% Control [±SE])			
		MDA-MB-231	Potency change (fold)	MCF-7	Potency change (fold)	MDA-MB-231	Efficacy change (fold)	MCF-7	Efficacy change (fold)
Bleomycin	PCI	27,500	.	750	.	6 (± 0)	.	5 (± 0)	.
Vinca alkaloids		350	+ 79	1.5	+ 500	7 (± 1)	- 1.2	4 (± 1)	+ 1.3
Taxanes		100,000	- 3.6	2,250	- 3.0	3 (± 1)	+ 2.0	14 (± 3)	- 2.8
Antimetabolites		n/a	n/a	n/a	n/a	63 (± 8)	- 10.5	46 (± 5)	- 9.2

5.6 PDT Controls

5.6.1 MDA-MB-231 cells – Dark Toxicity & PDT Control

As aforementioned, the same photosensitiser ($AlPcS_{2a}$, 5 µg/mL) and light dose (0.12 J/cm^2) was used across all PCI experiments (the 'PDT control') in both MDA-MB-231 and MCF-7 human breast adenocarcinoma cells and it is the average (mean) values observed from all of these experiments that is presented in Figure 105 and Figure 106. In addition to the determination of effects on these cells from PDT (that is, photosensitiser plus treatment light illumination), the dark toxicity of the photosensitiser was also investigated (that is, photosensitiser *without* treatment light illumination). Figure 105 shows that there *was* a significant difference in MDA-MB-231 viability between $AlPcS_{2a}$ dark toxicity (p = 0.006) and the $AlPcS_{2a}$ PDT experimental control (p = 0.001) versus control cells.

Furthermore, it was observed that the inherent $AlPcS_{2a}$ dark toxicity reduced cell viability to 84% (±4%) and that the PDT control (that is, the *estimated/predicted* PDT component of PCI treatment) reduced cell viability to 67% (±3%) in the MDA-MB-231 cell line.

5.6.2 MCF-7 cells – Dark Toxicity & PDT Control

Accordingly, dark toxicity and PDT cytotoxicity was also determined in the MCF-7 cell line (seen in Figure 106). Here, there *was* a significant difference in MCF-7 cell viability observed between $AlPcS_{2a}$ dark toxicity (p = 0.015) and the $AlPcS_{2a}$ PDT experimental control (p < 0.001) versus control cells. Moreover, it was observed that the inherent $AlPcS_{2a}$ dark toxicity reduced cell viability to 85% (±3%) and that the PDT control reduced cell viability to 61% (±2%) in the MCF-7 cell line.

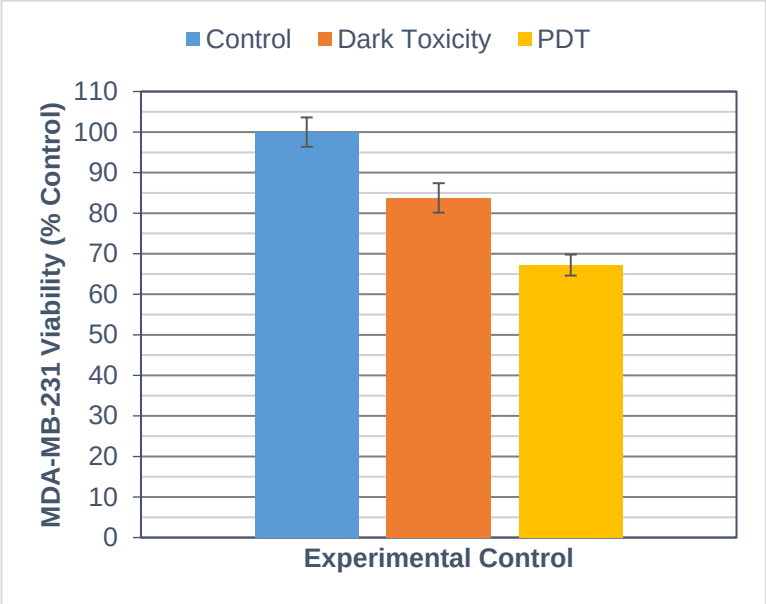

Figure 105. Reduction in MDA-MB-231 viability in 3D collagen hydrogels after AlPcS$_{2a}$ dark toxicity and AlPcS$_{2a}$ PDT. *Relative cellular viability (% of control) of MDA-MB-231 cells after incubation with 5 µg/mL AlPcS$_{2a}$ and with (PDT)/without (dark toxicity) treatment light exposure.*

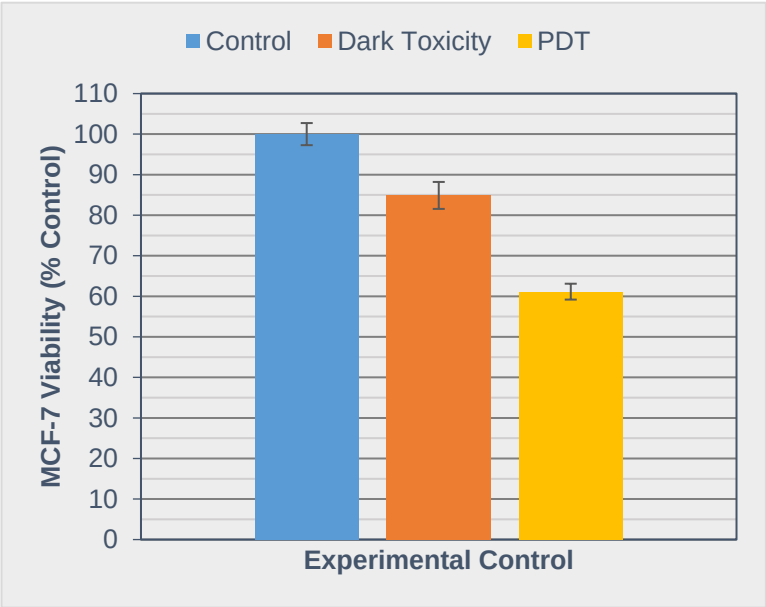

Figure 106. Reduction in MCF-7 viability in 3D collagen hydrogels after AlPcS$_{2a}$ dark toxicity and AlPcS$_{2a}$ PDT. *Relative cellular viability (% of control) of MCF-7 cells after incubation with 5 µg/mL AlPcS$_{2a}$ and with (PDT)/without (dark toxicity) treatment light exposure.*

5.6.3 MDA-MB-231 cells vs MCF-7 cells – PDT Control

With the specific consideration of the PDT control that was carried out alongside all of the different chemotherapy-PCI combinations, Figure 107 shows that there was *not* a significant difference (p = 0.442) in cell viability reduction for the AlPcS$_{2a}$ PDT control when comparing between the two breast cancer cell lines.

In addition, it was observed that the respective PDT controls reduced cell viability to 67% (±3%) and 61% (±2%) in the MDA-MB-231 and MCF-7 cell lines, respectively.

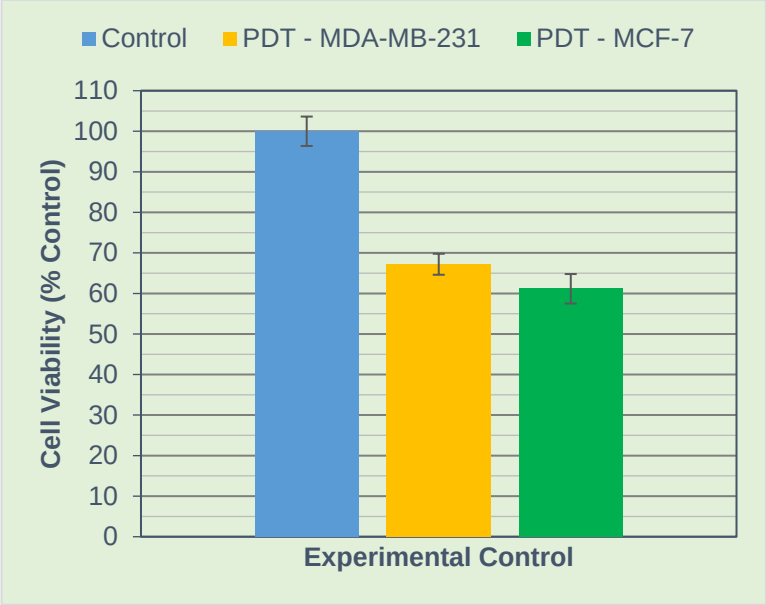

Figure 107. Reduction in breast cancer cell viability in 3D collagen hydrogels after AlPcS$_{2a}$ PDT. *Relative cellular viability (% of control) of MDA-MB-231 and MCF-7 cells after incubation with 5 µg/mL AlPcS$_{2a}$ plus treatment light exposure.*

5.7 Discussion

In keeping with the literature (2,53,189), our investigations demonstrated that AlPcS$_{2a}$ was an effective photosensitiser for both PDT and PCI applications in a 3D *in vitro* breast cancer model utilising MDA-MB-231 and MCF-7 cells.

First, with regard to PDT, increasing light energy density from 0.0-0.48 J/cm^2 (i.e. 0, 1, 2, 4 minutes illumination at 2.0 mW/cm^2) was shown to increase the cytotoxic effect of AlPcS$_{2a}$ PDT in a light dose-dependent manner in both MDA-MB-231 (TNBC) and MCF-7 (ER+) breast cancer cell lines (Figure 40, Figure 41, Figure 42, Figure 43). Moreover, this was also achieved in a concentration-dependent (AlPcS$_{2a}$) manner in both cell lines. Interestingly, in contrast to our findings with chemotherapy treatment, MDA-MB-231 cells were initially determined to be *more* sensitive to PDT (1 min) treatment than were MCF-7 cells. This was also reported in a recent study by Eng et al., (191) whereby the photochemical dose (utilising TPCS$_{2a}$) required to reduce cell viability by 50% was 3-fold higher for MCF-7 versus MDA-MB-231 cells (*NB. Although, see toward the end of this discussion section after PDT controls were collated across all of the PCI experiments*).

Importantly, $AlPcS_{2a}$ exhibited a limited dark toxicity in the absence of light treatment even at elevated concentrations - typically, around a 20% reduction in cell viability was the *maximum* effect observed (Figure 40 and Figure 42) - although many concentrations were actually much less toxic than this. There was no significant difference ($p = 0.250$) in $AlPcS_{2a}$ dark toxicity across the range of tested concentrations (0.1-100,000 nM) meaning that neither cell line was more sensitive to $AlPcS_{2a}$ under dark toxicity conditions. A low dark toxicity is important here as it indicates good light control measures during experimentation particularly in the context of differing PDT sensitivities between the two cell lines.

PCI studies *in vitro* have utilised various $AlPcS_{2a}$ concentrations (e.g. 1-20 µg/mL) and light energy densities (e.g. 0.75-3.0 J/cm^2) in combination, in order to achieve a "PDT dose" for use in PCI (168,192,193). Importantly, in order for the mechanism of PCI to function properly, PDT should be employed at a "sub-lethal" dose (46,47) – however, there appears to be no strict consensus as to the exact PDT dose lethality that ought to be used for PCI. In general, *in vitro* studies utilising breast cancer cells (all, in monolayer) appear to have used PDT doses ranging in "lethality" (i.e. the reduction in cell proliferation/viability/death) from approximately 15-50% (168,169,193).

In the landmark study by Berg et al., (188), whereby it was demonstrated that PCI-bleomycin could synergistically kill cancer cells, $AlPcS_{2a}$ was used at a concentration of 5 µg/mL (~6,800 nM). This concentration was shown to be effective across two very different cancer cell lines *in vitro* (i.e., V79 Chinese hamster lung fibroblasts; and, WiDr human primary adenocarcinoma). Moreover, Vikdal et al., (189) found that increasing $AlPcS_{2a}$ concentrations from 5 µg/mL to 20 µg/mL inhibited the intracellular trafficking of dextran (a model "drug" for pinocytosis/fluid-phase endocytosis) to $AlPcS_{2a}$-positive compartments by 47%. Consequently, this correlated with a 24% attenuation of PCI-efficacy with $AlPcS_{2a}$ 20 µg/mL versus $AlPcS_{2a}$ 5 µg/mL. In addition, Berstad et al., (193) used a 50% inhibitory PDT dose (IC_{50}/PDT_{50}) in successful [conventional] PCI experiments of immunotoxin delivery to breast cancer cells *in vitro* (MDA-MB-231 and Zr-75-1 cells). Finally, Eng et al., recently utilised a PDT_{50} photochemical dose in their PCI experiments to deliver an immunotoxin to TNBC cells (191). In the present work, utilising 5 µg/mL $AlPcS_{2a}$ correlates well with the observed PDT_{50} of MCF-7 cells but results in an approximate PDT_{70} for MDA-MB-231 cells (Figure 44).

However, upon recognition of the inherent resistance to chemotherapy of MDA-MB-231 cells and the uncertainties in treatment performance associated with 3D culture, along with light fluence and other aforementioned considerations, an $AlPcS_{2a}$ concentration of 5 µg/mL in combination with 1 min of red light illumination (0.12 J/cm^2) was taken forward to PCI experiments.

Given the preferred use of red light for PCI therapy, its effects on tumour growth are an important consideration. Red light is known to have a mitogenic effect based on its ability to activate cell division at certain spectral and dose ranges *in vitro* (194). Presently, its effects on cellular proliferation forms the empiric basis for the withholding of various clinical treatments involving red light (e.g. low-level light therapy) in cancer patients, for fear of promoting metastasis (195).

Suggestive of a harmful effect, Revazova demonstrated the acceleration of tumour growth *in vivo* (light regimen: 633 nm; total energy density: 21 J/cm^2) in a model of human gastric adenocarcinoma transplanted into immune-deficient athymic nude mice (190). In another *in vivo* study, the irradiation of squamous cell carcinomas (SCC) in the hamster cheek pouch (660 nm; 56 J/cm^2) caused significant progression of the severity of SCC as judged by histology (196). By contrast, a third study investigated the potential promotion of tumour growth by red-light (670 nm; total energy density: 186 J/cm^2) using a standard experimental mouse model of UV-induced SCC. The latter study failed to demonstrate a harmful effect of red light (administered topically *via* whole-body low-level laser therapy [LLLT]) on tumour growth in already developed cancerous skin lesions. Finally, in an *in vivo* PCI study involving mouse colon carcinoma tumours (CT.26CL25), red light treatment alone (652 nm; total energy density: 15-20 J/cm^2) was found to induce a 'small but significant' tumour growth enhancement versus control (71).

The latter study, in particular, demonstrates that the dosage of red light still remains an important consideration in PCI and is another reason (along with effects on oxygen consumption within tissues) for light fluence rates and totally energy density to be minimised as much as possible. Fortunately, the red light dosage (0.12 J/cm^2) used in our *in vitro* PCI experiments was shown to have no significant effect on cell viability in either breast cancer cell line versus controls (Figure 45).

Interestingly, the effect of red light *in vivo* has also been shown to involve immune responses which are known to be stimulated by phototherapy (195,197). For instance, one mechanism of *systemic* immune stimulation could result from red light penetration into, and the subsequent absorption by, tissues such as lymphatic nodes and vessels, as well as, bone marrow. These effects would also be in addition to the local photodynamic effects caused by interaction with endogenous porphyrins (197).

Now, with respect to the performance of PCI in the 3D *in vitro* breast cancer model (Table 4, Table 5, Table 6), PCI delivery of bleomycin (a model PCI chemotherapeutic drug) was seen to increase treatment potency (IC_{70}), compared with bleomycin chemotherapy, by ~2-fold and ~5-fold in MDA-MB-231 and MCF-7 cells, respectively. Similarly, PCI increased treatment efficacy at the highest tested concentration of 250,000 nM (E_{max}), versus bleomycin alone, by a factor of ~3 and 2 in each cell line, respectively. In keeping with previous findings relating to cell line sensitivities to chemotherapy, MCF-7 cells were found to be 37-fold (IC_{70}) more sensitive to PCI treatment than were MDA-MB-231 cells. Although, encouragingly, the E_{max} values from PCI-bleomycin were essentially the same for both cell lines. Moreover, the PCI-induced increase in treatment efficacy at this high concentration occurred to a greater extent in the TNBC cell line.

PCI of bleomycin was also seen to achieve synergy (i.e. when, $\alpha > 1$) in 63% and 88% of the tested bleomycin concentrations in MDA-MB-231 and MCF-7 cells, respectively. Thus, in line with reports in monolayer culture, our results demonstrate that bleomycin is also an effective PCI agent in a 3D *in vitro* model across a broad range of drug concentrations (0.5-250,000 nM). Interestingly, Mathews et al., (168) also utilised $AlPcS_{2a}$-bleomycin PCI in MDA-MB-231 and MCF-7 cells in monolayer, and reported a ~3-fold higher synergy value (α) for MDA-MB-231 cells (~9) versus MCF-7 cells (~3) - using the same synergy equation as our study. By contrast, the highest α values in the present study was identical for each cell line at 2.1 (Figure 49; Table 7).

Interestingly, the Mathews et al., study utilised a lower PDT/photochemical dose of between 15-25% and reported synergy with a low bleomycin concentration of ~350 nM. At this bleomycin concentration, our studies saw no synergy in MDA-MB-231 and only very mild

synergy in MCF-7 cells. Instead, the majority of bleomycin synergy was seen at the high bleomycin concentrations of between 50,000-250,000 nM. This demonstrates the importance of testing a broad range of drug concentrations in our 3D model – for had the tested bleomycin concentrations been less than 50,000 nM then PCI-bleomycin could have been deemed relatively ineffective. Furthermore, given the reported influence of higher concentrations of $AlPcS_{2a}$ affecting the compartmental co-localisation of photosensitiser and chemotherapeutic, it would be interesting to investigate (in future experiments) whether lower $AlPcS_{2a}$ concentrations affected treatment synergy outcomes. Moreover, whether different photochemical doses (e.g. PDT_{25}) affected overall PCI-bleomycin treatment outcomes. Specifically, in contrast to the parameters utilised in the present studies, Mathews et al., utilised a 5-fold lower $AlPcS_{2a}$ concentration (1 µg/mL) in combination with a ~6 to 8-fold higher energy density and only achieved a PDT lethality of between 15-25% (168). This dynamicity of PCI treatment parameters is somewhat indicative of the issues already emerging in the clinical setting. Indeed, difficulties in the optimisation of light-dosing (*via* interstitial tumour illumination) in a recent PCI-bleomycin clinical trial was cited amongst the primary reasons for the abrupt discontinuation of the trial itself (90). Further comparisons of PCI treatment effects between the Mathews et al., study and our own are difficult primarily owing to differences in PDT/photochemical doses and the treatment outcome assays used.

Collectively, the lower percentage of synergistic PCI-bleomycin combinations in MDA-MB-231 cells and the increased potency of PCI-bleomycin in MCF-7 cells, only in part support the generalised view, both in the literature and in the clinic, that the TNBC phenotype is inherently more resistant to therapy. Our data suggests that bleomycin concentration is the decisive factor, as, PCI-bleomycin increased treatment efficacy (cytotoxicity at 250,000 nM versus chemotherapy alone) to a greater extent in MDA-MB-231 cells, and was also seen to achieve a higher average synergy (α) value (when synergy did occur) in MDA-MB-231 cells.

In addition, single-agent bleomycin chemotherapy was found to be the most potent in both breast cancer cell lines but, provocatively, despite its pre-eminence as *the* model PCI chemotherapeutic drug, it was found *not* to be the most potent (IC_{70}) or efficacious (E_{max}) drug when delivered using PCI (Table 6). Moreover, in terms of the overall percentage of synergistic PCI combinations, *two* other chemotherapy drugs were seen to either equal or

improve upon the performance of bleomycin when delivered as part of a PCI regimen. Furthermore, some other chemotherapy drugs also achieved a higher outright synergy (α) value than bleomycin, as well as, a higher average α value (even if this was achieved at a lower percentage of overall combinations).

Beginning with the first group of new PCI drug candidates, the cytotoxicity of the vinca alkaloids was seen to be massively potentiated by delivery *via* PCI. In the MDA-MB-231 TNBC cell line, PCI was observed to increase treatment potency by 273-fold, 6,000-fold (IC_{50}), and ~2-fold versus chemotherapy alone for vinorelbine, vincristine, and vinblastine, respectively (Table 4). Moreover, treatment efficacy was equivalent for vinorelbine and vinblastine (viability reduced to 0% for chemotherapy and PCI) and was increased by PCI by a factor of ~3 for vincristine. PCI effects in the MCF-7 ER+ cell line were even more impressive. Compared to chemotherapy, PCI delivery increased the potency of treatment by 4,000-fold, 176,470-fold, and 1,000-fold for vinorelbine, vincristine and vinblastine, respectively. Similarly, treatment efficacy was equivalent for vinorelbine and vinblastine (0% for chemotherapy and PCI) and was increased, by PCI, by a factor of ~2 for vincristine. PCI-vincristine was seen to be the least efficacious of the vinca alkaloid PCI treatments (i.e. at 250,000 nM) but, almost paradoxically, achieved the greatest benefit from PCI in terms of potency. This indicates that PCI efficiency may be greater at lower chemotherapeutic concentrations for this particular drug. In general, though, both vinorelbine and vinblastine also achieved very impressive results in both TNBC and ER+ breast cancer cell lines when used as part of a PCI regimen. This is particularly promising for vinorelbine as it is presently one of the front-line chemotherapy drugs clinically-recommended for use in advanced breast cancer.

Likewise to PCI-bleomycin, PCI with each of the three vinca alkaloids was observed to be more potent in MCF-7 cells (than MDA-MB-231 cells). Particularly, PCI-vinorelbine was 55-fold and PCI-vinblastine was 6,400-fold more potent in the ER+ cell line. Interestingly, PCI-vincristine was similarly-potent in both cell lines but its efficacy at 250,000 nM was 2-fold greater in MCF-7 cells. Nevertheless, across all of the tested vincristine concentrations in the PCI group, there was *not* a significant difference ($p = 0.052$) in PCI-cytotoxicity seen between the two breast cancer cell lines. This similarity in performance from PCI-vincristine was one of the primary reasons for taking this combination forward to additional model variation and

formulation experiments; for, any subsequent significant differences observed would likely owe directly to these deliberate interventions. Collectively, though, the vinca alkaloid PCI data is indicative of an increased resistance to therapy on the part of the TNBC cells.

When used as part of a PCI regimen, each of the three investigated vinca alkaloids demonstrated synergism (Table 7). Encouragingly, despite PCI-vinorelbine only achieving synergy in 25% of the concentrations tested in MDA-MB-231 cells, when synergy did occur, it was highly so. For example, the highest α value achieved by PCI-vinorelbine in TNBC cells (3.7 at 100,000 nM) was greater than any of the other PCI-drug combinations in either cell line. Moreover, the average α value (2.5) was the second-highest out of all of the PCI-drug combinations. In addition, although slightly more PCI-vincristine concentrations were seen to be synergistic in MCF-7 cells (38%), the α values were much lower than those seen in MDA-MB-231 cells. PCI-vinblastine matched the synergistic performance of PCI-bleomycin in both cell lines, albeit with slightly lower average α values. PCI-vincristine surpassed even PCI-bleomycin in terms of treatment synergy, achieving 100% synergy in both cell lines. That is, vincristine attained a PCI-induced enhancement in cytotoxic effect in both TNBC and ER+ cell lines at *all* of the concentrations tested from 0.5-250,000 nM. Moreover, with PCI-vincristine, both the highest α value and the average α value were greater in both cell lines than PCI-bleomycin.

Interestingly, MCF-7 cells are classified as being relatively resistant to vincristine (198). However, the data presented here only somewhat supports this notion. For example, PCI-vincristine IC_{70} values in each breast cancer cell line were virtually identical which is in contrast to the rest of the PCI combinations which were invariably much more potent in the ER+ cells (Table 6). However, with vincristine administered as a single-agent chemotherapy, MCF-7 cells were seen to be ~3-fold *more* sensitive than MDA-MB-231 cells. Although it is possible, of course, that MCF-7 cells are indeed relatively vincristine-resistant when compared to most other cancers, but that MDA-MB-231 cells are simply *more* resistant again.

Vincristine is, along with the other vinca alkaloids, a microtubule-destabilising antimitotic chemotherapy drug initially derived from the leaves of the *Madagascar periwinkle*. Microtubules form one of the three primary protein components of the cellular cytoskeleton

which is itself responsible for the transport and positioning of intracellular organelles, as well as, the separation of chromatids during the anaphase of mitosis (199). Thus, microtubule-targeting agents such as these (and the taxanes) compromise microtubule dynamicity and, consequently, cell division is inhibited by the spindle assembly checkpoint (199). Interestingly, dynamicity is primarily affected at low concentrations with high concentrations affecting complete microtubule disassembly (200). If PCI efficiency was greater at low vincristine concentrations (i.e. during the compromised-dynamicity stage) then this could account for the observed disparities between the observed potency and efficacy of PCI-vincristine. That is, the tremendously potent effects at low concentrations (as signified by the differences in IC_{50}/IC_{70} values between chemotherapy and PCI) but then achieving only modest efficacy at the highest concentrations (though significant improvements over chemotherapy alone were still observed). Indeed, the highest synergy α value for PCI-vincristine in TNBC cells was achieved at 5 nM which is in contrast to the majority of other highest α values which were typically achieved at high concentrations. However, MCF-7 cells followed the general pattern of the other agents with the highest synergy being attained at high drug concentrations; this could also indicate some inherent resistance to vincristine.

Intriguingly, despite their widespread clinical use, the mechanisms linking microtubule poison-induced mitotic arrest and cell death still remain very much unexplored (187). Notwithstanding, disruption of the structure and function of the microtubule cytoskeleton alone is thought to exhibit lethal consequences for the cell (aside from those initiated by mitotic arrest). Indeed, drugs that target microtubules have demonstrated cytotoxicity in post-mitotic cells *in vivo* (e.g. neurons) (201); and clinical neurotoxicity is also one of the characteristic adverse effects of antimitotic agents.

Importantly in the context of PCI therapy, decreased microtubule dynamicity has also been shown to induce leakage of lysosomal protease cathepsins into the cytosol of various human cancer cells including those of breast (187), cervix (187), and lung (202). Thus, lysosomal integrity is reliant upon a fully-functioning microtubule network. Importantly, when released from lysosomes and into the cytosol, these cathepsins can trigger both caspase-dependent and caspase-independent mechanisms of cell death (51,203). Interestingly, stroma-induced alterations in cancer cell phenotype can also potentiate the expression and

microtubule-dependent release (into the ECM) of these lysosomal cysteine cathepsins (204). Thus, microtubule dynamicity will be diminished by antimitotic drugs which will, in turn, potentiate the release of the cathepsin proteases. This, subsequently, leaves the heavily cathepsin- and drug-laden lysosome as an attractive target for initiating cancer cell death. Not least by the action of PCI.

Groth-Pederson et al., first investigated the specific effect of vincristine chemotherapy on the lysosomes in HeLa (vincristine-sensitive) and MCF-7 (vincristine-resistant) cancer cells (187). Here, vincristine was seen to induce a “dramatic” increase in both the size and the number of lysosomes in both cell lines. Moreover, total lysosomal volume was increased and there was also an accompanying increase in cytosolic cysteine cathepsin concentration which was indicative of lysosomal destabilisation and permeabilisation. Interestingly, the authors posited that the increased lysosomal compartment volume was a result of the merging of pre-existing lysosomes and their defective turnover by exocytosis (which is dependent upon functioning microtubules) and not as a result of increased *de novo* synthesis.

After establishing that lysosomes are indeed targets of vincristine chemotherapy, Groth-Pederson and colleagues then combined vincristine with the anticancer agent siramesine whose dedicated mechanism of action involves the induction of lysosome destabilisation (205). Combined, these two agents attained a synergistic cytotoxic effect in both cell lines; achieving “massive cell death” in MCF-7 breast cancer cells even at low drug concentrations. Crucially, strong synergy was also observed when vincristine was substituted for the other microtubule-binding chemotherapy drugs vinorelbine (which is a semi-synthetic vincristine analogue) and paclitaxel (187) – both of which were also tested in the present study. In addition, the combination of vincristine and siramesine also produced substantial anti-tumour effects in a MCF-7 breast cancer xenograft *in vivo* model even at deliberately suboptimal doses of each drug.

In keeping with these data, the present study also investigated the microtubule-targeting therapeutic drugs docetaxel and paclitaxel. In MDA-MB-231 cells, PCI delivery did not increase docetaxel potency over chemotherapy but *did* increase paclitaxel potency by a factor of 3. By contrast, both drugs saw large increases in potency in MCF-7 cells when

delivered as part of a PCI regimen. Specifically, increases in potency over chemotherapy were 90-fold and 10-fold for docetaxel and paclitaxel, respectively. PCI-docetaxel efficacy at 250,000 nM was equivalent to chemotherapy in both cell lines. Interestingly, MDA-MB-231 cells were reduced to 0% viability and MCF-7 cells to 11% therefore PCI-docetaxel was *more* efficacious in the TNBC cells. This is important as docetaxel is another front-line chemotherapy drug recommended in advanced breast cancer. In line with previous observations, PCI-paclitaxel was also seen to achieve larger gains in efficacy at 250,000 nM in TNBC cells compared with ER+ cells. Moreover, in outright terms, PCI-paclitaxel was also more efficacious at 250,000 nM in MDA-MB-231 cells.

In terms of treatment outcomes between cell lines, PCI-docetaxel potency was 18-fold higher in MCF-7 cells, however, treatment efficacy at 250,000 nM was 11-fold higher in MDA-MB-231 cells. This could be due to the PDT/photochemical element of treatment predominating at lower drug concentrations before PCI interactions take over at higher drug concentrations. Intriguingly, a similar pattern was observed with PCI-paclitaxel whereby MCF-7 cells were 18-fold more sensitive in terms of potency and MDA-MB-231 cells were ~3-fold more sensitive in terms of treatment efficacy at the highest tested drug concentration.

Synergistic interactions were also observed upon the PCI delivery of docetaxel and paclitaxel. Encouragingly from a clinical perspective, PCI-docetaxel attained synergy in 50% of tested concentrations in both cell lines. Moreover, the highest synergy was seen at the same concentration in both cell lines (5,000 nM). By contrast, PCI-paclitaxel achieved synergy in only 13% and 25% of tested concentrations in MDA-MB-231 and MCF-7 cells, respectively. Although, in the TNBC cells, the highest synergy value was comparatively large (2.9) and actually the third-highest of all outright highest synergy values in both cell lines; behind only PCI-vinorelbine (3.7) and PCI-vincristine (3.0).

In relation to PCI-docetaxel, although potency and efficacy measures were equivalent to chemotherapy (in MDA-MB-231 cells), synergy was still attained in half of the concentrations which could be important at certain clinical doses. PCI-docetaxel also demonstrated an unusual dose-response at 500 nM (Figure 62) which could signify some

interaction between drug and sensitiser uptake, or possibly a preferential drug residence within the hydrogel itself at this docetaxel concentration.

Now, discerning the precise mechanisms of PCI-induced synergy observed with the tested microtubule-targeting agents will require further investigation. However, preliminary investigations were conducted into this matter using vinblastine connected to the fluorophore BODIPY™ (MW: 262.1 g/mol). Importantly, this molecule has a relatively low molecular weight and is, thus, unlikely to dramatically alter the uptake mechanism and kinetics of the parent drug. At the very least, the vinblastine-BODIPY™ conjugate is likely to be inherently more representative of vinca alkaloid behaviour in PCI than, say, the commonly used dextran-tagged fluorophores (189). Excitingly, the subsequent fluorescent-imaging of vinblastine-BODIPY™ in conjunction with the dedicated lysosome-targeting fluorophore Lysotracker® clearly shows the co-localisation of the two fluorophores (Figure 82). This signifies that the lysosomes were laden with the chemotherapy drug and tantalisingly suggests that the impressive vinca alkaloid results were achieved, at least in part, by means of a *classical* PCI mechanism of increased drug release to the cytoplasm.

The antimetabolite drugs gemcitabine and capecitabine performed relatively poorly in the 3D *in vitro* breast cancer models when compared to the vinca alkaloid and taxane agents. Whether in their PCI or chemotherapy guises, neither drug attained an IC_{70} value in either cell line and treatment efficacy at 250,000 nM was comparatively low. Some positives were observed with gemcitabine in that PCI delivery increased potency (IC_{50}) 2-fold and also attained some treatment synergy; 25% and 50% in TNBC and ER+ cells, respectively. PCI-capecitabine performance was particularly disappointing given capecitabine is also at the forefront of clinical recommendations in advanced breast cancer. There are several potential reasons for the poor performance of the antimetabolite drugs. Firstly, both are highly water-soluble and therefore may have preferred to accumulate and reside within the surrounding ECM provided by the hydrogel. Alternatively, as mentioned in the previous chapter, an increased expression of drug-metabolising enzymes has been observed in 3D-cultured cells so it is possible that, for example, elevated dihydropyrimidine dehydrogenase led to increased antimetabolite clearance. From a technical standpoint, it is also possible that the 18 h period of drug incubation was simply not long enough for the adequate uptake of these therapeutics.

Finally, the clinically-recommended combination of gemcitabine and paclitaxel also achieved very positive results from PCI-delivery compared with its use as a dual-agent chemotherapy. In MDA-MB-231 cells, PCI increased treatment potency by ~5-fold and treatment efficacy at 250,000 nM by 17-fold. Moreover, in MCF-7 cells, PCI massively increased treatment potency by 57,778-fold and treatment efficacy by ~3-fold. In line with previous findings, PCI of gemcitabine & paclitaxel was much more potent (IC_{70}) in MCF-7 than MDA-MB-231 cells (an 83,333-fold difference) but treatment was ~3-fold more efficacious (E_{max}) in MDA-MB-231 cells. In addition, a higher percentage of synergistic treatment combinations were seen in MDA-MB-231 cells (50%) compared with MCF-7 cells (25%) along with a higher average synergy α value.

In summary, at this point, PCI was seen to increase the potency and efficacy of several new PCI candidates. The microtubule-targeting chemotherapeutics performed particularly well and, in particular, the vinca alkaloids. In general, PCI increased treatment efficacy versus chemotherapy to a greater extent in the MDA-MB-231 TNBC cell line. By contrast, treatment potency versus chemotherapy was generally increased to a greater extent in the MCF-7 ER+ cell line. Encouragingly, the highest synergy values were generally seen in the TNBC cells and when combinations *were* synergistic, they tended to achieve a higher α value than treatment of ER+ cells (as indicated by their higher average α values). Conversely, the frequency of synergistic interactions for each PCI-drug combination was seen to slightly favour MCF-7 cells.

In addition to recognising promising new individual chemotherapy drug candidates, this work also aimed to highlight whole drug classes or modes of chemotherapy that could benefit from PCI and thus provide the groundwork for others to make their own investigations (Table 10). Indeed, data was pooled into the respective therapeutic drug classes (vinca alkaloids; taxanes; and, antimetabolites), and each drug class was then compared to bleomycin (a glycopeptide antibiotic). The long-standing position of bleomycin as the favoured chemotherapy drug for use in PCI studies also mandated its direct comparison with the individual agents (Table 8, Table 9). Encouragingly, these data collectively show that certain new PCI-drug combinations far exceeded the performance of PCI-bleomycin in terms of treatment potency, efficacy, and synergy.

Bleomycin monotherapy was seen to be the most potent chemotherapy in both TNBC and ER+ cell lines. On the other hand, the most efficacious chemotherapy in TNBC cells was a tie between vinorelbine, vinblastine, and docetaxel; with all achieving the maximum possible efficacy by reducing cell viability to 0% of control. As aforementioned, this correlates well with the clinical picture given that vinorelbine and docetaxel are recommended chemotherapies in advanced breast cancer (especially, TNBC). Similarly, of the eight chemotherapy drugs tested, vinorelbine and vinblastine were found to be the most efficacious in ER+ cells.

Now, in relation to the relative performances of the novel PCI-drug combinations compared with PCI-bleomycin, there were some prominent observations. Firstly, that vinca alkaloid PCI was generally massively more potent that PCI-bleomycin. Specifically, PCI-vinorelbine and PCI-vincristine were 100-fold and 61,111-fold *more* potent than PCI-bleomycin in MDA-MB-231 cells. Moreover, in MCF-7 cells, PCI-vinorelbine, PCI-vincristine, and PCI-vinblastine were 150-fold, 1,765-fold, and 60-fold *more* potent than PCI-bleomycin. Next, in terms of treatment efficacy, all PCI-vinca combinations were more efficacious than PCI-bleomycin in MDA-MB-231 cells by a factor of ~4-6. In addition, PCI-vinorelbine and PCI-vinblastine were more efficacious than PCI-bleomycin by a factor of 5 in MCF-7 cells. Other prominent observations include that PCI-docetaxel attained a 6-fold increase in efficacy over PCI-bleomycin in MDA-MB-231 cells. Furthermore, compared to PCI-bleomycin, PCI-gemcitabine & paclitaxel was similarly potent in MDA-MB-231 cells but was 1,667-fold *more* potent in MCF-7 cells. Moreover, this novel combination was also 6-fold more efficacious at 250,000 nM than was PCI-bleomycin. These findings are all highly important given that PCI-bleomycin has itself been considered an effective- and promising-enough PCI-therapy to warrant investigation in human clinical trials. Moreover, all of these agents have seen long-standing and extensive clinical use for various different cancer indications. Subsequently, their administration regimens, clinical precautions and monitoring, and adverse effect profiles are already well-characterised and well-known to clinicians.

PCI results were also pooled by chemotherapeutic drug class and compared to bleomycin-PCI. Collectively, vinca alkaloid-PCI was 79-fold and 500-fold more potent than bleomycin-PCI in MDA-MB-231 and MCF-7 cells, respectively. Meanwhile, efficacy was approximately equivalent to bleomycin-PCI across the two breast cancer cell lines. This

signifies the ability of vinca alkaloid PCI to rapidly and extensively reduce the cancer cell burden (compared with bleomycin-PCI) without compromising upon the overall treatment effect. Currently, there is at least two other chemotherapy drugs in the vinca alkaloid drug class that are approved for clinical use in cancer (vindesine and vinflunine). Based upon the results of the present work, these may also be promising candidates for PCI therapy. With regards to the taxanes, taken collectively, these agents were generally inferior to bleomycin-PCI apart from a 2-fold increase in efficacy in the TNBC cell line. Finally, the antimetabolite drug class were very much inferior to PCI with bleomycin.

Interestingly, following statistical analysis of *all* of the collated PDT control and dark toxicity control data (n=24), it was revealed that $AlPcS_{2a}$ photochemical treatment actually performed remarkably similarly in each cell line and was non-significantly different (Figure 107). This contrasts with the preliminary PDT experiments whereby MDA-MB-231 cells were seen to be more sensitive than MCF-7 cells (Figure 44). Ultimately, this was a good outcome in terms of the experimentation parameters achieved as it allows for a more direct comparison of PCI treatment effects between each cell line. However, it is not entirely clear why this disparity occurred. It is possible that differences in cell passage number could have played some part or that the $AlPcS_{2a}$ stock used for the initial PDT dose-response curves was somehow degraded or photo-bleached in some way. Nevertheless, a separate $AlPcS_{2a}$ stock solution was used for *all* of the PCI experiments (including in those experiments to follow in later Chapters).

Here, some potential limitations of PCI-delivery with the aforementioned chemotherapeutic agents is briefly mentioned. In general, they relate to issues around the neurotoxic and vesicant agents. For example, the vinca alkaloids are classified as 'vesicant' agents which means that they have the capacity to cause blistering and/or severe tissue injury and necrosis should they leak from a vein into the surrounding tissue during intravenous administration (206). Thus, although acute cellular concentrations would be dramatically lower than the concentrations at the administration stage - due to the *sink* condition and subsequent dilution within the blood compartment - the effect of releasing increased amounts of intracellular drug into nearby stromal and ECM compartments has not been thoroughly investigated. Theoretically, it could have unintended adverse consequences such as those

seen during extravasation. Conversely, such an effect in the surrounding tissue (i.e. close to the site of illumination) could even encourage and direct a more effective immune response to the illuminated region. Notwithstanding, should illuminated tumours be in close proximity to particularly sensitive structures such as neurons, this could potentiate issues with neurotoxicity. That said, amongst the promising drug candidates, some agents are well-known to be much more or less neurotoxic than others. These speculative considerations could justify the use of PCI-vinorelbine over PCI-vincristine, for instance, as vinorelbine is clinically regarded as a much less neurotoxic agent than vincristine and still achieved promising results when delivered using PCI. Moreover, it is also available as an oral tablet formulation which could lower the overall treatment cost and burden to healthcare systems.

Overall, these data have identified several new promising PCI drug candidates that outperformed PCI-bleomycin in terms of treatment potency, efficacy, and synergy in two different 3D *in vitro* models of breast cancer. In particular, the combination of PCI with microtubule-disturbing drugs appears to possess great future potential.

Chapter 6: PCI & Variations

6. Evaluation of PCI in a 3D *in vitro* Model with Regimen & Model Variations

6.1 Introduction

Following the evaluation of PCI treatments on 3D-cultured MDA-MB-231 and MCF-7 breast cancer cells utilising a *conventional* PCI regimen (that is, co-incubation of chemotherapy and $AlPcS_{2a}$ prior to light irradiation), further investigations were subsequently undertaken in order to evaluate the effect on treatment outcomes of variations in both PCI regimen and 3D-model parameters.

More specifically, the "*light-before*" PCI regimen was tested with selected chemotherapy drugs utilising the same $AlPcS_{2a}$ concentration (5 µg/mL) and light dose (660 nm; 0.12 J/cm^2) as previous experiments involving the conventional PCI regimen:

- *bleomycin* – due to its standing as a model PCI drug.
- *vincristine* – due to its emergence as a promising candidate for use in PCI delivery and because there was no significant difference observed in the effect of vincristine-PCI between MDA-MB-231 and MCF-7 cell lines; any subsequent significant differences resulting from treatment or model variations would therefore be scientifically interesting.
- *gemcitabine* – due to its generally poor all-round performance in the 3D model with respect to both chemotherapy and PCI treatment, therefore any resulting significant differences resulting from treatment or model variations would be scientifically interesting.

It is also important to note that the light-before (LB) PCI regimen necessarily mandates that chemotherapy drugs be added in a different sequence to the conventional PCI regimen. With this in mind, it was therefore necessary to conduct additional chemotherapy cytotoxicity experiments in order to more-accurately compare and contrast with the LB-PCI counterpart experiments.

In addition, because cell culture conditions including ECM geometries and 3D microstructures have been shown to dramatically influence cell morphology and cellular

responses to cytotoxic anticancer treatment, the effect of changes in hydrogel volume and hydrogel stiffness were also investigated. Importantly, these latter experiments involving 3D-model variations utilised the conventional PCI regimen and therefore mirrored previous PCI experiments in all but the deliberate model variations.

6.2 Variation 1: Light-Before PCI Regimen

6.2.1 Bleomycin

6.2.1.1 "Light-before" Bleomycin Chemotherapy vs Light-before Bleomycin PCI

6.2.1.1.1 MDA-MB-231 cells

Light-before (LB) PCI experiments began with bleomycin. As aforementioned, a new, "light-before" (LB) bleomycin chemotherapy cytotoxicity profile was performed in MDA-MB-231 cells in order to accurately compare to bleomycin LB-PCI (as shown in Figure 108). Here, there was *not* a significant difference ($p = 0.073$) in cell viability reduction observed between LB-chemotherapy and LB-PCI experimental groups. Bleomycin concentration *was* found to have a significant effect ($p < 0.001$) on cell viability reduction within each experimental group.

The $AlPcS_{2a}$ (5 µg/mL) PDT control conducted alongside these LB-PCI experiments reduced cell viability to 55% (±6%). With regard to treatment potency, IC_{70} values were found to be 36,000 nM and 30,000 nM for LB-chemotherapy and LB-PCI treatment groups, respectively. This represents a 1.2-fold reduction in IC_{70} in favour of LB-PCI. At the maximum tested concentration of 250,000 nM, cell viability was reduced to 20% (±1%) and 6% (±2%) in LB-chemotherapy and LB-PCI groups, respectively, which represents a 3.3-fold increase in efficacy at 250,000 nM in favour of LB-PCI.

6.2.1.1.2 MCF-7 cells

Similar LB-chemotherapy and LB-PCI experiments were then performed in MCF-7 cells (as shown in Figure 109). These experiments demonstrated that there was *not* a significant difference ($p = 0.192$) in cell viability reduction between LB-chemotherapy and LB-PCI experimental groups. Bleomycin concentration *was* found to have a significant effect ($p < 0.001$) on cell viability reduction within each experimental group.

The $AlPcS_{2a}$ (5 µg/mL) PDT control conducted alongside these LB-PCI experiments reduced cell viability to 38% (±3%). Pertaining to treatment IC_{70} values, these were estimated as 375 nM and 325 nM for LB-chemotherapy and LB-PCI treatment groups, respectively. This represents a 1.2-fold reduction in IC_{70} in favour of LB-PCI. In relation to treatment efficacy at the highest tested concentration of 250,000 nM, cell viability was reduced to 12% (±1%) and 6% (±2%) in LB-chemotherapy and LB-PCI groups, respectively. This signifies a 2-fold increase in treatment efficacy at 250,000 nM in favour of LB-PCI.

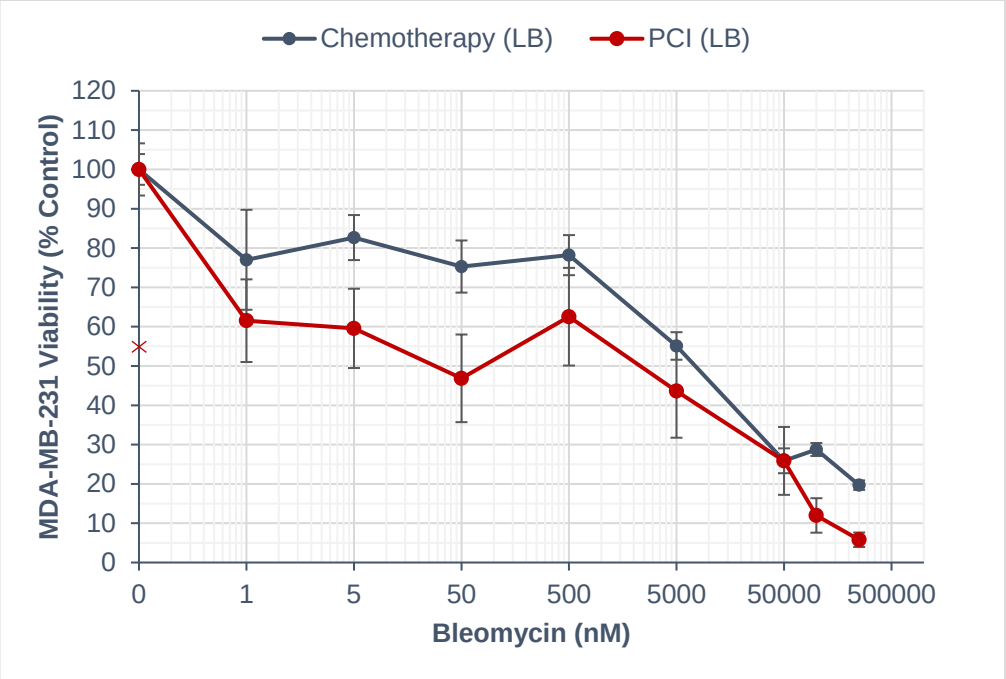

Figure 108. Reduction in MDA-MB-231 breast cancer cell viability in 3D collagen hydrogels after light-before bleomycin chemotherapy and light-before bleomycin PCI*. Relative cellular (% of control) of MDA-MB-231 cells after light-before regimen chemotherapy and PCI treatments at various bleomycin concentrations (0.5-250,000 nM).*

6.2.1.1.3 Light-before Bleomycin PCI – MDA-MB-231 cells vs MCF-7 cells

Next, the performance of bleomycin LB-PCI was compared between the MDA-MB-231 and MCF-7 breast cancer cell lines (see Figure 110). Here, it was observed that there was *not* a significant difference ($p = 0.067$) in cell viability reduction by bleomycin LB-PCI between the cell lines. Furthermore, bleomycin concentration *was* found to have a significant effect ($p < 0.001$) on cell viability reduction within each experimental group.

In addition, bleomycin LB-PCI combinations were seen to be more potent against MCF-7 cells across all concentrations tested. With regard to treatment potency, the IC_{70} values were found to be 30,000 nM and 325 nM for MDA-MB-231 and MCF-7 cells,

respectively. This represents a 92-fold IC_{70} reduction in favour of the MCF-7 cell line. At the maximum tested concentration of 250,000 nM, bleomycin LB-PCI was equally efficacious in both cell lines as cell viability was reduced to 6% (±2%).

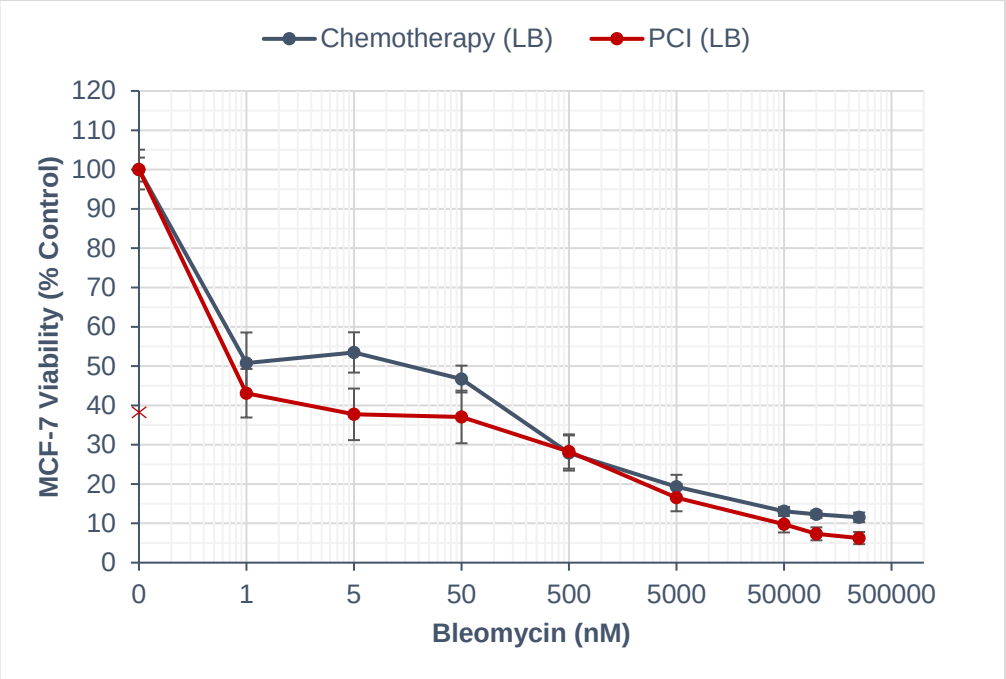

Figure 109. Reduction in MCF-7 breast cancer cell viability in 3D collagen hydrogels after light-before bleomycin chemotherapy and light-before bleomycin PCI*. Relative cellular viability (% of control) of MCF-7 cells after light-before regimen chemotherapy and PCI treatments at various bleomycin concentrations (0.5-250,000 nM).*

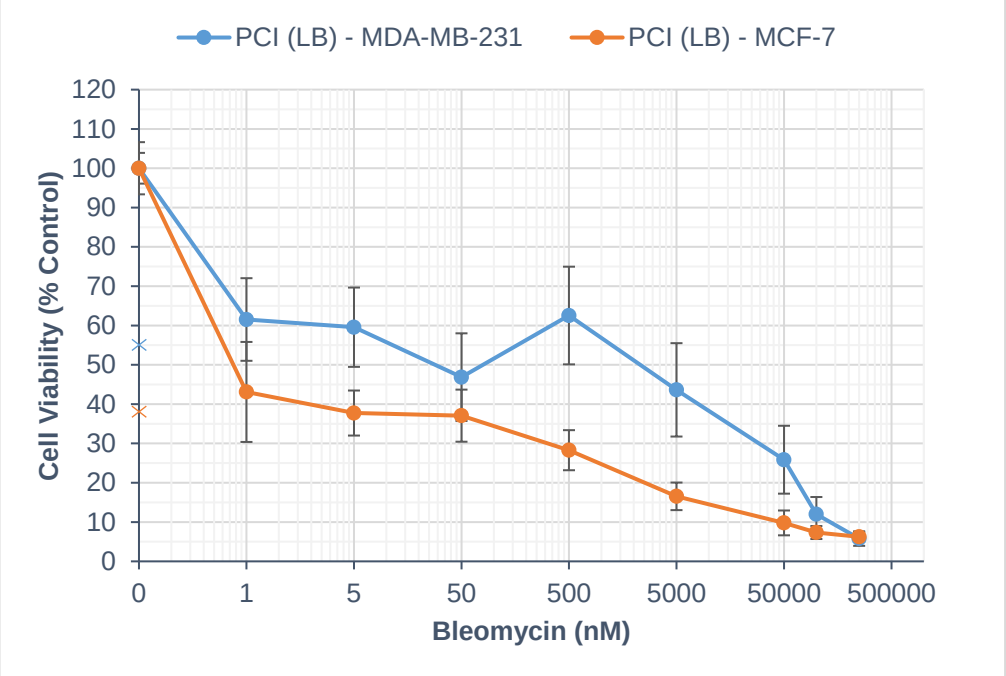

Figure 110. Reduction in breast cancer cell viability in 3D collagen hydrogels after light-before bleomycin PCI*. Relative cellular viability (% of control) of MDA-MB-231 and MCF-7 cells after light-before regimen PCI treatment at various bleomycin concentrations (0.5-250,000 nM).*

6.2.1.1.4 Treatment Synergy – Light-before Bleomycin PCI

Similarly to experiments utilising the conventional PCI regimen, synergy calculations were then performed from the PDT, LB-chemotherapy, and LB-PCI data. The bleomycin LB-PCI synergy plot (Figure 111) shows that 38% of bleomycin LB-PCI combinations were synergistic for the MDA-MB-231 cell line and that the highest *α* value achieved was 2.8 (±0.5) at 250,000 nM. Pertaining to synergy in the MCF-7 cell line, 0% of bleomycin LB-PCI combinations were synergistic (the highest *α* value achieved was an *antagonistic* 0.9 [±0.2] at 250,000 nM).

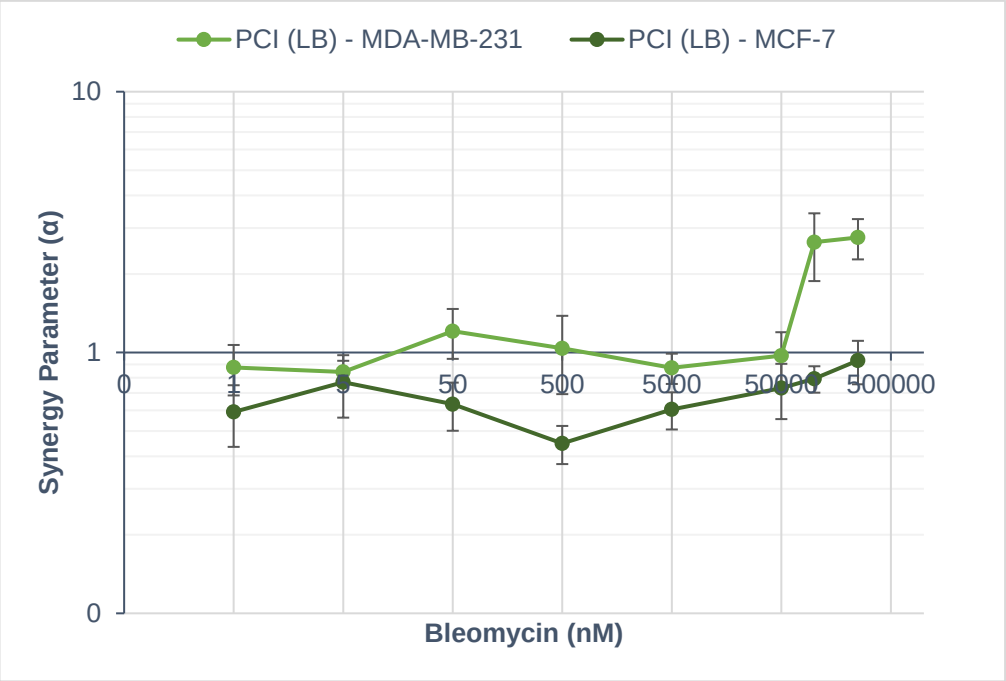

Figure 111. Synergy plot for light-before bleomycin-PCI combinations in MDA-MB-231 and MCF-7 breast cancer cells. *Synergy (α) was calculated from the individual cell viability results (specifically, survival/viability fraction) obtained for each respective LB treatment condition: LB-chemotherapy, LB-PDT, and LB-PCI.*

6.2.2 Vinca Alkaloids

6.2.2.1 "Light-before" Vincristine Chemotherapy vs Light-before Vincristine PCI

6.2.2.1.1 MDA-MB-231 cells

Following investigations utilising bleomycin, the next LB-PCI experiments were performed using the vinca alkaloid vincristine (Figure 112). Here, it was determined that there was *not* a significant difference ($p = 0.108$) in cell viability reduction between LB-chemotherapy and LB-PCI experimental groups. Furthermore, it was observed that vincristine concentration *did* have a significant effect ($p < 0.001$) on cell viability reduction within each experimental group.

The $AlPcS_{2a}$ (5 µg/mL) PDT control conducted alongside these LB-PCI experiments reduced cell viability to 57% (±8%). Concerning treatment potency, the IC_{70} values were estimated to be 175 nM and 0.40 nM for LB-chemotherapy and LB-PCI treatment groups, respectively. This represents a 438-fold reduction in IC_{70} in favour of LB-PCI. At the maximum tested concentration of 250,000 nM, cell viability was seen to be reduced to 24% (±3%) and 5% (±1%) in LB-chemotherapy and LB-PCI groups, respectively. This represents a 4.8-fold increase in treatment efficacy at 250,000 nM in favour of LB-PCI.

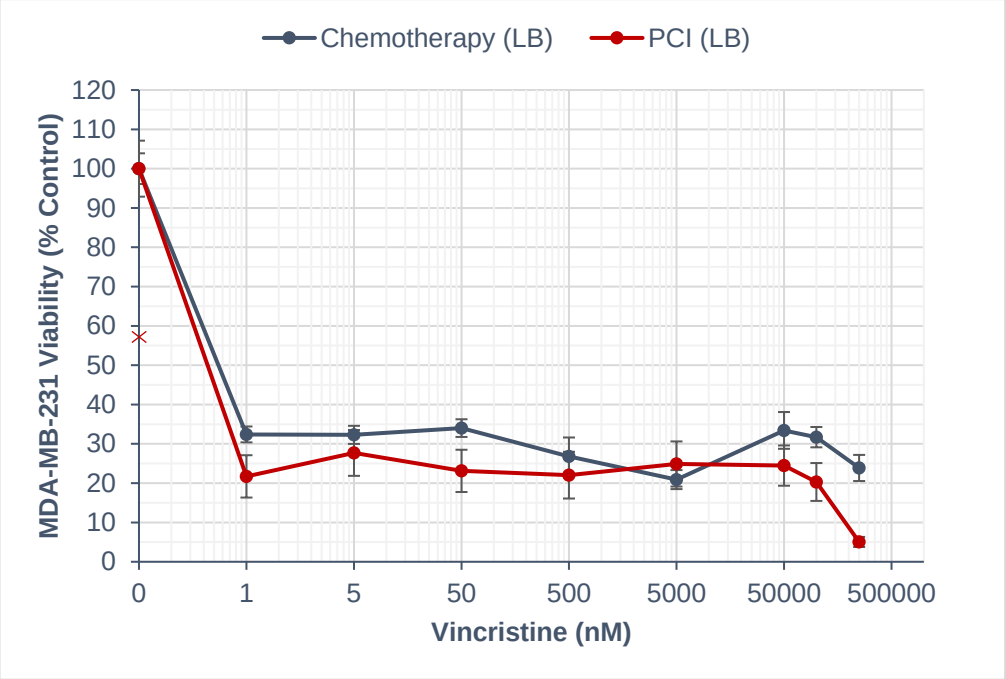

Figure 112. Reduction in MDA-MB-231 breast cancer cell viability in 3D collagen hydrogels after light-before vincristine chemotherapy and light-before vincristine PCI*. Relative cellular viability (% of control) of MDA-MB-231 cells after light-before regimen chemotherapy and PCI treatments at various vincristine concentrations (0.5-250,000 nM).*

6.2.2.1.2 MCF-7 cells

The vincristine LB-chemotherapy and LB-PCI experiments were then repeated in MCF-7 cells (Figure 113). Here, a significant difference ($p < 0.001$) in cell viability reduction *was* observed between LB-chemotherapy and LB-PCI experimental groups. Furthermore, vincristine concentration *did* have a significant effect ($p < 0.001$) on cell viability reduction within each experimental group.

The $AlPcS_{2a}$ (5 µg/mL) PDT control conducted alongside these LB-PCI experiments reduced cell viability to 40% (±4%). Pertaining to treatment IC_{70} values, these were found to be 500 nM and 0.375 nM for LB-chemotherapy and LB-PCI treatment groups, respectively. This signifies a 1,333-fold reduction in IC_{70} in favour of LB-PCI. At the highest tested concentration of 250,000 nM, cell viability was reduced to 19% (±2%) and 4% (±1%) in LB-chemotherapy and LB-PCI groups, respectively. These E_{max} values represent a 4.8-fold increase in treatment efficacy at 250,000 nM in favour of LB-PCI.

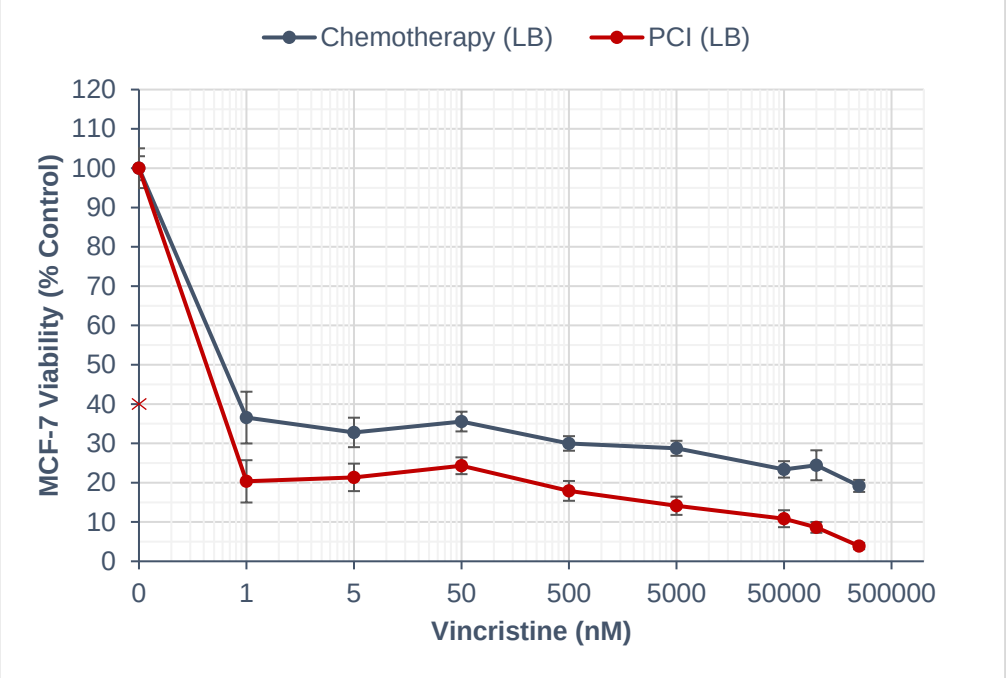

Figure 113. Reduction in MCF-7 breast cancer cell viability in 3D collagen hydrogels after light-before vincristine chemotherapy and light-before vincristine PCI*. Relative cellular viability (% of control) of MCF-7 cells after light-before regimen chemotherapy and PCI treatments at various vincristine concentrations (0.5-250,000 nM).*

6.2.2.1.3 Light-before Vincristine PCI – MDA-MB-231 cells vs MCF-7 cells

Vincristine LB-PCI was then compared between MDA-MB-231 and MCF-7 cells (as seen in Figure 114). From these comparisons, it was determined that there was *not* a significant difference (p = 0.255) in cell viability reduction by vincristine LB-PCI between MDA-MB-231 and MCF-7 cell lines. In addition, vincristine concentration *did* have a significant effect (p < 0.001) on cell viability reduction within each experimental group.

It can be determined from Figure 114 that vincristine LB-PCI IC_{70} values were 0.40 nM and 0.38 nM for MDA-MB-231 and MCF-7 cells, respectively, which essentially represents

an equipotent performance in both cell lines. Moreover, at the maximum tested concentration of 250,000 nM, vincristine LB-PCI was essentially equally effective in both cell lines as cell viability was reduced to 5% (±1%) and 4% (±1%) in MDA-MB-231 and MCF-7 cells, respectively.

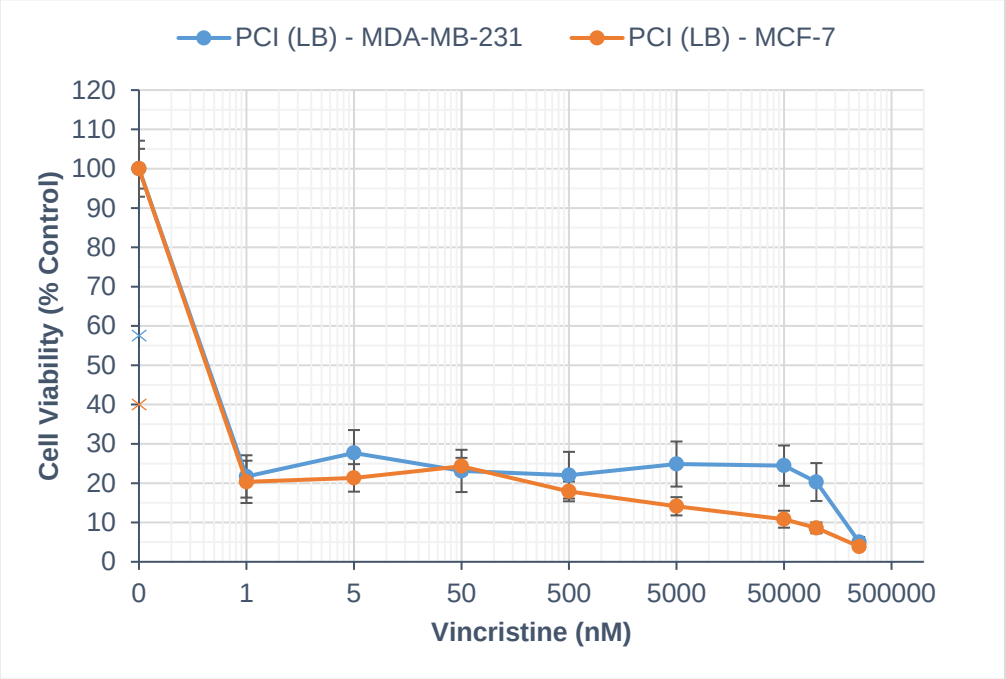

Figure 114. Reduction in breast cancer cell viability in 3D collagen hydrogels after light-before vincristine PCI. *Relative cellular viability (% of control) of MDA-MB-231 and MCF-7 cells after light-before regimen PCI treatment at various vincristine concentrations (0.5-250,000 nM).*

6.2.2.1.4 MDA-MB-231 and MCF-7 Treatment Synergy – Light-before Vincristine PCI

Synergy calculations were then performed (shown below in Figure 115) and it was determined that 88% of vincristine LB-PCI combinations were synergistic for the MDA-MB-231 cell line and that the highest *α* value achieved was 3.5 (±0.4) at 250,000 nM. With regard to the MCF-7 cell line, 50% of vincristine LB-PCI combinations were synergistic and the highest *α* value achieved was 3.4 (±1.1) at 250,000 nM.

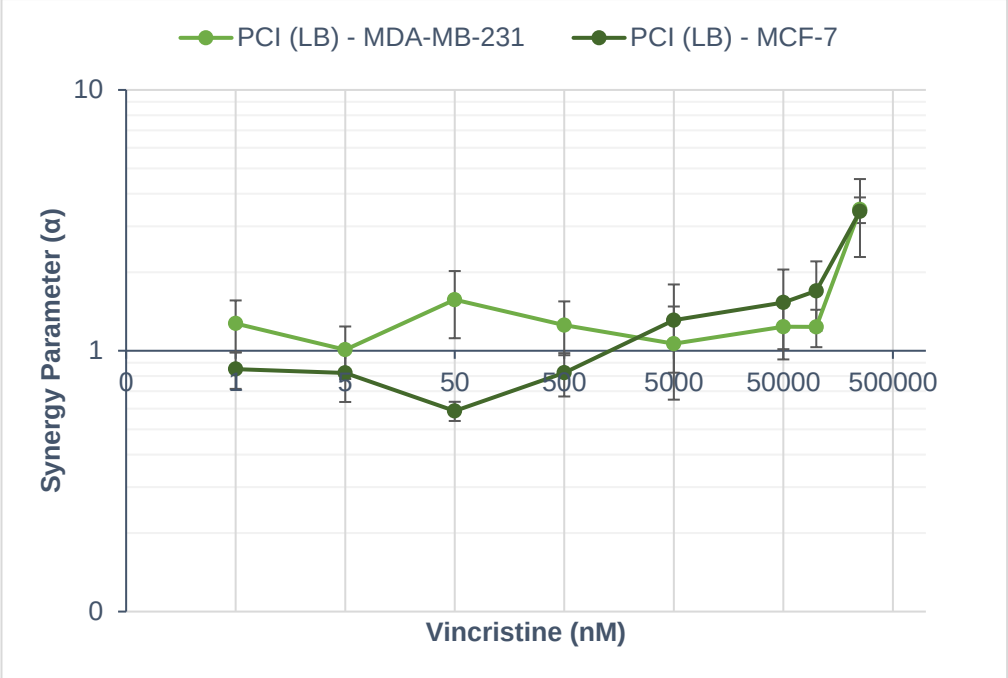

Figure 115. Synergy plot for light-before vincristine-PCI combinations in MDA-MB-231 and MCF-7 breast cancer cells. *Synergy (α) was calculated from the individual cell viability results (specifically, survival/viability fraction) obtained for each respective LB treatment condition: LB-chemotherapy, LB-PDT, and LB-PCI.*

6.2.3 Antimetabolites

6.2.3.1 "Light-before" Gemcitabine Chemotherapy vs Light-before Gemcitabine PCI

6.2.3.1.1 MDA-MB-231 cells

Light-before experimentation was then carried out utilising the antimetabolite chemotherapy drug gemcitabine. Here, it was observed that there was *not* a significant difference ($p = 0.998$) in cell viability reduction between LB-chemotherapy and LB-PCI experimental groups (Figure 116). In addition, gemcitabine concentration *did* have a significant effect ($p < 0.001$) on cell viability reduction within each experimental group.

The $AlPcS_{2a}$ (5 µg/mL) PDT control conducted alongside these LB-PCI experiments reduced cell viability to 38% (±5%). Pertaining to treatment potency, IC_{70} values were *not attained* for either treatment group, although, IC_{50} values *were* obtained and were found to be 75 nM and 1,000 nM for LB-chemotherapy and LB-PCI treatment groups, respectively. This represents a 13.3-fold reduction in IC_{50} in favour of LB-chemotherapy. At the highest tested concentration of 250,000 nM, it was observed that both treatment groups reduced cell viability to 40% (±3%; ±6%) in LB-chemotherapy and LB-PCI groups, respectively.

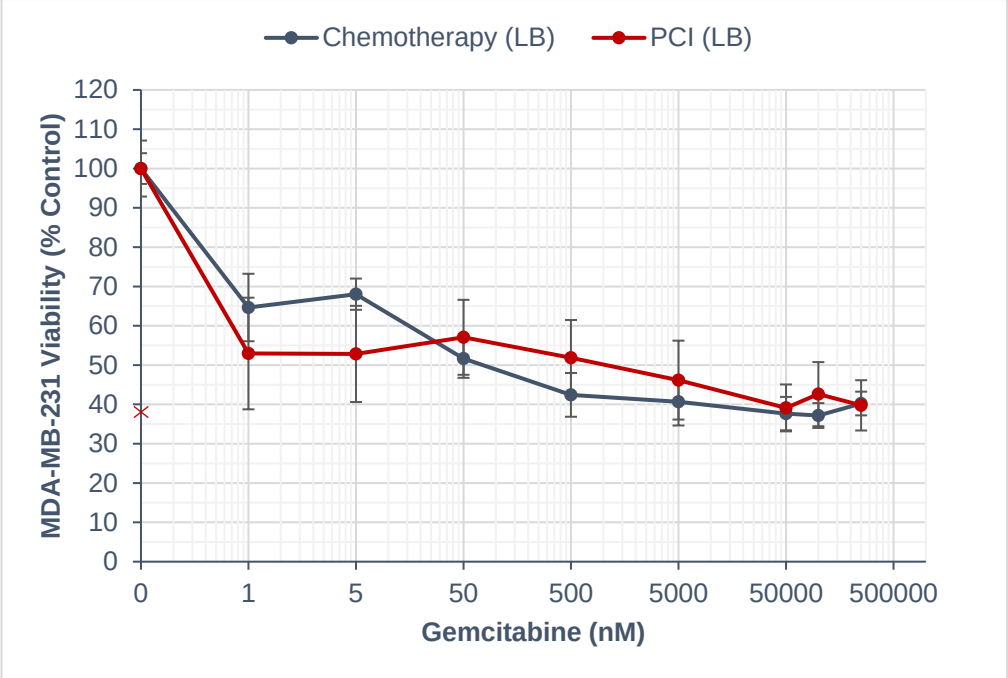

Figure 116. Reduction in MDA-MB-231 breast cancer cell viability in 3D collagen hydrogels after light-before gemcitabine chemotherapy and light-before vincristine PCI*. Relative cellular viability (% of control) of MDA-MB-231 cells after light-before regimen chemotherapy and PCI treatments at various vincristine concentrations (0.5-250,000 nM).*

6.2.3.1.2 MCF-7 cells

Gemcitabine LB-chemotherapy and LB-PCI were then carried out in MCF-7 cells (as seen in Figure 117). From these experiments it was determined that there was *not* a significant difference (p = 0.119) in cell viability reduction between LB-chemotherapy and LB-PCI experimental groups. In addition, gemcitabine concentration *did* have a significant effect (p < 0.001) on cell viability reduction within each experimental group.

The $AlPcS_{2a}$ (5 µg/mL) PDT control conducted alongside these LB-PCI experiments reduced cell viability to 26% (±3%). In relation to treatment potency, IC_{70} values were found to be 8,750 nM and 1 nM for LB-chemotherapy and LB-PCI treatment groups, respectively. This signifies an 8,750-fold reduction in IC_{70} in favour of LB-PCI. With regard to treatment E_{max} at the maximum tested concentration of 250,000 nM, cell viability was found to be 32% (±4%) and 23% (±3%) in LB-chemotherapy and LB-PCI groups, respectively. These values represent a 1.4-fold increase in treatment efficacy at 250,000 nM in favour of LB-PCI.

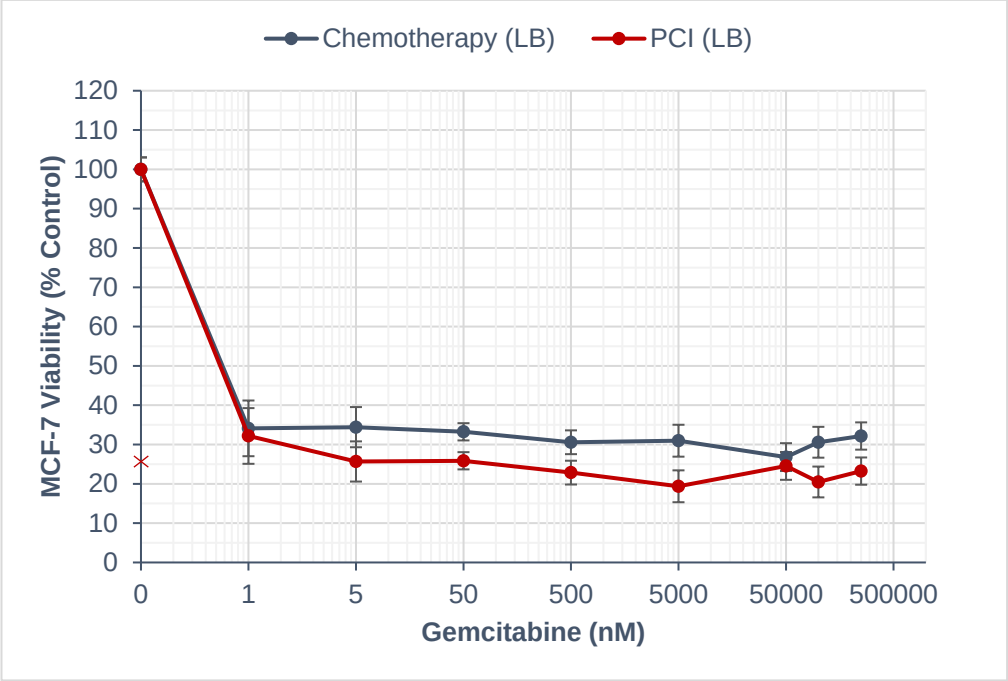

Figure 117. Reduction in MCF-7 breast cancer cell viability in 3D collagen hydrogels after light-before gemcitabine chemotherapy and light-before gemcitabine PCI*. Relative cellular viability (% of control) of MCF-7 cells after light-before regimen chemotherapy and PCI treatments at various gemcitabine concentrations (0.5-250,000 nM).*

6.2.3.1.3 Light-before Gemcitabine PCI – MDA-MB-231 cells vs MCF-7 cells

Gemcitabine LB-PCI was then compared between each breast cancer cell line (as shown in Figure 118). Figure 118 shows that there *was* a significant difference ($p = 0.013$) in cell viability reduction by gemcitabine LB-PCI between MDA-MB-231 and MCF-7 cell lines. Furthermore, gemcitabine concentration had a significant effect ($p < 0.001$) on cell viability reduction within each experimental group.

From these comparisons it can be observed that gemcitabine LB-PCI combinations were more potent against MCF-7 cells across all of the concentrations tested. Concerning gemcitabine LB-PCI potency, the IC_{70} was *not attained* and was 1 nM for MDA-MB-231 and MCF-7 cells, respectively. In addition, the IC_{50} was found to be 1,000 nM and 0.275 nM for MDA-MB-231 and MCF-7 cells, respectively, which signifies a 3,636-fold IC_{50} reduction in favour of MCF-7 cells. At the highest tested concentration of 250,000 nM, gemcitabine LB-PCI reduced cell viability to 40% (±6%) and 23% (±3%) in MDA-MB-231 and MCF-7 cells, respectively. This represents a 1.7-fold increase in treatment efficacy at 250,000 nM for MCF-7 cells.

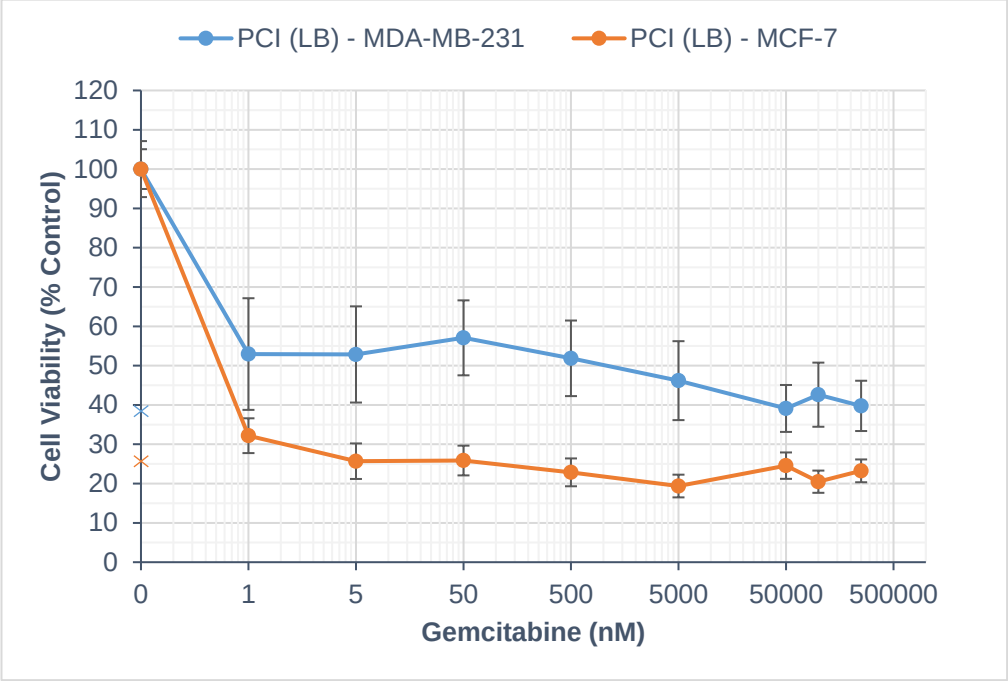

Figure 118. Reduction in breast cancer cell viability in 3D collagen hydrogels after light-before gemcitabine PCI*. Relative cellular viability (% of control) of MDA-MB-231 and MCF-7 cells after light-before regimen PCI treatment at various gemcitabine concentrations (0.5-250,000 nM).*

6.2.3.1.3 Treatment Synergy – Light-before Gemcitabine PCI

Synergy calculations were then performed in order to ascertain a greater understanding of the effects of gemcitabine LB-PCI versus gemcitabine LB-chemotherapy. As seen in the synergy plot (Figure 119), 0% of gemcitabine LB-PCI combinations were synergistic for the MDA-MB-231 cell line (the highest α value being 0.7 [±0.2] at 0.5 nM and 5 nM). With regard to the MCF-7 cell line, 0% of gemcitabine LB-PCI combinations were synergistic (the highest α value being 0.5 [±0.1] at 5 nM and 5,000 nM). Both α values signify treatment antagonism.

6.2.4 Results summary

6.2.4.1 Treatment potency (IC_{70}) and treatment efficacy (E_{max})

The key treatment effects indicative of LB-treatment potency and efficacy (IC_{70}; E_{max}) were identified from the respective LB-chemotherapy and LB-PCI cytotoxicity profiles for each drug and were compared to each other (Table 11).

The key treatment effects (IC_{70}; E_{max}) of LB-PCI were then compared between the two breast cancer cell lines (as shown in Table 12).

6.2.4.2 Treatment Synergy

Next, the treatment synergy values achieved by LB-PCI were identified and summarised (see Table 13 below). Specifically, the results obtained for the percentage of synergistic treatment combinations, the highest *α* values achieved and at what drug concentrations. In addition, the average *α* value achieved by the LB-PCI combinations was calculated and is also reported in Table 13.

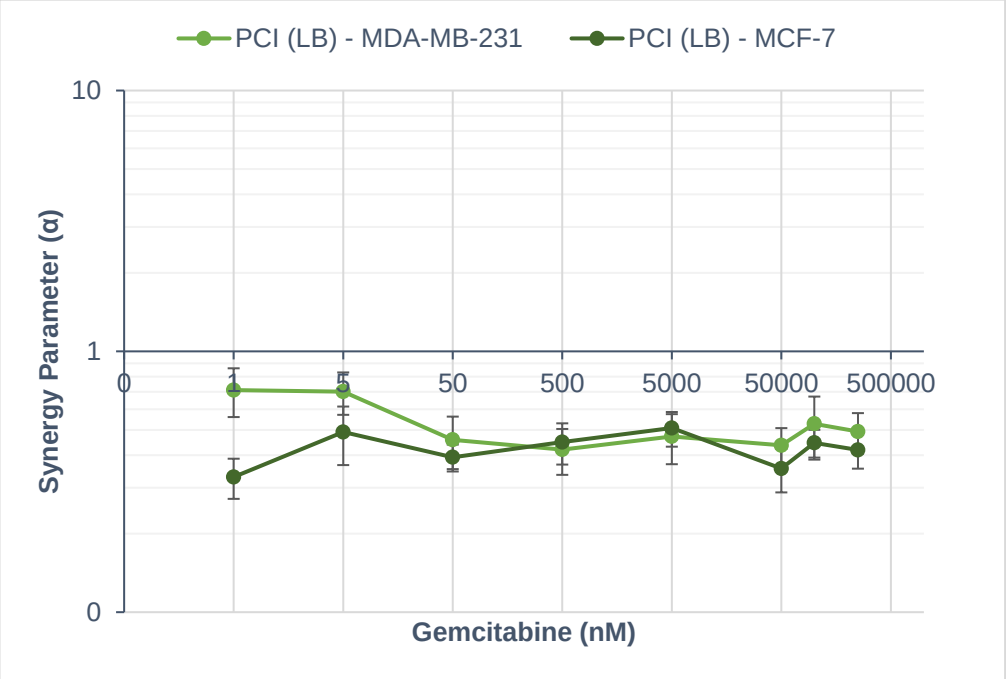

***Figure 119. Synergy plot for light-before gemcitabine-PCI combinations in MDA-MB-231 and MCF-7 breast cancer cells**. Synergy (α) was calculated from the individual cell viability results (specifically, survival/viability fraction) obtained for each respective LB treatment condition: LB-chemotherapy, LB-PDT, and LB-PCI.*

Table 11. Summary and comparison of key treatment effects (IC_{70}; E_{max}) of "light-before" chemotherapy and light-before PCI treatment effects in MDA-MB-231 and MCF-7 cells in 3D collagen hydrogels.

Chemotherapy Drug	Treatment	IC_{70} (nM)				E_{max} (% Control [±SE])			
		MDA-MB-231	*Potency change (fold)*	*MCF-7*	*Potency change (fold)*	*MDA-MB-231*	*Efficacy change (fold)*	*MCF-7*	*Efficacy change (fold)*
Bleomycin	LB Chemotherapy	36,000	.	375	.	20 (± 1)	.	12 (± 1)	.
Vincristine		175	.	500	.	24 (± 3)	.	19 (± 2)	.
Gemcitabine		75 (IC_{50})	+ 13.3	8,750	.	40 (± 3)	≡	32 (±4)	.
Bleomycin	LB PCI	30,000	+ 1.2	325	+ 1.2	6 (± 2)	+ 3.3	6 (± 2)	+ 2.0
Vincristine		0.40	+ 438	0.375	+ 1,333	5 (± 1)	+ 4.8	4 (± 1)	+ 4.8
Gemcitabine		1,000 (IC_{50})	.	1 / 0.275 (IC_{50})	+ 8,750	40 (± 6)	≡	23 (± 3)	+ 1.4

Table 12. Summary of light-before PCI IC_{70} and E_{max} values with treatment effects compared between MDA-MB-231 and MCF-7 human breast cancer cell lines.

Chemotherapy Drug	Treatment	IC_{70} (nM)				E_{max} (% Control [±SE])			
		MDA-MB-231	Potency change (fold)	MCF-7	Potency change (fold)	MDA-MB-231	Efficacy change (fold)	MCF-7	Efficacy change (fold)
Bleomycin	LB PCI	30,000	.	325	+ 92	6 (± 2)	≡	6 (± 2)	≡
Vincristine		0.40	.	0.38	+1.1	5 (± 1)	+ 1.3	4 (± 1)	.
Gemcitabine		1,000 (IC_{50})	.	0.275 (IC_{50})	+ 3,636	40 (± 6)	.	23 (± 3)	+ 1.7

Table 13. Summary of treatment synergy values from light-before PCI treatment combinations on MDA-MB-231 and MCF-7 human breast cancer cells in 3D collagen hydrogels.

Chemotherapy Drug	Treatment	Synergy (α)							
		MDA-MB-231				MCF-7			
		Synergistic combinations (%) / Ave (α)		Highest α value	Conc (nM)	Synergistic combinations (%) / Ave (α)		Highest α value	Conc (nM)
Bleomycin	LB PCI	38	2.2 (±0.5)	2.8 (±0.5)	250,000	0	0.7 (±0.2)	0.9 (±0.2)	250,000
Vincristine		88	1.6 (±0.3)	3.5 (± 0.4)	250,000	50	2.0 (±0.7)	3.4 (± 1.1)	250,000
Gemcitabine		0	0.5 (±0.1)	0.7 (± 0.2)	0.5 & 5	0	0.4 (±0.1)	0.5 (± 0.1)	5 & 5,000

6.3 Variation 2: Gel Stiffness - RTC 2 mg/mL vs RTC 5 mg/mL vs Monolayer

Following the investigations into the effect of a different PCI regimen on treatment cytotoxicity, the effect of other variations were also then pursued; only this time, they were in relation to the 3D model rather than the treatment regimen. More specifically, the effect on PCI treatment cytotoxicity of changes to both hydrogel volume and hydrogel stiffness was investigated. The effect of hydrogel stiffness was explored first, with comparisons of cell lines 3D-cultured in 2 mg/mL rat tail collagen, 5 mg/mL rat tail collagen, and also in monolayer. As previously introduced, cell-stromal interactions and 3D microenvironment can play a crucial role in treatment responses.

6.3.1 Bleomycin

6.3.1.1 Bleomycin PCI

6.3.1.1.1 MDA-MB-231 cells

Experiments investigating the effect of hydrogel stiffness on PCI cytotoxicity began with the glycopeptide antibiotic bleomycin. Figure 120 shows that there *was* a significant difference (*p*

= 0.023) in cell viability reduction between rat tail collagen (RTC) 2 mg/mL and RTC 5 mg/mL experimental groups after bleomycin-PCI exposure. However, this figure also shows that there was *not* a significant difference (p = 0.604) between RTC 2 mg/mL and monolayer-cultured MDA-MB-231 cells. Furthermore, bleomycin concentration had a significant effect (p < 0.001) on cell viability reduction within each experimental group.

The $AlPcS_{2a}$ (5 µg/mL) PDT control conducted alongside these PCI experiments reduced cell viability to 67% (±3%), 55% (±6%), and 61% (±2%) in RTC 2 mg/mL, RTC 5 mg/mL, and monolayer experimental groups, respectively. With regard to treatment potency, IC_{70} values were 27,500 nM, 8,750 nM, and 75,000 nM for RTC 2 mg/mL, RTC 5 mg/mL, and monolayer groups, respectively. This represents a 3.1-fold reduction in IC_{70} in favour of RTC 5 mg/mL versus 2 mg/mL and 2.7-fold in favour of 2 mg/mL versus monolayer. At the maximum tested concentration of 250,000 nM, cell viability was reduced to 6% (±0%), 4% (±1%), and 5% (±0%) in RTC 2 mg/mL, RTC 5 mg/mL, and monolayer groups, respectively. Thus, treatment efficacy at 250,000 nM was essentially equal between the various environmental hydrogel stiffness conditions.

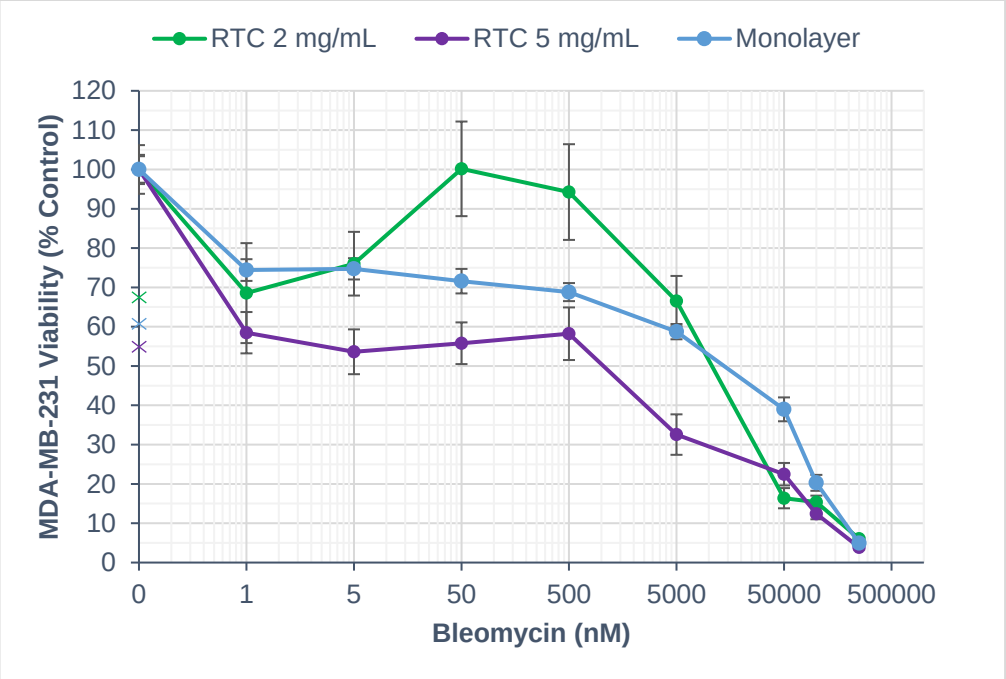

Figure 120. Reduction in MDA-MB-231 breast cancer cell viability in 3D collagen hydrogels of varying stiffness and monolayer culture after bleomycin PCI*. Relative cellular viability (% of control) of MDA-MB-231 cells 3D-cultured in RTC 2 mg/mL and RTC 5 mg/mL hydrogels and monolayer culture after PCI treatment at various bleomycin concentrations (0.5-250,000 nM).*

6.3.1.1.2 MCF-7 cells

Next, the variations in hydrogel stiffness experiments were performed in MCF-7 cells (as shown in Figure 121). Here, it was observed that there was *not* a significant difference (p = 0.536) in cell viability reduction between RTC 2 mg/mL and RTC 5 mg/mL experimental groups after bleomycin-PCI exposure. However, Figure 121 shows that there *was* a significant difference (p < 0.001) between RTC 2 mg/mL and monolayer-cultured MCF-7 cells. Furthermore, bleomycin concentration had a significant effect (p < 0.001) on cell viability reduction within each experimental group.

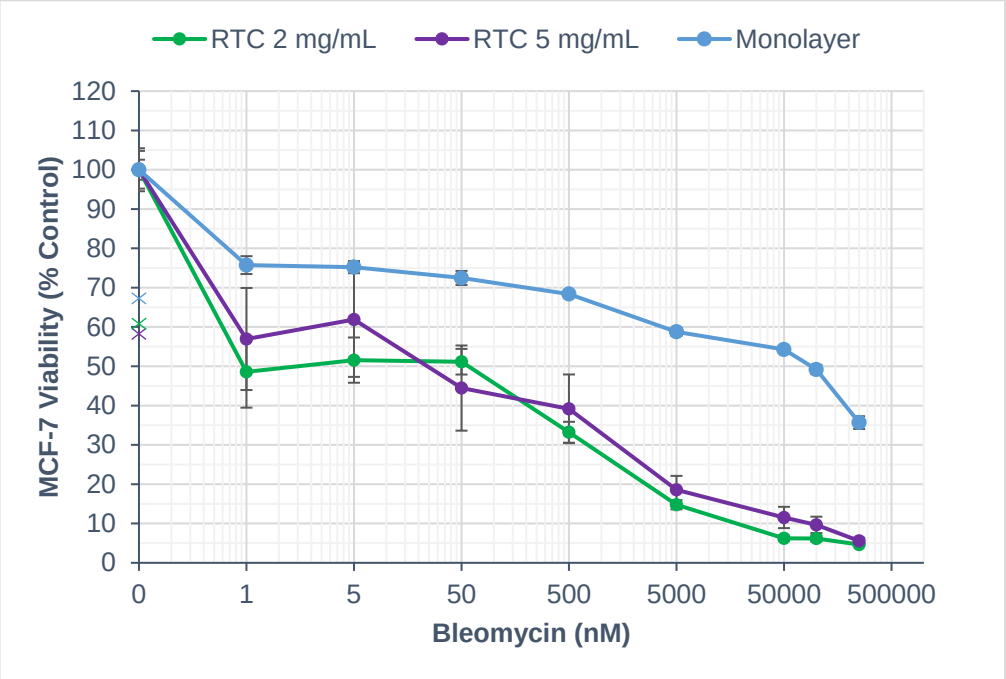

Figure 121. Reduction in MCF-7 breast cancer cell viability in 3D collagen hydrogels of varying stiffness and monolayer culture after bleomycin PCI. *Relative cellular viability (% of control) of MCF-7 cells 3D-cultured in RTC 2 mg/mL and RTC 5 mg/mL hydrogels and monolayer culture after PCI treatment at various bleomycin concentrations (0.5-250,000 nM).*

The $AlPcS_{2a}$ (5 µg/mL) PDT control conducted alongside these PCI experiments reduced cell viability to 61% (±2%), 58% (±10%), and 67% (±1%) in RTC 2 mg/mL, RTC 5 mg/mL, and monolayer experimental groups, respectively. Pertaining to treatment potency, the IC_{70} values were 750 nM, 1,375 nM, and was *not attained* for RTC 2 mg/mL, RTC 5 mg/mL, and monolayer groups, respectively. This signifies a 1.8-fold reduction in IC_{70} in favour of RTC 2 mg/mL versus 5 mg/mL. The IC_{50} was 0.45 nM, 23 nM, and 90,000 nM for RTC 2 mg/mL, RTC 5 mg/mL, and monolayer groups, respectively. This represents a 51-fold reduction in IC_{50} in favour of RTC 2 mg/mL versus RTC 5 mg/mL and a 200,000-fold reduction

versus monolayer. At the maximum tested concentration of 250,000 nM, cell viability was reduced to 5% (±0%) and 6% (±1%) in RTC 2 mg/mL and RTC 5 mg/mL groups, respectively, which essentially represents an equivalent bleomycin-PCI efficacy at 250,000 nM in 3D-culture. However, in monolayer, 250,000 nM bleomycin-PCI reduced cell viability to 36% (±2%) which represents a ~6-7-fold increase in PCI treatment efficacy in favour of 3D culture.

6.3.1.1.2 MDA-MB-231 cells vs MCF-7 cells – RTC 5 mg/mL

NB. The effect of bleomycin-PCI in RTC 2 mg/mL hydrogels and compared between MDA-MB-231 and MCF-7 cell lines can be seen in Figure 48.

Upon comparison of bleomycin-PCI cytotoxicity between MDA-MB-231 and MCF-7 cell lines that were 3D-cultured in RTC 5 mg/mL hydrogels (see Figure 122), it was observed that there was *not* a significant difference (p = 0.386) in cell viability reduction between the MDA-MB-231 and MCF-7 cell lines. In addition, bleomycin concentration *did* have a significant effect (p < 0.001) on cell viability reduction within each experimental group.

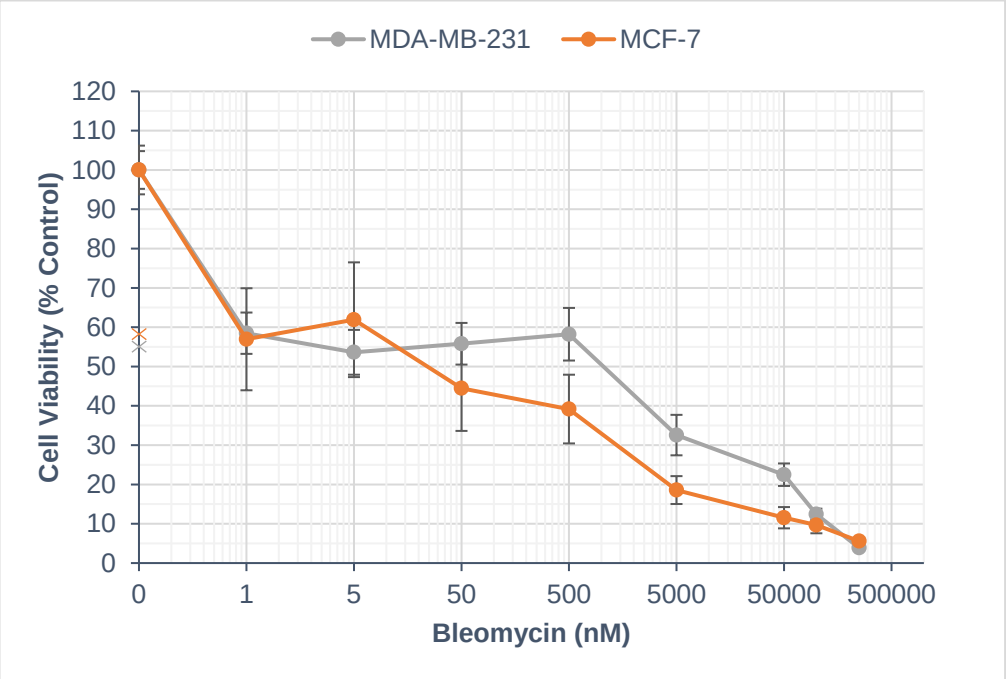

Figure 122. Reduction in breast cancer cell viability in 3D collagen 5 mg/mL hydrogels after bleomycin PCI*. Relative cellular viability (% of control) of MDA-MB-231 and MCF-7 cells 3D-cultured in RTC 5 mg/mL hydrogels after PCI treatment at various bleomycin concentrations (0.5-250,000 nM).*

The $AlPcS_{2a}$ (5 µg/mL) PDT control conducted alongside these PCI experiments reduced cell viability to 55% (±6%) and 58% (±10%) in MDA-MB-231 and MCF-7, respectively. In relation to treatment potency, the IC_{70} values obtained were 8,750 nM and 1,375 nM for

MDA-MB-231 and MCF-7 groups, respectively. This represents a 6.4-fold reduction in IC_{70} in favour of the MCF-7 cell line. At the maximum tested concentration of 250,000 nM, cell viability was reduced to 4% (±1%) and 6% (±1%) in MDA-MB-231 and MCF-7 cells, respectively. This signifies a 1.5-fold increase in treatment efficacy at 250,000 nM in favour of the MDA-MB-231 cell line.

6.3.1.1.3 MDA-MB-231 cells vs MCF-7 cells – Monolayer

Next, similar bleomycin-PCI comparisons were made for MDA-MB-231 and MCF-7 cells cultured in monolayer (as shown in Figure 123). Here, it was observed that there *was* a significant difference ($p < 0.001$) in cell viability reduction between MDA-MB-231 and MCF-7 cells cultured in monolayer after bleomycin-PCI exposure. In addition, bleomycin concentration had a significant effect ($p < 0.001$) on cell viability reduction within each experimental group.

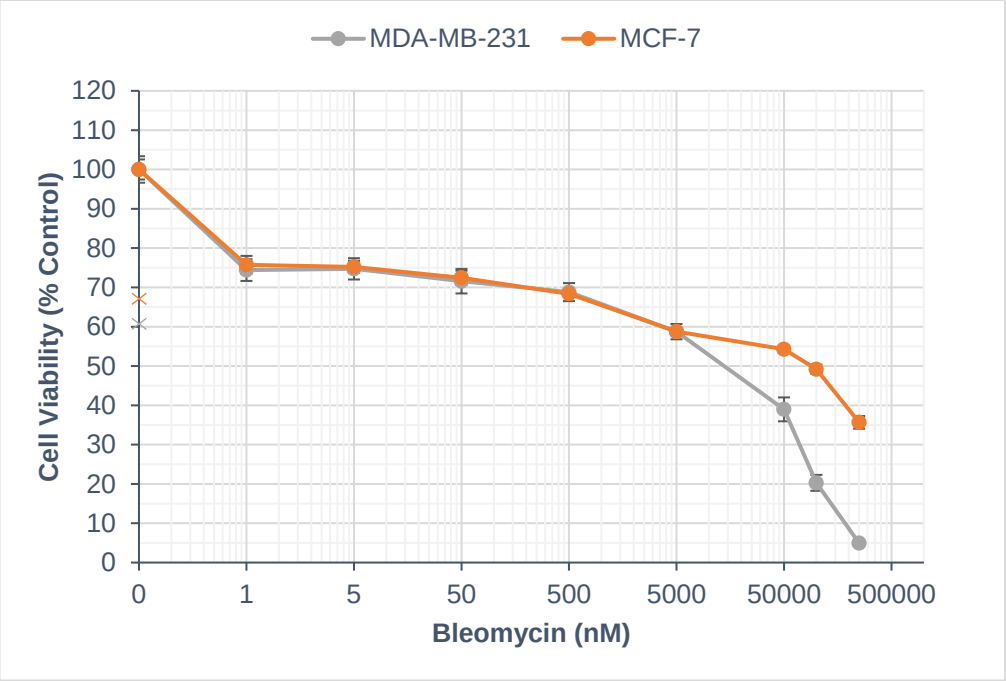

Figure 123. Reduction in breast cancer cell viability in monolayer culture after bleomycin PCI. *Relative cellular viability (% of control) of MDA-MB-231 and MCF-7 cells cultured in monolayer after PCI treatment at various bleomycin concentrations (0.5-250,000 nM).*

The $AlPcS_{2a}$ (5 µg/mL) PDT control conducted alongside these PCI experiments reduced cell viability to 61% (±2%) and 67% (±1%) in MDA-MB-231 and MCF-7, respectively. With regard to treatment potency, IC_{70} values were 75,000 nM and *not attained* for MDA-MB-231 and MCF-7 groups, respectively. Treatment IC_{50} was 13,750 nM and 90,000 nM for MDA-

MB-231 and MCF-7 cells, respectively, which represents a 6.5-fold reduction in IC_{50} in favour of the MDA-MB-231 cell line. At the highest tested concentration of 250,000 nM, cell viability was reduced to 5% (±0%) and 36% (±2%) in MDA-MB-231 and MCF-7 cells, respectively. These E_{max} values signify a 7.2-fold increase in treatment efficacy at 250,000 nM in favour of the MDA-MB-231 cell line.

6.3.2 Vinca Alkaloids

6.3.2.1 Vincristine PCI

6.3.2.1.1 MDA-MB-231 cells

Following investigations with bleomycin-PCI, the next chemotherapeutic to evaluate with 3D model variations was the vinca alkaloid vincristine. Below, Figure 124 shows that there was *not* a significant difference in cell viability reduction between RTC 5 mg/mL (p = 0.939) and monolayer (p = 0.374) experimental groups versus RTC 2 mg/mL after vincristine-PCI exposure. In addition, vincristine concentration had a significant effect (p < 0.001) on cell viability reduction within each experimental group.

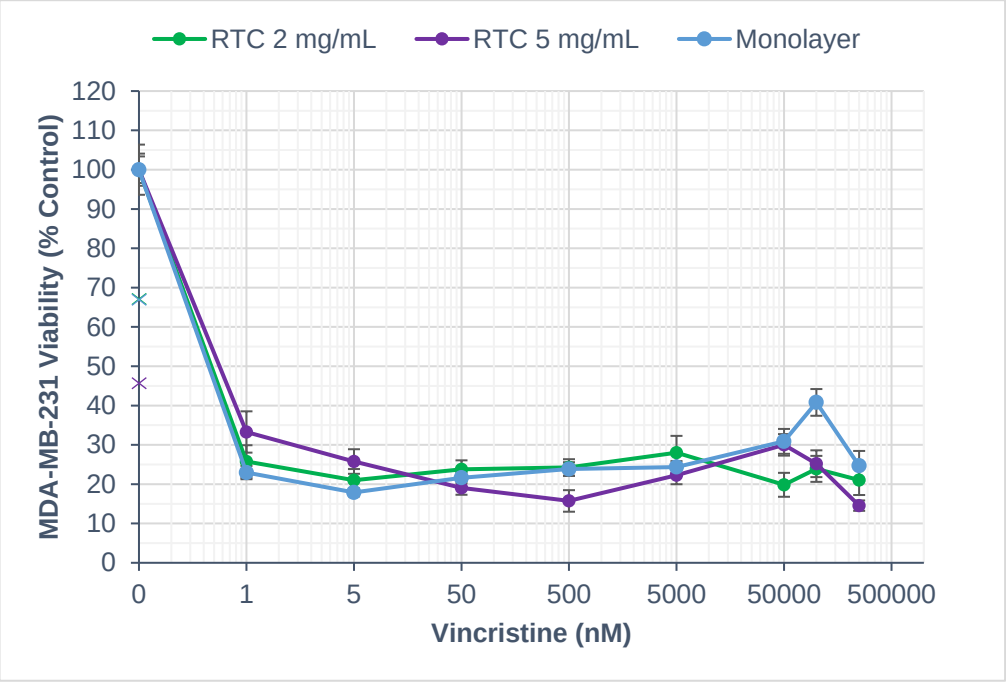

Figure 124. Reduction in MDA-MB-231 breast cancer cell viability in 3D collagen hydrogels of varying stiffness and monolayer culture after vincristine PCI. *Relative cellular viability (% of control) of MDA-MB-231 cells 3D-cultured in RTC 2 mg/mL and RTC 5 mg/mL hydrogels and in monolayer after PCI treatment at various vincristine concentrations (0.5-250,000 nM).*

The $AlPcS_{2a}$ (5 µg/mL) PDT control conducted alongside these PCI experiments reduced cell viability to 67% (±3%), 46% (±6%), and 67% (±3%) in RTC 2 mg/mL, RTC 5 mg/mL, and monolayer experimental groups, respectively. In relation to treatment potency, the IC_{70} values were 0.45 nM, 1.25 nM, and 0.40 nM for RTC 2 mg/mL, RTC 5 mg/mL, and monolayer groups, respectively. This represents a 2.8-fold reduction in IC_{70} in favour of RTC 2 mg/mL and 3.1-fold in favour of monolayer both versus RTC 5 mg/mL. At the maximum tested concentration of 250,000 nM, cell viability was reduced to 21% (±4%), 15% (±1%), and 25% (±4%) in RTC 2 mg/mL, RTC 5 mg/mL, and monolayer groups, respectively. This represents a 1.4-fold and 1.7-fold increase in treatment efficacy at 250,000 nM in favour of RTC 5 mg/mL versus RTC 2 mg/mL and monolayer, respectively. There was also a notable increase in cell viability between 5,000-100,000 nM in the monolayer group and between 500-50,000 nM in the RTC 5 mg/mL group.

6.3.2.1.2 MCF-7 cells

Next, these variations in hydrogel stiffness were evaluated on MCF-7 cells (as shown in Figure 125). Here, it was observed that there was *not* a significant difference ($p = 0.882$) in cell viability reduction between RTC 2 mg/mL and RTC 5 mg/mL experimental groups after vincristine-PCI exposure. However, the same figure shows that there *was* a significant difference ($p < 0.001$) between RTC 2 mg/mL and monolayer-cultured MCF-7 cells. Furthermore, vincristine concentration had a significant effect ($p < 0.001$) on cell viability reduction within each experimental group.

The $AlPcS_{2a}$ (5 µg/mL) PDT control conducted alongside these PCI experiments reduced cell viability to 57% (±6%), 62% (±12%), and 74% (±1%) in RTC 2 mg/mL, RTC 5 mg/mL, and monolayer experimental groups, respectively. Concerning treatment potency, the IC_{70} values were estimated to be 0.425 nM, 0.475 nM, and 12,500 nM for RTC 2 mg/mL, RTC 5 mg/mL, and monolayer groups, respectively. This represents a 29,412-fold and 26,316-fold reduction in IC_{70} in favour of RTC 2 mg/mL and 5 mg/mL (3D culture) versus monolayer, respectively. At the maximum tested concentration of 250,000 nM, cell viability was reduced to 10% (±1%) and 9% (±3%) in RTC 2 mg/mL and RTC 5 mg/mL groups, respectively. This represents an essentially equivalent treatment efficacy at 250,000 nM for the 3D culture

experimental groups. However, 250,000 nM vincristine-PCI reduced cell viability to 20% (±2%) which represents a 2-fold increase in treatment efficacy in favour of 3D culture versus monolayer.

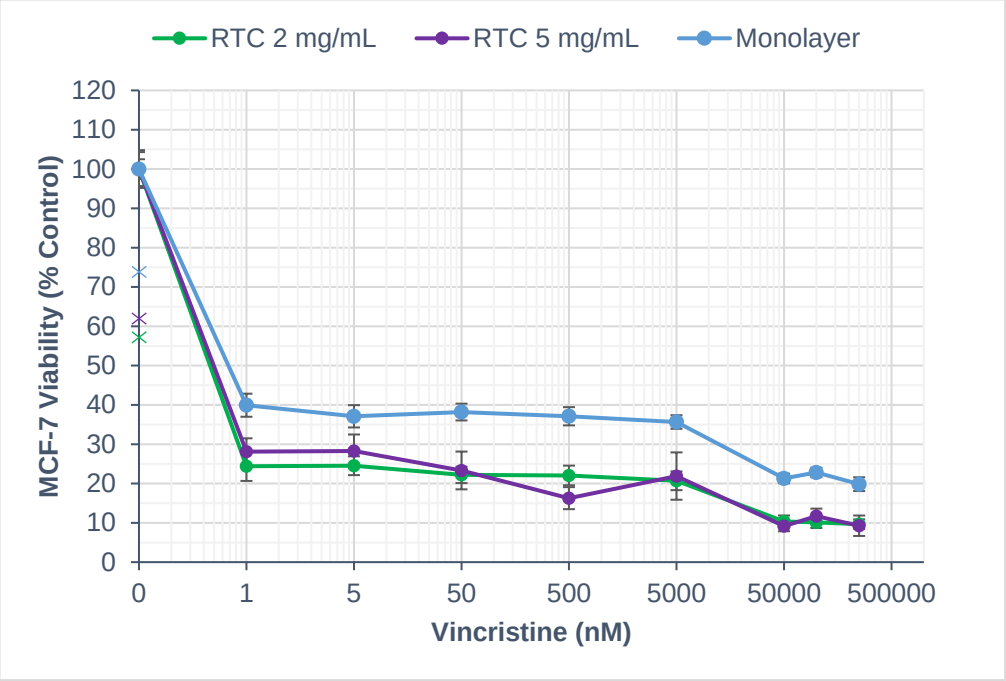

Figure 125. Reduction in MCF-7 breast cancer cell viability in 3D collagen hydrogels of varying stiffness and monolayer culture after vincristine PCI*. Relative cellular viability (% of control) of MCF-7 cells 3D-cultured in RTC 2 mg/mL and RTC 5 mg/mL hydrogels and monolayer culture after PCI treatment at various vincristine concentrations (0.5-250,000 nM).*

6.3.2.1.3 MDA-MB-231 cells vs MCF-7 cells – RTC 5 mg/mL

NB. The effect of vincristine-PCI in RTC 2 mg/mL hydrogels and compared between MDA-MB-231 and MCF-7 cell lines can be seen in Figure 56.

It was then necessary to compare the cytotoxicity of vincristine-PCI on MDA-MB-231 and MCF-7 cells 3D-cultured in RTC 5 mg/mL (as shown in Figure 126). Here, it was observed that there was *not* a significant difference ($p = 0.209$) in cell viability reduction between MDA-MB-231 and MCF-7 cells 3D-cultured in RTC 5 mg/mL hydrogels after vincristine-PCI exposure. In addition, vincristine concentration had a significant effect ($p < 0.001$) on cell viability reduction within each experimental group.

The $AlPcS_{2a}$ (5 µg/mL) PDT control conducted alongside these PCI experiments reduced cell viability to 46% (±6%) and 62% (±12%) in MDA-MB-231 and MCF-7, respectively. With regard to treatment IC_{70} values, they were found to be 1.25 nM and 0.475 nM for MDA-

MB-231 and MCF-7 groups, respectively. This signifies a 2.6-fold reduction in IC_{70} in favour of MCF-7 cells. At the maximum tested concentration of 250,000 nM, cell viability was reduced to 15% (±1%) and 9% (±3%) in MDA-MB-231 and MCF-7 cells, respectively. These E_{max} values represent a 1.7-fold increase in treatment efficacy at 250,000 nM in favour of MCF-7 cells.

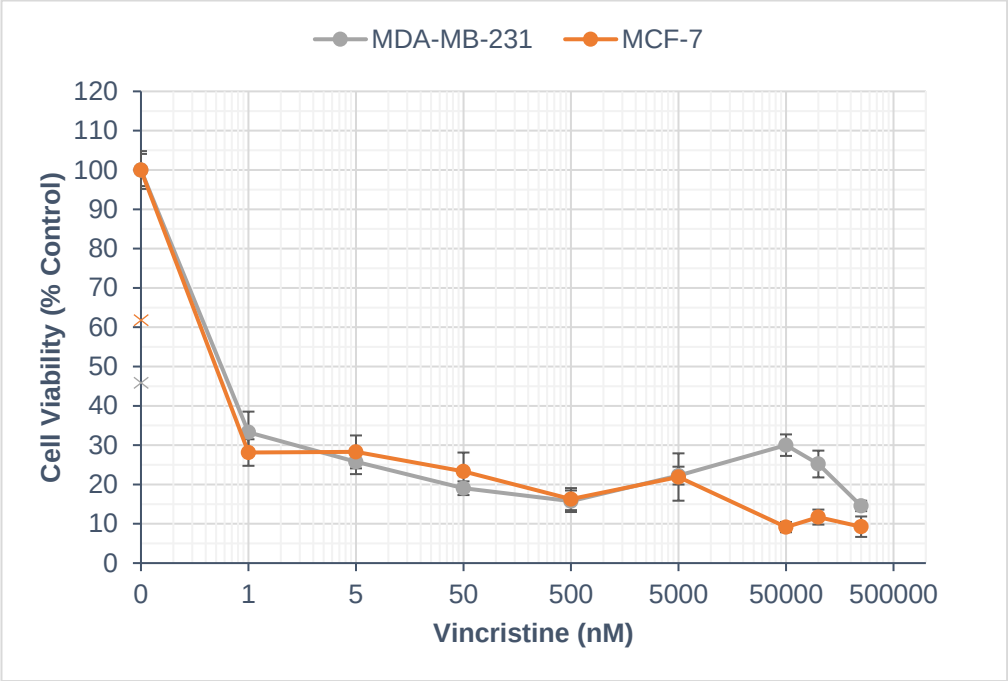

Figure 126. Reduction in breast cancer cell viability in 3D collagen 5 mg/mL hydrogels after vincristine PCI*. Relative cellular viability (% of control) of MDA-MB-231 and MCF-7 cells 3D-cultured in RTC 5 mg/mL hydrogels after PCI treatment at various vincristine concentrations (0.5-250,000 nM).*

6.3.2.1.4 MDA-MB-231 cells vs MCF-7 cells – Monolayer

Monolayer comparisons between the cell lines then followed (as shown in Figure 127). From these experiments, it was observed that there *was* a significant difference (p = 0.016) in cell viability reduction between MDA-MB-231 and MCF-7 cells cultured in monolayer after vincristine-PCI exposure. Furthermore, vincristine concentration had a significant effect (p < 0.001) on cell viability reduction within each cell line.

The $AlPcS_{2a}$ (5 µg/mL) PDT control conducted alongside these PCI experiments reduced cell viability to 67% (±3%) and 74% (±1%) in MDA-MB-231 and MCF-7, respectively. Pertaining to treatment potency, the IC_{70} values were estimated to be 0.40 nM and 12,500 nM for MDA-MB-231 and MCF-7 groups, respectively. This represents a 31,250-fold reduction in

IC_{70} in favour of MDA-MB-231 cells. At the maximum tested concentration of 250,000 nM, cell viability was seen to be reduced to 25% (±4%) and 20% (±2%) in MDA-MB-231 and MCF-7 cells, respectively. This signifies a 1.3-fold increase in treatment efficacy at 250,000 nM in favour of MCF-7 cells. In addition, a gradual rise in MDA-MB-231 cell viability was also observed from 5-5,000 nM and then a separate, notable increase and peak between 5,000-100,000 nM.

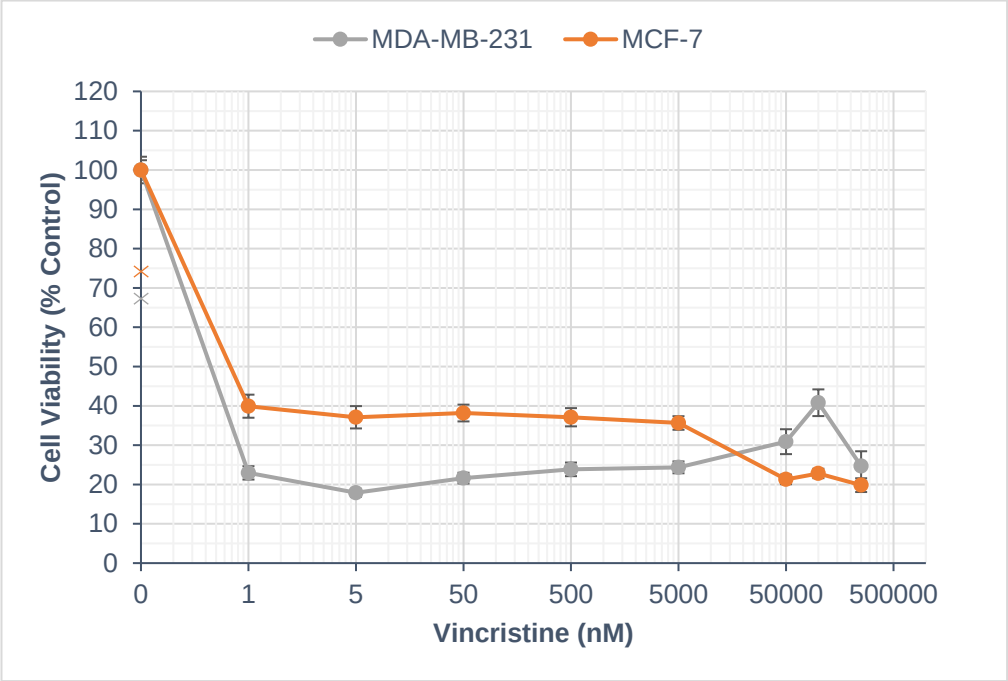

Figure 127. Reduction in breast cancer cell viability in monolayer culture after vincristine PCI. *Relative cellular viability (% of control) of MDA-MB-231 and MCF-7 cells cultured in monolayer after PCI treatment at various vincristine concentrations (0.5-250,000 nM).*

6.3.3 Results summary

6.3.3.1 Treatment potency (IC_{70}) and treatment efficacy (E_{max})

The key treatment effects indicative of PCI treatment potency and efficacy (that is, IC_{70}; E_{max}) were identified from the respective cytotoxicity profiles for each drug in each culture condition (hydrogel stiffness and monolayer) and were compared to RTC 2 mg/mL for each cell line (Table 14).

The key cytotoxic effects (IC_{70}; E_{max}) of PCI treatment in hydrogels of different stiffness and monolayer were then compared between the two breast cancer cell lines (as shown below in Table 15).

Table 14. Summary of PCI treatment cytotoxicity in different 3D model culture conditions and monolayer (hydrogel stiffness and monolayer) and compared against RTC 2 mg/mL 3D culture.

Chemotherapy Drug PCI	Hydrogel Stiffness	IC_{70} (nM)				E_{max} (% Control [±SE])			
		MDA-MB-231	Potency change (fold)	MCF-7	Potency change (fold)	MDA-MB-231	Efficacy change (fold)	MCF-7	Efficacy change (fold)
Bleomycin	2 mg/L	27,500	.	750 / 0.45 (IC_{50})	.	6 (±0)	.	5 (± 0)	.
Vincristine		0.45	.	0.425	.	21 (±4)	.	10 (±1)	.
Bleomycin	5 mg/mL	8,750	+ 3.1	1,375 / 23 (IC_{50})	- 1.8 / - 51 (IC_{50})	4 (±1)	+ 1.5	6 (± 1)	- 1.2
Vincristine		1.25	- 2.8	0.475	- 1.1	15 (±1)	+ 1.4	9 (±3)	+ 1.1
Bleomycin	Monolayer	75,000	- 2.7	n/a / 90,000 (IC_{50})	n/a / - 200,000 (IC_{50})	5 (±0)	+ 1.2	36 (± 2)	- 7.2
Vincristine		0.40	+ 1.1	12,500	- 29,411	25 (±4)	- 1.2	20 (±2)	- 2.0

Table 15. Summary of PCI treatment cytotoxicity in different 3D model culture conditions and monolayer (hydrogel stiffness) and compared between MDA-MB-231 and MCF-7 human breast cancer cells.

Chemotherapy Drug PCI	Hydrogel Stiffness	IC_{70} (nM)				E_{max} (% Control [±SE])			
		MDA-MB-231	Potency change (fold)	MCF-7	Potency change (fold)	MDA-MB-231	Efficacy change (fold)	MCF-7	Efficacy change (fold)
Bleomycin	2 mg/L	27,500	-	750	+ 37	6 (±0)	-	5 (±0)	+ 1.2
Vincristine		0.45	-	0.425	+ 1.1	21 (±4)	-	10 (±1)	+ 2
Bleomycin	5 mg/mL	8,750	.	1,375	+ 6.4	4 (±1)	+ 1.5	6 (±1)	.
Vincristine		1.25	.	0.475	+ 2.6	15 (±1)	.	9 (±3)	+ 1.7
Bleomycin	Monolayer	75,000 / 13,750 (IC_{50})	.	n/a / 90,000 (IC_{50})	+ 6.5 (IC_{50})	5 (±0)	+ 7.2	36 (± 2)	.
Vincristine		0.40	+ 31,250	12,500	.	25 (±4)	.	20 (±2)	+ 1.3

6.3.4 Rheological studies

6.3.4.1 Mechanical analysis of hydrogel stiffness

Rheological studies proved that the rat tail collagen (RTC) type I hydrogels increased in mechanical stiffness in a concentration-dependent manner from 2 mg/mL to 5 mg/mL (Figure 128). Moreover, the mechanical properties of the two collagen preparations differed significantly (p = 0.013). For instance, at 1 H_z, the RTC 2 mg/mL hydrogel has a stiffness of ~30 Pa which is around a 5-fold lower mechanical stiffness (or complex modulus) than the

RTC 5 mg/mL hydrogel (~140 Pa). In addition, it can be observed that the complex modulus increased with the increase in the vibration frequency (H_z).

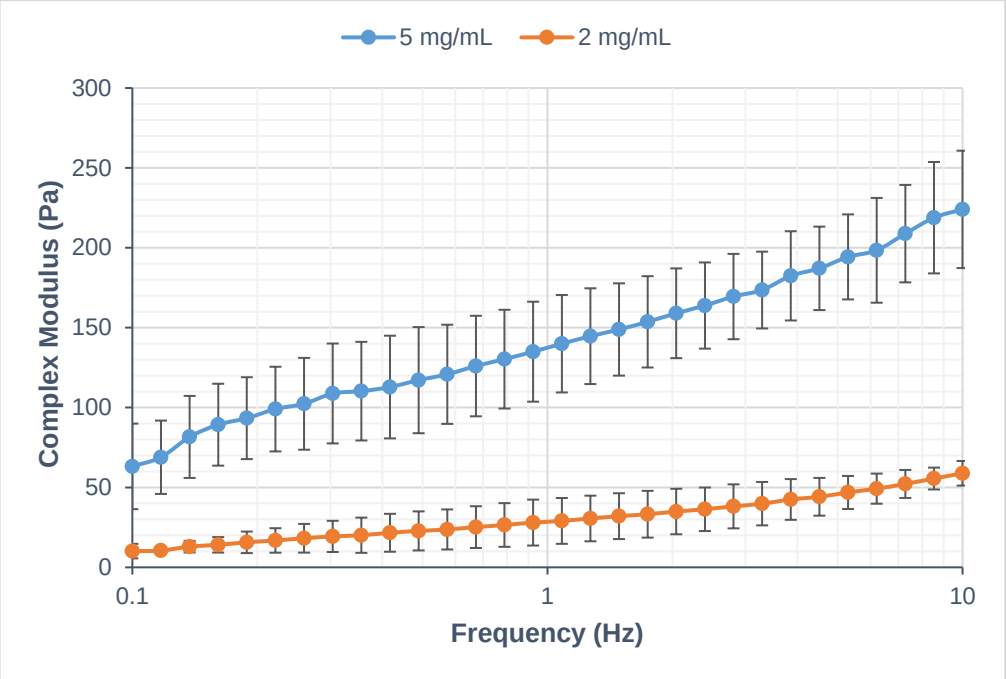

Figure 128. Collagen hydrogel stiffness increases in a concentration-dependent manner. *The complex modulus (Pa) of 2 mg/mL and 5 mg/mL collagen hydrogels measured at different frequencies (H_z).*

6.4 Variation 3: Gel Volume - 25 µL vs 75 µL vs Monolayer

Following the investigations into the effect of a different hydrogel stiffness and monolayer culture on PCI treatment cytotoxicity, the effect(s) of other variations were then also pursued. Namely, the effect of hydrogel volume (25 µL versus 75 µL and monolayer) was then explored using RTC 2 mg/mL hydrogels which have been used in the vast majority of the present work (including, for example, the initial chemotherapeutic and PCI investigations). The use of a larger, 75 µL hydrogel, meant that cancer cells were more widely dispersed within the 3D ECM which could affect, for instance, cell-cell and cell-matrix interactions, and therefore, in turn, cellular responses to treatment.

6.4.1 Bleomycin

6.4.1.1 Bleomycin PCI

6.4.1.1.1 MDA-MB-231 cells

Initial experiments into the effects of hydrogel volume on PCI cytotoxicity began with bleomycin-PCI (as shown in Figure 129).

Here, it was observed that there *was* a significant difference (p = 0.008) in cell viability reduction between 25 µL and 75 µL experimental groups after bleomycin-PCI exposure. However, Figure 129 shows that there was *not* a significant difference (p = 0.604) between 25 µL and monolayer-cultured MDA-MB-231 cells. In addition, bleomycin concentration had a significant effect (p < 0.001) on cell viability reduction within each experimental group.

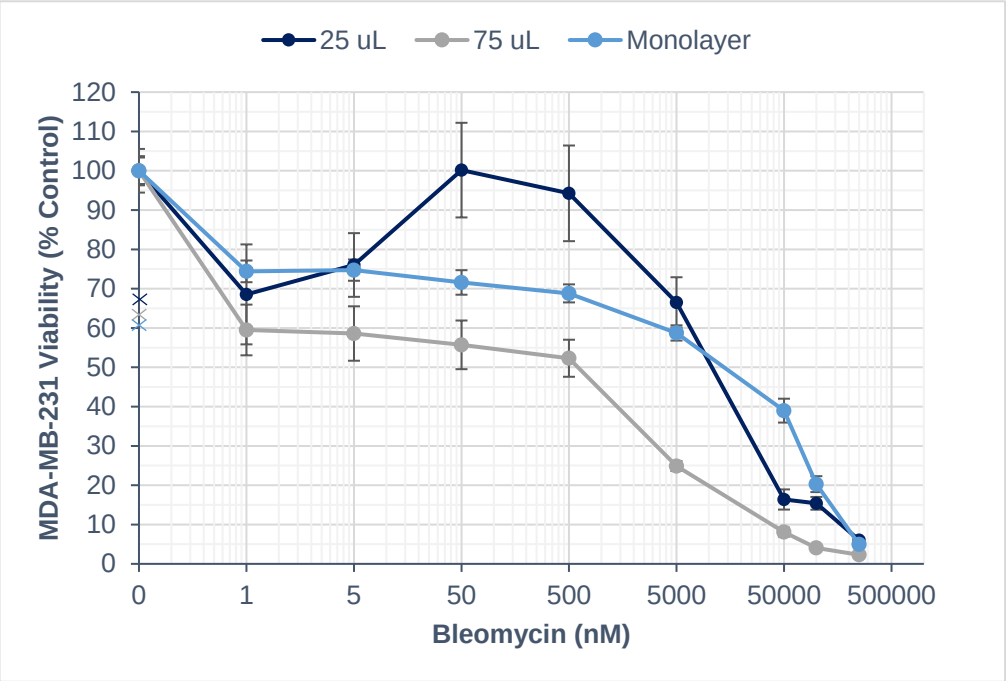

Figure 129. Reduction in MDA-MB-231 breast cancer cell viability in 3D collagen hydrogels of varying volume and monolayer culture after bleomycin PCI. *Relative cellular viability (% of control) of MDA-MB-231 cells 3D-cultured in 25 µL and 75 µL hydrogels and monolayer culture after PCI treatment at various bleomycin concentrations (0.5-250,000 nM).*

The $AlPcS_{2a}$ (5 µg/mL) PDT control conducted alongside these PCI experiments reduced cell viability to 67% (±3%), 63% (±5%), and 61% (±2%) in 25 µL, 75 µL, and monolayer experimental groups, respectively. With regard to treatment potency, IC_{70} values were found to be 27,500 nM, 10,000 nM, and 75,000 nM for 25 µL, 75 µL, and monolayer groups, respectively. This represents a 2.7-fold reduction in IC_{70} in favour of 25 µL versus monolayer and a 2.8-fold reduction in favour of 75 µL versus 25 µL. At the highest tested concentration of 250,000 nM, cell viability was reduced to 6% (±0%), 2% (±0%), and 5% (±0%) in 25 µL, 75 µL, and monolayer groups, respectively. Thus, treatment efficacy was 2.5-3-fold in favour of the 75 µL hydrogel volume at 250,000 nM.

6.4.1.1.2 MCF-7 cells

Following this, similar investigations were made with the MCF-7 cell line (as shown in Figure 130). From these experiments it could be determined that there *was* a significant difference (p = 0.003) in cell viability reduction between 25 µL and 75 µL experimental groups after bleomycin-PCI exposure. Moreover, Figure 130 shows that there *was* a significant difference (p < 0.001) between 25 µL and monolayer-cultured MCF-7 cells. Furthermore, bleomycin concentration had a significant effect (p < 0.001) on cell viability reduction within each experimental group.

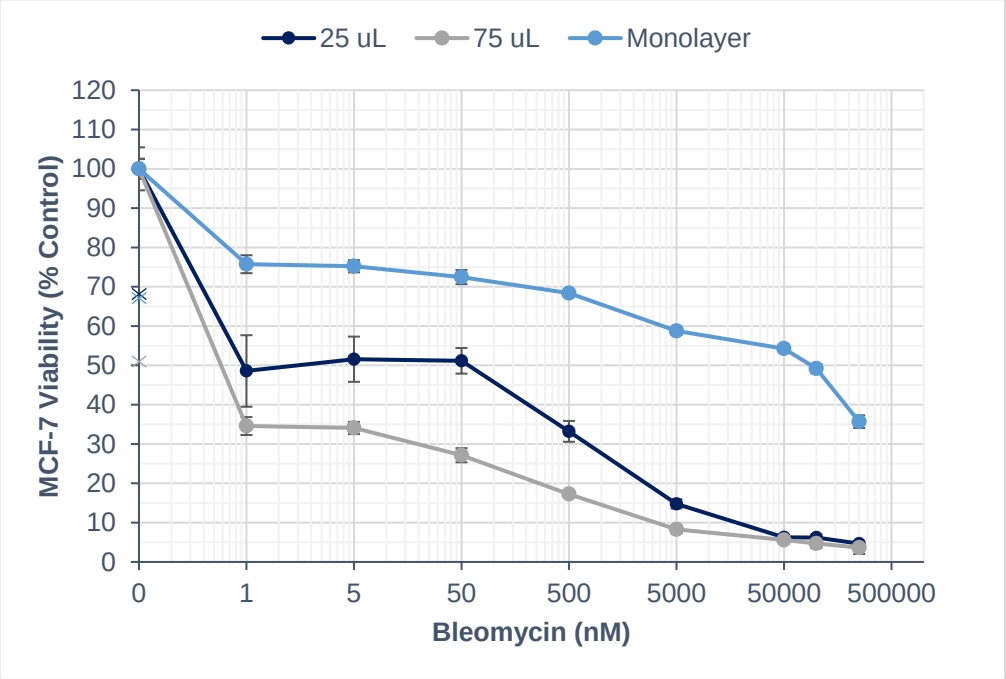

Figure 130. Reduction in MCF-7 breast cancer cell viability in 3D collagen hydrogels of varying gel volume and monolayer culture after bleomycin PCI. *Relative cellular viability (% of control) of MCF-7 cells 3D-cultured in 25 µL and 75 µL 2 mg/mL hydrogels and monolayer culture after PCI treatment at various bleomycin concentrations (0.5-250,000 nM).*

The $AlPcS_{2a}$ (5 µg/mL) PDT control conducted alongside these PCI experiments reduced cell viability to 68% (±4%), 51% (±6%), and 67% (±1%) in 25 µL, 75 µL, and monolayer experimental groups, respectively. In relation to treatment potency, IC_{70} values were 750 nM, 20 nM, and was *not attained* for 25 µL, 75 µL, and monolayer groups, respectively. This represents a 38-fold reduction in IC_{70} in favour of 75 µL versus 25 µL. Pertaining to treatment IC_{50}, these values were 0.45 nM, 0.30 nM, and 90,000 nM for 25 µL, 75 µL, and monolayer groups, respectively. Versus monolayer culture, these values signify a 200,000-fold reduction in IC_{70} in favour of 25 µL and a 300,000-fold reduction in favour of 75

µL. At the highest tested concentration of 250,000 nM, cell viability was reduced to 5% (±0%) and 4% (±0%) in 25 µL and 75 µL groups, respectively. This essentially represents an equivalent treatment efficacy for 3D culture at 250,000 nM. However, in monolayer culture, bleomycin-PCI was seen to reduce cell viability to 36% (±2%) which represents an ~8-fold increase in treatment efficacy in favour of 3D culture at 250,000 nM.

6.4.1.1.3 MDA-MB-231 cells vs MCF-7 cells – 75 µL

NB. Breast cancer cell line comparisons of bleomycin-PCI cytotoxicity in 25 µL (RTC 2 mg/mL) hydrogels and monolayer culture are shown in Figure 48 & Figure 123, respectively; therefore, only the 75 µL comparisons follow.

Below, Figure 131 shows that there *was* a significant difference ($p < 0.001$) in cell viability reduction between MDA-MB-231 and MCF-7 cells 3D-cultured in 75 µL hydrogels after bleomycin-PCI exposure. Furthermore, bleomycin concentration had a significant effect ($p < 0.001$) on cell viability reduction within each experimental group.

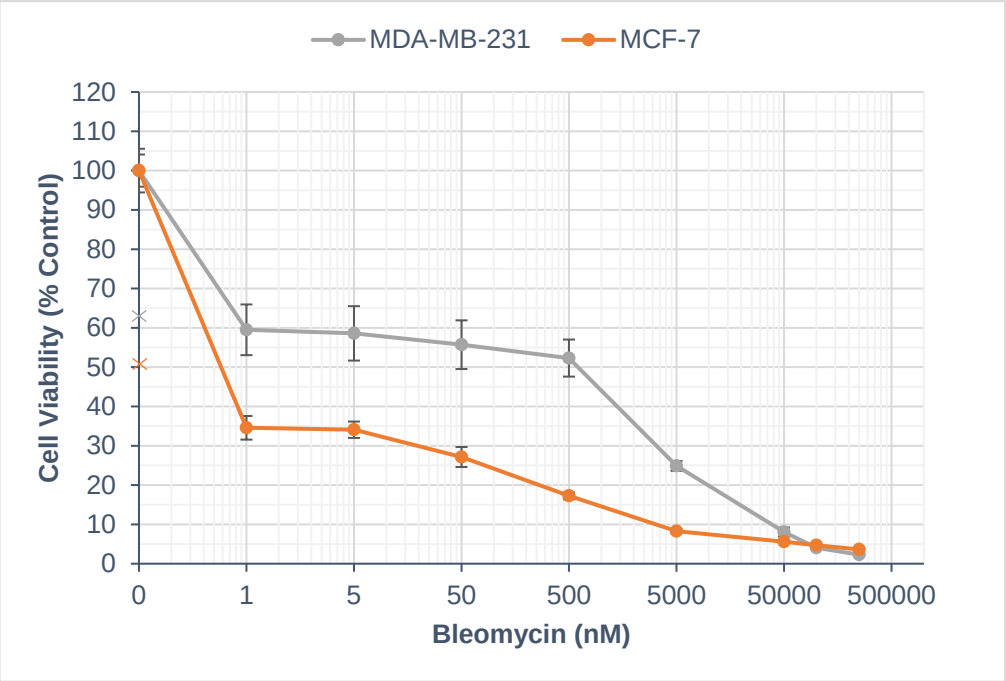

Figure 131. Reduction in breast cancer cell viability in 3D 75 µL collagen hydrogels after bleomycin PCI*. Relative cellular viability (% of control) of MDA-MB-231 and MCF-7 cells 3D-cultured in 75 µL hydrogels after PCI treatment at various bleomycin concentrations (0.5-250,000 nM).*

The $AlPcS_{2a}$ (5 µg/mL) PDT control conducted alongside these PCI experiments reduced cell viability to 63% (±5%) and 51% (±6%) in MDA-MB-231 and MCF-7, respectively.

Pertaining to treatment potency, the IC_{70} was found to be 3,250 nM and 20 nM for MDA-MB-231 and MCF-7 groups, respectively. This represents a 500-fold reduction in IC_{70} in favour of MCF-7 cells. At the highest tested concentration of 250,000 nM, cell viability was seen to be reduced to 2% (±0%) and 4% (±0%) in MDA-MB-231 and MCF-7 cells, respectively. This represents a 2-fold increase in treatment efficacy in favour of MDA-MB-231 cells at 250,000 nM.

6.4.2 Vinca Alkaloids

6.4.2.1 Vincristine PCI

6.4.2.1.1 MDA-MB-231 cells

Following the investigations with bleomycin-PCI, PCI utilising the vinca alkaloid vincristine was next to be evaluated with the changes in 3D hydrogel volume (as seen in Figure 132). Here, it was observed that there *was* a significant difference (p = 0.029) in cell viability reduction between 25 µL and 75 µL experimental groups after bleomycin-PCI exposure. However, there was *not* a significant difference (p = 0.374) seen between 25 µL and monolayer. In addition, vincristine concentration had a significant effect (p < 0.001) on cell viability reduction within each experimental group.

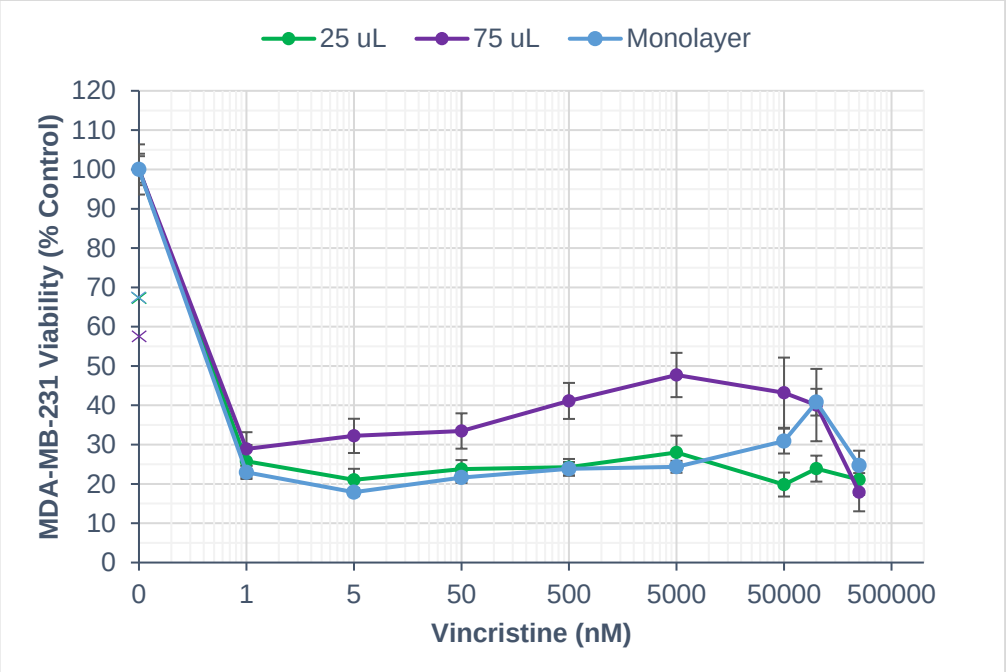

Figure 132. Reduction in MDA-MB-231 breast cancer cell viability in 3D collagen hydrogels of varying volume and monolayer culture after vincristine PCI. *Relative cellular viability (% of control) of MDA-MB-231 cells 3D-cultured in 25 µL and 75 µL hydrogels and monolayer culture after PCI treatment at various vincristine concentrations (0.5-250,000 nM).*

The $AlPcS_{2a}$ (5 µg/mL) PDT control conducted alongside these PCI experiments reduced cell viability to 67% (±3%), 57% (±6%), and 67% (±3%) in 25 µL, 75 µL, and monolayer experimental groups, respectively. Here, treatment IC_{70} values were estimated to be 0.45 nM, 0.475 nM, and 0.40 nM for 25 µL, 75 µL, and monolayer groups, respectively, which represents an essentially equipotent IC_{70} for each treatment group. At the highest tested concentration of 250,000 nM, cell viability was seen to be reduced to 21% (±4%), 18% (±5%), and 25% (±4%) in 25 µL, 75 µL, and monolayer groups, respectively. This represents a 1.2-fold and 1.4-fold increase in treatment efficacy in favour of 75 µL versus 25 µL and monolayer, respectively. There was also a notable increase in cell viability between 5,000-100,000 nM in the monolayer group which was not present in the 25 µL and 75 µL 3D-culture conditions. Furthermore, there was also a gradual increase in cell viability observed between 0.5-5,000 nM in the 75 µL group.

6.4.2.1.2 MCF-7 cells

Similar experiments were then conducted in MCF-7 cells (as seen below in Figure 133). Here, it was observed that there *was* a significant difference ($p = 0.001$) in cell viability reduction between 25 µL and 75 µL, as well as, in 25 µL and monolayer ($p < 0.001$) experimental groups after vincristine-PCI exposure. Furthermore, vincristine concentration had a significant effect ($p < 0.001$) on cell viability reduction within each experimental group.

The $AlPcS_{2a}$ (5 µg/mL) PDT control conducted alongside these PCI experiments reduced cell viability to 57% (±6%), 33% (±4%), and 74% (±1%) in 25 µL, 75 µL, and monolayer experimental groups, respectively. Concerning treatment potency, the IC_{70} values were 0.425 nM, 0.35 nM, and 12,500 nM for 25 µL, 75 µL, and monolayer groups, respectively. This represents a 1.2-fold reduction in IC_{70} in favour of 25 µL versus 75 µL, a 29,412-fold reduction in IC_{70} for 25 µL versus monolayer, and, a 35,714-fold reduction in IC_{70} for 75 µL versus monolayer. At the maximum tested concentration of 250,000 nM, cell viability was seen to be reduced to 10% (±1%) and 5% (±0%) in 25 µL and 75 µL groups, respectively - a 2-fold increase in treatment efficacy in favour of 75 µL. However, in monolayer culture, vincristine-PCI was seen to reduce cell viability to 20% (±2%) which represents a 2-fold (for

25 µL) and 4-fold (for 75 µL) increase in treatment efficacy at 250,000 nM in favour of 3D culture versus monolayer.

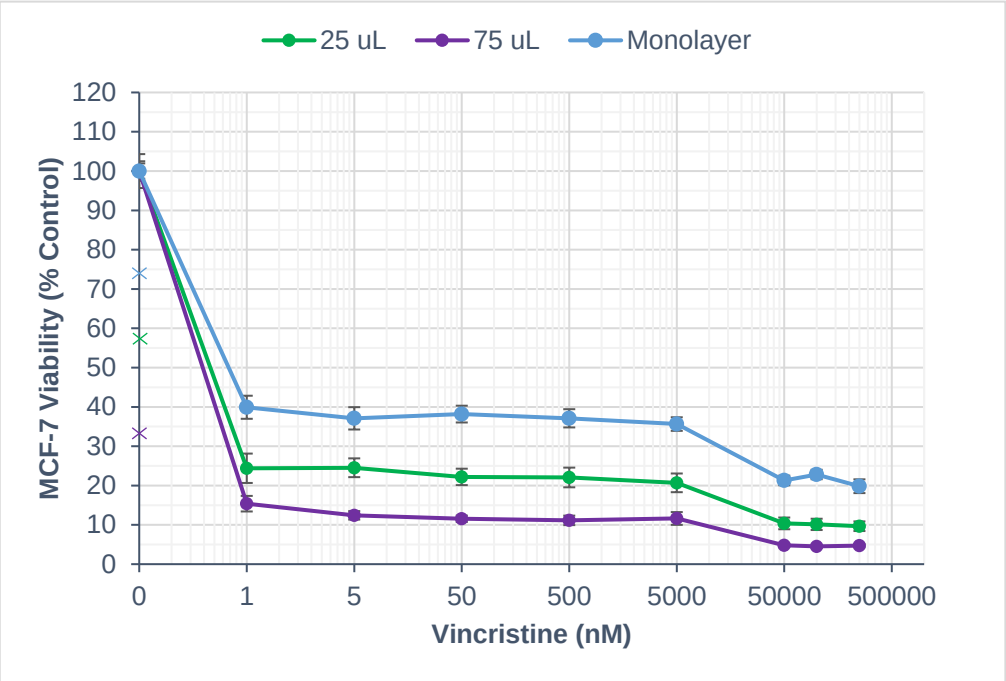

Figure 133. Reduction in MCF-7 breast cancer cell viability in 3D collagen hydrogels of varying volume and monolayer culture after vincristine PCI*. Relative cellular viability (% of control) of MCF-7 cells 3D-cultured in 25 µL and 75 µL hydrogels and monolayer culture after PCI treatment at various vincristine concentrations (0.5-250,000 nM).*

6.4.2.1.3 MDA-MB-231 cells vs MCF-7 cells – 75 µL

NB. Breast cancer cell line comparisons of vincristine-PCI cytotoxicity in 25 µL (RTC 2 mg/mL) hydrogels and monolayer culture are shown in Figure 56 & Figure 127, respectively; therefore only the 75 µL comparisons follow.

Cell line comparisons of vincristine-PCI cytotoxicity in 75 µL hydrogels were then made (as shown in Figure 134). Here, it was observed that there *was* a significant difference ($p < 0.001$) in cell viability reduction between MDA-MB-231 and MCF-7 cells 3D-cultured in 75 µL hydrogels after vincristine-PCI exposure. Furthermore, vincristine concentration had a significant effect ($p < 0.001$) on cell viability reduction within each experimental group.

The $AlPcS_{2a}$ (5 µg/mL) PDT control conducted alongside these PCI experiments reduced cell viability to 57% (±6%) and 33% (±4%) in MDA-MB-231 and MCF-7, respectively. Concerning treatment potency, the IC_{70} values were 0.475 nM and 0.35 nM for MDA-MB-231 and MCF-7 groups, respectively. This signifies a 1.4-fold reduction in IC_{70} in favour of MCF-

7 cells. At the highest tested concentration of 250,000 nM, cell viability was seen to be reduced to 18% (±5%) and 5% (±0%) in MDA-MB-231 and MCF-7 cells, respectively. These E_{max} values show a 3.6-fold increase in treatment efficacy at 250,000 nM in favour of MCF-7 cells. In addition, there was also a notable increase in cell viability observed between 50-5,000 nM in the MDA-MB-231 cell line that was not present in the MCF-7 cell line.

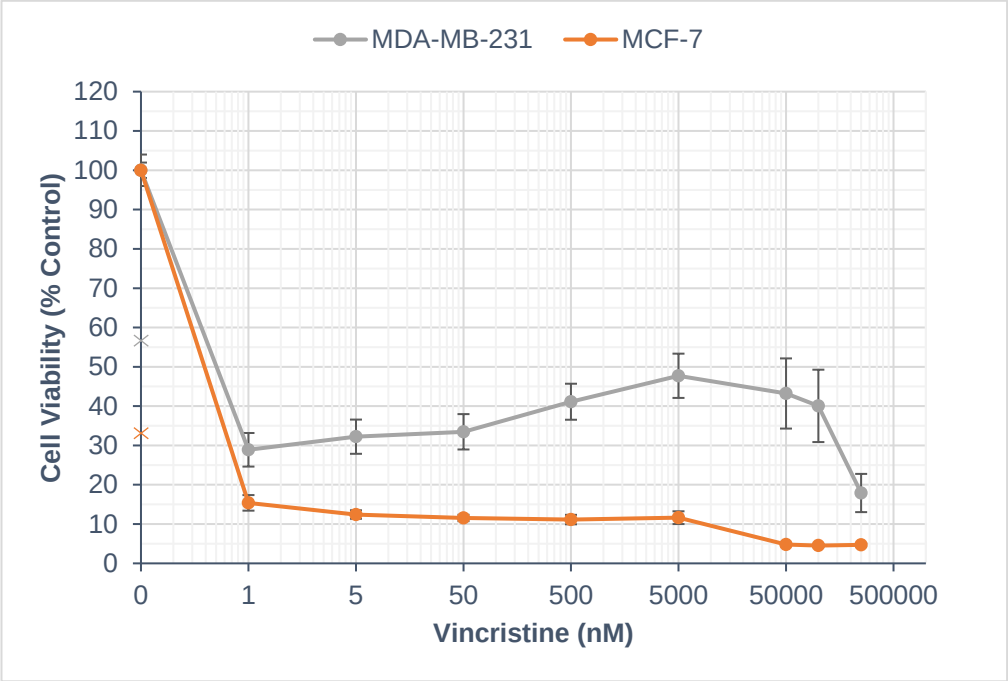

Figure 134. Reduction in breast cancer cell viability in 3D 75 µL collagen hydrogels after vincristine PCI. *Relative cellular viability (% of control) of MDA-MB-231 and MCF-7 cells 3D-cultured in 75 µL hydrogels after PCI treatment at various vincristine concentrations (0.5-250,000 nM).*

6.4.3 Results summary

6.4.3.1 Treatment potency (IC_{70}) and treatment efficacy (E_{max})

The key treatment effects indicative of PCI treatment potency and efficacy (that is, IC_{70}; E_{max}) were identified from the respective cytotoxicity profiles for each drug in each culture condition and were compared to 25 µL (RTC 2 mg/mL) hydrogels for each cell line (Table 16).

The key cytotoxic effects (IC_{70}; E_{max}) of PCI treatment in hydrogels of different volumes and monolayer were then compared between the two breast cancer cell lines (as shown in Table 17).

Table 16. Summary of PCI treatment cytotoxicity in different 3D model culture conditions (hydrogel volume) and compared with 25 µL collagen hydrogels.

Chemotherapy Drug	Hydrogel Volume	IC_{70} (nM)				E_{max} (% Control [±SE])			
		MDA-MB-231	Potency change (fold)	MCF-7	Potency change (fold)	MDA-MB-231	Efficacy change (fold)	MCF-7	Efficacy change (fold)
Bleomycin	25 µL	27,500	.	750 / 0.45 (IC_{50})	.	6 (±0)	.	5 (± 0)	.
Vincristine		0.45	.	0.425	.	21 (±4)	.	10 (±1)	.
Bleomycin	75 µL	3,250	+ 8.5	20 / 0.30 (IC_{50})	+ 38 / + 1.5 (IC_{50})	2 (±0)	+ 3.0	4 (±0)	+ 1.3
Vincristine		0.475	- 1.1	0.35	+ 1.2	18 (±5)	+ 1.2	5 (±0)	+ 2.0
Bleomycin	Monolayer	75,000	- 2.7	n/a / 90,000 (IC_{50})	- 200,000 (IC_{50})	5 (±0)	+ 1.2	36 (± 2)	+ 7.2
Vincristine		0.40	+ 1.1	12,500	- 29,412	25 (±4)	- 1.2	20 (±2)	- 2.0

Table 17. Summary of PCI treatment cytotoxicity in different 3D model culture conditions (hydrogel volume) and compared between MDA-MB-231 and MCF-7 human breast cancer cells.

Chemotherapy Drug	Hydrogel Volume	IC_{70} (nM)				E_{max} (% Control [±SE])			
		MDA-MB-231	Potency change (fold)	MCF-7	Potency change (fold)	MDA-MB-231	Efficacy change (fold)	MCF-7	Efficacy change (fold)
Bleomycin	25 µL	27,500	.	750	+ 37	6 (±0)	.	5 (±0)	+ 1.2
Vincristine		0.45	.	0.425	+ 1.1	21 (±4)	.	10 (±1)	+ 2
Bleomycin	75 µL	3,250	.	20	+ 163	2 (±0)	+ 2.0	4 (±0)	.
Vincristine		0.475	.	0.35	+ 1.4	18 (±5)	.	5 (±0)	+ 3.6
Bleomycin	Monolayer	75,000 / 13,750 (IC_{50})	.	n/a / 90,000 (IC_{50})	+ 6.5 (IC_{50})	5 (±0)	+ 7.2	36 (± 2)	.
Vincristine		0.40	+ 31,250	12,500	.	25 (±4)	.	20 (±2)	+ 1.3

6.4.4 Microscopy studies

6.4.4.1 Cell proximity between 25 µL and 75 µL volume hydrogels

Figure 135 & Figure 136 show that at the same magnification (x 20) and thickness of scanned section (200 µm), both MDA-MB-231 and MCF-7 human breast cancer cells are in closer 3D-proximity to each other in 25 µL volume hydrogels (*left*) than in 75 µL hydrogels (*right*).

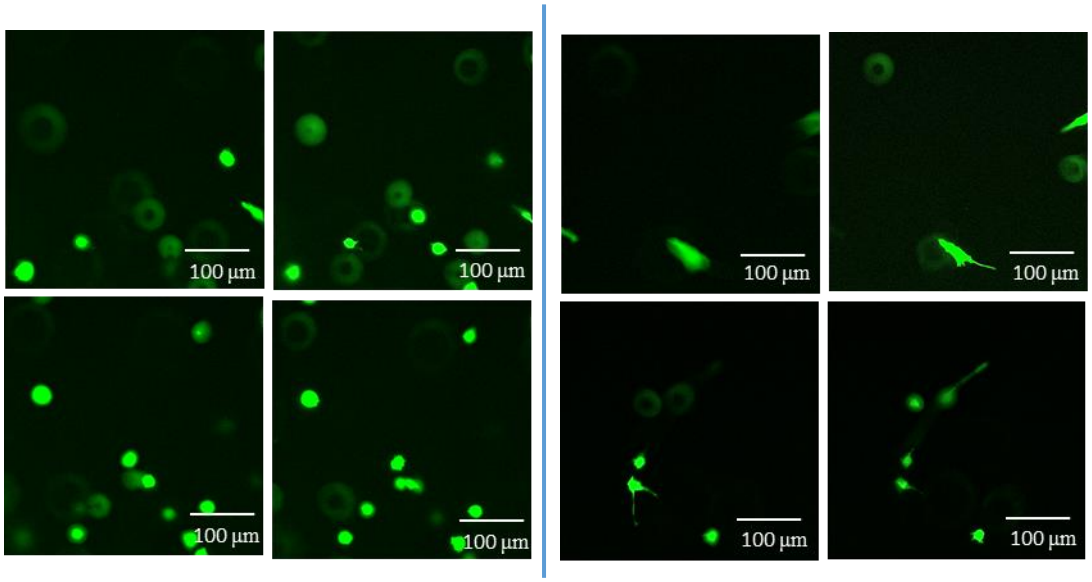

Figure 135. MDA-MB-231 cells are in closer 3D proximity to each other in 25 µL RTC hydrogels. *MDA-MB-231 cells are shown in 25 µL (left) and 75 µL (right) RTC hydrogels. Magnification x 20.*

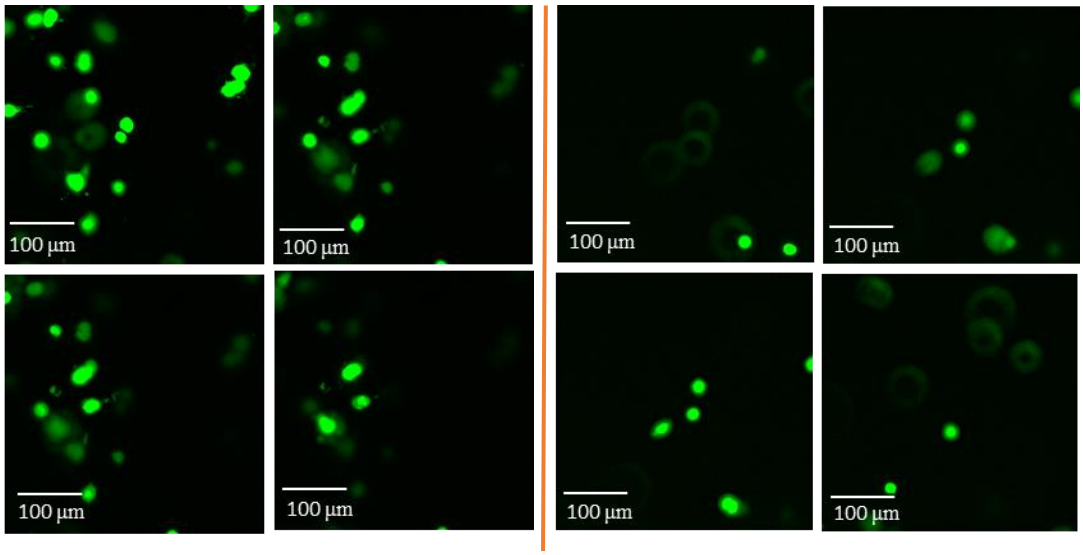

Figure 136. MCF-7 cells are in closer 3D proximity to each other in 25 µL RTC hydrogels. *MCF-7 cells are shown in 25 µL (left) and 75 µL (right) RTC hydrogels. Magnification x 20.*

6.5 Discussion

Following the testing of numerous individual chemotherapy drugs as a part of an $AlPcS_{2a}$-mediated PCI regimen, three compounds were selected and taken forward to experiments involving variations in PCI regimen, as well as, variations in the 3D model itself.

Briefly, these drugs were selected based upon the differing performances when delivered *via* PCI. First, PCI-bleomycin is essentially the gold-standard comparator at present as it has shown preclinical efficacy sufficient-enough that it has progressed to clinical studies

in humans (47). Second, PCI-vincristine has emerged as a promising new candidate and registered the highest potency and 100% synergy in both cell lines. Moreover, PCI-vincristine performance was non-significantly different between the breast cancer cell lines and its efficacy was not maximal in either cell line, whereas, the other PCI-vinca agents were maximally effective. Thirdly, PCI-gemcitabine performed relatively poorly all-round so any significant improvements in performance as a result of either regimen or model variations would be scientifically interesting (and potentially therapeutically useful).

As previously mentioned, an alternative PCI regimen also exists whereby the 'PDT' or photochemical component of PCI therapy is carried out *before* the administration of the chemotherapeutic agent. It has been posited that following photochemical treatment, the photochemically-damaged lysosomes and lysosomal membranes then fuse with intact and undamaged lysosomes (and lysosomal membranes) to form a composite lysosomal compartment that is relatively more permeable. This increased permeability then, in turn, results in an increased leakage of any therapeutic agent that is subsequently administered (after photochemical treatment) and sequestered within the lysosome. This leakage would then ultimately result in a higher cytosolic concentration of the chemotherapeutic component and, thus, an increased opportunity for the chemotherapy to exert its therapeutic action. In addition, as has been previously described, increased lysosomal permeability and content-leakage can itself lead to the initiation of a separate cell death mechanism mediated by cell-death initiating cathepsin enzymes.

Importantly, although the "light-after" (i.e., conventional) and light-before (LB) PCI regimens were kept the same as far as was practically possible, the necessary technical and methodological differences between each regimen meant that they differed sufficiently that direct comparisons can only be tentative. For instance, the overall duration of LB experimentation was extended by 24 h which meant that the overall effect of the PDT/photochemical component was comparatively greater in the LB regimen. The synergy attainment may therefore provide the preferred basis of comparison between the alternative regimens.

Nonetheless, the LB investigations yielded some interesting results by comparison to the conventional regimen. By way of example, in terms of PCI treatment potency, LB PCI-bleomycin was observed to perform more-poorly versus its counterpart chemotherapy experiments ('LB chemotherapy') but was equivalent in terms of efficacy. Similarly to findings with conventional PCI-bleomycin, LB PCI-bleomycin was more potent in MCF-7 cells. Although, here, the preference in potency for MCF-7 cells was enhanced approximately 3-fold again versus conventional PCI (preference for MCF-7 cells over MDA-MB-231 cells: PCI: 37-fold; LB PCI: 92-fold). In terms of synergy, LB PCI-bleomycin achieved 38% and 0% synergy in MDA-MB-231 and MCF-7 cells, respectively. So, interestingly, despite LB PCI-bleomycin being more potent in MCF-7 cells, these were not synergistic interactions. By contrast, the highest synergy value in MDA-MB-231 cells exceeded that achieved in the conventional regimen; as did the average synergy (α) value. However, MDA-MB-231 synergy was ultimately observed in 2-fold fewer LB PCI-bleomycin combinations than conventional PCI (PCI: 63%; LB PCI: 38%).

Now to consider LB PCI-vincristine: although LB PCI-vincristine potency values did not reach the heights of the conventional regimen, this PCI-drug combination still performed impressively with 438-fold and 1,333-fold increases in potency over LB chemotherapy in MDA-MB-231 and MCF-7 cells, respectively. Interestingly, LB PCI-vincristine potency was very similar across both cell lines *and* PCI regimens at around 0.40 nM. With regards to treatment efficacy, vincristine attained greater benefit from the LB regimen with 5-fold increases in both cell lines (versus 3- and 2-fold with conventional PCI). Furthermore, LB PCI-vincristine was more efficacious (outright) than PCI-vincristine. Additionally, LB PCI-vincristine achieved 88% and 50% synergy in MDA-MB-231 and MCF-7 cells, respectively, whereas conventional PCI saw 100% synergy in both cancer cell lines. The highest synergy values were virtually the same in each cell line and were both higher than those achieved by conventional PCI. Moreover, a higher average α value was observed with LB PCI-vincristine in MCF-7 cells, however, fewer synergistic combinations were observed in this cell line.

Similarly to findings with the conventional PCI regimen, LB PCI-gemcitabine also performed poorly. Interestingly, though, potency was increased by 8,750-fold versus LB chemotherapy. However, when considered together with the synergy results (0% synergy in

both cell lines), it can be determined that this benefit likely arose solely from the photochemical treatment component of PCI therapy. Nevertheless, it illustrates just how powerful combination regimens (i.e. chemotherapy plus PDT) can be at reducing tumour burden when compared with single-agent chemotherapy.

In contrast to the present study (albeit with differing chemotherapeutics and/or cell lines), a PCI-bleomycin *in vitro* study by Høgset and colleagues (188) - utilising V79 cells (Chinese hamster lung fibroblasts) and $TPPS_{2a}$ - found no difference in treatment cytotoxicity between conventional and LB PCI regimens. In another study (79), PCI-gelonin treatment of THX cells (human malignant melanoma) using 20 µg/mL $AlPcS_{2a}$, found that a LB PCI regimen exhibited a "much stronger" cytotoxicity than did conventional PCI. These findings therefore show that the benefit derived from the opposing PCI strategies can vary depending upon the type of cell being treated and the macromolecule being delivered.

The next set of methodological variations involved varying the stiffness of 3D hydrogels of the same volume (25 µL) by means of using different concentrations of collagen type I (2 mg/mL and 5 mg/mL), as well as, culturing cells on a stiff plastic substrate (i.e., monolayer culture). Rheological studies demonstrated that there was a considerable difference in stiffness between RTC 2 mg/mL and RTC 5 mg/mL hydrogels (Figure 128). A higher collagen concentration provides a higher mechanical stability to the hydrogel (117). Similarly, at higher frequencies, water molecules likely move out of the hydrogel which *stiffens* the ECM owing to the closer proximity of the collagen fibrils.

Both *in vitro* and *in vivo*, the stiffness of the tumour microenvironment has been shown to modulate cellular responses to chemotherapy and also to influence the transition of cells to a more invasive and malignant phenotype (119). The primary advantage of culturing cells in 3D *in vitro* is therefore that, in comparison to traditional monolayer culture, the microenvironment is more representative of tumours *in situ*. Advantages of investigating drug candidates and chemotherapeutic mechanisms in 3D include: (i) the presence of oxygen and nutrient gradients; (ii) increased cell-cell interactions from cells forming 3D aggregates; (iii) non-uniform exposure to treatment; (iv) ECM-to-cell signalling; (v) different rates of cellular proliferation throughout the 3D structure; and, (vi) impact of specific stromal/tumour cells in

the tumour microenvironment (particularly in heterotypic cell cultures) (119). Thus, the evaluation of treatment effects on cells in 3D has the potential to be more representative of *in vivo* responses.

Interestingly, hydrogel stiffness was also shown to modulate responses to PCI treatment. In the stiffer 5 mg/mL [collagen type I] hydrogels, the potency of PCI-bleomycin was increased ~3-fold in MDA-MB-231 cells compared with 2 mg/mL hydrogels. Conversely, PCI-bleomycin potency was *decreased* ~2-fold in MCF-7 cells cultured in RTC 5 mg/mL. Moreover, in monolayer culture, PCI-bleomycin was ~3-fold *less* potent in MDA-MB-231 cells. Further, PCI-bleomycin potency (IC_{50}; as IC_{70} was not achieved) was massively reduced in monolayer MCF-7 cells; specifically, by a factor of 200,000. This could, in part, be due to an increased cellular proliferation in monolayer versus in 3D. Indeed, rates of MCF-7 cell proliferation have previously been shown to be substantially reduced when grown in 3D collagen hydrogels (186). This finding demonstrates the value of evaluating treatments in more biomimetic conditions. With 5 mg/mL hydrogels, PCI-bleomycin efficacy at the highest tested bleomycin concentration of 250,000 nM were broadly similar to 2 mg/mL hydrogels across both cell lines. Again, though, monolayer-cultured MCF-7 cells were the exception exhibiting a ~7-fold resistance to PCI-bleomycin efficacy (versus 2 mg/mL 3D culture conditions). These differences could also arise from differences in cell-cell and cell-ECM interactions between the three culture conditions. In monolayer culture, for instance, cell-cell interactions are likely to predominate owing to the lack of ECM. By contrast, however, 3D cultures retain extensive ECM structures; with differences in stiffness possibly affecting the penetration of cell-cell and cell-ECM signalling molecules induced by exposure to treatment.

Comparisons of drug-PCI potency and efficacy outcomes between each cell line in the separate culture conditions yielded some very interesting results (Table 14). Crucially, PCI-bleomycin and PCI-vincristine were seen to be more potent in the MCF-7 ER+ cell line in 3D culture conditions (both 2 mg/mL and 5 mg/mL). However, the exact opposite was observed with these very same treatments in monolayer culture conditions. Both PCI-bleomycin (~7 fold *[IC_{50}]*) and PCI-vincristine (31,250-fold) were much more potent in the MDA-MB-231 TNBC cell line when these treatments were evaluated in monolayer culture. In general, the very same pattern was also observed with regard to the efficacy of each

respective PCI treatment. These dramatic differences in both the general trend of PCI treatment outcomes and the outright numbers between 3D and monolayer culture suggest that monolayer systems are limited in their capacity to model cytotoxic treatment outcomes.

The importance of microenvironment stiffness was also demonstrated as differences in treatment outcomes (potency, particularly) were observed between the two 3D culture conditions. Briefly, in 5 mg/mL hydrogels, there was a smaller disparity in PCI-bleomycin cytotoxic effect (in terms of potency) between each cell line; ~6-fold in favour of MCF-7 cells. That is, the effect of PCI-bleomycin was *more* similar in each cell line than it was in 2 mg/mL hydrogels where there was a larger 37-fold disparity in PCI-bleomycin effect between each cell line (again, in favour of MCF-7 cells). Conversely, the opposite was true of PCI-vincristine whereby treatment effects (potency) between each cell line were *more* similar in the 2 mg/mL hydrogels (differed by 1.1-fold in favour of MCF-7 cells) and were more disparate in 5 mg/mL hydrogels (differed by ~3-fold in favour of MCF-7 cells).

Additional observations with regard to PCI-vincristine include that MDA-MB-231 cells cultured in stiffer 5 mg/mL hydrogels were ~3-fold more resistant to treatment versus 2 mg/mL hydrogels – although absolute IC_{70} concentrations were still very low for both at 0.45 nM (2 mg/mL) and 1.25 nM (5 mg/mL). Other treatment comparisons between cell lines and 3D culture conditions demonstrated that PCI-vincristine was essentially equipotent and only slightly more efficacious in 5 mg/mL conditions versus 2 mg/mL. By contrast, comparisons with monolayer culture again revealed dramatically different treatment responses. PCI-vincristine treatment of MDA-MB-231 cells in monolayer yielded very similar IC_{70} values to 2 mg/mL hydrogels (differing only by a factor of 1.1). However, contrastingly, PCI-vincristine treatment of monolayer MCF-7 cells was 29,411-fold less potent than in 2 mg/mL 3D culture conditions. PCI-vincristine at 250,000 nM was also 2-fold less efficacious than MCF-7 cells cultured in 2 mg/mL 3D culture.

The third methodological variation that was investigated was that of the effect on treatment outcomes of hydrogel volume. Specifically, 25 µL and 75 µL 3D collagen hydrogels (both 2 mg/mL) and monolayer culture. The majority of differences in treatment outcomes between 25 µL hydrogels (i.e. 2 mg/mL hydrogels) and monolayer have already been outlined

previously in this discussion section. Nevertheless, some interesting observations were also seen with respect to differences between 25 µL and 75 µL 3D hydrogels.

For instance, PCI-bleomycin was found to be 8.5-fold and 38-fold *more* potent in MDA-MB-231 and MCF-7 cells when these cells were cultured in 75 µL hydrogels (versus 25 µL hydrogels). Increases in efficacy were more subtle but they were both in favour of the 75 µL hydrogels. Intriguingly, PCI-vincristine once-again demonstrated a remarkably consistent potency and efficacy in 75 µL hydrogels when compared to those achieved throughout virtually all of the separate treatment, regimen, and cell line variations – with an IC_{70} of ~ 0.40 nM in both cell lines and an E_{max} of ~20% (MDA-MB-231) and ~7% (MCF-7). Again, though, results from monolayer culture is the standout exception as maximum dose PCI-vincristine *only* reduced cell viability to 20% in MCF-7 ER+ cells. In addition, PCI-bleomycin in 75 µL hydrogels was found to be 163-fold more potent in favour of MCF-7 cells (Table 17) which is a much greater disparity than that observed in 25 µL hydrogels (37-fold).

Collectively, these data demonstrate that both PCI regimen and cell culture conditions can have a dramatic impact upon PCI treatment outcomes. In fact, in some instances, PCI-bleomycin was observed to be much diminished by changes in PCI regimen. Furthermore, the potency of PCI treatment was also seen to be completely opposite between monolayer and 3D culture conditions. In addition, microenvironment parameters including hydrogel stiffness and volume were also seen to modulate treatment outcomes. Finally, PCI-vincristine appears to be a remarkably consistent PCI modality across different *in vitro* models of breast cancer.

Section C: 3D *In Vitro* Studies - Formulation

Chapter 7: Evaluation of PCI & Nanoformulations

7. Evaluation of Light Treatments and Nanoformulations

7.1 Introduction

With regard to anticancer therapy, chemotherapy drugs still remain at the forefront of preferred treatment options for the majority of solid and haematological malignancies. Many of these cytotoxic agents have well-recognised modes of action and, in corollary, modes of toxicity which commonly manifest in a dose-dependent manner. Thus, improving the therapeutic indices of these vital anticancer compounds remains an important initiative; amongst these novel strategies are technologies such as PCI and nano-formulations.

Following the extensive evaluation of chemotherapy and PCI treatment cytotoxicity on 3D-cultured MDA-MB-231 and MCF-7 human breast adenocarcinoma cells, several key promising drug candidates emerged. Subsequently, further experimental investigations were undertaken in order to evaluate the performance of these key drug-PCI combinations in an additional 3D *in vitro* model of cancer; namely, a pancreatic cancer model. Moreover, in addition to the utilisation of promising new PCI drug candidates (and the model PCI drug bleomycin), this subsequent work also involved the use of pharmaceutical nanoformulation techniques. These novel formulations (including an in-house developed nanoformulation) were primarily used in order to try to improve the therapeutic indices of *gemcitabine* due to its comparatively poor all-round performance both as a single-agent chemotherapy and as part of a PCI regimen (Figure 137).

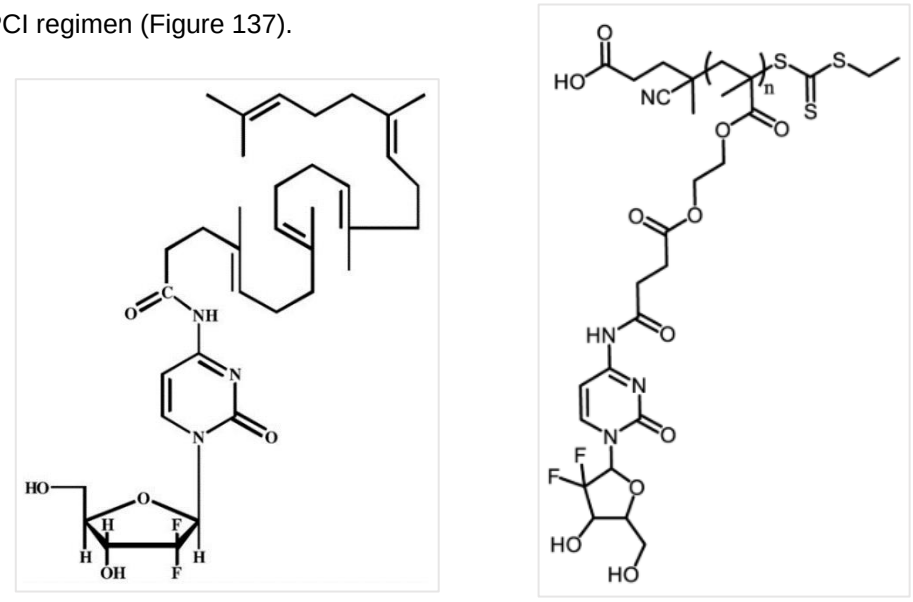

Figure 137. Chemical structures of the gemcitabine nanoformulations. *Squalene-gemcitabine (left) and polymer-gemcitabine (right).*

More specifically, select chemotherapy drugs (bleomycin, vincristine, and gemcitabine) were tested against 3D-cultured MiaPaCa-2 pancreatic cancer cells and, then, also combined with the same $AlPcS_{2a}$ concentration (5 µg/mL) and light dose (660 nm; 0.12 J/cm^2) as previously used in PCI experiments. This allowed for, for example, PCI-performance comparisons between different types of cancer. In addition, the aforementioned pharmaceutical formulation techniques involved the use of squalene- and polymer-formulations of gemcitabine (a front-line pancreatic cancer chemotherapeutic) which were tested in formulation-PCI experiments before being contrasted against their "standard" drug-PCI counterparts.

7.2. Bleomycin

7.2.1 Bleomycin Chemotherapy vs Bleomycin PCI

7.2.1.1 MiaPaCa-2 cells

Experiments utilising the MiaPaCa-2 pancreatic cancer cell line began with the glycopeptide antibiotic bleomycin. Similarly to previous experiments in the 3D *in vitro* breast cancer models, a chemotherapy cytotoxic profile was established first before then combining these drug concentrations with the photosensitiser and light necessary for PCI experimentation. As shown in Figure 138, there *was* a significant difference ($p = 0.010$) in cell viability reduction between chemotherapy and PCI experimental groups. Furthermore, bleomycin concentration had a significant effect ($p < 0.001$) on cell viability reduction within each experimental group.

The $AlPcS_{2a}$ (5 µg/mL) PDT control conducted alongside these PCI experiments was found to reduce cell viability to 42% (±5%). With regard to treatment potency, the IC_{70} values were estimated to be 150,000 nM for the chemotherapy group and 500 nM for the PCI group, respectively. This represents a 300-fold reduction in IC_{70} in favour of the PCI group. With respect to treatment efficacy at the maximum tested concentration of 250,000 nM, cell viability was reduced to 20% (±3%) and 5% (±1%) for chemotherapy and PCI groups, respectively. These E_{max} values signify a 4-fold increase in treatment efficacy at 250,000 nM for the PCI group.

7.2.1.2 Bleomycin PCI - MiaPaCa-2 cells vs MDA-MB-231 cells vs MCF-7 cells

Next, the performance of bleomycin-PCI was compared between each of the three cancer cell lines utilised thus far (as shown in Figure 139). Here, there *was* a significant difference ($p < 0.001$) in cell viability reduction observed between each cell line.

The $AlPcS_{2a}$ (5 µg/mL) PDT control conducted alongside these PCI experiments was found to reduce cell viability to 76% (±6%), 68% (±4%), and 42% (±5%) for MDA-MB-231, MCF-7, and MiaPaCa-2 cell lines, respectively. It can be determined from Figure 139 that bleomycin-PCI treatment combinations were generally more potent against MCF-7 and MiaPaCa-2 cells than MDA-MB-231 cells across the various tested concentrations. With respect to treatment potency, the IC_{70} values were 25,000 nM, 750 nM, and 500 nM for MDA-MB-231, MCF-7, and MiaPaCa-2 cells, respectively. This signifies a 50-fold and 1.5-fold reduction in IC_{70} in favour of MiaPaCa-2 cells versus MDA-MB-231 cells and MCF-7 cells, respectively. At the maximum tested concentration of 250,000 nM, cell viability was seen to be reduced to 6% (±0%), 5% (±0%), and 5% (±1%) in MDA-MB-231 cells, MCF-7 cells, and MiaPaCa-2 cells, respectively. These E_{max} values demonstrate that bleomycin-PCI was essentially equally-efficacious at 250,000 nM across the three cell lines.

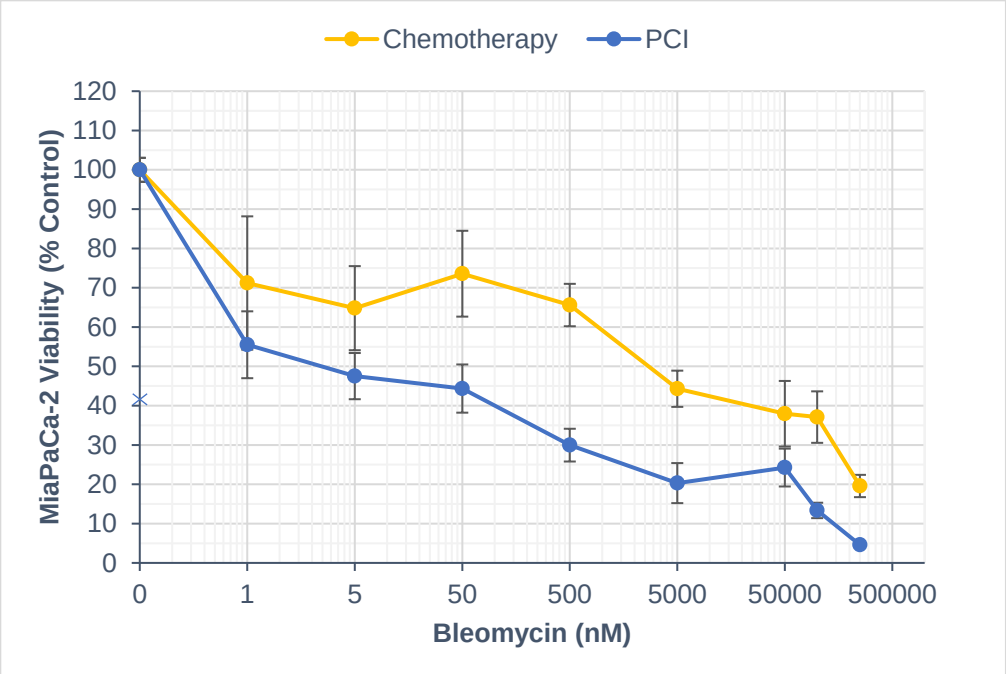

Figure 138. Reduction in MiaPaCa-2 pancreatic cancer cell viability in 3D collagen hydrogels after bleomycin chemotherapy and bleomycin PCI*. Relative cellular viability (% of control) of MiaPaCa-2 cells after chemotherapy and PCI treatment at various bleomycin concentrations (0.5-250,000 nM).*

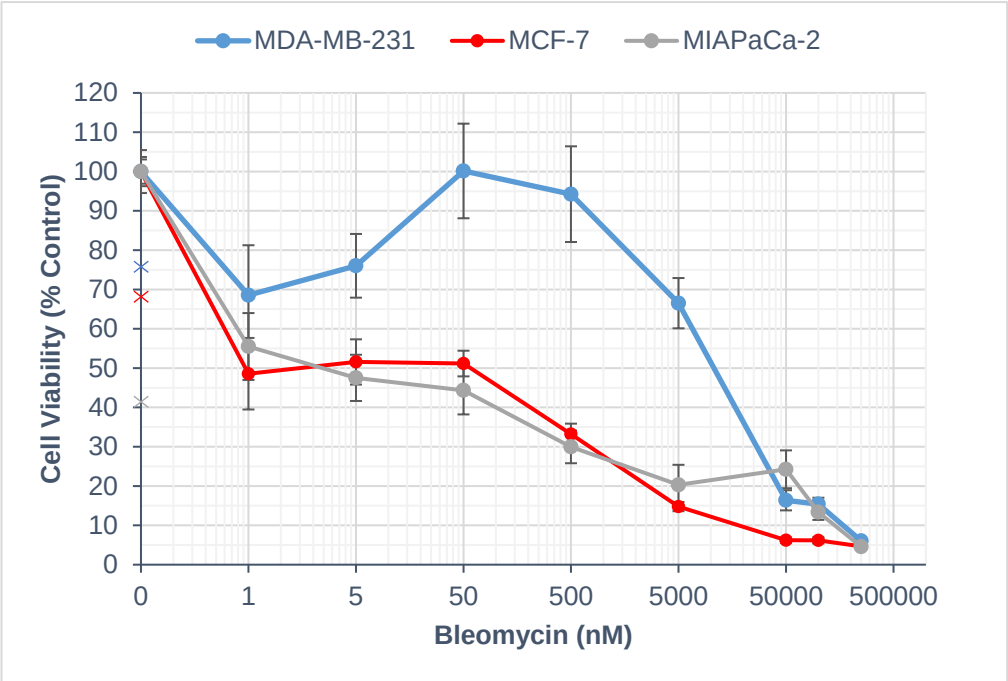

Figure 139. Reduction in cancer cell viability in 3D collagen hydrogels after bleomycin PCI. *Relative cellular viability (% of control) of MDA-MB-231, MCF-7, and MiaPaCa-2 cells after PCI treatment at various bleomycin concentrations (0.5-250,000 nM).*

7.2.1.2 Treatment Synergy

Synergy calculations were then performed (see the synergy plot below in Figure 140) and it was determined that 50% of bleomycin-PCI combinations were synergistic for the MiaPaCa-2 cell line and that the highest α value achieved was 2.1 (±0.3) at 250,000 nM.

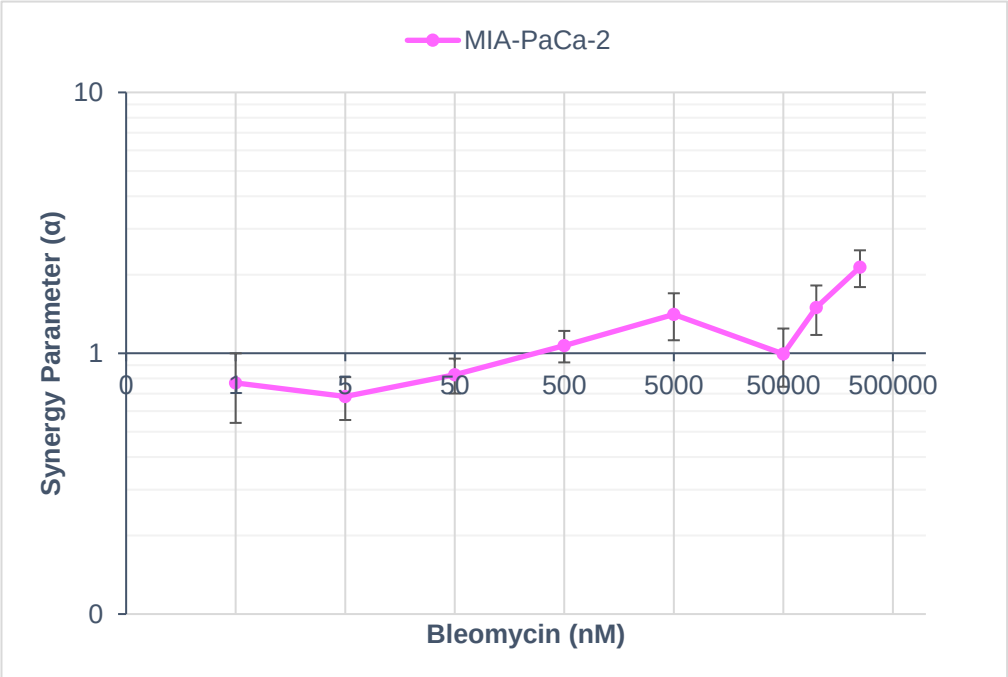

Figure 140. Synergy plot for bleomycin-PCI combinations in MiaPaCa-2 pancreatic cancer cells. *Synergy (α) was calculated from the individual cell viability results (specifically, survival/viability fraction) obtained for each respective treatment condition: chemotherapy, PDT, and PCI.*

7.3 Vinca Alkaloids

7.3.1 Vincristine Chemotherapy vs Vincristine PCI

7.3.1.1 MiaPaCa-2 cells

The next chemotherapy drug to be tested in MiaPaCa-2 cells in both its chemotherapy and PCI guises was the vinca alkaloid vincristine (as shown in Figure 141). Here, it was determined that there *was* a significant difference ($p < 0.001$) in cell viability reduction between chemotherapy and PCI experimental groups. Furthermore, vincristine concentration had a significant effect ($p < 0.001$) on cell viability reduction within each experimental group.

The $AlPcS_{2a}$ (5 µg/mL) PDT control conducted alongside these PCI experiments was found to reduce cell viability to 55% (±5%) for MiaPaCa-2 cells. It can also be determined from Figure 141 that vincristine-PCI treatment combinations were more potent than chemotherapy across all concentrations tested. Concerning treatment potency, the IC_{70} values were *not attained* and 0.475 nM for chemotherapy and PCI groups, respectively. Treatment IC_{50} values were found to be 0.40 nM and 0.25 nM which represents a 1.6-fold IC_{50} reduction in favour of PCI. At the highest tested concentration of 250,000 nM, cell viability was seen to be reduced to 33% (±2%) and 7% (±1%) for chemotherapy and PCI groups, respectively. This represents a 4.7-fold increase in treatment efficacy at 250,000 nM in favour of PCI.

7.3.1.2 Vincristine PCI: MiaPaCa-2 cells vs MDA-MB-231 cells vs MCF-7 cells

Next, the performance of vincristine-PCI was compared between each of the three cell lines (as shown in Figure 142). Here, it was observed that there *was* a significant difference ($p = 0.025$) in cell viability reduction by vincristine-PCI between each cell line.

The $AlPcS_{2a}$ (5 µg/mL) PDT control conducted alongside these PCI experiments was found to reduce cell viability to 53% (±4%), 57% (±6%), and 55% (±5%) for MDA-MB-231, MCF-7, and MiaPaCa-2 cell lines, respectively. It can also be seen from Figure 142 that vincristine-PCI treatment combinations were, in general, similarly potent against each cell line with defined differences appearing only at the highest concentrations tested. With regard to treatment potency, the IC_{70} values were found to be essentially equipotent with values of 0.45 nM, 0.40 nM, and 0.475 nM for MDA-MB-231 cells, MCF-7 cells, and MiaPaCa-2 cells,

respectively. At the maximum tested concentration of 250,000 nM, cell viability was reduced to 21% (±4%), 10% (±1%) and 7% (±1%) in MDA-MB-231 cells, MCF-7 cells, and MiaPaCa-2 cells, respectively. This signifies a 2.1-fold and 3-fold increase in vincristine-PCI efficacy at 250,000 nM in favour of MCF-7 and MiaPaCa-2 cells, respectively, versus MDA-MB-231 cells.

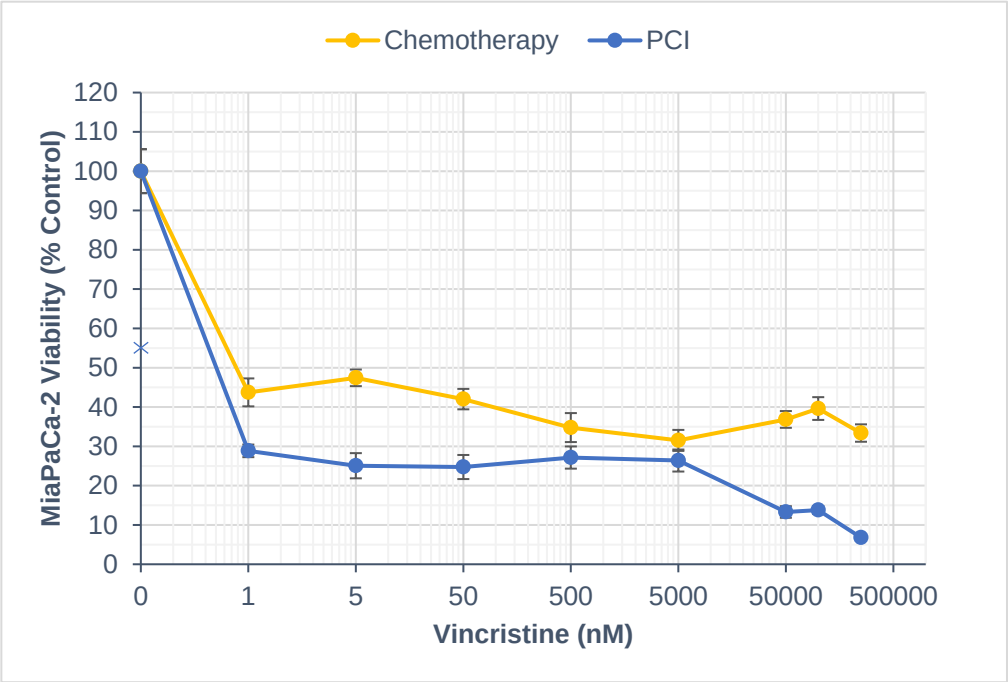

Figure 141. Reduction in MiaPaCa-2 pancreatic cancer cell viability in 3D collagen hydrogels after vincristine chemotherapy and vincristine PCI*. Relative cellular viability (% of control) of MiaPaCa-2 cells after chemotherapy and PCI treatment at various vincristine concentrations (0.5-250,000 nM).*

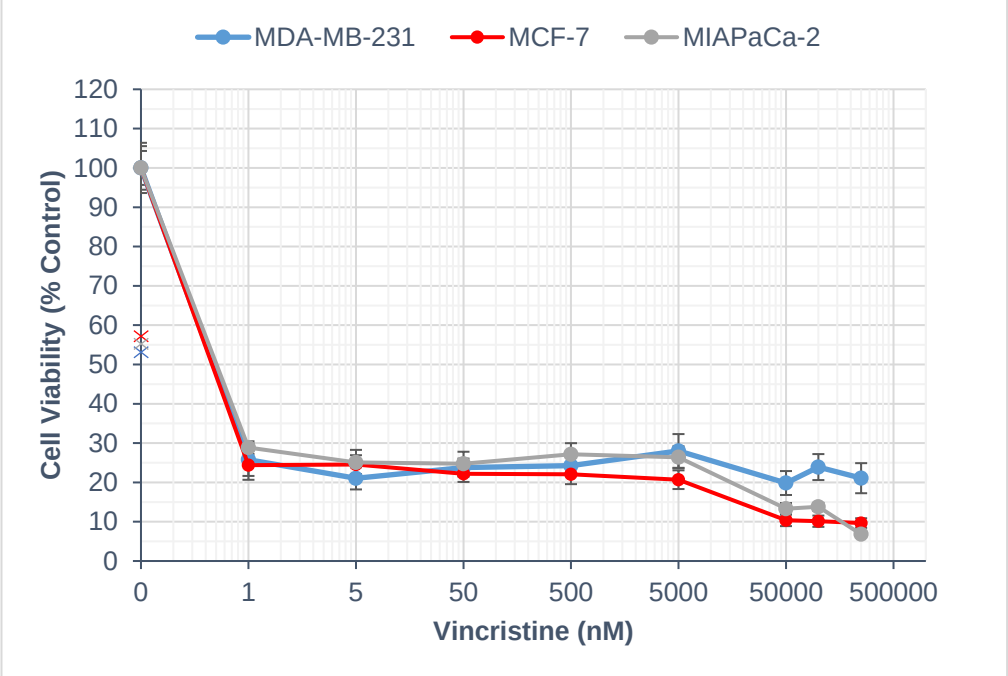

Figure 142. Reduction in cancer cell viability in 3D collagen hydrogels after vincristine PCI*. Relative cellular viability (% of control) of MDA-MB-231, MCF-7, and MiaPaCa-2 cells after PCI treatment at various vincristine concentrations (0.5-250,000 nM).*

7.3.1.3 Treatment Synergy

Synergy calculations were then performed (see the synergy plot below in Figure 143) and it was determined that 63% of bleomycin-PCI combinations were synergistic for the MiaPaCa-2 cell line and the highest *α* value achieved was 2.9 (±0.3) at 250,000 nM.

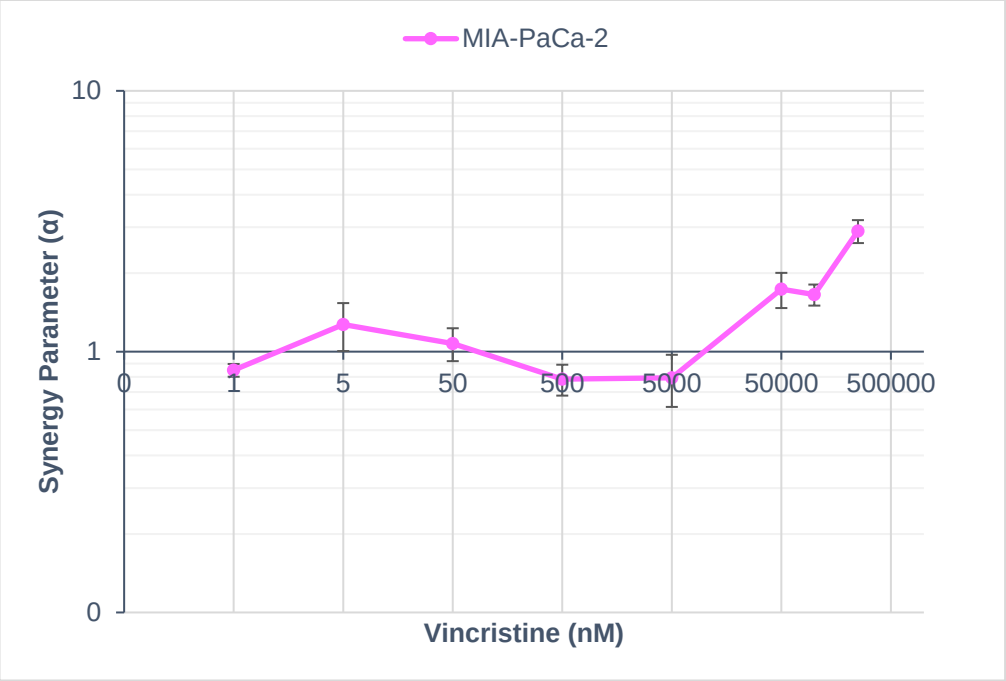

***Figure 143. Synergy plot for vincristine-PCI combinations in MiaPaCa-2 pancreatic cancer cells**. Synergy (α) was calculated from the individual cell viability results (specifically, survival/viability fraction) obtained for each respective treatment condition: chemotherapy, PDT, and PCI.*

7.4 Antimetabolites

7.4.1 Gemcitabine Chemotherapy vs Gemcitabine PCI

7.4.1.1 MiaPaCa-2 cells

Following the experiments utilising bleomycin and vincristine, gemcitabine was the next chemotherapy drug to be tested in the 3D pancreatic cancer model (as shown below in Figure 144). Here, there *was* a significant difference ($p < 0.001$) in cell viability reduction observed between chemotherapy and PCI experimental groups. Furthermore, gemcitabine concentration had a significant effect ($p < 0.001$) on cell viability reduction within each experimental group.

The $AlPcS_{2a}$ (5 µg/mL) PDT control conducted alongside these PCI experiments was found to reduce cell viability to 57% (±2%). It can be seen from Figure 144 that gemcitabine-PCI treatment combinations were more potent than chemotherapy across all concentrations

tested. Pertaining to treatment potency, the IC_{70} was *not attained* and was 5,000 nM for chemotherapy and PCI groups, respectively. Treatment IC_{50} was 4,500 nM and 0.40 nM which represents an 11,250-fold IC_{50} reduction in favour of PCI. At the maximum tested concentration of 250,000 nM, cell viability was reduced to 33% (±3%) and 24% (±2%) for chemotherapy and PCI groups, respectively. This represents a 1.4-fold increase in treatment efficacy at 250,000 nM in favour of PCI.

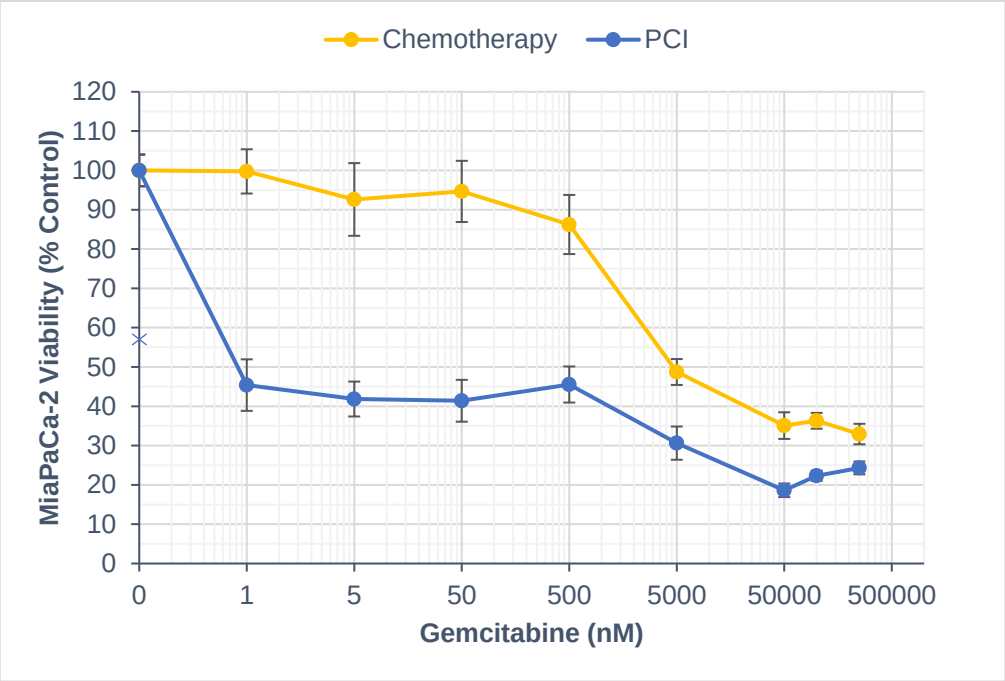

Figure 144. Reduction in MiaPaCa-2 pancreatic cancer cell viability in 3D collagen hydrogels after gemcitabine chemotherapy and gemcitabine PCI*. Relative cellular viability (% of control) of MiaPaCa-2 cells after chemotherapy and PCI treatment at various gemcitabine concentrations (0.5-250,000 nM).*

7.4.1.2 Gemcitabine PCI: MiaPaCa-2 cells vs MDA-MB-231 cells vs MCF-7 cells

Next, the performance of gemcitabine-PCI was compared between each of the three cell lines utilised thus far (as shown in Figure 145). Here, it was observed that there *was* a significant difference (p = 0.011) in cell viability reduction by gemcitabine-PCI between each cell line.

The $AlPcS_{2a}$ (5 µg/mL) PDT control conducted alongside these PCI experiments was found to reduce cell viability to 72% (±9%), 95% (±5%), and 57% (±2%) for MDA-MB-231, MCF-7, and MiaPaCa-2 cell lines, respectively. It can also be seen from Figure 145 that gemcitabine-PCI treatment combinations were more potent against MiaPaCa-2 cells at all concentrations tested. Treatment IC_{70} was 5,000 nM for MiaPaCa-2 cells but was *not attained*

in the breast cancer cell lines. Treatment IC_{50} values were 12 nM, 20 nM, and 0.40 nM for MDA-MB-231 cells, MCF-7 cells, and MiaPaCa-2 cells, respectively, which represents a 30-fold and 50-fold reduction in favour of MiaPaCa-2 cells versus MDA-MB-231 and MCF-7 cells, respectively. At the maximum tested concentration of 250,000 nM, cell viability was reduced to 40% (±5%), 43% (±3%) and 24% (±2%) in MDA-MB-231 cells, MCF-7 cells, and MiaPaCa-2 cells, respectively. These E_{max} values represent a 1.7-fold and 1.8-fold increase in gemcitabine-PCI efficacy at 250,000 nM in favour of MiaPaCa-2 cells versus MDA-MB-231 and MCF-7 cells, respectively.

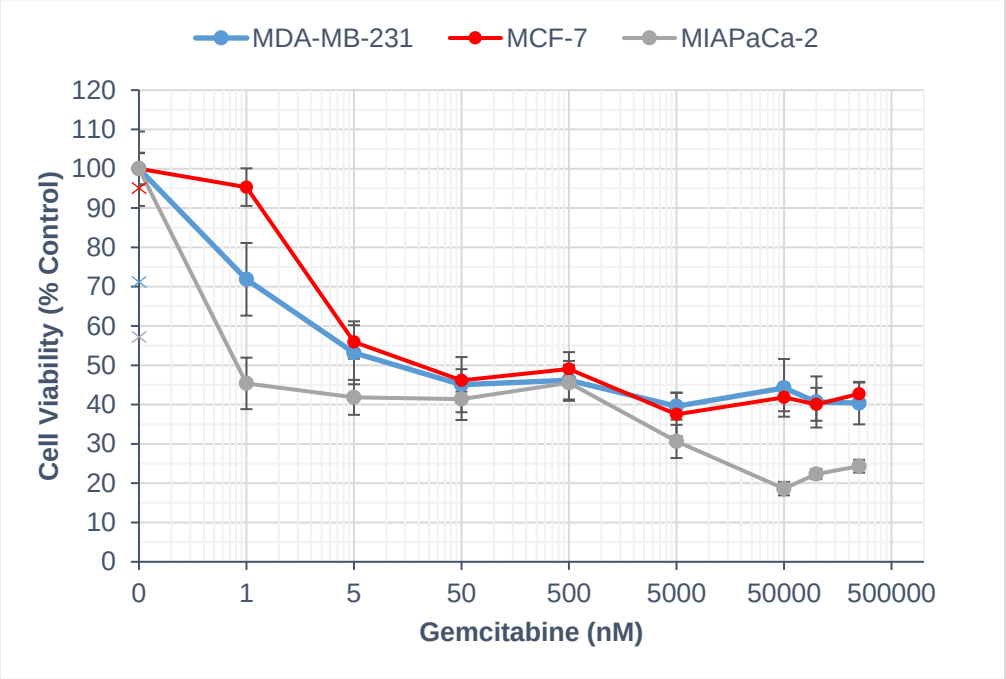

Figure 145. Reduction in cancer cell viability in 3D collagen hydrogels after gemcitabine PCI. *Relative cellular viability (% of control) of MDA-MB-231, MCF-7, and MiaPaCa-2 cells after PCI treatment at various gemcitabine concentrations (0.5-250,000 nM).*

7.4.1.3 Treatment Synergy

Synergy calculations were then performed (see the synergy plot in Figure 146) and it was determined that 75% of gemcitabine-PCI combinations were synergistic for the MiaPaCa-2 cell line and the highest α value achieved was 1.5 (±0.2) at 50 nM.

7.5 Results summary

7.5.1 Treatment potency (IC_{70}) and treatment efficacy (E_{max})

The key treatment effects indicative of chemotherapy and PCI treatment potency and efficacy (that is, IC_{70} and E_{max}) were identified from the respective cytotoxicity profiles for each drug in

each cell line. Moreover, PCI values were compared against the respective chemotherapy values for each chemotherapeutic drug (as shown in Table 18).

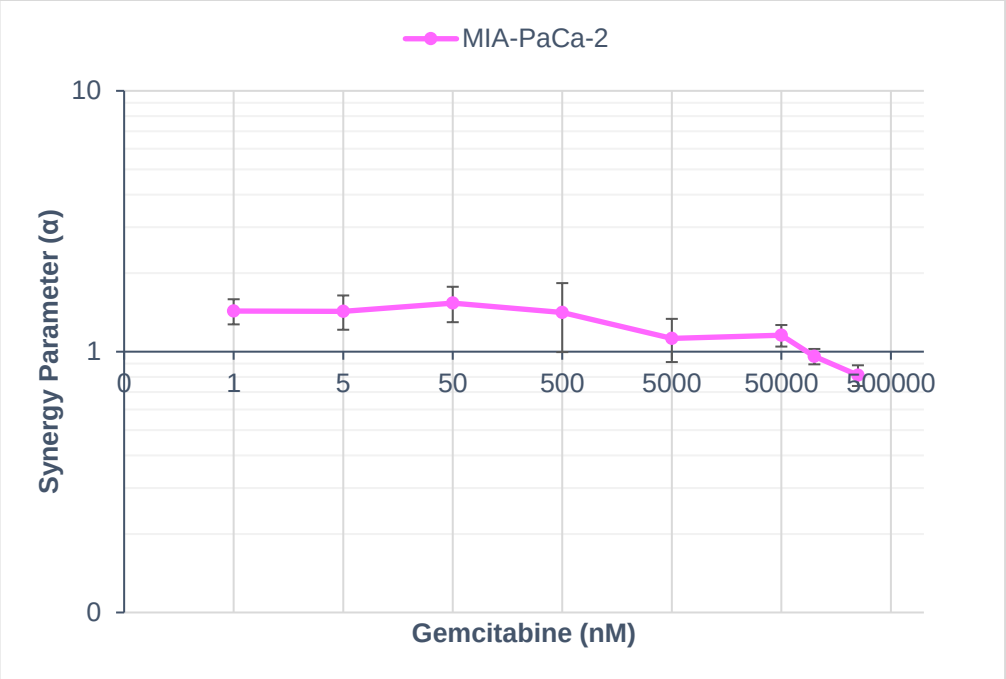

Figure 146. Synergy plot for gemcitabine-PCI combinations in MiaPaCa-2 pancreatic cancer cells. *Synergy (α) was calculated from the individual cell viability results (specifically, survival/viability fraction) obtained for each respective treatment condition: chemotherapy, PDT, and PCI.*

Table 18. Summary of chemotherapy and PCI treatment cytotoxicity in a 3D* pancreatic cancer model in vitro *with comparisons between each treatment group

Chemotherapy Drug	Treatment	IC_{70} (nM)		E_{max} (% Control [±SE])	
		MiaPaCa-2	*Potency change (fold)*	*MiaPaCa-2*	*Efficacy change (fold)*
Bleomycin	Chemotherapy	150,000	.	20% (±3%)	.
Vincristine		n/a / 0.40 (IC_{50})	.	33% (±2%)	.
Gemcitabine		n/a / 4,500 (IC_{50})	.	33% (±3%)	.
Bleomycin	PCI	500	+ 300	5% (±1%)	+ 4.0
Vincristine		0.475 / 0.25 (IC_{50})	+ 1.6 (IC_{50})	7% (±1%)	+ 4.7
Gemcitabine		5,000 / 0.40 (IC_{50})	+ 11,250 (IC_{50})	24% (±2%)	+ 1.4

The key cytotoxic effects (IC_{70}; E_{max}) of PCI treatment utilising bleomycin, vincristine, and gemcitabine were then compared between the three cancer cell lines used in this work (as shown in Table 19). In addition, the cell lines within which the treatments were most potent were also identified.

Table 19. Summary of PCI treatment cytotoxicity in the different in vitro 3D cancer models with treatment potency between cell lines compared to the most potent/efficacious cell line.

PCI Drug	IC_{70} (nM)						E_{max} (% Control [±SE])					
	MDA-MB-231	*Potency change (fold)*	*MCF-7*	*Potency change (fold)*	*MiaPaCa-2*	*Potency change (fold)*	*MDA-MB-231*	*Efficacy change (fold)*	*MCF-7*	*Efficacy change (fold)*	*MiaPaCa-2*	*Efficacy change (fold)*
Bleomycin	25,000	- 50	750	- 1.5	500	.	6% (±0%)	- 1.2	5% (±0%)	.	5% (±1%)	.
Vincristine	0.45	- 1.1	0.40	.	0.475	- 1.2	21% (±4%)	- 3.0	10% (±1%)	- 1.4	7% (±1%)	.
Gemcitabine	n/a / 12 (IC_{50})	. / - 30 (IC_{50})	n/a / 20 (IC_{50})	. / - 50 (IC_{50})	5,000 / 0.40 (IC_{50})	.	40% (±5%)	- 1.7	43% (±3%)	- 1.8	24% (±2%)	.

Table 20. Summary of synergy values obtained from PCI treatment combinations on MDA-MB-231 and MCF-7 human breast cancer cells in addition to MiaPaCa-2 human pancreatic cancer cells within 3D collagen hydrogels.

Chemotherapy Drug	Treatment	Synergy (α)											
		MDA-MB-231				*MCF-7*				*MiaPaCa-2*			
		Synergistic combinations (%) / Ave (α)		*Highest α value*	*Conc (nM)*	*Synergistic combinations (%) / Ave (α)*		*Highest α value*	*Conc (nM)*	*Synergistic combinations (%) / Ave (α)*		*Highest α value*	*Conc (nM)*
Bleomycin	PCI	63	1.7 (±0.2)	2.1 (±0.1)	250,000	88	1.6 (±0.3)	2.1 (±0.6)	50,000 & 100,000	50	1.5 (±0.3)	2.1 (±0.3)	250,000
Vincristine		100	2.0 (±0.3)	3.0 (±0.4)	5	100	1.7 (±0.4)	2.6 (±0.7)	50,000 & 100,000	63	1.7 (±0.3)	2.9 (±0.3)	250,000
Gemcitabine		25	1.2 (±0.2)	1.2 (±0.1)	100,000	50	1.3 (±0.2)	1.4 (±0.2)	5	75	1.3 (±0.2)	1.5 (±0.2)	50

7.5.2 Treatment Synergy

Next, the treatment synergy values achieved by PCI in MiaPaCa-2 pancreatic cancer cells were identified and summarised (see Table 20). Specifically, the results obtained for the percentage of synergistic treatment combinations identified, the highest α values achieved and at what drug concentrations. In addition, the average α value achieved by the synergistic PCI combinations was calculated and is also reported in Table 20.

7.6 Chemotherapy & Lysosome Co-localisation

7.6.1 Vinblastine & Lysotracker

Vinblastine was not tested in dose-response experiments in MiaPaCa-2 pancreatic cancer cells, however, the fluorescent BODIPY™-vinblastine conjugate served as a good model for small molecule drug uptake and localisation in this cell line. Here, fluorescence imaging of fluorescently-tagged vinblastine chemotherapy (*green*; 10,000 nM) and Lysotracker™ (*red*; 75 nM) showed that the subcellular localisation of chemotherapy *was* indeed within lysosomal compartments - as shown by the orange-yellow colour within the cells of the composite image of Figure 147.

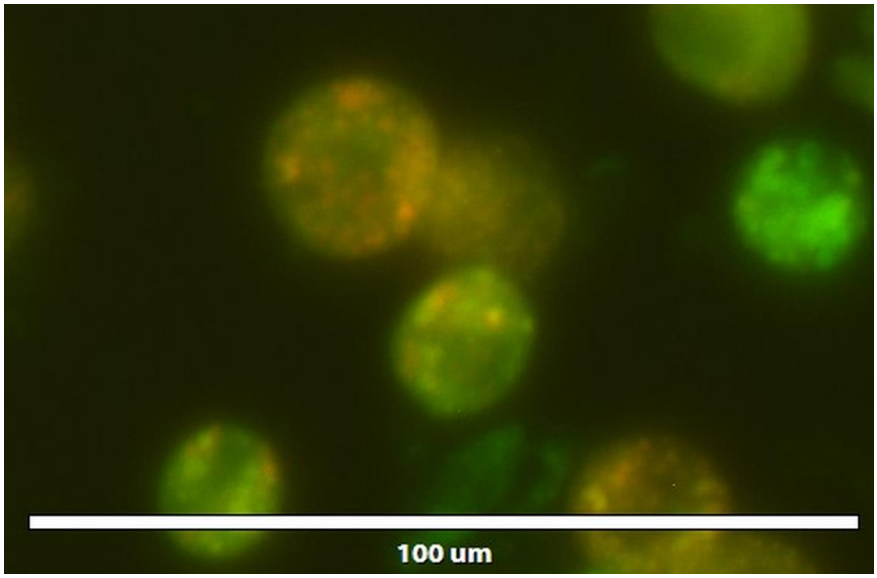

Figure 147. Co-localisation of chemotherapy and lysosome. *Fluorescence microscopy of MiaPaCa-2 cells incubated (18 h) with fluorescently-tagged vinblastine (green) lysotracker (red). This composite image combines both. The scale bar shown is 100 µm.*

7.7 MiaPaCa-2 Cell death

7.7.1 Live/dead imaging

Vinblastine was again used as a model small molecule chemotherapy drug in MiaPaCa-2 pancreatic cancer cells. Live cells (*green*) are shown with dead cells (*red*) in Figure 148 and it can be seen that dead cells predominate after only 18 h incubation with chemotherapy (vinblastine). These experiments demonstrate that the decrease in cell viability resulting from the various chemotherapy and PCI treatments actually corresponds to cell *death*.

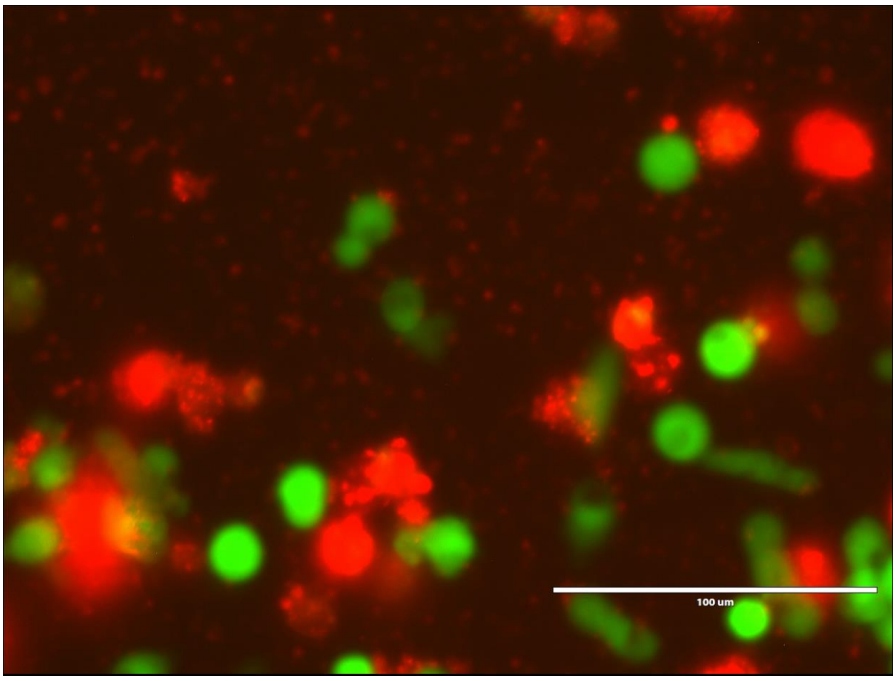

Figure 148. Dead MiaPaCa-2 cells after chemotherapy. *Fluorescent imaging of MiaPaCa-2 cells showing live (green) and dead (red) cells following 18 h incubation with vinblastine (10,000 nM). The scale bar shown is 100 µm.*

7.8 Gemcitabine Nanoformulations & PCI

Following the evaluation of both chemotherapy and PCI with the pre-selected chemotherapeutics of bleomycin, vincristine, and gemcitabine in the pancreatic cancer (MiaPaCa-2) 3D *in vitro* model, gemcitabine was chosen in order to determine whether its therapeutic indices could be improved by pharmaceutical formulation techniques.

More specifically, two separate gemcitabine formulation derivatives were employed: the first, a squalene-gemcitabine conjugate and, the second, a polymer-gemcitabine conjugate. The squalene-gemcitabine conjugate utilises the important precursor biomolecule

squalene in order to target specific receptors on the cancer cell surface and thus increase its cellular uptake (207). The polymer-gemcitabine conjugate utilises a more 'classic' formulation approach whereby cellular uptake is enhanced owing to the increased physical size and molecular weight of the biocompatible drug-polymer conjugate versus its drug-only counterpart (164). Both formulations self-assemble into nanosized particles and were used as model nano-objects in order to evaluate whether PCI protocols could further augment their cytotoxic activity.

7.8.1 Nanoparticle Characterisation

7.8.1.1 SqGem and Gemcitabine-Polymer Formulations

7.8.1.1.1 Particle size distribution

Nanoparticle characterisation involved DLS measurement of each of the gemcitabine formulations. This revealed that SqGem nanoparticles were larger in size, on average, at 430 nm. Further, SqGem nanoparticles were ~3-fold more uniform in their distribution than were gemcitabine-polymer nanoparticles (Figure 149; Table 21). By contrast, gemcitabine-polymer nanoparticles were around ~3-fold smaller in size than the SqGem nanoparticles at 130 nm.

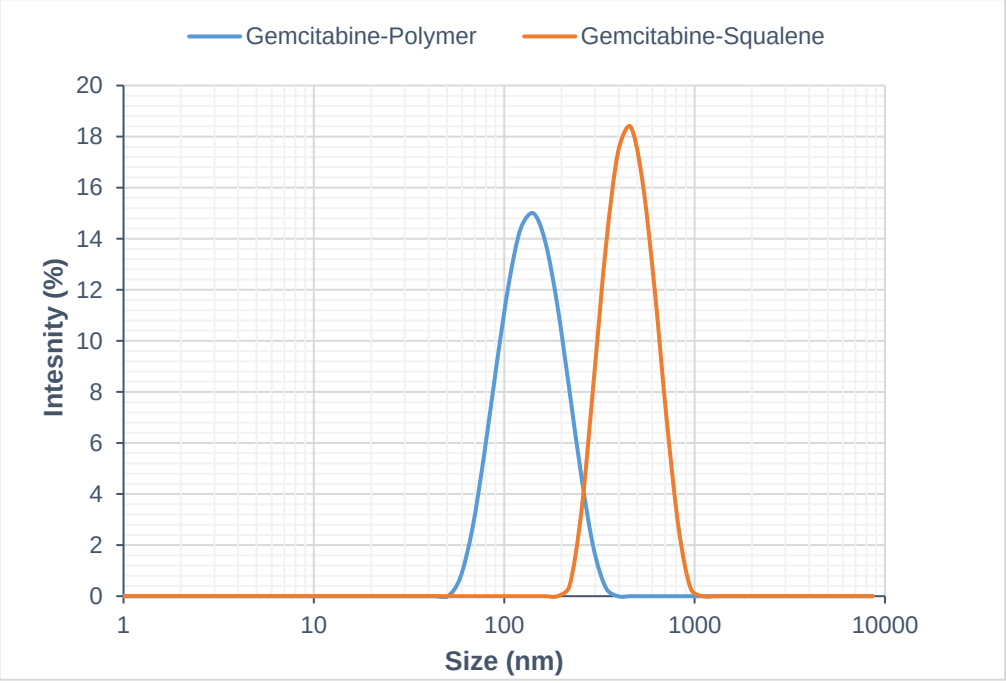

Figure 149. SqGem nanoparticles were larger and more uniform in their distribution. *Particle size distribution of SqGem (gemcitabine-squalene) and gemcitabine-polymer formulations as determined by DLS measurement.*

Table 21. SqGem nanoparticles were larger and more uniform in their distribution. *The average particle size (nm) and the polydispersity index (PDI) of SqGem and gemcitabine-polymer formulations as determined by DLS measurement.*

Formulation	Z-Average (d.nm)	PDI
Gemcitabine-Polymer	130	0.30
Gemcitabine-Squalene (SqGem)	430	0.08

7.8.2 MiaPaCa-2 cells

7.8.2.1 Gemcitabine Chemotherapy vs Gemcitabine PCI vs SqGem

Before the gemcitabine-squalene (SqGem) formulation was combined with PCI, it was first tested as a standalone chemotherapeutic agent akin to previous chemotherapy experiments. Here, it is compared to the previous gemcitabine chemotherapy and gemcitabine-PCI investigations in MiaPaCa-2 cells (see Figure 150). These experiments demonstrated that there *was* a significant difference in cell viability reduction for SqGem when compared with gemcitabine chemotherapy (p = 0.001) and gemcitabine-PCI (p = 0.005). Furthermore, gemcitabine concentration had a significant effect (p < 0.001) on cell viability reduction within each experimental group including SqGem.

The $AlPcS_{2a}$ (5 µg/mL) PDT control conducted alongside these PCI experiments was found to reduce cell viability to 57% (±2%). With regard to treatment potency, the respective IC_{70} values were *not attained*, 5,000 nM, and 3,500 nM for chemotherapy, PCI, and SqGem groups, respectively. This signifies a 1.4-fold reduction in favour of the SqGem formulation. Treatment IC_{50} was 4,500 nM, 0.40 nM, and 875 nM which represents an 11,250-fold and 2,188-fold reduction in IC_{50} in favour of PCI against chemotherapy and SqGem, respectively. At the maximum tested concentration of 250,000 nM, cell viability was seen to be reduced to 33% (±3%), 24% (±2%), and 0% (±0%) for chemotherapy, PCI, and SqGem groups, respectively. These E_{max} values represent a 33-fold and 24-fold increase in treatment efficacy at 250,000 nM for the SqGem formulation.

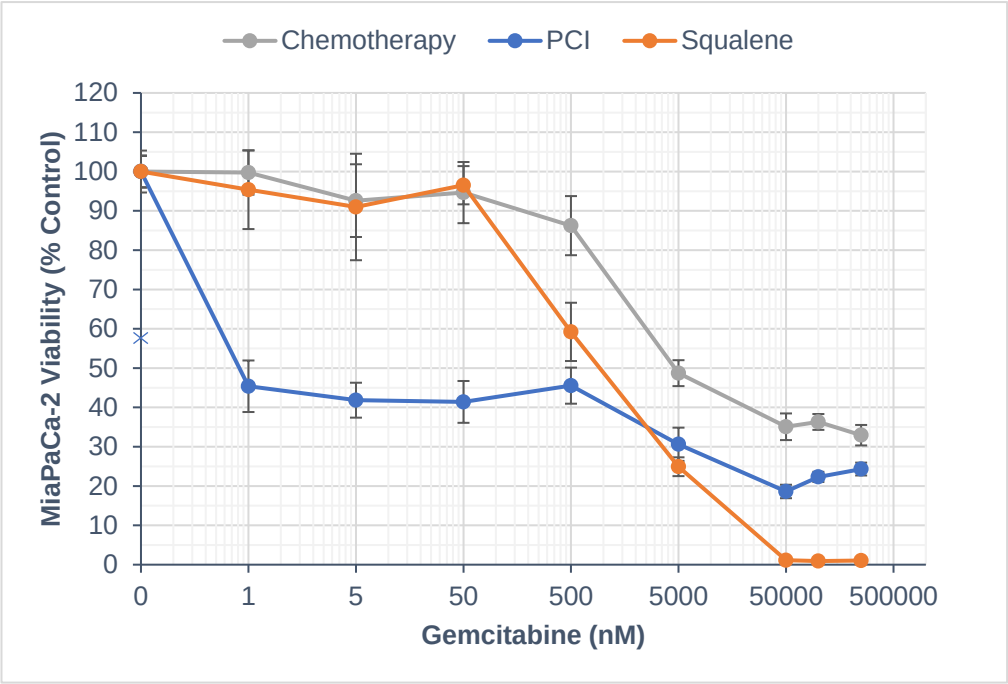

Figure 150. Reduction in MiaPaCa-2 pancreatic cancer cell viability in 3D collagen hydrogels after gemcitabine chemotherapy, gemcitabine-PCI, and SqGem treatment*. Relative cellular viability (% of control) of MiaPaCa-2 cells after chemotherapy, PCI, and SqGem treatment at various gemcitabine concentrations (0.5-250,000 nM).*

7.8.2.2 Gemcitabine Chemotherapy vs Gemcitabine PCI vs SqGem PCI

Next, the SqGem formulation was delivered via PCI utilising the same photosensitiser concentration and light dose as used in previous PCI experiments. These experiments are shown compared with gemcitabine chemotherapy and gemcitabine-PCI in MiaPaCa-2 cells (as shown in Figure 151). Here, it was determined that there *was* a significant difference in cell viability reduction for SqGem PCI when compared with gemcitabine chemotherapy ($p < 0.001$) and gemcitabine PCI ($p = 0.023$). Furthermore, gemcitabine concentration had a significant effect ($p < 0.001$) on cell viability reduction within each experimental group.

The $AlPcS_{2a}$ (5 µg/mL) PDT control conducted alongside the SqGem PCI experiments was found to reduce cell viability to 51% (±3%). Pertaining to treatment potency, the IC_{70} values were *not attained*, 5,000 nM, and 4,000 nM for chemotherapy, PCI, and SqGem-PCI groups, respectively. This signifies a 1.3-fold reduction in IC_{70} in favour of SqGem PCI over PCI. Furthermore, treatment IC_{50} was estimated to be 4,500 nM, 0.40 nM, 0.40 nM which represents a 36,000-fold reduction in favour of PCI and SqGem PCI over chemotherapy. At the highest tested concentration of 250,000 nM, cell viability was found to be reduced to 33%

(±3%), 24% (±2%), and 0% (±0%) for chemotherapy, PCI, and SqGem PCI groups, respectively. This represents a 33-fold and 24-fold increase in treatment efficacy at 250,000 nM for SqGem PCI versus the other treatment conditions. In addition, PCI and SqGem PCI treatments were similarly potent at lower gemcitabine concentrations with SqGem PCI then becoming more potent than PCI from approximately 500 nM and above.

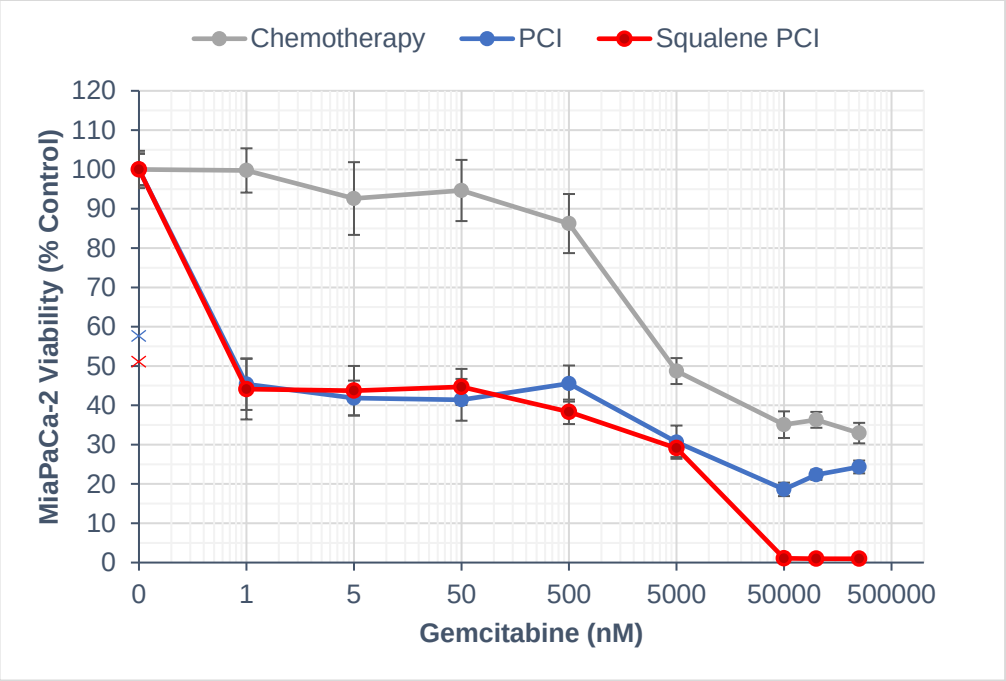

Figure 151. Reduction in MiaPaCa-2 pancreatic cancer cell viability in 3D collagen hydrogels after gemcitabine chemotherapy, gemcitabine PCI, and SqGem PCI treatment*. Relative cellular viability (% of control) of MiaPaCa-2 cells after chemotherapy, PCI, and SqGem PCI treatment at various gemcitabine concentrations (0.5-250,000 nM).*

7.8.2.3 SqGem vs SqGem PCI

Following comparisons with chemotherapy and PCI, the SqGem formulation experiments were then compared – that is, the SqGem formulation in its non-PCI and PCI guises. Here, it can be seen from Figure 152 that there *was* a significant difference (p = 0.001) in cell viability reduction between SqGem and SqGem PCI experimental groups.

The $AlPcS_{2a}$ (5 µg/mL) PDT control conducted alongside these PCI experiments was found to reduce cell viability to 51% (±3%). It can also be observed from Figure 152 that SqGem PCI treatment combinations were more potent against MiaPaCa-2 cells at low and middle concentrations, in particular 0.5-500 nM. With regard to treatment potency, the IC_{70} values were 3,500 nM and 4,000 nM for SqGem and SqGem PCI groups, respectively, which

represents a 1.1-fold difference. However, treatment IC_{50} values were found to be 875 nM and 0.40 nM for SqGem and SqGem PCI groups, respectively. This signifies a 2,188-fold reduction in IC_{50} in favour of SqGem PCI. Pertaining to treatment efficacy, both of the SqGem and SqGem PCI treatment groups were seen to reduce cell viability to 0% at the maximum tested concentration of 250,000 nM. Moreover, both treatment conditions reduced cell viability to 0% of control at the 5-fold lower concentration of 50,000 nM.

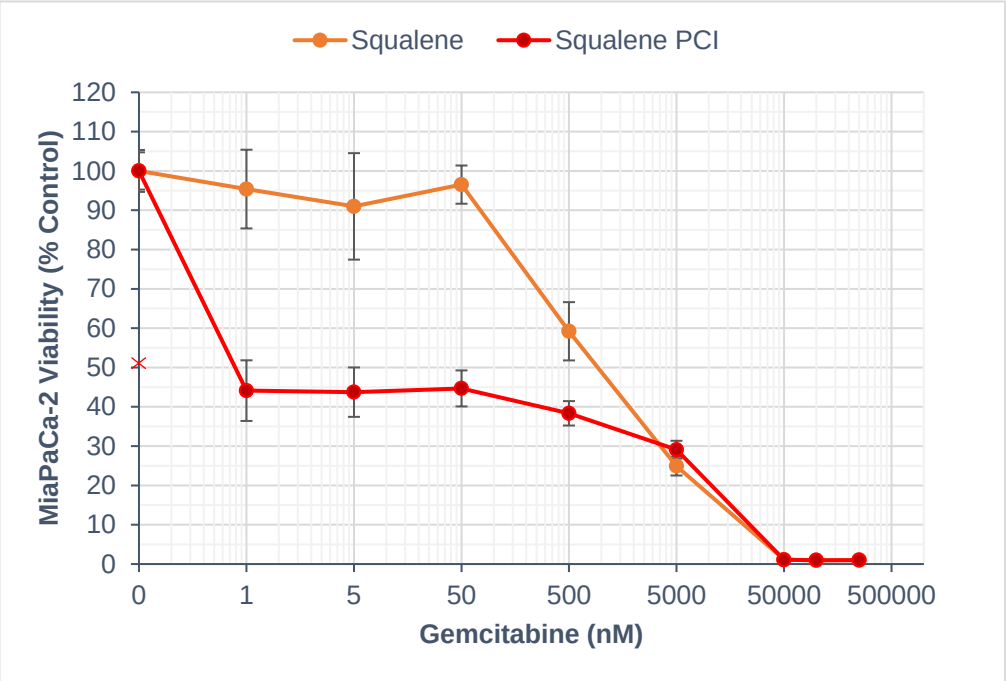

Figure 152. Reduction in MiaPaCa-2 pancreatic cancer cell viability in 3D collagen hydrogels after SqGem and SqGem PCI*. Relative cellular viability (% of control) of MiaPaCa-2 cells after SqGem and SqGem PCI treatment at various gemcitabine concentrations (0.5-250,000 nM).*

7.8.2.4 Gemcitabine Chemotherapy vs Gemcitabine PCI vs Gemcitabine-Polymer PCI

The second gemcitabine formulation was then evaluated in the *in vitro* 3D pancreatic cancer model. Below, Figure 153 shows the gemcitabine-polymer formulation compared with gemcitabine chemotherapy and gemcitabine-PCI. Here, it was determined that there *was* a significant difference in cell viability reduction for gemcitabine-polymer PCI when compared with gemcitabine chemotherapy (p = 0.010) and gemcitabine-PCI (p = 0.017); although the latter was in *favour* of gemcitabine-PCI. Furthermore, gemcitabine concentration had a significant effect (p < 0.001) on cell viability reduction within each experimental group.

The $AlPcS_{2a}$ (5 µg/mL) PDT control conducted alongside the gemcitabine-polymer PCI experiments was found to reduce cell viability to 47% (±6%). Concerning treatment potency, IC_{70} values were *not attained*, 5,000 nM, and 162,500 nM for chemotherapy, PCI, and polymer-PCI groups, respectively. This represents a 33-fold reduction in favour of PCI versus polymer-PCI. Treatment IC_{50} was 4,500 nM, 0.40 nM, 750 nM which represents an 11,250-fold and 1,875-fold reduction in IC_{50} in favour of PCI against chemotherapy and polymer-PCI, respectively. At the maximum tested concentration of 250,000 nM, cell viability was reduced to 33% (±3%), 24% (±2%), and 27% (±3%) for chemotherapy, PCI, and polymer-PCI groups, respectively. This signifies a 1.4-fold and 1.2-fold increase in treatment efficacy at 250,000 nM for PCI.

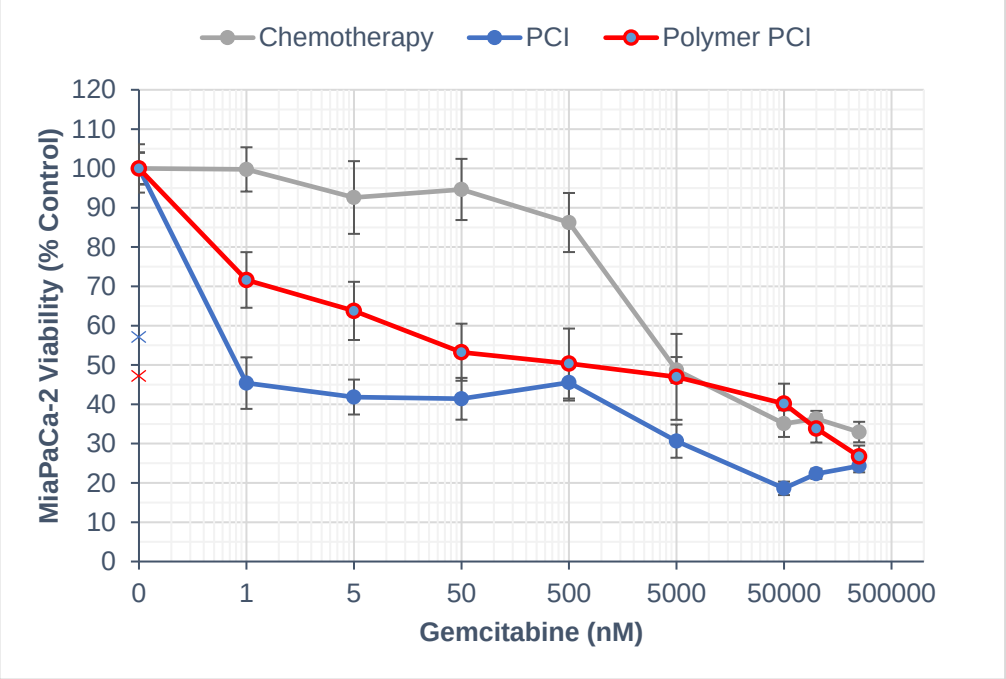

Figure 153. Reduction in MiaPaCa-2 pancreatic cancer cell viability in 3D collagen hydrogels after gemcitabine chemotherapy, gemcitabine PCI, and gemcitabine-polymer PCI treatment. *Relative cellular viability (% of control) of MiaPaCa-2 cells after chemotherapy, PCI, and gemcitabine-polymer PCI treatment at various gemcitabine concentrations (0.5-250,000 nM).*

7.8.2.5 SqGem PCI vs Gemcitabine-Polymer PCI

Next, it was pertinent to compare the PCI-performance of the gemcitabine formulations against 3D-cultured MiaPaCa-2 cells (as shown below in Figure 154). Here, it was determined that there *was* a significant difference (p = 0.001) in cell viability reduction between SqGem PCI and gemcitabine-polymer experimental groups.

The $AlPcS_{2a}$ (5 µg/mL) PDT control conducted alongside these PCI experiments was found to reduce cell viability to 51% (±3%) and 47% (±6%) for SqGem PCI and gemcitabine-polymer PCI, respectively. It can be observed from Figure 154 that SqGem PCI treatment combinations were more potent than polymer-PCI combinations at all of the drug concentrations tested. With regard to treatment potency, the IC_{70} values were estimated to be 4,000 nM and 162,500 nM for SqGem PCI and polymer-PCI groups, respectively. These values represent a 41-fold reduction in IC_{70} in favour of SqGem PCI. At the maximum tested concentration of 250,000 nM, SqGem PCI reduced cell viability to 0% (±0%) whereas polymer-PCI reduced cell viability to 27% (±3%). This represents a 27-fold increase in treatment efficacy at 250,000 nM in favour of SqGem PCI.

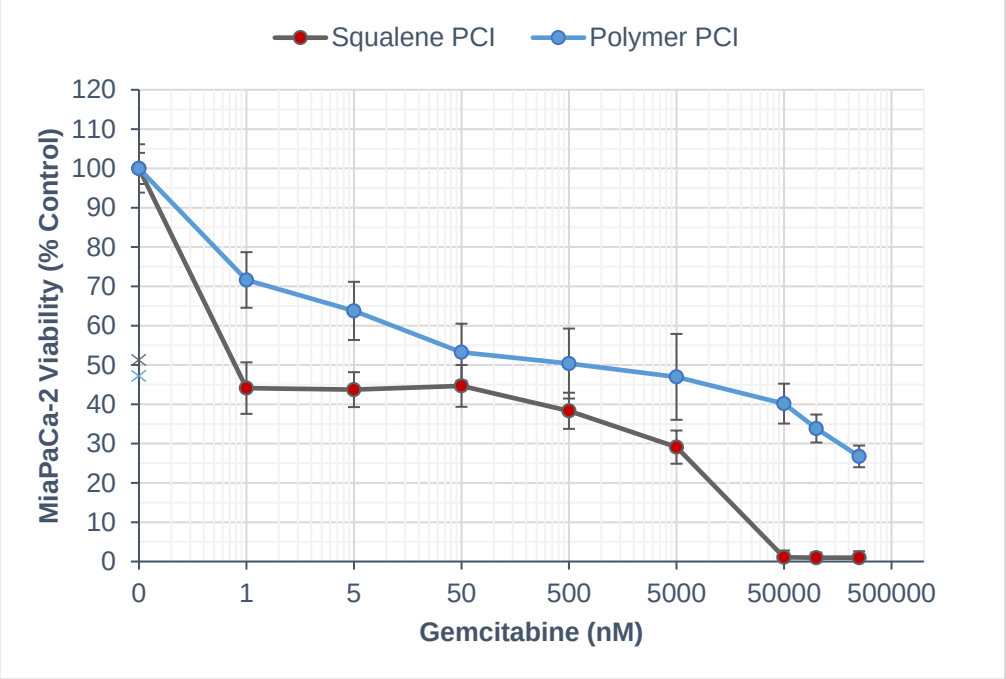

Figure 154. Reduction in MiaPaCa-2 pancreatic cancer cell viability in 3D collagen hydrogels after PCI treatment with gemcitabine formulations*. Relative cellular viability (% of control) of MiaPaCa-2 cells after SqGem PCI and gemcitabine-polymer PCI treatment at various gemcitabine concentrations (0.5-250,000 nM).*

7.8.2.6 Treatment Synergy

7.8.2.6.1 SqGem PCI

7.8.2.6.1.1 Synergy vs Gemcitabine Chemotherapy and Gemcitabine PCI

Synergy calculations were then performed (the synergy plot can be seen in Figure 155) for SqGem PCI treatment. Here, comparisons were made to both gemcitabine chemotherapy

and gemcitabine PCI treatments in MiaPaCa-2 cells in order to determine whether SqGem PCI exhibited any benefit over PCI treatment as well as over chemotherapy. From these calculations it was determined that 88% and 100% of SqGem PCI combinations were synergistic in the MiaPaCa-2 cell line versus gemcitabine chemotherapy and gemcitabine-PCI, respectively. Furthermore, the highest *α* values achieved were found to be 21 (±3) at 100,000 nM versus chemotherapy and 26 (±2) at 250,000 nM versus PCI.

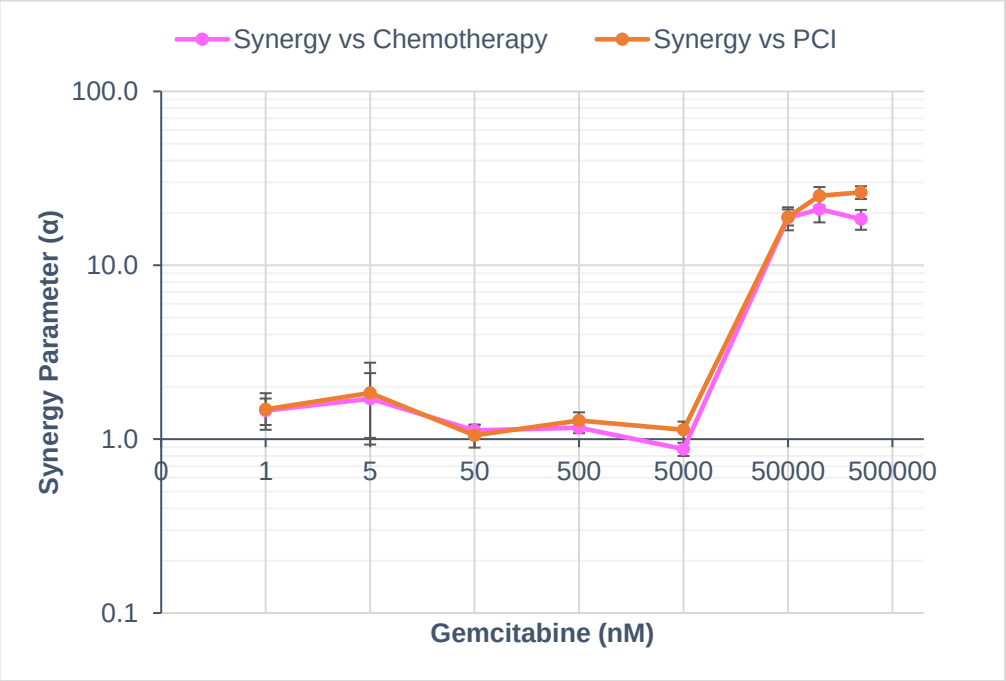

Figure 155. Synergy plot for SqGem PCI treatment combinations in MiaPaCa-2 pancreatic cancer cells. *Synergy (α) was calculated from the individual cell viability results (specifically, survival/viability fraction) obtained for each respective treatment condition: chemotherapy, PDT, and PCI, and here compared against chemotherapy and PCI treatments. NB. Y-axis scale is 0.1-100.*

7.8.2.6.1.2 Synergy vs Formulations: SqGem and Gemcitabine-Polymer PCI

Next, synergy calculations were then performed (the synergy plot can be seen in Figure 156) for SqGem PCI treatment versus the other formulation treatments. Namely, comparisons were made to SqGem and gemcitabine-polymer PCI in order to determine whether SqGem PCI exhibited any benefit over these treatments. From these calculations it was determined that 38% and 100% of SqGem PCI combinations were synergistic in the MiaPaCa-2 cell line versus SqGem and gemcitabine-polymer PCI treatment, respectively. The highest *α* values achieved were 1.7 (±0.7) at 5 nM versus SqGem and 41 (±4) at 50,000 nM versus gemcitabine-polymer PCI, respectively.

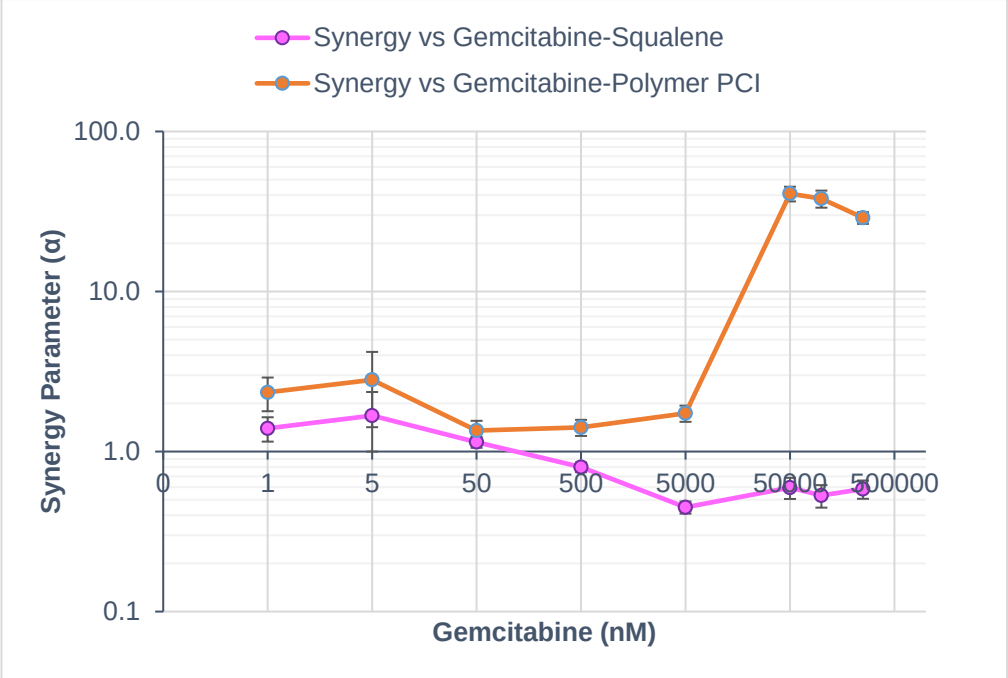

Figure 156. Synergy plot for SqGem PCI treatment combinations against the other tested formulations in MiaPaCa-2 pancreatic cancer cells. *Synergy (α) was calculated from the individual cell viability results (specifically, survival/viability fraction) obtained for each respective treatment condition: chemotherapy, PDT, and PCI, and are here compared against SqGem and gemcitabine-polymer PCI treatment. NB. Y-axis scale is 0.1-100.*

7.8.2.6.2 Gemcitabine-Polymer PCI

7.8.2.6.2.1 Synergy vs Gemcitabine Chemotherapy and Gemcitabine PCI

Synergy calculations were then performed (the synergy plot can be seen in Figure 157) for gemcitabine-polymer PCI treatment. Here, comparisons were made to both gemcitabine chemotherapy and gemcitabine PCI treatments in MiaPaCa-2 cells in order to determine whether polymer-PCI exhibited any benefit over PCI treatment as well as over chemotherapy. Again, in relation to each of the synergy figures, “Synergy vs Chemotherapy” here (and thenceforth), in fact denotes comparisons to both chemotherapy *and* PDT (as standalone individual treatments) as has been the case with all previous synergy calculations. From these calculations it was determined that 0% and 25% of gemcitabine-polymer PCI combinations were synergistic in the MiaPaCa-2 cell line versus gemcitabine chemotherapy and gemcitabine PCI treatment, respectively. The highest α values achieved were 1.0 (±0.2) at 50 nM (i.e. an additive effect) versus chemotherapy and 1.9 (±0.8) at 5,000 nM versus PCI, respectively.

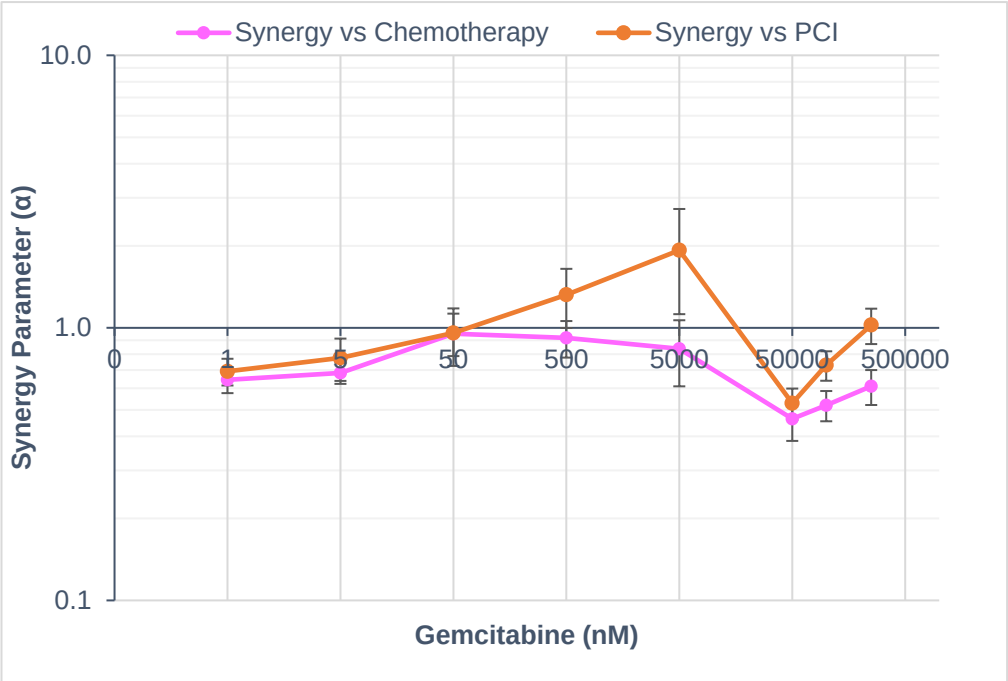

Figure 157. Synergy plot for gemcitabine-polymer PCI treatment combinations in MiaPaCa-2 pancreatic cancer cells. *Synergy (α) was calculated from the individual cell viability results (specifically, survival/viability fraction) obtained for each respective treatment condition: chemotherapy, PDT, and PCI, and are here compared against gemcitabine chemotherapy and gemcitabine PCI treatment.*

7.8.3 MDA-MB-231 cells

Following the evaluation of the gemcitabine formulations in the MiaPaCa-2 pancreatic cancer cell model, similar experiments were then conducted utilising the previous MDA-MB-231 breast cancer cell model. This would, for example, allow for performance comparisons to be made of the novel formulation-PCI combinations in distinctly-different types of cancer.

7.8.3.1 SqGem PCI vs Gemcitabine Chemotherapy vs Gemcitabine PCI

SqGem PCI therapy was carried out against MDA-MB-231 cells and compared with chemotherapy and PCI (as shown in Figure 158). Here, it was observed that there *was* a significant difference in cell viability reduction for SqGem PCI when compared with gemcitabine chemotherapy ($p < 0.001$) and gemcitabine-PCI ($p = 0.006$). Furthermore, gemcitabine concentration had a significant effect ($p < 0.001$) on cell viability reduction within each experimental group.

The $AlPcS_{2a}$ (5 µg/mL) PDT control conducted alongside the SqGem PCI experiments was found to reduce cell viability to 43% (±5%). With regard to treatment potency, the IC_{70} values were *not attained* for either chemotherapy or PCI groups but was 10,000 nM for SqGem PCI. In addition, treatment IC_{50} was *not attained*, 12.5 nM, and 0.30 nM for chemotherapy, PCI, and SqGem PCI groups, respectively. This represents a 42-fold reduction in IC_{50} in favour of SqGem PCI. At the maximum tested concentration of 250,000 nM, cell viability was found to be reduced to 56% (±6%), 40% (±5%), and 0% (±0%) for chemotherapy, PCI, and SqGem PCI groups, respectively. This represents a 56-fold and 40-fold increase in treatment efficacy at 250,000 nM for SqGem PCI versus chemotherapy and PCI.

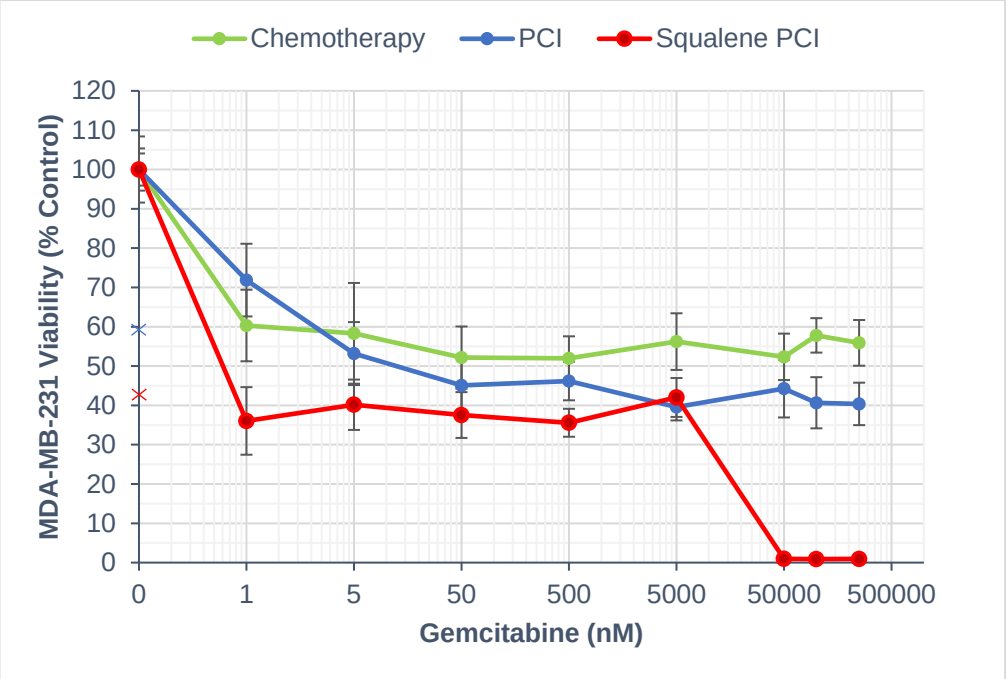

Figure 158. Reduction in MDA-MB-231 breast cancer cell viability in 3D collagen hydrogels after gemcitabine chemotherapy, gemcitabine PCI, and SqGem PCI treatment*. Relative cellular viability (% of control) of MDA-MB-231 cells after chemotherapy, PCI, and SqGem PCI treatment at various gemcitabine concentrations (0.5-250,000 nM).*

7.8.3.2 Gemcitabine-Polymer PCI vs Gemcitabine Chemotherapy vs Gemcitabine PCI

Following experimentation with the first gemcitabine formulation (SqGem), the second gemcitabine-polymer formulation was then tested against the MDA-MB-231 breast cancer cells (in its PCI guise). Similarly, comparisons were made to gemcitabine chemotherapy and gemcitabine PCI (as shown in Figure 159). Here, it was observed that there was *not* a significant difference in cell viability reduction for gemcitabine-polymer PCI when compared with gemcitabine chemotherapy (p = 0.107) and gemcitabine-PCI (p = 0.799). In addition,

gemcitabine concentration had a significant effect ($p < 0.001$) on cell viability reduction within each experimental group.

The $AlPcS_{2a}$ (5 µg/mL) PDT control conducted alongside the gemcitabine-polymer PCI experiments was found to reduce cell viability to 44% (±5%). With regard to treatment potency, IC_{70} values was *not attained* for either chemotherapy or PCI groups and was 200,000 nM for polymer-PCI. Treatment IC_{50} was found to be *not attained*, 12.5 nM, and 5 nM for chemotherapy, PCI, and polymer-PCI groups, respectively. This represents a 2.5-fold reduction in IC_{50} in favour of gemcitabine-polymer PCI versus gemcitabine PCI. At the maximum tested concentration of 250,000 nM, cell viability was seen to be reduced to 56% (±6%), 40% (±5%), and 28% (±4%) for chemotherapy, PCI, and polymer-PCI groups, respectively. These E_{max} values signify a 2-fold and 1.4-fold increase in treatment efficacy at 250,000 nM for polymer-PCI versus chemotherapy and PCI.

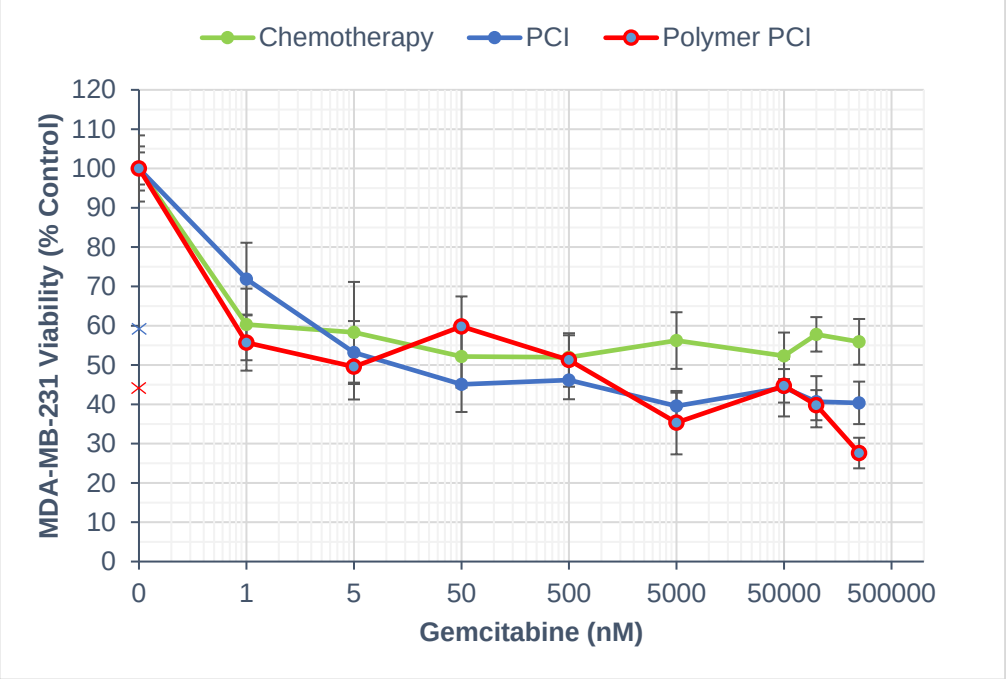

Figure 159. Reduction in MDA-MB-231 breast cancer cell viability in 3D collagen hydrogels after gemcitabine chemotherapy, gemcitabine PCI, and gemcitabine-polymer PCI treatment*. Relative cellular viability (% of control) of MDA-MB-231 cells after chemotherapy, PCI, and gemcitabine-polymer PCI treatment at various gemcitabine concentrations (0.5-250,000 nM).*

7.8.3.3 SqGem PCI vs Gemcitabine-Polymer PCI

The performance of the gemcitabine formulations were then compared against each other (as shown in Figure 160). Here, it was observed that there *was* a significant difference ($p = 0.006$) in cell viability reduction between SqGem PCI and polymer-PCI experimental groups.

The $AlPcS_{2a}$ (5 µg/mL) PDT control conducted alongside these PCI experiments was found to reduce cell viability to 43% (±5%) and 44% (±5%) for SqGem PCI and gemcitabine-polymer PCI, respectively. It can be observed from Figure 160 that gemcitabine- SqGem PCI treatment combinations were more potent than polymer-PCI combinations against MDA-MB-231 cells across the vast majority of concentrations tested. Pertaining to formulation treatment potency, the respective IC_{70} values were 10,000 nM and 200,000 nM for SqGem PCI and polymer-PCI treatment groups. This represents a 20-fold reduction in favour of SqGem PCI. At the maximum tested concentration of 250,000 nM, SqGem PCI reduced cell viability to 0% (±0%) whereas polymer-PCI reduced cell viability to 28% (±4%). This represents a 28-fold increase in treatment efficacy at 250,000 nM in favour of SqGem PCI.

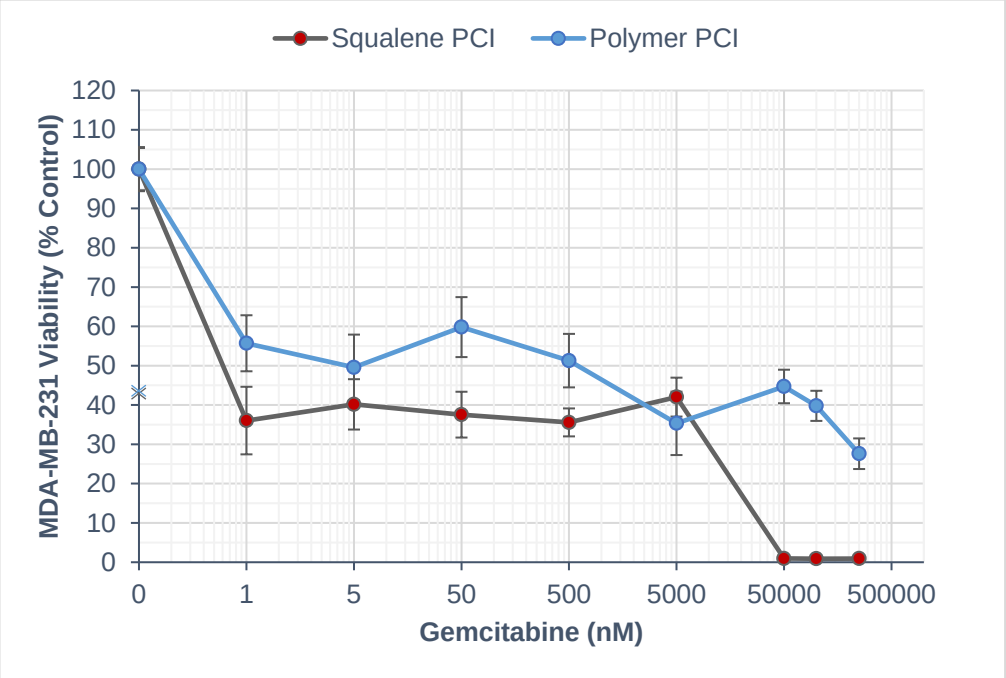

Figure 160. Reduction in MDA-MB-231 breast cancer cell viability in 3D collagen hydrogels after PCI treatment with gemcitabine formulations*. Relative cellular viability (% of control) of MDA-MB-231 cells after SqGem PCI and gemcitabine-polymer PCI treatment at various gemcitabine concentrations (0.5-250,000 nM).*

7.8.3.3 Treatment Synergy

7.8.3.3.1 SqGem PCI

7.8.3.3.1.1 Synergy vs Gemcitabine Chemotherapy vs Gemcitabine PCI

Synergy calculations were then performed (the synergy plot can be seen in Figure 161) for SqGem PCI treatment in MDA-MB-231 cells. Here, comparisons were made to both chemotherapy and PCI treatments. From these calculations it was determined that 50% and

88% of SqGem PCI combinations were synergistic in the MDA-MB-231 cell line versus gemcitabine chemotherapy and gemcitabine-PCI, respectively. The highest *α* values achieved were 30 (±5) at 100,000 nM versus chemotherapy and 50 (±5) at 50,000 nM versus PCI.

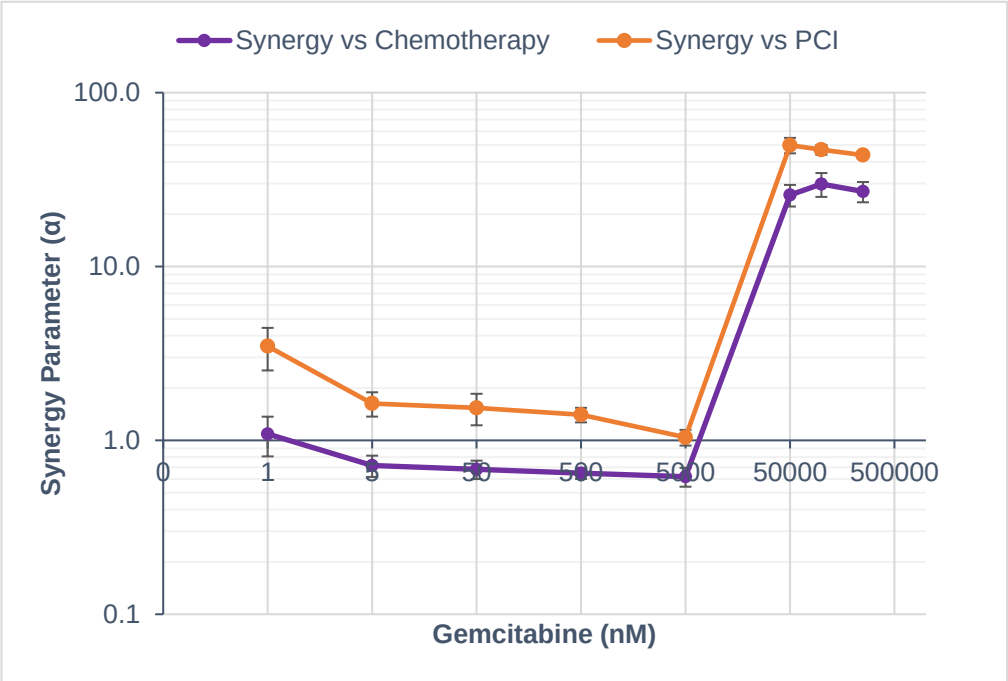

Figure 161. Synergy plot for SqGem PCI treatment combinations versus gemcitabine chemotherapy (& PDT) and gemcitabine PCI in MDA-MB-231 cells. *Synergy (α) was calculated from the individual cell viability results (specifically, survival/viability fraction) obtained for each respective treatment condition: chemotherapy, PDT, and PCI, and are here compared against gemcitabine chemotherapy and gemcitabine PCI treatment. NB. Y-axis scale is 0.1-100.*

7.8.3.3.1.2 Synergy vs Formulations: Gemcitabine-Polymer PCI

Synergy calculations were then performed (the synergy plot can be seen in Figure 162) for SqGem PCI treatment compared with gemcitabine-polymer PCI. Here, it was determined that 88% of SqGem PCI combinations were synergistic in the MiaPaCa-2 cell line versus gemcitabine-polymer PCI treatment. The highest *α* value achieved were 50 (±5) at 50,000 nM versus gemcitabine-polymer PCI.

7.8.3.3.2 Gemcitabine-Polymer PCI

7.8.3.3.2.1 Synergy vs Gemcitabine Chemotherapy and Gemcitabine PCI

Synergy calculations were then performed for the gemcitabine-polymer formulation and compared with gemcitabine chemotherapy and gemcitabine-PCI. Figure 163 shows that 13% and 88% of gemcitabine-polymer PCI combinations were synergistic in the MDA-MB-231 cell

line versus gemcitabine chemotherapy and gemcitabine-PCI, respectively. The highest *α* values achieved were 1.5 (±0.7) at 5,000 nM versus chemotherapy and 3.7 (±2) at 5,000 nM versus PCI.

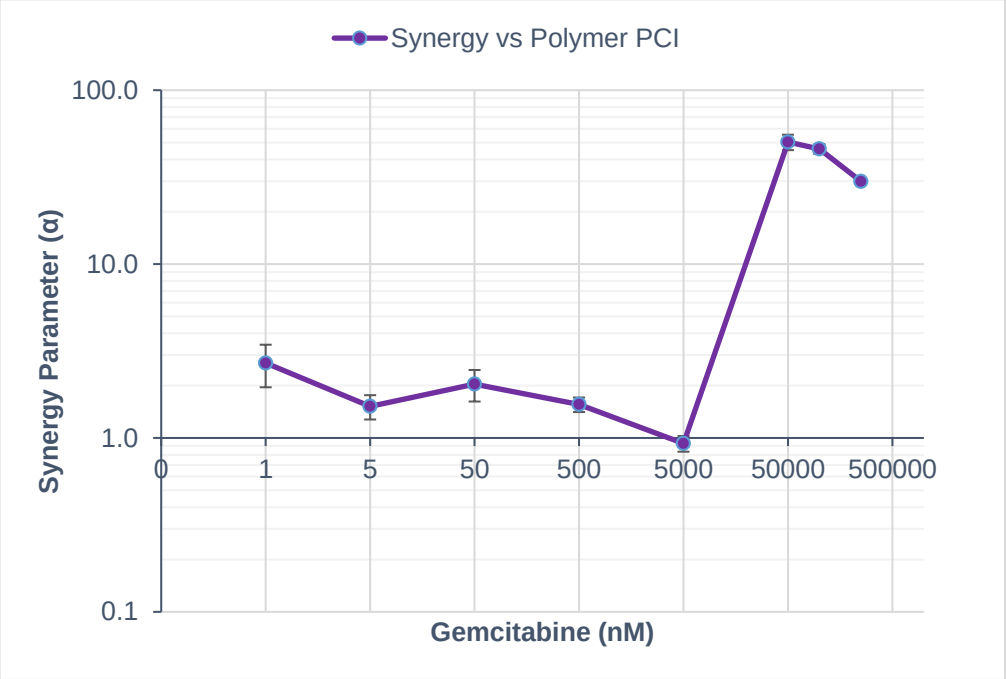

Figure 162. Synergy plot for SqGem PCI treatment combinations against gemcitabine-polymer PCI in MDA-MB-231 breast cancer cells. *Synergy (α) was calculated from the individual cell viability results (specifically, survival/viability fraction) obtained for each respective treatment condition: chemotherapy, PDT, and PCI, and are here compared against gemcitabine-polymer PCI treatment. NB. Y-axis scale is 0.1-100.*

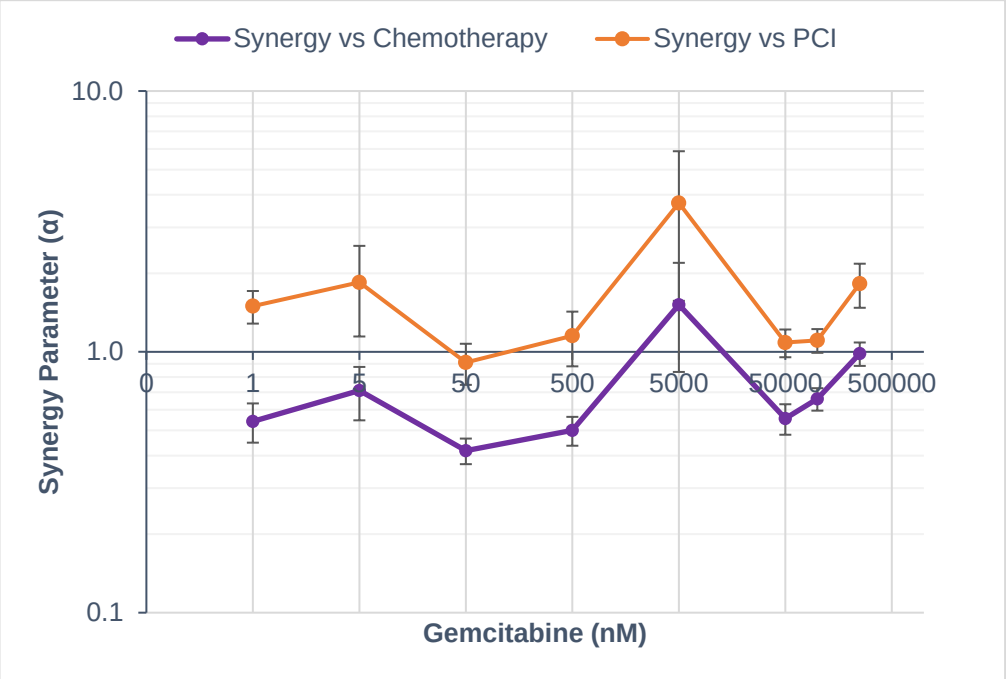

Figure 163. Synergy plot for gemcitabine-polymer PCI treatment combinations versus gemcitabine chemotherapy (& PDT) and gemcitabine PCI in MDA-MB-231 cells. *Synergy (α) was calculated from the individual cell viability results (specifically, survival/viability fraction) obtained for each respective treatment condition: chemotherapy, PDT, and PCI, and are here compared against gemcitabine chemotherapy and gemcitabine-PCI treatment.*

7.8.4 Gemcitabine Formulation Comparisons: MiaPaCa-2 cells vs MDA-MB-231 cells

It was then pertinent to compare the PCI-performance of the gemcitabine formulations on MiaPaCa-2 and MDA-MB-231 cells. That is, between pancreatic cancer cells and breast cancer cells.

7.8.4.1 SqGem PCI

Following statistical analysis of SqGem PCI cytotoxicity in both of the MiaPaCa-2 and MDA-MB-231 cell lines (see Figure 164), it was determined that there was *not* a significant difference (p = 0.805) in cell viability reduction between the cancer cell lines as a result of treatment.

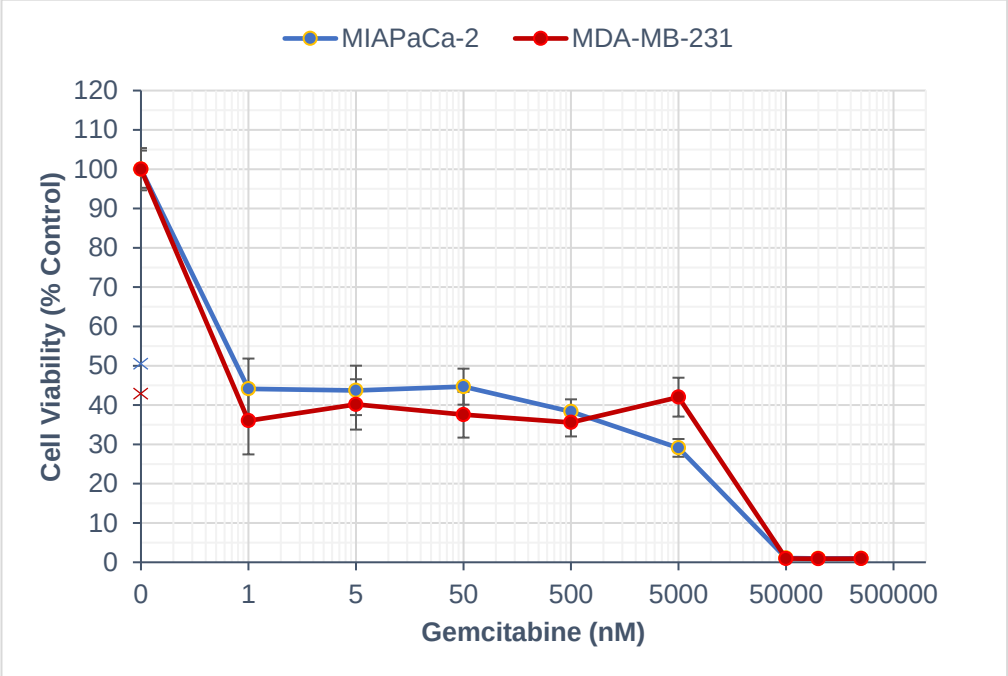

Figure 164. Reduction in MiaPaCa-2 and MDA-MB-231 cancer cell viability in 3D collagen hydrogels after SqGem PCI treatment*. Relative cellular viability (% of control) of MiaPaCa-2 and MDA-MB-231 cells after SqGem PCI treatment at various gemcitabine concentrations (0.5-250,000 nM).*

The $AlPcS_{2a}$ (5 µg/mL) PDT control conducted alongside these PCI experiments was found to reduce cell viability to 51% (±3%) and 43% (±5%) for MiaPaCa-2 and MDA-MB-231 cells, respectively. It can be observed from Figure 164 that SqGem PCI treatment combinations were generally more potent against MDA-MB-231 cells, however, performance was broadly similar across the various concentrations tested (as the statistical non-

significance result demonstrated). Concerning treatment potency, the IC_{70} values were 4,000 nM and 10,000 nM for MiaPaCa-2 and MDA-MB-231 cells, respectively. This represents a 2.5-fold reduction in favour of the pancreatic cancer cell line. At the maximum tested concentration of 250,000 nM, SqGem PCI was found to reduce cell viability to 0% (±0%) in both the pancreatic and breast cancer cell lines. Maximum efficacy (i.e. cell viability reduced to 0% of control) was also achieved at 50,000 nM in both cell lines.

7.8.4.2 Gemcitabine-Polymer PCI

The PCI-performance of the gemcitabine-polymer formulation was then compared between the pancreatic and triple-negative breast cancer cell lines (as shown in Figure 165). Here, it was observed that there was *not* a significant difference (p = 0.719) in cell viability reduction resulting from gemcitabine-polymer PCI between MiaPaCa-2 and MDA-MB-231 cell lines.

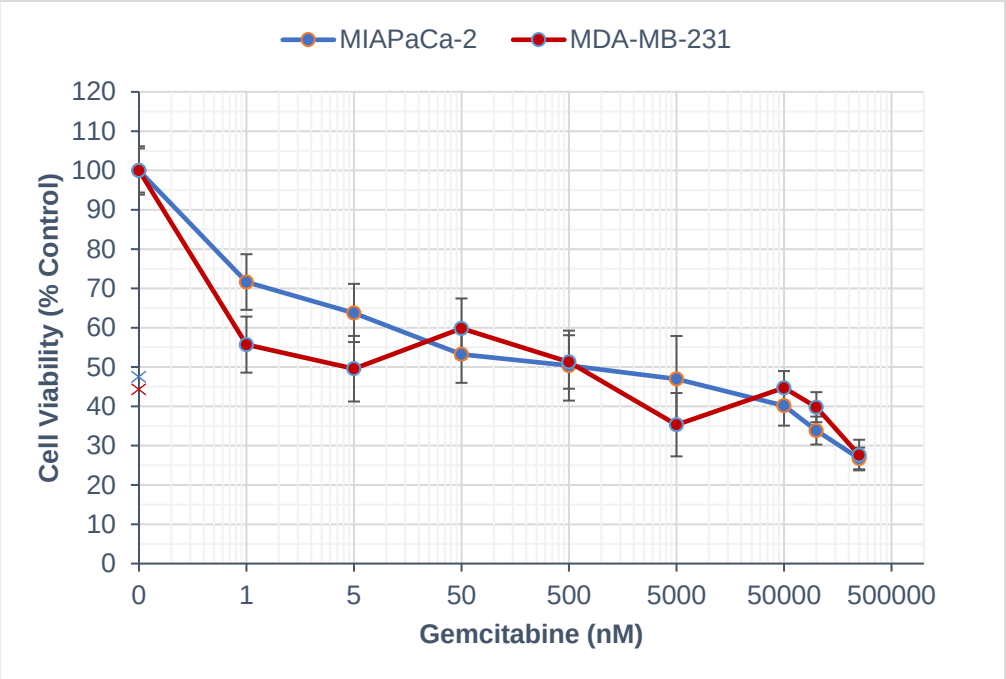

Figure 165. Reduction in MiaPaCa-2 and MDA-MB-231 cancer cell viability in 3D collagen hydrogels after gemcitabine-polymer PCI treatment. *Relative cellular viability (% of control) of MiaPaCa-2 and MDA-MB-231 cells after gemcitabine-polymer PCI treatment at various gemcitabine concentrations (0.5-250,000 nM).*

The $AlPcS_{2a}$ (5 µg/mL) PDT control conducted alongside these PCI experiments was found to reduce cell viability to 47% (±6%) and 44% (±5%) for MiaPaCa-2 and MDA-MB-231 cells, respectively. It can be observed from Figure 165 that polymer-PCI treatment combinations performed similarly in each cell line across the various concentrations tested. With regard to treatment potency, the IC_{70} values were estimated to be 162,500 nM and

200,000 nM for SqGem PCI and polymer-PCI groups, respectively. This represents a 1.2-fold reduction in IC_{70} in favour of MiaPaCa-2 cells. At the maximum tested concentration of 250,000 nM, polymer-PCI treatment was seen to reduce cell viability to 27% (±3%) and 28% (±4%) in MiaPaCa-2 and MDA-MB-231 cells, respectively. This demonstrated that gemcitabine-polymer PCI treatment was equipotent for both the pancreatic and breast cancer cell lines.

7.8.5 Results summary

7.8.5.1 Treatment potency (IC_{70}) and treatment efficacy (E_{max})

The key effects indicative of treatment potency and efficacy (that is, IC_{70} and E_{max}) of the various gemcitabine-based cytotoxic treatments in MiaPaCa-2 and MDA-MB-231 cells were identified from the respective cytotoxicity profiles for each treatment and were compared to gemcitabine-PCI (as shown in Table 22).

The key cytotoxic effects (IC_{70}; E_{max}) of each gemcitabine-based treatment were then compared between the MiaPaCa-2 pancreatic cancer and MDA-MB-231 breast cancer cell lines (as shown in Table 23).

Table 22. Summary of the cytotoxic effects on 3D-cultured MiaPaCa-2 and MDA-MB-231 cells resulting from various gemcitabine-based treatments and compared with gemcitabine PCI.

Gemcitabine Treatment	IC_{70} (nM)				E_{max} (% Control [±SE])			
	MiaPaCa-2	***Potency change (fold)***	***MDA-MB-231***	***Potency change (fold)***	***MiaPaCa-2***	***Efficacy change (fold)***	***MDA-MB-231***	***Efficacy change (fold)***
Chemotherapy	n/a / 4,500 (IC_{50})	- 11,250 (IC_{50})	n/a / n/a (IC_{50})	n/a	33% (±3%)	- 1.4	56% (±6%)	- 1.4
PCI *(Comparator)*	5,000 / 0.40 (IC_{50})	.	n/a / 12.5 (IC_{50})	.	24% (±2%)	.	40% (±5%)	.
-Squalene	3,500 / 875 (IC_{50})	+ 1.4 / - 2,188 (IC_{50})	.	.	0% (±0%)	+ 24	.	.
-Squalene PCI	4,000 / 0.40 (IC_{50})	+ 1.3 / ≡ (IC_{50})	10,000 / 0.30 (IC_{50})	+ 42 (IC_{50})	0% (±0%)	+ 24	0% (±0%)	+ 40
-Polymer PCI	162,500 / 750 (IC_{50})	- 33 / - 1,875	200,000 / 5 (IC_{50})	+ 2.5 (IC_{50})	27% (±3%)	- 1.1	28% (±4%)	+ 1.4

Table 23. Summary of the cytotoxic effects on 3D-cultured MiaPaCa-2 and MDA-MB-231 cells resulting from various gemcitabine-based treatments and compared between each cell line.

Gemcitabine Treatment	IC_{70} (nM)				E_{max} (% Control [±SE])			
	MiaPaCa-2	*Potency change (fold)*	*MDA-MB-231*	*Potency change (fold)*	*MiaPaCa-2*	*Efficacy change (fold)*	*MDA-MB-231*	*Efficacy change (fold)*
Chemotherapy	n/a / 4,500 (IC_{50})	.	n/a / n/a	.	33% (±3%)	+ 1.7	56% (±6%)	.
PCI	5,000 / 0.40 (IC_{50})	+ 31.3 (IC_{50})	n/a / 12.5 (IC_{50})	.	24% (±2%)	+ 1.7	40% (±5%)	.
-Squalene	3,500 / 875 (IC_{50})	.	.	.	0% (±0%)	.	.	.
-Squalene PCI	4,000 / 0.40 (IC_{50})	+ 2.5 / .	10,000 / 0.30 (IC_{50})	. / + 1.3 (IC_{50})	0% (±0%)	≡	0% (±0%)	≡
-Polymer PCI	162,500 / 750 (IC_{50})	+ 1.2 / .	200,000 / 5 (IC_{50})	. / + 150 (IC_{50})	27% (±3%)	≡	28% (±4%)	≡

7.8.5.2 Treatment Synergy

Next, the treatment synergy values achieved by the various gemcitabine-based cytotoxic treatments were identified and summarised (see Table 24). Specifically, the results obtained for the percentage of synergistic treatment combinations, the highest *α* values achieved and at what drug concentrations. In addition, the average *α* value achieved by the synergistic treatment combinations was calculated and is also reported in Table 24.

Table 24. Summary of treatment synergy from various gemcitabine-based treatments in MiaPaCa-2 and MDA-MB-231 cancer cells in 3D collagen hydrogels.

Chemotherapy Drug / Formulation	Comparator	Synergy (α)							
		MiaPaCa-2				MDA-MB-231			
		Synergistic combinations (%) / Ave		*Highest α value*	*Conc (nM)*	*Synergistic combinations (%) / Ave*		*Highest α value*	*Conc (nM)*
Gemcitabine PCI	Chemotherapy (& PDT)	75	1.3 (±0.2)	1.5 (±0.2)	50	25	1.2 (±0.2)	1.2 (±0.1)	100,000
SqGem PCI		88	9.1 (±1.4)	21.0 (±3.4)	100,000	50	20.9 (±3.1)	29.8 (±4.7)	100,000
Gemcitabine-Polymer PCI		0	0.7 (±0.1)	1.0 (±0.2)	50	13	1.5 (±0.7)	1.5 (±0.7)	5,000
SqGem PCI	PCI	100	9.6 (±1.1)	26.3 (±2.2)	250,000	88	21.2 (±1.5)	49.8 (±5.1)	50,000
Gemcitabine-Polymer PCI		25	1.6 (±0.6)	1.9 (±0.8)	5,000	88	1.7 (±0.6)	3.7 (±2.0)	5,000
SqGem PCI	SqGem	38	1.4 (±0.3)	1.7 (±0.7)	5	.	.	.	.
SqGem PCI	Gemcitabine-Polymer PCI	100	14.7 (±1.7))	40.9 (±4.3)	50,000	88	19.1 (±1.4)	50.4 (±5.1)	50,000

7.8.6 Discussion

Previous chapters have demonstrated the ability of PCI to improve treatment outcomes over chemotherapy in two separate 3D *in vitro* models of breast cancer. Next, selected PCI-drug combinations (PCI-bleomycin; PCI-vincristine; and, PCI-gemcitabine) were tested in a 3D *in vitro* model of pancreatic cancer model utilising MiaPaCa-2 cells and collagen hydrogels (type I, 25 µL, 2 mg/mL). As outlined beforehand, pancreatic cancer is a notoriously difficult cancer to treat and has relatively few treatment options. Of these, gemcitabine (alongside FOLFIRINOX) is at the fore-front of clinical treatment recommendations both as a single-agent and in combinational therapy. Subsequently, in addition to evaluating the performance of PCI-bleomycin, two gemcitabine formulations were also combined with PCI and tested in the 3D pancreatic cancer model.

In keeping with previous experiments, initial investigations began with the model PCI chemotherapeutic drug bleomycin. When compared to bleomycin chemotherapy in MiaPaCa-2 cells, PCI-bleomycin increased the potency of treatment by 300-fold and increased efficacy at the highest tested bleomycin concentration by a factor of 4. Both of these PCI-induced increases (potency, in particular) were higher than those achieved in the breast cancer cell lines. Moreover, PCI-bleomycin was most potent and most efficacious (although outright E_{max} values were virtually the same) in MiaPaCa-2 cells when compared to the breast cancer cell lines. Treatment synergy was achieved in 50% of PCI-bleomycin combinations in MiaPaCa-2 cells which was lowest of the three *in vitro* 3D cancer models (25 µL hydrogels). The average α value was also lower, however, the highest α value matched those seen in MDA-MB-231 and MCF-7 cells (all, α = 2.1).

With regard to PCI-vincristine in MiaPaCa-2 cells, treatment potency (IC_{50}) was increased ~2-fold and treatment efficacy increased ~5-fold versus vincristine chemotherapy. Again, upon comparison with the previously reported IC_{70} values, PCI-vincristine performed very consistently once more; with an IC_{70} of 0.48 nM. As previously alluded to, the potency of PCI-vincristine was therefore remarkably similar across all of the various cancer models. With regard to overall efficacy, PCI-vincristine was most efficacious in MiaPaCa-2 cells; outperforming MDA-MB-231 and MCF-7 cells by a factor of 3 and 1.4, respectively. In terms

of synergy, 63% of PCI-vincristine combinations achieved synergistic interactions. Although this is fewer than the breast cancer cell lines, both the average α value (1.7) and the highest α value (2.9) were comparable. This demonstrates, therefore, that when synergy did occur, is was to a similar extent as that achieved in the breast cancer models.

Gemcitabine chemotherapy did not achieve the IC_{70} concentration in MiaPaCa-2 cells therefore, as in previous cases, potency comparisons were made using the IC_{50} concentrations. Here, PCI-gemcitabine potency was 11,250-fold greater than gemcitabine chemotherapy in MiaPaca-2 cells. A modest increase in treatment efficacy at 250,000 nM (E_{max}) was also observed with PCI in comparison to chemotherapy. In terms of outright potency (IC_{70}), PCI-vincristine performed the best (0.48 nM) in MiaPaCa-2 cells, followed by PCI-bleomycin (500 nM), and then PCI gemcitabine (5,000 nM). Interestingly, though, IC_{50} comparisons between the three cancer models reveal that PCI-gemcitabine was much more potent and efficacious in MiaPaCa-2 cells than the breast cancer cell lines. This correlates well with the place of gemcitabine at the forefront of pancreatic cancer treatment. That said, as with potency, both PCI-bleomycin and PCI-vincristine were more efficacious at 250,000 nM than was PCI-gemcitabine in MiaPaCa-2 pancreatic cancer cells. In addition, 75% of PCI-gemcitabine combinations were synergistic in pancreatic cancer cells which was higher than both breast cancer cell lines. Moreover, PCI-gemcitabine achieved its highest α value (1.5) and highest average α value (1.3) in MiaPaCa-2 cells. Yet, although synergy in MiaPaCa-2 cells occurred more frequently with PCI-gemcitabine, when it did occur, it was on average lower than both PCI-bleomycin and PCI-vincristine.

Encouragingly, all three PCI-drug combinations were, in general, found to be most potent *and* most efficacious against 3D-cultured MiaPaCa-2 human pancreatic cancer cells when compared with MDA-MB-231 and MCF-7 human breast cancer cells. Plus, although PCI-gemcitabine was most cytotoxic in MiaPaCa-2 cells when compared with its performance in the breast cancer models, it was, in general, less efficacious and less potent than the other PCI-drug combinations evaluated in MiaPaCa-2 cells.

The final group of experiments involved the use of novel gemcitabine formulations in conjunction with PCI technology. Namely, a methacrylate-based gemcitabine-monomer

conjugate which was then RAFT-polymerised to form a gemcitabine-polymer conjugate (164). The resulting conjugates formed well-defined nanoparticles of 130 nm in size in aqueous suspension (Table 21, Figure 149); which has also been previously reported (164). The second formulation was a squalene derivative of gemcitabine (SqGem). These bioconjugates spontaneously aggregate in water and were seen to form nanoparticles of 430 nm in size. This size is larger than that reported in the literature where nanoparticles of ~100-200 nm have typically been formed (153). Further optimisation of the nanoparticle formation method might have brought the overall size more in line with the literature. However, there *are* clinical formulations that exist with "larger-sized" nanoparticles. For instance, the PDT formulation Visudyne® is an intravenously-administered liposomal formulation of the photosensitiser verteporfin with nanoparticles of around 300 nm in size (208). The larger size of the SqGem nanoparticles might also favour endocytic uptake which would be beneficial in PCI. Notwithstanding, the primary concern of this work was the cytotoxic performance of the nanoparticle formulation(s) rather than the optimisation of nanoparticle size.

The addition of squalene and polymer moieties to gemcitabine is deliberately performed at the 4-amino position in order to inhibit its rapid deamination and, thus, its degradation. This conjugation converts native gemcitabine into a more amphiphilic compound capable of interaction with cellular membranes (209). For instance, in addition to endocytic uptake, SqGem nanoparticles have been shown to passively diffuse into tumour cells and accumulate within cellular and organelle membranes (210). In terms of antitumour cytotoxicity *in vitro* (and *in vivo*), SqGem has been shown to be significantly superior to gemcitabine chemotherapy in both gemcitabine-sensitive and -resistant pancreatic tumour models (210).

Indeed, in the present study, SqGem monotherapy was found to be both more potent (1.4-fold) and much more efficacious at 250,000 nM (24-fold) in MiaPaCa-2 cells than even PCI-gemcitabine. Similarly, PCI-delivery of SqGem was 1.4-fold and 42-fold (IC_{50}) more potent than PCI-gemcitabine in MiaPaCa-2 cells and MDA-MB-231 cells, respectively. Combined SqGem and PCI also yielded impressive results over PCI-gemcitabine in terms of overall treatment efficacy at 250,000 nM. Specifically, PCI-SqGem increased cytotoxicity 24-fold and 40-fold in MiaPaCa-2 and MDA-MB-231 cancer cell lines, respectively (Table 22). These results are particularly salient, as, MiaPaCa-2 cells are classified as being moderately

resistant to gemcitabine (209). Thus, pancreatic cancers with a greater gemcitabine sensitivity (e.g. Capan1 or BxPC3) could potentially derive an even greater therapeutic benefit from this novel PCI-SqGem combination.

Upon comparison of the pancreatic cancer and TNBC cell lines, PCI-SqGem was found to be 2.5-fold more potent (IC_{70}) in MiaPaCa-2 cells. In terms of efficacy, this formulation-PCI combination was maximally efficacious in both cell lines. The magnitude of the cytotoxicity exhibited by this powerful PCI-drug combination can also be realised upon the additional observation that maximal efficacy was achieved at a concentration of 50,000 nM. By contrast, the majority of PCI-drug combinations (save for PCI-vinorelbine and PCI-vinblastine) failed to achieve maximal efficacy even at the 5-fold higher concentration of 250,000 nM.

PCI-SqGem also produced extremely impressive results in terms of treatment synergy across multiple comparators and in both MiaPaCa-2 and MDA-MB-231 cells. For instance, when compared with PCI-gemcitabine, PCI-SqGem generated synergistic interactions in 100% and 88% of PCI-SqGem combinations in MiaPaCa-2 and MDA-MB-231 cells, respectively. Moreover, the highest α values were massively higher than those obtained from other PCI-drug combinations at 26.3 (MiaPaCa-2) and 49.8 (MDA-MB-231), respectively. Similarly, average α values were elevated to 9.6 and 21.2 for the pancreatic cancer and TNBC cells, respectively. Interestingly, on comparing the respective performances of PCI-SqGem and SqGem in MiaPaCa-2 cells (Figure 152, Table 22, Table 23): it can be observed that although the majority of cytotoxic benefit was derived from the formulation element, delivery *via* PCI still produced additional benefit over SqGem alone. Specifically, 38% of PCI-SqGem combinations were found to be synergistic versus SqGem and all of these occurred at the lower concentrations of between 0.5-50 nM.

As previously introduced, squalene is a substrate of the LDL receptor (LDLR) – a receptor known to be moderately- and highly-expressed in MiaPaCa-2 and MDA-MB-231 cells, respectively (153,211). Indeed, a LDLR-driven benefit from the formulation of gemcitabine with squalene in these cancer cell lines is supported by the data presented in this study. Although, admittedly, striking results were seen in both pancreatic and TNBC cells, in

general, MDA-MB-231 cells were seen to benefit to a greater extent. Sobot et al., recently reported that cellular uptake of SqGem nanoparticles was greater in high-LDLR, MDA-MB-231 cells versus low-LDLR, MCF-7 cells (153). Moreover, this study demonstrated both *in vitro* and *in vivo* that SqGem molecules spontaneously associate and interact with blood plasma lipoproteins which then act as an endogenous carrier of this drug-lipid bioconjugate (SqGem). In experiments with human blood, Sobot and colleagues also showed that SqGem has a 500-fold higher affinity for LDL in comparison to albumin. By contrast, free gemcitabine was primarily recovered in the water phase (without association with LDL or any other plasma proteins). These observations could also support our earlier hypothesis that the water-soluble free gemcitabine preferentially accumulated in ECM compartments during chemotherapy and PCI-gemcitabine experiments – thus reducing drug uptake and the subsequent therapeutic effect. Finally, endocytic uptake of LDL has been proven to be highly increased in rapidly growing malignant cancer cells (212). This could account for the PCI-induced synergistic interactions observed at lower SqGem concentrations in MiaPaca-2 cells.

Interestingly, it has also been reported that squalene itself has the potential to inhibit cancer cell proliferation through decreasing oncogene (e.g. ras) activation (152). In essence, squalene decreases farnesyl pyrophosphate levels which is an essential enzyme required in the mechanism of activating cytosolic proteins expressed by oncogenes such as ras. In reducing farnesyl pyrophosphate levels, the necessary relocation of proteins to the plasma membrane (where they are activated) is also reduced. Incidentally, photochemical damage to cellular membranes during PCI could also disrupt this type of required relocation and the subsequent signal-transduction of cell-transforming activity. Importantly, both pancreatic and breast cancers are associated with ras mutations so, in the event of inhibition by squalene, this could further explain why such remarkable therapeutic gains were observed from the SqGem formulation (159).

In terms of treatment potency, PCI delivery of the second, polymer-gemcitabine formulation was found to be much inferior to PCI-gemcitabine in MiaPaCa-2 cells and slightly superior (IC_{50}) in MDA-MB-231 cells. Across all of the tested concentrations, polymer-gemcitabine PCI performed similarly in each cell line (no significant difference) and was essentially equivalently efficacious at 250,000 nM. Interestingly, though, PCI of gemcitabine-

polymer was synergistic in 88% of concentrations in TNBC cells (Figure 163, Table 24) when compared with PCI-gemcitabine; but synergistic in only 13% of concentrations when compared with chemotherapy (& PDT – i.e. as separate components). This can be understood when recognising that PCI-gemcitabine was generally highly antagonistic in its cytotoxic effect when combined in a PCI regimen - versus when synergy treatment effects were calculated using gemcitabine chemotherapy as a standalone treatment (in conjunction with PDT).

The relatively poor performance of the gemcitabine-polymer formulation is not altogether surprising in light of the literature that has been previously published by our group (164). Namely, that the benefit over gemcitabine chemotherapy (and, potentially, PCI-gemcitabine) seems to be derived over a longer time-frame (in MiaPaCa-2 cells, at least) than the ~5 days of experimentation that was carried out in the present work. Thus, the real utility of this formulation in PCI experiments might only be truly realised with more prolonged experiments whereby the depot-like effect can be fully exploited.

The data presented here therefore indicate that SqGem greatly enhanced the cellular uptake of gemcitabine *via* LDLR uptake and thus potentiated its cytotoxic effect in a synergistic manner. Moreover, squalene can itself induce anticancer intracellular events. The utilisation of SqGem as part of a PCI regimen can enhance all-round treatment performance yet further (particularly at lower drug concentrations). The impressive results of PCI-SqGem are therefore likely to be the result of a convergence of multiple cytotoxic mechanisms coming together in order to produce a potent, efficacious, and synergistic treatment modality.

As outlined throughout this Thesis, both PCI and SqGem have favourable pharmacological and toxicological characteristics which could benefit clinical translation. Indeed, the clinical use of PCI has already been shown to be safe and effective in humans (47,90); and, an ongoing clinical trial is currently exploring the use of PCI and gemcitabine for non-resectable cholangiocarcinoma (91). In addition, SqGem combines an endogenous lipid biomolecule (squalene) with an already well-known chemotherapy drug (gemcitabine). Preclinical *in vivo* studies have also shown that squalenoylation of gemcitabine favourably modifies drug pharmacokinetics and biodistribution. Moreover, that it results in a considerably

higher drug distribution to the organs of the reticuloendothelial system (RES), such as the liver and spleen – which are common sites for cancer metastases (210). Crucially, these favourable SqGem properties could also translate to treatment in humans, too, as intravenously-administered SqGem has been shown to strongly interact with cholesterol-rich lipoproteins, such as LDL, which are central to the RES (153). Although optimisation of light-dosing schedules still presents a real challenge to clinicians and PCI researchers alike, the impressive treatment outcomes outlined herein make PCI-SqGem a prime candidate for further preclinical and clinical investigations in the anticancer therapeutic space.

Chapter 8: General Conclusions & Future Work

8. General Conclusions and Future Work

8.1 Conclusions

In total, eight chemotherapy drugs were evaluated for their therapeutic activity against MDA-MB-231 and MCF-7 human breast cancer cell lines embedded within a 3D *in vitro* model. These cell lines each represent a breast cancer subtype (TNBC and luminal A, respectively) which exhibit different molecular characteristics (including morphology and gene expression), response to chemotherapy, and prognosis at a clinical level.

In regard to cellular responses to chemotherapy, MDA-MB-231 cells were much more resistant to cytotoxic drug treatment than were MCF-7 cells. This included increased resistance to those front-line chemotherapy drugs recommended for advanced breast cancer in the clinical setting; that is, docetaxel, vinorelbine, and capecitabine.

In general, the vinca alkaloid drug class performed very well in all of the conditions and cell lines. Furthermore, the most potent and efficacious drugs in each experimental group (48 h and 72 h), for each breast cancer cell line, aligned very well with the drugs recommended in the clinical setting for advanced breast cancer; in particular, vinorelbine and docetaxel. Our investigations demonstrated that $AlPcS_{2a}$ was an effective photosensitiser for both PDT and PCI applications in the 3D *in vitro* breast cancer models.

Importantly, effective PCI therapy was achieved for numerous PCI-drug combinations at a low light fluence rate (2.0 mW/cm^2) and total red light dosage (0.12 J/cm^2). Moreover, this light dosage alone was shown not to increase cell viability.

In keeping with previous studies, PCI-bleomycin was found to potentiate treatment cytotoxicity over bleomycin chemotherapy alone and in a synergistic manner. Interestingly, the PCI-induced increases in treatment efficacy were also seen to occur to a greater extent in the more-resistant MDA-MB-231 cells. Moreover, although PCI-bleomycin *did* perform relatively well, after investigations with the panel of chemotherapy drugs, it was found *not* to be the most potent or efficacious drug when delivered using PCI. Moreover, in terms of the overall percentage of synergistic PCI combinations, *two* other chemotherapy drugs were seen

to either equal or improve upon the performance of bleomycin in this regard. Furthermore, some other chemotherapy drugs also achieved a higher outright synergy (α) value than bleomycin, as well as, a higher average α value (even if this was achieved at a lower percentage of overall combinations).

Excitingly, the cytotoxicity of the vinca alkaloid drugs was seen to be massively potentiated by delivery *via* PCI in both breast cancer models. High degrees of synergy were also observed upon PCI delivery of each of vinorelbine, vincristine, and vinblastine. PCI-docetaxel was also seen to be more efficacious in the TNBC cells (than ER+ cells) and produced treatment synergy. This is particularly promising for vinorelbine and docetaxel as both are front-line chemotherapy drugs recommended in clinical guidelines for advanced breast cancer. Finally, the clinically-recommended combination of gemcitabine and paclitaxel also achieved very positive results from PCI-delivery compared with chemotherapy.

The cytotoxicity profiles and microscopy data presented here also support the literature with respect to the lysosome being a target of microtubule-targeting chemotherapy drugs. It is posited that the inherent destabilising effect of these agents in combination with the lysosome-targeting modality of PCI is what produced the impressive synergistic interactions (especially, with the vinca alkaloids).

Overall, the data presented in this thesis has identified several new promising PCI drug candidates that outperformed PCI-bleomycin in terms of treatment potency, efficacy, and synergy in two different 3D *in vitro* models of breast cancer. The combination of PCI with microtubule-targeting drugs, in particular, appears to possess great future potential.

Experiments whereby key PCI and 3D model parameters were altered also demonstrated that both PCI regimen and cell culture conditions can have a dramatic impact upon PCI treatment outcomes. In fact, in some instances, PCI-bleomycin was much diminished by changes in PCI regimen and the potency of PCI treatment was seen to be completely opposite between monolayer and 3D culture conditions. In addition, microenvironment parameters including hydrogel stiffness and hydrogel volume were also seen to modulate treatment outcomes. Excitingly, PCI-vincristine appears to be a remarkably consistent PCI modality across various *in vitro* models of cancer.

The final chapter utilised an additional 3D *in vitro* model of pancreatic cancer. Pancreatic cancer is a notoriously difficult cancer to treat and has limited treatment options, therefore, three PCI-drug combinations, as well, as novel nanoformulations were tested against MiaPaCa-2 human pancreatic cancer cells. Due to gemcitabine being at the forefront of clinical treatment recommendations (both as monotherapy and in combinational regimens) for this malady it featured heavily in these latter investigations, despite demonstrating relatively poor performance in previous breast cancer models.

Encouragingly, all three PCI-drug combinations (PCI-bleomycin, PCI-vincristine, and PCI-gemcitabine) were generally found to be most potent *and* most efficacious against 3D-cultured MiaPaCa-2 human pancreatic cancer cells when compared with the human breast cancer cells. That said, PCI-gemcitabine was mostly outperformed by the other two PCI-drug combinations evaluated in MiaPaCa-2 cells.

Finally, the final group of experiments involved the use of novel gemcitabine nanoformulations in conjunction with PCI technology. Namely, a gemcitabine-polymer conjugate and a squalene bioconjugate derivative of gemcitabine (SqGem). PCI-SqGem was found to be a powerful PCI-drug treatment modality achieving maximal efficacy at doses much lower than any other PCI-drug combination. PCI-SqGem also produced extremely impressive results in terms of treatment synergy across multiple comparators and in both MiaPaCa-2 and MDA-MB-231 cells. It is posited that this resulted from the combination of LDLR-targeting with the inherent anticancer effects of squalene itself (in addition to the other benefits of PCI delivery). In relation to the polymer-gemcitabine nanoformulation, performance was seen to be relatively poor. However, the real utility of this formulation in PCI experiments might only be truly realised with more prolonged experiments whereby the depot-like effect can be fully exploited.

8.2 Future Work

The PCI treatment modality allows for almost an infinite combination of different variables but the ones established and outlined in this work may form a good basis for those wishing to conduct further investigations. For instance, combining these promising PCI-drugs with the

$TPCS_{2a}$ photosensitiser would be pertinent given its recent use in the clinical setting (47). Moreover, this work identified several promising new PCI-drug combinations and also tentatively put forward the drug classes from which additional promise may be derived. There is still, therefore, a multitude of other chemotherapy drugs awaiting testing for compatibility with PCI; with the microtubule-targeting agents chief amongst the prime candidates to begin with.

Moreover, PCI-vincristine performed very consistently across various conditions so it would be interesting to see how this PCI combination would perform in other cancer types. The natural progression of this work would be to test these promising combinations in *in vivo* models of the cancers that have been modelled *in vitro* in this work. In particular, the pancreatic and triple-negative breast cancer types. It would also be interesting to investigate whether the high potency of the PCI-vinca alkaloid combinations across a large-range of concentrations would help offset some of the light-dosing issues experienced in the clinic. Furthermore, it would be pertinent to explore whether these potent regimens could be used in some kind of cancer vaccine.

The promising drug candidates in this work also have several clinical indications for anticancer treatment so there also remains numerous other human cancer cell lines upon which to test these potent combinations. It is hoped that the testing of these combinations in a biomimetic 3D model will allow for the better alignment of treatment outcomes between the *in vitro* and *in vivo* setting and, hopefully, better-inform how these agents might behave in the clinical setting. In addition, the modelling of the cytotoxic effects of these therapeutic agents may be further aided by the use of a heterotypic cell culture system combining both cancer- and stromal-cell components.

All of the chemotherapy drugs utilised in this work are already clinically-approved and are well-known to clinicians and healthcare authorities worldwide. It is hoped that this work will, following the appropriate preclinical testing, ultimately stimulate trials in humans in order that cancer patients can benefit from these potent treatment combinations.

Finally, the SqGem formulation was seen to be particularly potent and efficacious and achieved impressive synergy interactions across two different types of aggressive cancers

with poor clinical prognoses. This nanoformulation therefore warrants further investigation in other cancer models whether as a single-agent chemotherapy or as a part of a PCI regimen.

Reference List

1. Dolmans DE, Fukumura D, Jain RK. Photodynamic therapy for cancer. *Nat Rev Cancer*. 2003;3(5): 375–380.

2. Josefsen LB, Boyle RW. Photodynamic therapy and the development of metal-based photosensitisers. *Met Based Drugs*. 2008;2008.

3. Finsen NR. *Phototherapy*. London: Arnold; 1901.

4. Raab O. Uber die wirkung fluoreszierender stoffe auf infusorien. *Zeitung Biol*. 1900;39: 524–526.

5. von Tappeiner H, Jesionek A. Therapeutische versuche mit fluoreszierenden stoffen. *Muench Med*. 1903;47: 2042–2044.

6. Prime J. Les accidents toxiques par l'eosinate de sodium. Paris: Jouve and Boyer; 1900.

7. Hausmann W. Die sensiblisierende wirkung des hematoporphyrins. *Biochem Zeitung*. 1911;30: 276–316.

8. Meyer–Betz F. Untersuchungen uber die biologische photodynamische wirkung des hematoporphyrins und anderer derivative des blut und galenafarbstoffs. *Dtsch Arch Klin*. 1913;112: 476–503.

9. Schwartz SK, Absolon K, Vermund H. Some relationships of porphyrins, X-rays and tumours. *Univ Minn Med Bull*. 1955;27: 7–8.

10. Lipson RL, Baldes EJ, Olsen A. The use of a derivative of hematoporhyrin in tumor detection. *J Natl Cancer Inst*. 1961;26: 1–11.

11. Diamond I, Mcdonagh A, Wilson C, Granelli S, Nielsen S, Jaenicke R. Photodynamic therapy of malignant tumours. *Lancet*. 1972;300(7788): 1175–1177.

12. Dougherty TJ, Grindey GB, Fiel R, Weishaupt KR, Boyle DG. Photoradiation therapy. II. Cure of animal tumors with hematoporphyrin and light. *J Natl Cancer Inst*. 1975;55(1): 115–121.

13. Dougherty TJ, Kaufman JE, Goldfarb A, Weishaupt KR, Boyle D, Mittleman A. Photoradiation therapy for treatment of malignant tumors. *Cancer Res*. 1978;38(8): 2628–2635.

14. Kelly JF, Snell ME, Berenbauai MC. Photodynamic destruction of human bladder carcinoma. *Br J Cancer*. 1975;31(2): 237–244.

15. Brown SB, Brown EA, Walker I. The present and future role of photodynamic therapy in cancer treatment. *Lancet Oncol* [Internet]. 2004;5(8): 497–508. Available from: http://www.ncbi.nlm.nih.gov/pubmed/15288239 [Accessed 2nd August 2018].

16. Huang Z. A review of progress in clinical photodynamic therapy. *Technol Cancer Res Treat*. 2005;4(3): 283–293.

17. Szeimies RM, Matheson RT, Davis SA, Bhatia AC, Frambach Y, Klövekorn W, et al. Topical methyl aminolevulinate photodynamic therapy using red light-emitting diode light for multiple actinic keratoses: A randomized study. *Dermatologic Surg*. 2009;35(4): 586–592.

18. van Straten D, Mashayekhi V, de Bruijn HS, Oliveira S, Robinson DJ. Oncologic photodynamic therapy: Basic principles, current clinical status and future directions. *Cancers (Basel)*. 2017;9(2): 1–54.

19. Luo D, Carter KA, Miranda D, Lovell JF. Chemophototherapy: An emerging treatment option for solid tumors. *Adv Sci*. 2017;4(1): 1–24.

20. Moan J, Berg K. The photodegrdation of Porphyrins in cells can be used to estimate the lifetime of singlet oxygen. *Photochem Photobiol*. 1991;53(4): 549–553.

21. Woodburn KW, Vardaxis NJ, Hill JS, Kaye AH, Phillips DR. Subcellular localisation of porphyrins using confocal laser scanning microscopy. *Photochem Photobiol*. 1991;54(5): 725–732.

22. Weizman E, Rothmann C, Greenbaum L, Shainberg A, Adamek M, Ehrenberg B, et al. Mitochondrial localization and photodamage during photodynamic therapy with tetraphenylporphines. *J Photochem Photobiol B Biol*. 2000;59(1–3): 92–102.

23. Raymond KN, Pierre VC. Next generation, high relaxivity gadolinium MRI agents. *Bioconjugate Chem*. 2005;16(1): 3–8.

24. Berg K, Prasmickaite L, Selbo PK, Hellum M, Bonsted A, Høgset A. Photochemical internalization (PCI)--a novel technology for release of macromolecules from endocytic vesicles. *Oftalmologia* [Internet]. 2003;56(1): 67–71. Available from: http://www.ncbi.nlm.nih.gov/pubmed/12886687 [Accessed 4th August 2018].

25. Henderson BW, Dougherty TJ. How does photodynamic therapy work? *Photochem Photobiol*. 1992;55(1): 145–57.

26. Oliveira CS, Turchiello R, Kowaltowski AJ, Indig GL, Baptista MS. Major determinants of photoinduced cell death: Subcellular localization versus photosensitization efficiency. *Free Radic Biol Med*. 2011;51(4): 824–833.

27. Igney FH, Krammer PH. Death and anti-death: tumour resistance to apoptosis. *Nat Rev Cancer* [Internet]. 2002;2(4): 277–288. Available from: http://www.nature.com/doifinder/10.1038/nrc776 [Accessed 4th August 2018].

28. Wu S, Xing D. Mechanism of mitochondrial membrane permeabilization during apoptosis under photofrin-mediated photodynamic therapy. *J Xray Sci Technol*. 2012;20(3): 363–372.

29. Nagata S, Obana A, Gohto Y, Nakajima S. Necrotic and apoptotic cell death of human malignant melanoma cells following photodynamic therapy using an amphiphilic photosensitizer, ATX-S10(Na). *Lasers Surg Med*. 2003;33(1): 64–70.

30. Levine B, Klionsky DJ. Development by self-digestion: Molecular mechanisms and biological functions of autophagy. *Dev Cell*. 2004;6(4): 463–477.

31. Inguscio V, Panzarini E, Dini L. Autophagy contributes to the death/survival balance in cancer photodynamic therapy. *Cells* [Internet]. 2012;1(3): 464–491. Available from: http://www.mdpi.com/2073-4409/1/3/464 [Accessed 5th August 2018].

32. Kessel DH, Price M, Reiners JJ. ATG7 deficiency suppresses apoptosis and cell death induced by lysosomal photodamage. *Autophagy*. 2012;8(9): 1333–1341.

33. Castano AP, Demidova TN, Hamblin MR. Mechanisms in photodynamic therapy: Part three - Photosensitizer pharmacokinetics, biodistribution, tumor localization and modes of tumor destruction. *Photodiagnosis Photodyn Ther*. 2005;2(2):91–106.

34. Dolmans DE, Kadambi A, Hill JS, Flores KR, Gerber JN, Walker JP, et al. Targeting tumor vasculature and cancer cells in orthotopic breast tumor by fractionated photosensitizer dosing photodynamic therapy. *Cancer Res*. 2002;62(15): 4289–4294.

35. Castano A, Mroz P, Hamblin M. Photodynamic therapy and anti-tumour immunity. *Nat Rev Cancer* [Internet]. 2006;6(7): 535–545. Available from: http://www.nature.com/nrc/journal/v6/n7/abs/nrc1894.html [Accessed 6th August 2018].

36. Vabulas RM, Wagner H, Schild H. Heat shock proteins as ligands of toll-like receptors. *Curr Top Microbiol Immunol* [Internet]. 2002;270: 169–184. Available from: http://www.ncbi.nlm.nih.gov/pubmed/12467251 [Accessed 6th August 2018].

37. Korbelik M, Dougherty GJ. Photodynamic therapy-mediated immune response against subcutaneous mouse tumors. *Cancer Res*. 1999;59(8): 1941–1946.

38. Gollnick SO, Vaughan L, Henderson BW. Generation of effective antitumor vaccines using photodynamic therapy. *Cancer Res*. 2002;62(6): 1604–1608.

39. Hopper C. Photodynamic therapy: a clinical reality in the treatment of cancer. *Lancet Oncol* [Internet]. 2000;1(4): 212–219. Available from: http://www.sciencedirect.com/science/article/pii/S1470204500001662 [Accessed 7th August 2018].

40. Shafirstein G, Bellnier D, Oakley E, Hamilton S, Potasek M, Beeson K, et al. Interstitial Photodynamic Therapy — A Focused Review. *Cancers (Basel)*. 2017;9(2): 1–14.

41. Li LB, Xie JM, Zhang XN, Chen JZ, Luo YL, Zhang LY, et al. Retrospective study of photodynamic therapy vs photodynamic therapy combined with chemotherapy and chemotherapy alone on advanced esophageal cancer. *Photodiagnosis Photodyn Ther* [Internet]. 2010;7(3): 139–143. Available from: https://www.sciencedirect.com/science/article/abs/pii/S1572100010000670?via%3Dihub [Accessed 7th August 2018].

42. Zuluaga MF, Lange N. Combination of photodynamic therapy with anti-cancer agents. *Curr Med Chem* [Internet]. 2008;15(17): 1655–1673. Available from: http://www.eurekaselect.com/openurl/content.php?genre=article&issn=0929-8673&volume=15&issue=17&spage=1655 [Accessed 8th August 2018].

43. Cowled PA, Mackenzie L, Forbes IJ. Pharmacological Modulation of Photodynamic Therapy with Hematoporphyrin Derivative and Light. *Cancer Res*. 1987;47(4): 971–974.

44. Canti G, Nicolin A, Cubeddu R, Taroni P, Bandieramonte G, Valentini G. Antitumor efficacy of the combination of photodynamic therapy and chemotherapy in murine tumors. *Cancer Lett* [Internet]. 1998;125(1–2): 39–44. Available from: http://www.ncbi.nlm.nih.gov/pubmed/9566694 [Accessed 10th August 2018].

45. Sun G, Anderson MA, Gorospe EC, Leggett CL, Lutzke LS, Wong Kee Song LM, et al. Synergistic effects of photodynamic therapy with HPPH and gemcitabine in pancreatic cancer cell lines. *Lasers Surg Med*. 2012;44(9): 755–761.

46. Berg K, Selbo PK, Prasmickaite L, Tjelle TE, Sandvig K, Moan J, et al. Photochemical internalization: A novel technology for delivery of macromolecules into cytosol. *Cancer Res*. 1999;59(6): 1180–1183.

47. Sultan AA, Jerjes W, Berg K, Høgset A, Mosse CA, Hamoudi R, et al. Disulfonated tetraphenyl chlorin (TPCS2a)-induced photochemical internalisation of bleomycin in patients with solid malignancies: a phase 1, dose-escalation, first-in-man trial. *Lancet Oncol*. 2016;17(9): 1217–1229.

48. Weyergang A, Berstad MEB, Bull-Hansen B, Olsen CE, Selbo PK, Berg K. Photochemical activation of drugs for the treatment of therapy-resistant cancers. *Photochem Photobiol Sci* [Internet]. 2015;14(8): 1465–1475. Available from: http://xlink.rsc.org/?DOI=C5PP00029G [Accessed 11th August 2018].

49. Selbo PK, Weyergang A, Høgset A, Norum OJ, Berstad MB, Vikdal M, et al. Photochemical internalization provides time- and space-controlled endolysosomal escape of therapeutic molecules. *J Control Release*. 2010;148(1): 2–12.

50. de Duve C. The lysosome in retrospect. In: *Lysosome in Biology and Pathology* (Dingle JT, Fell HB., eds). Amsterdam: North-Holland; 1969; 3–40.

51. Kroemer G, Jäättelä M. Lysosomes and autophagy in cell death control. *Nature Rev Cancer*. 2005;5(11): 886–897.

52. Høgset A, Prasmickaite L, Selbo PK, Hellum M, Engesæter B, Bonsted A, et al. Photochemical internalisation in drug and gene delivery. *Adv Drug Deliv Rev*. 2004;56(1): 95–115.

53. De Pinillos Bayona AM, Moore CM, Loizidou M, MacRobert AJ, Woodhams JH. Enhancing the efficacy of cytotoxic agents for cancer therapy using photochemical internalisation. *Int J Cancer*. 2016;138(5): 1049–1057.

54. Norum OJ, Gaustad JV, Angell-Petersen E, Rofstad EK, Peng Q, Giercksky KE, et al. Photochemical internalization of bleomycin is superior to photodynamic therapy due to the therapeutic effect in the tumor periphery. *Photochem Photobiol*. 2009;85(3): 740–749.

55. Norum OJ, Giercksky KE, Berg K. Photochemical internalization as an adjunct to marginal surgery in a human sarcoma model. *Photochem Photobiol Sci*. 2009;8: 758–762.

56. Norum OJ, Bruland ØS, Gorunova L, Berg K. Photochemical internalization of bleomycin before external-beam radiotherapy improves locoregional control in a human sarcoma model. *Int J Radiat Oncol Biol Phys*. 2009;75(3): 878–885.

57. Norum OJ, Fremstedal AS, Weyergang A, Golab J, Berg K. Photochemical delivery of bleomycin induces T-cell activation of importance for curative effect and systemic anti-tumor immunity. *J Control Release*. 2017;268: 120–127.

58. Zahreddine H, Borden KL. Mechanisms and insights into drug resistance in cancer. *Front Pharmacol*. 2013;4(28).

59. Woodhams J, Lou PJ, Selbo PK, Mosse A, Oukrif D, MacRobert A, et al. Intracellular re-localisation by photochemical internalisation enhances the cytotoxic effect of gelonin--quantitative studies in normal rat liver. *J Control Release* [Internet]. 2010;142(3): 347–353. Available from: http://www.ncbi.nlm.nih.gov/pubmed/19932724 [Accessed 13th August 2018].

60. Selbo PK, Sivam G, Fodstad Y, Sandvig K, Berg K. In vivo documentation of photochemical internalization, a novel approach to site specific cancer therapy. *Int J Cancer*. 2001;92(5): 761–766.

61. Norum OJ, Selbo PK, Weyergang A, Giercksky KE, Berg K. Photochemical internalization (PCI) in cancer therapy: From bench towards bedside medicine. *J Photochem Photobiol B Biol* [Internet]. 2009;96(2): 83–92. Available from: http://dx.doi.org/10.1016/j.jphotobiol.2009.04.012 [Accessed 13th August 2018].

62. Waeckerle-Men Y, Mauracher A, Håkerud M, Mohanan D, Kündig TM, Høgset A, et al. Photochemical targeting of antigens to the cytosol for stimulation of MHC class-I-restricted T-cell responses. *Eur J Pharm Biopharm*. 2013;85(1): 34–41.

63. Håkerud M, Waeckerle-Men Y, Selbo PK, Kündig TM, Høgset A, Johansen P. Intradermal photosensitisation facilitates stimulation of MHC class-I restricted CD8 T-cell responses of co-administered antigen. *J Control Release*. 2014;174(1): 143–150.

64. Doherty GJ, McMahon HT. Mechanisms of endocytosis. *Annu Rev Biochem* [Internet]. 2009;78(1): 857–902. Available from: http://www.annualreviews.org/doi/10.1146/annurev.biochem.78.081307.110540 [Accessed 13th August 2018].

65. Gèze M, Morlière P, Mazière JC, Smith KM, Santus R. Lysosomes, a key target of hydrophobic photosensitizers proposed for photochemotherapeutic applications. *J Photochem Photobiol B Biol*. 1993;20(1): 23–35.

66. Prasmickaite L, Høgset A, Berg K. Evaluation of different photosensitizers for use in photochemical gene transfection. *Photochem Photobiol*. 2001;73(4): 388–395.

67. Berg K, Selbo PK, Weyergang A, Dietze A, Prasmickaite L, Bonsted A, et al. Porphyrin-related photosensitizers for cancer imaging and therapeutic applications. *J Microsc*. 2005;218(2): 133–147.

68. Ali H, van Lier JE. Metal complexes as photo- and radiosensitizers. *Chem Rev*. 1999;99(9): 2379–2450.

69. Master A, Livingston M, Sen Gupta A. Photodynamic nanomedicine in the treatment of solid tumors: Perspectives and challenges. *J Control Release* [Internet]. 2013;168(1): 88–102. Available from: http://dx.doi.org/10.1016/j.jconrel.2013.02.020 [Accessed 13th August 2018].

70. Ali S, Muhammad S, Khurshid A, Ikram M, Maqsood M, Fisher C, et al. Effective phthalocyanines mediated photodynamic therapy with doxorubicin or methotrexate combination therapy at sub-micromolar concentrations in vitro. *Photodiagnosis Photodyn Ther*. 2018;22: 51–64.

71. Berg K, Nordstrand S, Selbo PK, Tran DT, Angell-Petersen E, Høgset A. Disulfonated tetraphenyl chlorin (TPCS2a), a novel photosensitizer developed for clinical utilization of photochemical internalization. *Photochem Photobiol Sci* [Internet]. 2011;10(10): 1637–1651. Available from: http://www.ncbi.nlm.nih.gov/pubmed/21773635 [Accessed 13th August 2018].

72. Veber DF, Johnson SR, Cheng H, Smith BR, Ward KW, Kopple KD. Molecular properties that influence the oral bioavailability of drug candidates. *J Med Chem*. 2002;45: 2615–2623.

73. Kyowa Kirin Ltd. Bleo-Kyowa Powder for solution for injection. *Summary of Product Characteristics* [Internet]. 2016. Available from: http://www.medicines.org.uk/emc/medicine/26918 [Accessed 13th August 2018].

74. Linnert M, Gehl J. Bleomycin treatment of brain tumors: an evaluation. *Anticancer Drugs*. 2009;20(3): 157–164.

75. Adigbli DK, Wilson DG, Farooqui N, Sousi E, Risley P, Taylor I, et al. Photochemical internalisation of chemotherapy potentiates killing of multidrug-resistant breast and bladder cancer cells. *Br J Cancer* [Internet]. 2007;97(4): 502–512. Available from: https://www.nature.com/articles/6603895 [Accessed 14th August 2018].

76. Lou PJ, Lai PS, Shieh MJ, MacRobert AJ, Berg K, Bown SG. Reversal of doxorubicin resistance in breast cancer cells by photochemical internalization. *Int J Cancer*. 2006;119(11): 2692–2698.

77. Berg K, Høgset A, Prasmickaite L, Weyergang A, Bonsted A, Dietze A, et al. Photochemical internalization (PCI): A novel technology for activation of endocytosed therapeutic agents. *Med Laser Appl*. 2006;21(4): 239–250.

78. Eiklid K, Olsnes S, Pihl A. Entry of lethal doses of abrin, ricin and modeccin into the cytosol of HeLa cells. *Exp Cell Res*. 1980;126(2): 321–326.

79. Prasmickaite L, Høgset A, Selbo PK, Engesaeter BØ, Hellum M, Berg K. Photochemical disruption of endocytic vesicles before delivery of drugs: a new strategy for cancer therapy. *Br J Cancer*. 2002;86(4): 652–657.

80. Fretz MM, Høgset A, Koning GA, Jiskoot W, Storm G. Cytosolic delivery of liposomally targeted proteins induced by photochemical internalization. *Pharm Res*. 2007;24(11): 2040–2047.

81. Lai PS, Pai CL, Peng CL, Shieh MJ, Berg K, Lou PJ. Enhanced cytotoxicity of saporin by polyamidoamine dendrimer conjugation and photochemical internalization. *J Biomed Mater Res - Part A*. 2008;87(1): 147–155.

82. Lu HL, Syu WJ, Nishiyama N, Kataoka K, Lai PS. Dendrimer phthalocyanine-encapsulated polymeric micelle-mediated photochemical internalization extends the efficacy of photodynamic therapy and overcomes drug-resistance in vivo. *J Control Release*. 2011;155(3): 458–64.

83. Tian J, Xu L, Xue Y, Jiang X, Zhang W. Enhancing photochemical internalization of DOX through a porphyrin-based amphiphilic block copolymer. *Biomacromolecules*. 2017;18(12): 3992–4001.

84. Pasparakis G, Manouras T, Vamvakaki M, Argitis P. Harnessing photochemical internalization with dual degradable nanoparticles for combinatorial photo-chemotherapy. *Nat Commun* [Internet]. 2014;5: 3623. Available from: http://www.nature.com/ncomms/2014/140407/ncomms4623/full/ncomms4623.html [Accessed 14th August 2018].

85. Zhu K, Liu G, Hu J, Liu S. Near-infrared light-activated photochemical internalization of reduction-responsive polyprodrug vesicles for synergistic photodynamic therapy and chemotherapy. *Biomacromolecules*. 2017;18(8): 2571–2582.

86. Høgset A, Engesæter BO, Prasmickaite L, Berg K, Fodstad Ø, Mælandsmo GM. Light-induced adenovirus gene transfer, an efficient and specific gene delivery technology for cancer gene therapy. *Cancer Gene Ther*. 2002;9(4): 365–371.

87. Shafirstein G, Battoo A, Harris K, Baumann H, Gollnick SO, Lindenmann J, et al. Photodynamic therapy of non-small cell lung cancer narrative review and future directions. *Ann Am Thorac Soc*. 2016;13(2): 265–275.

88. Agostinis P, Berg K, Cengel KA, Foster TH, Girotti AW, Gollnick SO, et al. Photodynamic therapy of cancer: an update. *CA Cancer J Clin* [Internet]. 2011;61(4): 250–281. Available from: https://www.ncbi.nlm.nih.gov/pmc/articles/PMC3209659/ [Accessed 15th August 2018].

89. Shin D, Christie C, Ju D, Nair RK, Molina S, Berg K, et al. Photochemical internalization enhanced macrophage delivered chemotherapy. *Photodiagnosis Photodyn Ther*. 2018;21: 156–162.

90. PCI Biotech AS. Update on the ENHANCE study. *Press Release* [Internet]. 2015. Available from: http://pcibiotech.no/update-on-the-enhance-study/ [Accessed 15th August 2018].

91. PCI Biotech AS. A phase I/II study safety and efficacy study of PCI of gemcitabine and chemotherapy in patients with cholangiocarcinomas. *Webpage* [Internet]. 2016. Available from: https://clinicaltrials.gov/ct2/show/NCT01900158 [Accessed 15th August 2018].

92. Cancer Research UK. Breast cancer statistics. *Webpage* [Internet]. 2018. Available from: https://www.cancerresearchuk.org/health-professional/cancer-

statistics/statistics-by-cancer-type/breast-cancer#heading-Zero [Accessed 15th August 2018].

93. Vargo-Gogola T, Rosen JM. Modelling breast cancer: One size does not fit all. *Nat Rev Cancer*. 2007;7(9): 659–672.

94. Harrison RG, Greenman MJ, Mall FP, Jackson CM. Observations of the living developing nerve fiber. *Anat Rec*. 1907;1(5): 116–128.

95. Gey GO, Coffmann WD, Kubicek MT. Tissue culture studies of the proliferative capacity of cervical carcinoma and normal epithelium. *Cancer Res*. 1952;12: 264–265.

96. Lacroix M, Leclercq G. Relevance of breast cancer cell lines as models for breast tumours: an update. *Breast Cancer Res Treat* [Internet]. 2004;83(3): 249–289. Available from: http://www.ncbi.nlm.nih.gov/entrez/query.fcgi?cmd=Retrieve&db=PubMed&dopt=Citation&list_uids=14758095 [Accessed 15th August 2018].

97. Lasfargues EY, Ozzello L. Cultivation of human breast carcinomas. *J Natl Cancer Inst*. 1958;21(6): 1131–1147.

98. Cailleau R, Olivé M, Cruciger QV, Coffman W, Kubicek M, Lasfargues E, et al. Long-term human breast carcinoma cell lines of metastatic origin: Preliminary characterization. *In Vitro* [Internet]. 1978;14(11): 911–915. Available from: http://link.springer.com/10.1007/BF02616120 [Accessed 15th August 2018].

99. Soule HD, Vazguez J, Long A, Albert S, Brennan M. A human cell line from a pleural effusion derived from a breast carcinoma. *J Natl Cancer Inst* [Internet]. 1973;51(5): 1409–1416. Available from: http://www.ncbi.nlm.nih.gov/pubmed/4357757 [Accessed 16th August 2018].

100. Holliday DL, Speirs V. Choosing the right cell line for breast cancer research. *Breast Cancer Res*. 2011;13(4): 215.

101. Speirs V, Shaaban AM. The rising incidence of male breast cancer. *Breast Cancer Res Treat*. 2009;115(2): 429–430.

102. Vaclova T, Maguire S, Pugh M, Barry P, Orr N. Molecular and genomic characterization of a newly established male breast cancer cell line. In: *AACR Annual Meeting* [Internet]. 2017;77(13): 816. Available from: http://cancerres.aacrjournals.org/content/77/13_Supplement/816 [Accessed 16th August 2018].

103. Perou CM, Sørile T, Eisen MB, Van De Rijn M, Jeffrey SS, Ress CA, et al. Molecular portraits of human breast tumours. *Nature*. 2000;406(6797): 747–752.

104. Sorlie T, Perou CM, Tibshirani R, Aas T, Geisler S, Johnsen H, et al. Gene expression patterns of breast carcinomas distinguish tumor subclasses with clinical implications. *Proc Natl Acad Sci U S A* [Internet]. 2001;98(19): 10869–10874. Available from: https://www.ncbi.nlm.nih.gov/pmc/articles/PMC58566/ [Accessed 16th August 2018].

105. Osborne CK, Hobbs K, Clark GM. Effect of estrogens and antiestrogens on growth of human breast cancer cells in athymic nude mice. *Cancer Res* [Internet]. 1985;45(2): 584–590. Available from: http://www.ncbi.nlm.nih.gov/pubmed/3967234 [Accessed 16th August 2018].

106. Johnston SJ, Cheung KL. Fulvestrant - a novel endocrine therapy for breast cancer. *Curr Med Chem* [Internet]. 2010;17(10): 902–914. Available from: http://www.ncbi.nlm.nih.gov/pubmed/20156170 [Accessed 16th August 2018].

107. Neve RM, Chin K, Fridlyand J, Yeh J, Frederick L, Fevr T, et al. A collection of breast cancer cell lines for the study of functionally. *Cancer Cell*. 2009;10(6): 515–527.

108. Weigelt B, Bosma AJ, Hart AA, Rodenhuis S, van't Veer LJ. Marker genes for circulating tumour cells predict survival in metastasized breast cancer patients. *Br J Cancer* [Internet]. 2003;88(7): 1091–1094. Available from: http://www.nature.com/articles/6600868 [Accessed 16th August 2018].

109. Yamada KM, Cukierman E. Modeling tissue morphogenesis and cancer in 3D. *Cell*. 2007;130(4): 601–610.

110. Birgersdotter A, Sandberg R, Ernberg I. Gene expression perturbation in vitro—A growing case for three-dimensional (3D) culture systems. *Semin Cancer Biol*. 2005;15(5): 405–412.

111. Breslin S, O'Driscoll L. Three-dimensional cell culture: The missing link in drug discovery. *Drug Discov Today*. 2013;18(5–6): 240–249.

112. Weaver VM, Petersen OW, Wang F, Larabell CA, Briand P, Damsky C, et al. Reversion of the malignant phenotype of human breast cells in three-dimensional culture and in vivo by integrin blocking antibodies. *J Cell Biol* [Internet]. 1997;137(1): 231–245. Available from: http://jcb.rupress.org/content/137/1/231 [Accessed 17th August 2018].

113. Vinci M, Gowan S, Boxall F, Patterson L, Zimmermann M, Court W, et al. Advances in establishment and analysis of 3D tumour spheroid-based functional assays for target validation and drug evaluation. *BMC Biol* [Internet]. 2012;10(1): 29. Available from: http://www.ncbi.nlm.nih.gov/pubmed/22439642 [Accessed 17th August 2018].

114. Ivascu A, Kubbies M. Rapid generation of single-tumor spheroids for high-throughput cell function and toxicity analysis. *J Biomol Screen*. 2006;11(8): 922–932.

115. Tung YC, Hsiao AY, Allen SG, Torisawa YS, Ho M, Takayama S. High-throughput 3D spheroid culture and drug testing using a 384 hanging drop array. *Analyst*. 2011;136(3): 473–478.

116. Nirmalanandhan VS, Duren A, Hendricks P, Vielhauer G, Sittampalam GS. Activity of anticancer agents in a three-dimensional cell culture model. *Assay Drug Dev Technol* [Internet]. 2010;8(5): 581–590. Available from: http://www.ncbi.nlm.nih.gov/pubmed/20662735 [Accessed 17th August 2018].

117. Stevens MM. Exploring and engineering the cell surface interface. *Science* [Internet]. 2005;310(5751): 1135–1138. Available from: http://www.ncbi.nlm.nih.gov/pubmed/16293749 [Accessed 17th August 2018].

118. Lee GY, Kenny PA, Lee EH, Bissell MJ. Three-dimensional culture models of normal and malignant breast epithelial cells. *Nat Methods*. 2010;4(4): 359–365.

119. Lovitt C, Shelper T, Avery V. Advanced cell culture techniques for cancer drug discovery. *Biology (Basel)*. 2014;3(2): 345–367.

120. David L, Dulong V, Le Cerf D, Cazin L, Lamacz M, Vannier JP. Hyaluronan hydrogel: An appropriate three-dimensional model for evaluation of anticancer drug sensitivity. *Acta Biomater*. 2008;4(2): 256–263.

121. Chen SY, Hung PJ, Lee PJ. Microfluidic array for three-dimensional perfusion culture of human mammary epithelial cells. *Biomed Microdevices*. 2011;13(4): 753–758.

122. Butcher DT, Alliston T, Weaver VM. A tense situation: Forcing tumour progression. *Nat Rev Cancer*. 2009;9(2): 108-122.

123. Gennisson JL, Grenier N, Combe C, Tanter M. Supersonic shear wave elastography of in vivo pig kidney: Influence of blood pressure, urinary pressure and tissue anisotropy. *Ultrasound Med Biol*. 2012;38(9): 1559-1567.

124. Wei SC, Fattet L, Tsai JH, Guo Y, Pai VH, Majeski HE, et al. Matrix stiffness drives epithelial-mesenchymal transition and tumour metastasis through a TWIST1-G3BP2 mechanotransduction pathway. *Nat Cell Biol*. 2015;17(5): 678–688.

125. Guzman A, Ziperstein MJ, Kaufman LJ. The effect of fibrillar matrix architecture on tumor cell invasion of physically challenging environments. *Biomaterials*. 2014;35(25): 6954–6963.

126. Joyce JA. Therapeutic targeting of the tumor microenvironment. *Cancer Cell*. 2005;7(6): 513–520.

127. Holliday DL, Brouilette KT, Markert A, Gordon LA, Jones JL. Novel multicellular organotypic models of normal and malignant breast: Tools for dissecting the role of the microenvironment in breast cancer progression. *Breast Cancer Res*. 2009;11(1): R3.

128. Goswami S, Sahai E, Wyckoff JB, Epidermal CF-, Cammer M, Cox D, et al. Macrophages promote the invasion of breast carcinoma cells via a colony-stimulating factor-1/epidermal growth factor paracrine loop. *Cancer Res*. 2005;65(12): 5278–5283.

129. Shekhar MP, Werdell J, Tait L. Interaction with endothelial cells is a prerequisite for branching ductal-alveolar morphogenesis and hyperplasia of preneoplastic human breast epithelial cells: Regulation by estrogen. *Cancer Res*. 2000;60(2): 439–449.

130. Camp JT, Elloumi F, Roman-Perez E, Rein J, Stewart DA, Harrell JC, et al. Interactions with fibroblasts are distinct in basal-like and luminal breast cancers. *Mol Cancer Res* [Internet]. 2011;9(1): 3–13. Available from: http://mcr.aacrjournals.org/cgi/doi/10.1158/1541-7786.MCR-10-0372 [Accessed 18th August 2018].

131. Hopkins AL. Network pharmacology: The next paradigm in drug discovery. *Nat Chem Biol*. 2008;4(11): 682–690.

132. Voskoglou-Nomikos T, Pater JL, Seymour L. Clinical predictive value of the in vitro cell line, human xenograft, and mouse allograft preclinical cancer models. *Clin Cancer Res*. 2003;9(11): 4227–4239.

133. Makhoul I, Montgomery CO, Gaddy D, Suva LJ. The best of both worlds - managing the cancer, saving the bone. *Nat Rev Endocrinol* [Internet]. 2016;12(1): 29–42. Available from: http://www.ncbi.nlm.nih.gov/pubmed/26503674 [Accessed 18th August 2018].

134. Rahib L, Smith BD, Aizenberg R, Rosenzweig AB, Fleshman JM, Matrisian LM. Projecting cancer incidence and deaths to 2030: The unexpected burden of thyroid, liver, and pancreas cancers in the United States. *Cancer Res*. 2014;74(11): 2913–2921.

135. Jemal A, Bray F, Center MM, Ferlay J, Ward E, Forman D. Global cancer statistics. *CA Cancer J Clin*. 2011;61(2): 69–90.

136. Siegel R, Miller K, Jemal A. Cancer statistics, 2015. *CA Cancer J Clin*. 2015;65(1): 5–29.

137. Forman D, Bray F, Brewster D, Gombe Mbalawa C, Kohler B, Piñeros M, et al. Cancer incidence in five continents, Vol. X. *Scientific Publication* [Internet]. 2014. Available from: http://ci5.iarc.fr/CI5I-X/old/vol10/CI5vol10.pdf [Accessed 18th August 2018].

138. Kleeff J, Korc M, Apte M, La Vecchia C, Johnson CD, Biankin AV, et al. Pancreatic cancer. *Nat Rev Dis Prim* [Internet]. 2016;2(April):1–23. Available from: http://dx.doi.org/10.1038/nrdp.2016.22 [Accessed 18th August 2018].

139. Ghosn M, Ibrahim T, Assi T, El Rassy E, Kourie HR, Kattan J. Dilemma of first line regimens in metastatic pancreatic adenocarcinoma. *World J Gastroenterol*. 2016;22(46): 10124–10130.

140. He J, Ahuja N, Makary MA, Cameron JL, Eckhauser FE, Choti MA, et al. 2564 resected periampullary adenocarcinomas at a single institution: Trends over three decades. *HPB (Oxford)*. 2014;16(1): 83–90.

141. Maitra A, Hruban RH. Pancreatic cancer. *Annu Rev Pathol*. 2008;3: 157–188.

142. Moher D, Liberati A, Tetzlaff J, Altman DG, Altman D, Antes G, et al. Preferred reporting items for systematic reviews and meta-analyses: The PRISMA statement. *PLoS Med*. 2009;6(7).

143. Rahib L, Fleshman JM, Matrisian LM, Berlin JD. Evaluation of pancreatic cancer clinical trials and benchmarks for clinically meaningful future trials: A systematic review. *JAMA Oncol* [Internet]. 2016;2(9): 1209–1216. Available from: http://oncology.jamanetwork.com/article.aspx?doi=10.1001/jamaoncol.2016.0585 [Accessed 19th August 2018].

144. Puls TJ, Tan X, Whittington CF, Voytik-Harbin SL. 3D collagen fibrillar microstructure guides pancreatic cancer cell phenotype and serves as a critical design parameter for phenotypic models of EMT. *PLoS One*. 2017;12(11): 1–25.

145. Ma J, Jemal A. The rise and fall of cancer mortality in the USA: Why does pancreatic cancer not follow the trend? *Future Oncol*. 2013;9(7): 917–919.

146. Moreira L, Bakir B, Chatterji P, Dantes Z, Reichert M, Rustgi AK. Pancreas 3D organoids: Current and future aspects as a research platform for personalized medicine in pancreatic cancer. *Cell Mol Gastroenterol Hepatol* [Internet]. 2018;5(3): 289–298. Available from: https://doi.org/10.1016/j.jcmgh.2017.12.004 [Accessed 19th August 2018].

147. National Institute for Health and Care Excellence (NICE). Managing advanced breast cancer. *Advanced Breast Cancer* [Internet]. 2018. Available from: https://pathways.nice.org.uk/pathways/advanced-breast-cancer#path=view%3A/pathways/advanced-breast-cancer/managing-advanced-breast-cancer.xml&content=view-index [Accessed 20th August 2018].

148. National Institute for Health and Care Excellence (NICE). Managing pancreatic cancer. *Pancreatic Cancer* [Internet]. 2018. Available from: https://pathways.nice.org.uk/pathways/pancreatic-cancer#path=view%3A/pathways/pancreatic-cancer/managing-pancreatic-cancer.xml&content=view-index [Accessed 20th August 2018].

149. Hajatdoost L, Sedaghat K, Walker E, Thomas J, Kosari S. Chemotherapy in pancreatic cancer: A systematic review. *Medicina (Kaunas)* [Internet]. 2018;54(3): 48. Available from: http://www.mdpi.com/1010-660X/54/3/48 [Accessed 20th August 2018].

150. Von Hoff DD, Ervin T, Arena FP, Chiorean EG, Infante J, Moore M, et al. Increased survival in pancreatic cancer with nab-paclitaxel plus gemcitabine. *N Engl J Med*. 2013;369(18): 1691–1703.

151. Olive KP, Jacobetz MA, Davidson CJ, Gopinathan A, McIntyre D, Honess D, et al. Inhibition of Hedgehog signaling enhances delivery of chemotherapy in a mouse model of pancreatic cancer. *Science*. 2009;324(5933): 1457–1461.

152. Reddy LH, Couvreur P. Squalene: A natural triterpene for use in disease management and therapy. *Adv Drug Deliv Rev*. 2009;61(15): 1412–1426.

153. Sobot D, Mura S, Yesylevskyy SO, Dalbin L, Cayre F, Bort G, et al. Conjugation of squalene to gemcitabine as unique approach exploiting endogenous lipoproteins for drug delivery. *Nat Commun*. 2017;8(May): 15678.

154. Peñuelas J, Munné-Bosch S. Isoprenoids: An evolutionary pool for photoprotection. *Trends Plant Sci*. 2005;10(4): 166–169.

155. Kelly GS. Squalene and its potential clinical uses. *Altern Med Rev*. 1999;4(1): 29–36.

156. Mathews J. Sharks still intrigue cancer researchers. *J Natl Cancer Inst*. 1992;84(13): 1000–1002.

157. Owen RW, Haubner R, Würtele G, Hull WE, Spiegelhalder B, Bartsch H. Olives and olive oil in cancer prevention. *Eur J Cancer Prev*. 2004;13(4): 319–326.

158. Relas H, Gylling H, Miettinen TA. Fate of intravenously administered squalene and plant sterols in human subjects. *J Lipid Res*. 2001;42(6): 988–994.

159. Newmark HL. Squalene, olive oil, and and cancer risk: A review and hypothesis. *Cancer Epidemiol Biomarkers Prev*. 1997;6(12): 1101–1103.

160. Couvreur P, Vauthier C. Nanotechnology: Intelligent design to treat complex disease. *Pharm Res*. 2006;23(7): 1417–1450.

161. Bergman AM, Pinedo HM, Peters GJ. Determinants of resistance to 2′,2′-difluorodeoxycytidine (gemcitabine). *Drug Resist Updat*. 2002;5(1): 19–33.

162. Couvreur P, Stella B, Harivardhan Reddy L, Hillaireau H, Dubernet C, Desmaële D, et al. Squalenoyl nanomedicines as potential therapeutics. *Nano Lett*. 2006;6(11): 2544–2548.

163. Ambike A, Rosilio V, Stella B, Lepeêtre-Mouelhi S, Couvreur P. Interaction of self-assembled squalenoyl gemcitabine nanoparticles with phospholipid-cholesterol monolayers mimicking a biomembrane. *Langmuir*. 2011;27(8): 4891–4899.

164. Joubert F, Martin L, Perrier S, Pasparakis G. Development of a gemcitabine-polymer conjugate with prolonged cytotoxicity against a pancreatic cancer cell line. *ACS Macro Lett* [Internet]. 2017;6(5): 535–540. Available from: http://pubs.acs.org/doi/abs/10.1021/acsmacrolett.7b00160 [Accessed 9th September 2018].

165. Promega Ltd. CellTiter-Glo® 3D Cell Viability Assay. *Technical Manual* [Internet]. 2015. Available from: https://www.promega.com/-/media/files/resources/protocols/technical-manuals/101/celltiter-glo-3d-cell-viability-assay-protocol.pdf [Accessed 9th September 2018].

166. Field A. *Discovering Statistics using IBM SPSS Statistics*. 4th ed. London: Sage Publications; 2013.

167. Chou TC, Talalay P. Quantitative analysis of dose-effect relationships: the combined effects of multiple drugs or enzyme inhibitors. *Adv Enzyme Regul*. 1984;22(C): 27–55.

168. Mathews MS, Vo V, Shih EC, Zamora G, Sun CH, Madsen, SJ, et al. Photochemical internalization-mediated delivery of chemotherapeutic agents in human breast tumor cell lines. *J Env Pathol Toxicol Oncol*. 2012;31(1): 49–59.

169. Martinez A, Bayona DP, Woodhams JH, Pye H, Hamoudi RA, Moore CM, et al. Efficacy of photochemical internalisation using disulfonated chlorin and porphyrin photosensitisers : An in vitro study in 2D and 3D prostate cancer models. *Cancer Lett*. 2017;393: 68–75.

170. Gidding CE, Kellie SJ, Kamps WA, De Graaf SS. Vincristine revisited. *Crit Rev Oncol Hematol*. 1999;29(3): 267–287.

171. Gregory RK, Smith IE. Vinorelbine - a clinical review. *Br J Cancer* [Internet]. 2000;82(12): 1907–1913. Available from: https://www.ncbi.nlm.nih.gov/pmc/articles/PMC2363259/pdf/82-6691203a.pdf [Accessed 10th September 2018].

172. Moudi M, Go R, Yien CY, Nazre M. Vinca alkaloids. *Int J Prev Med*. 2013;4(11): 1131–1135.

173. Ngan VK, Bellman K, Hill BT, Wilson L, Jordan MA. Mechanism of mitotic block and inhibition of cell proliferation by the semisynthetic Vinca alkaloids vinorelbine and its newer derivative vinflunine. *Mol Pharmacol*. 2001;60(1): 225–232.

174. von Minckwitz G. Docetaxel/anthracycline combinations for breast cancer treatment. *Expert Opin Pharmacother* [Internet]. 2007;8(4): 485–495. Available from: http://www.tandfonline.com/doi/full/10.1517/14656566.8.4.485 [Accessed 10th September 2018].

175. Jordan MA, Wilson L. Microtubules as a target for anticancer drugs. *Nat Rev Cancer*. 2004;4(4): 253–265.

176. Ma P, Mumper RJ. Paclitaxel nano-delivery systems: A comprehensive review. *J Nanomed Nanotechnol*. 2013;4(2): 1000164.

177. Heinemann V. Gemcitabine in metastatic breast cancer. *Expert Rev Anticancer Ther*. 2005;5(3): 429–443.

178. Walko CM, Lindley C. Capecitabine: A review. *Clin Ther*. 2005;27(1): 23–44.

179. Herschkowitz JI, Simin K, Weigman VJ, Mikaelian I, Usary J, Hu Z, et al. Identification of conserved gene expression features between murine mammary carcinoma models and human breast tumors. *Genome Biol* [Internet]. 2007;8(5): R76. Available from: http://genomebiology.com/2007/8/5/R76 [Accessed 11th September 2018].

180. Pelicano H, Zhang W, Liu J, Hammoudi N, Dai J, Xu RH, et al. Mitochondrial dysfunction in some triple-negative breast cancer cell lines: role of mTOR pathway and therapeutic potential. *Breast Cancer Res* [Internet]. 2014;16(5): 434. Available from: http://www.ncbi.nlm.nih.gov/pubmed/25209360 [Accessed 11th September 2018].

181. Lanning NJ, Castle JP, Singh SJ, Leon AN, Tovar EA, Sanghera A, et al. Metabolic profiling of triple-negative breast cancer cells reveals metabolic vulnerabilities. *Cancer Metab* [Internet]. 2017;5(1): 6. Available from: http://cancerandmetabolism.biomedcentral.com/articles/10.1186/s40170-017-0168-x [Accessed 12th September 2018].

182. ATCC. MDA-MB-231 (ATCC® HTB-26TM). *Monograph* [Internet]. 2016. Available from: https://www.lgcstandards-atcc.org/Products/All/HTB-26.aspx?geo_country=gb [Accessed 12th September 2018].

183. ATCC. MCF7 (ATCC® HTB-22TM). *Monograph* [Internet]. 2018. Available from: https://www.lgcstandards-atcc.org/Products/All/HTB-22.aspx?geo_country=gb#specifications [Accessed 12th September 2018].

184. Wang F, Yang Y. Inhibition of PKM2 sensitizes triple-negative breast cancer cells to doxorubicin. *Biochem Biophys Res Commun*. 2014;454(3):465–470.

185. Rowinsky E. The Vina Alkaloids. In: *Cancer Medicine* (Kufe D, Pollock R, Weichselbaum R, Bast Jr R, Gansler T, Holland J, et al., eds). 6th ed. Ontario: BC Decker; 2003.

186. Breslin S, O'Driscoll L. The relevance of using 3D cell cultures, in addition to 2D monolayer cultures, when evaluating breast cancer drug sensitivity and resistance. *Oncotarget*. 2016;7(29): 45745–45756.

187. Groth-Pedersen L, Ostenfeld MS, Høyer-Hansen M, Nylandsted J, Jäättelä M. Vincristine induces dramatic lysosomal changes and sensitizes cancer cells to lysosome-destabilizing siramesine. *Cancer Res*. 2007;67(5): 2217–2225.

188. Berg K, Dietze A, Kaalhus O, Høgset A. Site-specific drug delivery by photochemical internalization enhances the antitumor effect of bleomycin. *Clin Cancer Res*. 2005;11(23): 8476–8485.

189. Vikdal M, Generalov R, Berg K. The photosensitizer disulfonated aluminum phthalocyanine reduces uptake and alters trafficking of fluid phase endocytosed drugs in vascular endothelial cells-impact on efficacy of photochemical internalization. *Biochem Pharmacol* [Internet]. 2013;86(6): 748–758. Available from: http://dx.doi.org/10.1016/j.bcp.2013.07.011 [Accessed 13th September 2018].

190. Revazova E, Bryzgalov I, Ivanov IS, Sebastian J, Keller G, Watson J. Stimulation of the growth of human tumor by low-power laser irradiation. *Bull Exp Biol Med* [Internet]. 2001;132(2): 778–779. Available from: http://www.ncbi.nlm.nih.gov/pubmed/11713565 [Accessed 13th September 2018].

191. Eng MS, Kaur J, Prasmickaite L, Engesæter B, Weyergang A, Skarpen E, et al. Enhanced targeting of triple-negative breast carcinoma and malignant melanoma by photochemical internalization of CSPG4-targeting immunotoxins. *Photochem Photobiol Sci*. 2018;17(5): 539–551.

192. Weyergang A, Berg K, Kaalhus O, Peng Q, Selbo PK. Photodynamic therapy targets the mTOR signaling network in vitro and in vivo. *Mol Pharm*. 2008;6(1): 255–264.

193. Berstad MB, Weyergang A, Berg K. Photochemical internalization (PCI) of HER2-targeted toxins: Synergy is dependent on the treatment sequence. *Biochim Biophys Acta* [Internet]. 2012;1820(12): 1849–1858. Available from: http://dx.doi.org/10.1016/j.bbagen.2012.08.027 [Accessed 13th September 2018].

194. Moore P, Ridgway TD, Higbee RG, Howard EW, Lucroy MD. Effect of wavelength on low-intensity laser irradiation-stimulated cell proliferation in vitro. *Lasers Surg Med*. 2005;36(1): 8–12.

195. Lanzafame RJ. Photobiomodulation and cancer and other musings. *Photomed Laser Surg* [Internet]. 2011;29(1): 3–4. Available from: http://www.ncbi.nlm.nih.gov/pubmed/21219219 [Accessed 14th September 2018].

196. de C. Monteiro JS, Pinheiro AN, de Oliveira SC, Aciole GT, Sousa JA, Cangussú MC, et al. Influence of laser phototherapy (λ660 nm) on the outcome of oral chemical carcinogenesis on the hamster cheek pouch model: histological study. *Photomed Laser Surg* [Internet]. 2011;29(11): 741–745. Available from: http://www.ncbi.nlm.nih.gov/pubmed/21718118 [Accessed 14th September 2018].

197. Myakishev-Rempel M, Stadler I, Brondon P, Axe DR, Friedman M, Nardia FB, et al. A preliminary study of the safety of red light phototherapy of tissues harboring cancer. *Photomed Laser Surg*. 2012;30(9): 551–558.

198. Muller M, Meijer C, Zaman GJ, Borst P, Scheper RJ, Mulder NH, et al. Overexpression of the gene encoding the multidrug resistance-associated protein results in increased ATP-dependent glutathione S-conjugate transport. *Proc Natl Acad Sci U S A*. 1994;91(26): 13033–13037.

199. Honore S, Pasquier E, Braguer D. Understanding microtubule dynamics for improved cancer therapy. *Cell Mol Life Sci*. 2005;62(24): 3039–3056.

200. Jordan MA, Thrower D, Wilson L. Mechanism of inhibition of cell proliferation by Vinca alkaloids. *Cancer Res*. 1991;51(8): 2212–2222.

201. Duflos A, Kruczynski A, Barret JM. Novel aspects of natural and modified vinca alkaloids. *Curr Med Chem Anticancer Agents*. 2002;2(1): 55–70.

202. Bröker LE, Huisman C, Span SW, Rodriguez JA, Kruyt FA, Giaccone G. Cathepsin B mediates caspase-independent cell death induced by microtubule stabilizing agents in non-small cell lung cancer cells. *Cancer Res*. 2004;64(1): 27–30.

203. Cirman T, Orešić K, Mazovec GD, Turk V, Reed JC, Myers RM, et al. Selective disruption of lysosomes in HeLa cells triggers apoptosis mediated by cleavage of Bid by multiple papain-like lysosomal cathepsins. *J Biol Chem*. 2004;279(5): 3578–3587.

204. Sloane BF, Yan S, Podgorski I, Linebaugh BE, Cher ML, Mai J, et al. Cathepsin B and tumor proteolysis: Contribution of the tumor microenvironment. *Semin Cancer Biol*. 2005;15(2): 149–157.

205. Ostenfeld MS, Fehrenbacher N, Hoyer-Hansen M, Thomsen C, Farkas T, Jäättelä M. Effective tumor cell death by σ-2 receptor ligand siramesine involves lysosomal leakage and oxidative stress. *Cancer Res*. 2005;65(19): 8975–8983.

206. Gilbar PJ, Carrington CV. The incidence of extravasation of vinca alkaloids supplied in syringes or mini-bags. *J Oncol Pharm Pract*. 2006;12(2): 113–118.

207. Sobot D, Mura S, Yesylevskyy SO, Dalbin L, Cayre F, Bort G, et al. Conjugation of squalene to gemcitabine as unique approach exploiting endogenous lipoproteins for drug delivery. *Nat Commun* [Internet]. 2017;8: 15678. Available from: http://www.nature.com/doifinder/10.1038/ncomms15678 [Accessed 16th September 2018].

208. Bulbake U, Doppalapudi S, Kommineni N, Khan W. Liposomal formulations in clinical use: An updated review. *Pharmaceutics*. 2017;9(2).

209. Maksimenko A, Caron J, Mougin J, Desmaële D, Couvreur P. Gemcitabine-based therapy for pancreatic cancer using the squalenoyl nucleoside monophosphate nanoassemblies. *Int J Pharm* [Internet]. 2015;482(1–2): 38–46. Available from: http://dx.doi.org/10.1016/j.ijpharm.2014.11.009 [Accessed 16th September 2018].

210. Bigand C, Hajri A, Parmentier C, Couvreur P, Réjiba S, Reddy LH. Squalenoyl gemcitabine nanomedicine overcomes the low efficacy of gemcitabine therapy in

pancreatic cancer. *Nanomedicine* [Internet]. 2011;7(6): 841–849. Available from: http://dx.doi.org/10.1016/j.nano.2011.02.012 [Accessed 17th September 2018].

211. Felt SA, Droby GN, Grdzelishvili VZ. Ruxolitinib and polycation combination treatment overcomes multiple mechanisms of resistance of pancreatic cancer cells to oncolytic vesicular stomatitis virus. *J Virol*. 2017;91(16): pii e00461-17.

212. Gal D, MacDonald PC, Porter JC, Simpson ER. Cholesterol metabolism in cancer cells in monolayer culture. III. Low-density lipoprotein metabolism. *Int J Cancer*. 1981;28(3): 315–319.